Evolution of Nuclear Structure: From Semi-Magicity to Magicity in the Neutron-Rich Copper Isotopes

Serge Franchoo

Habilitation à diriger des recherches

université PARIS-SACLAY

Evolution de la structure nucléaire : De semi-magicité à magicité dans les isotopes de cuivre riches en neutrons

Habilitation à diriger des recherches de l'Université Paris-Saclay

présentée et soutenue à Orsay, le 28 mai 2021, par

Serge Franchoo

Composition du jury

Michael BENTLEY Professeur, Université de York, Royaume-Uni	Rapporteur
Thomas NILSSON Professeur, Université de technologie de Chalmers, Suède	Rapporteur
Berta RUBIO Professeure, Institut de physique corpusculaire, Valence, Espagne	Rapportrice
Olivier SORLIN Directeur de Recherche, CNRS	Examinateur
Tiina SUOMIJÄRVI Professeure, Université Paris-Saclay	Examinatrice

université
PARIS-SACLAY

Titre : Evolution de la structure nucléaire : De semi-magicité à magicité dans les isotopes de cuivre riches en neutrons

Mots clés : structure nucléaire, noyaux exotiques, isotopes de cuivre

Title : Evolution of Nuclear Structure: From Semi-Magicity to Magicity in the Neutron-Rich Copper Isotopes

Keywords : nuclear structure, exotic nuclei, copper isotopes

Abstract : The neutron-rich copper isotopes have generated substantial interest over the last decades, thanks to the simple picture they present of a single proton outside the closed Z = 28 nickel core. At the semi-magic neutron number N = 40, the single-particle nature of the lowest excited states affirms itself through distinct and sudden structural changes. It remains firmly apparent along the isotopic chain, which is illustrated by the transparent interpretation of weakly coupled valence particles that holds for the odd-odd isotopes. The availability of competing configurations, however, never stays far away, and provides fertile ground for the appearance of shape coexistence at the N = 50 magic number. In this contribution we intend to bring together the extensive experimental input from various probes involving transfer reactions, in-flight, decay as well as laser spectroscopy over the last twenty years, and offer an overview of the theoretical endeavour by which it has been accompanied.

Evolution de la structure nucléaire :

De semi-magicité à magicité

dans

les isotopes de cuivre riches en neutrons

SERGE FRANCHOO

UNIVERSITÉ PARIS-SACLAY (2021)

L'homme n'est qu'un roseau, le plus faible de la nature, mais c'est un roseau pensant. Il ne faut pas que l'univers entier s'arme pour l'écraser ; une vapeur, une goutte d'eau suffit pour le tuer. Mais quand l'univers l'écraserait, l'homme serait encore plus noble que ce qui le tue puisqu'il sait qu'il meurt et l'avantage que l'univers a sur lui, l'univers n'en sait rien. Toute notre dignité consiste donc en la pensée. C'est de là qu'il faut nous relever et non de l'espace et de la durée, que nous ne saurions remplir. Travaillons donc à bien penser : voilà le principe de la morale.

Pascal, Pensées, fr. 186

Je voyois aussi beaucoup à Chamberi un Jacobin Professeur de physique, bon homme de moine dont j'ai oublié le nom, et qui faisoit souvent de petites expériences qui m'amusoient extrémement. Je voulus à son exemple faire de l'encre de sympathie. Pour cet effet après avoir rempli une bouteille plus qu'à demi de chaux vive, d'orpiment et d'eau je la bouchai bien. L'effervescence commença presque à l'instant très violemment. Je courus à la bouteille pour la déboucher mais je n'y fus pas à tems ; elle me sauta au visage comme une bombe. J'avalai de l'orpiment, de la chaux, j'en faillis mourir. Je restai aveugle plus de six semaines, et j'appris ainsi à ne pas me mêler de physique expérimentale sans en savoir les élémens.

Rousseau, Confessions, Livre cinquième

Contents

Chapter 1

Introduction

We set off with a brief sketch of the origins of the nuclear shell model. The magic numbers it portends have been professed to come under stress and possibly dissolve far from stability, a phenomenon we illustrate for $N = 20$. We then explore the status of $N = 28$. The tortuous road the theoretical understanding of these findings has followed is put under the spotlight, from the overlap of single-particle orbitals to shape coexistence and the peculiar role of the spin-orbit and tensor components in the nuclear interaction. In the subsequent sections we shall then turn to a review of the experimental literature on the neutron-rich copper isotopes, which we take under the microscope in this work, before examining the available theoretical effort that specifically focusses on the nickel region.

1.1 The early days

It has been said that the dawn of nuclear structure broke with the discovery of the neutron by James Chadwick in 1932. Certainly the event proved most prolific. Having the piece at hand, James Bartlett added protons and neutrons in a consecutive manner and ranked among the first to devise a shell structure both for the α particle and the ^{16}O nucleus [Bar32a]. Trying to move beyond, it was deemed possible to include also electrons in the core, but this turned out to be a frustrating exercise [Bar32b]. Against the background of an ongoing controversy whether the nucleus would be built from protons and neutrons in separate shells or agglutinating α particles instead, Kurt

Guggenheimer at the Collège de France in Paris opted for the former. He identified discontinuities in the nuclear binding energies when the neutron count reaches 50 or 82 particles and went on to publish perhaps the very first nuclear chart [Gug34]. Incidentally he swapped the p in isotopes for an n in the new word isotones he proposed.

His colleague Walter Elsasser at the nearby Institut Poincaré listed the possible energy levels of a spherical well that would rule the particles independently and for which he adopted the familiar spectroscopic labels $spdfgh$, figuring out along the way that also 126 would be a member of the select club of peculiar numbers [Els34a]. To arrive at the shell closures at 50 and 82, Elsasser proposed to skip the $2s$ and $2p$ orbitals from the filling sequence, arguing that they would dissolve as proper structures once they sink from the Fermi surface in the lighter nuclei to the inner bulk in the heavier ones [Els34b]. The eight particles would rearrange in the next available envelopes and complete assemblies would accordingly be reached earlier, 58 becoming 50 ($1s^2 1p^6 1d^{10} 2s^2 1f^{14} 2p^6 1g^{18} \rightarrow 1s^2 1p^6 1d^{10} 1f^{14} 1g^{18}$) and 90 becoming 82 ($1s^2 1p^6 1d^{10} 2s^2 1f^{14} 2p^6 1g^{18} 2d^{10} 1h^{22} \rightarrow 1s^2 1p^6 1d^{10} 1f^{14} 1g^{18} 2d^{10} 1h^{22}$, note that $3s^2$ was believed to lie above $1h^{22}$). To construct 126 from quantum numbers several combinations subsisted, but the scientific community remained largely at sea at what possibly happened between oxygen and tin.

Eugene Wigner, who had meanwhile engaged in an intricate endeavour to calculate nuclear binding energies, with little misgivings wrote that "the single-particle picture is known to be an insufficient approximation" [Wig37]. So when the nuclear shell model was introduced through four separate articles in the journal Physical Review in 1949 [Hax49, Fee49a, Nor49, Goe49], it came as a surprise that an independent-particle model turned out to be the most fruitful matrix for understanding the correlation between spin and shell structure that slowly was becoming clear. While Maria Goeppert-Mayer much later would reply that "the shell model, although proposed by theoreticians, really corresponds to the experimentalist's approach" [Goe63], Wigner would be credited for calling the cluster of grumpy behenians "magic numbers" [Aud06].

A simple potential well was sufficient to explain the increased stability at 8 and 20, but shrewd skill was required to correctly assign quantum numbers to strings of successive particles in the heavier nuclei. The observed regularities, however, had pressed

	8	14	20	28	50
Haxel, Jensen, Suess		$1s1p1d_{5/2}$		$1d_{3/2}2s1f_{7/2}$	$1f_{5/2}2p1g_{9/2}$
Feenberg, Hammack	$1s1p$		$2s1d$		
	$1s1p$				$1d1f1g$
Nordheim	$1s1p$		$2s1d$		$1f2p2d$
Goeppert-Mayer	$1s1p$		$1d2s$	$1f_{7/2}$	$1f_{5/2}2p1g_{9/2}$

Table 1.1: Magic numbers up to 50 according to different early authors. Taken from [Hax49, Fee49a, Nor49, Goe49]

people to try out reshuffling the possible levels in contrasting manners. A short but useful note in the literature that was published the same year explained the difference between three of the four attempts [Fee49b]. Eugene Feenberg and Kenyon Hammack pushed up in energy all states with radial nodes, like it had been suggested by Elsasser fifteen years before. Thereby they explicitly promoted the image of a hollow nucleus and ascribed it to the repulsive action of the Coulomb force in its centre. Lothar Nordheim applied the opposite hypothesis by energetically favouring radial nodes, shifting $2d$ before $1g$. He painted a picture of a rigid nucleus where high angular momentum is unwanted, the balance of forces now being in favour of the strong interaction. Maria Goeppert-Mayer, on the other hand, chose not to intervene in the ordering of the states but instead introduced a strong spin-orbit interaction. Splitting apart the parallel and antiparallel orientations, the magic numbers at 28 and at 50 were found from the downwards displacement of the $f_{7/2}$ and $g_{9/2}$ orbitals, respectively. The authors of the short note overlooked an earlier brief letter by Otto Haxel, Hans Jensen and Hans Suess, which nevertheless were the first to show how the magic numbers could be produced from lifting the degeneracy of the $j_< = \ell - 1/2$ and $j_> = \ell + 1/2$ partner orbitals by a sufficiently strong spin-orbit force [Hax49]. Curiously enough and perhaps the reason for its disregard was the prediction of the first magic number at 14, found from the unguarded lowering of the $1d_{5/2}$ orbital. An overview of the four proposals is given in table 1.1.

Since its early days, the shell model has withstood many tests of time. Next to

isotopic abundances, masses and spins, also electric and magnetic moments, the existence of isomerism and β-decay properties have been in line with shell structure and the underlying idea of a single nucleon moving in an average field. Among much fruitless effort to understand why the relativistic Thomas precession could not account for the magnitude of the spin-orbit splitting, even including an attempt to deduce the spin-orbit force from a tensor interaction instead [Kei51], Kenneth Case and Abraham Pais at Princeton in their analysis of nucleon-nucleon scattering purposely modelled the spin-orbit force by the derivative of the central potential V_c,

$$V_{ls}(r) = -\alpha_{ls} \, \frac{1}{r} \frac{\partial V_c}{\partial r} \, \boldsymbol{L} \cdot \boldsymbol{S} \tag{1.1}$$

with the two-body operators $\boldsymbol{L} = (\boldsymbol{r}_1 - \boldsymbol{r}_2) \times (\boldsymbol{p}_1 - \boldsymbol{p}_2)$ and $\boldsymbol{S} = \boldsymbol{\sigma}_1 + \boldsymbol{\sigma}_2$, while actually chosing a Yukawa form for V_c [Cas50].[1] In spite of the labyrinth of manifold interpretations that still lay open ahead, it remained all the same most remarkable that the energy gaps created by the spin-orbit force are of the same order of magnitude as the harmonic oscillator gaps.

Nonetheless, whereas for many years the magic numbers seemed firmly established, all of a sudden their anchorage started to wash away. One of the first magic numbers to disappear was $N = 20$ in neutron-rich neon, sodium and magnesium. When the masses of the ^{31,32}Na isotopes were measured at the Cern proton synchrotron, they deviated from the predictions by various models available at the time [Thi75]. Hartree-Fock calculations built on the Vautherin-Brink Skyrme force forthwith led Xavier Campi and his coworkers at Orsay and Massachusetts to interpret the anomaly as a sign of deformation [Cam75]. More precisely the $1/2^-$ and $3/2^-$ levels that sprout from the $\nu f_{7/2}$ orbital like a Nilsson scheme would cross into the *sd* shell once a prolate shape sets in. The authors did not distinguish this design from a tantamount change in the spin-orbit force in a single-particle view, which would lower the $\nu f_{7/2}$ orbital close enough to the $\nu d_{3/2}$ one for filling of the former to be favoured.

The treatment of deformation of the nucleus is a most fundamental question. When Markus Fierz in Zürich spelled out the general formula for the proton-neutron interaction from first principles, he had found it to contain a tensor term [Fie37]. Hideki

[1] David Inglis had put forward a $1/r \; dV/dr$ radial dependence for the spin-orbit coupling several years before but did so merely from the argument that the force is the gradiant of the potential [Ing36]

Yukawa in Osaka derived the same result from the Proca field equation for a massive vector boson, so the tensor force was seen to originate in the postulate of a heavy spin-1 meson that mediates the nuclear interaction [Yuk38]. The idea was discarded in favour of the spinless pion, but it would emerge again soon after precisely in the context of deformation. Based on the fascinating observation of an electric quadrupole moment for the deuteron by Jerome Kellogg and colleagues at Columbia university in 1939 [Kel39], William Rarita and Julian Schwinger at the opposite shore at Berkeley positively posited the existence of a spin-spin tensor force in the nucleus [Rar41]. Its common expression,

$$S_{12} = \frac{3(\boldsymbol{\sigma}_1 \cdot \boldsymbol{r}_{12})(\boldsymbol{\sigma}_2 \cdot \boldsymbol{r}_{12})}{r_{12}^2} - \boldsymbol{\sigma}_1 \cdot \boldsymbol{\sigma}_2, \tag{1.2}$$

couples spin and space coordinates and therefore does no longer preserve the orbital angular momentum. Besides the spin-orbit interaction, it is the only other non-central force that charge independence and invariance requirements allow for. Held responsible for the occurrence of asymmetrical charge distributions, the tensor force needs lies at the origin of nuclear deformation. However, it could not be readily linked to the behaviour of individual single-particle orbitals and its proper place in the shell model presented a puzzle.

Searching to escape from the deadlock, but also confronted with the catastrophic diversion of human endeavour into the war effort, theoretical thinking held its breath ere it fell back from the shell model into renewed paths of subatomic synergy. So in 1950 at Columbia university again the reality of quadrupole moments was duly recognised by James Rainwater as a proof for spheroidal rather than spherical shapes [Rai50]. Soon afterwards his idea was elaborated upon by Aage Bohr and Ben Mottelson at Copenhagen to formulate their collective picture of nuclear matter [Boh53]. Philip Elliott working at Harwell near Oxford, overlooking the site of the first nuclear reactor in western Europe, proposed the SU(3) symmetry in an attempt to bridge the shell model and the collective approach [Ell58]. The model he engineered governs in the eight dimensions that correspond to the three orbital angular momentum and the five quadrupole operators.

Not readily able to accommodate the tensor force, the shell model took a different approach. Amos de-Shalit at the venerable Massachusetts Institute of Technology and

Maurice Goldhaber at rustic Brookhaven contrived a way in which deformation could stem from overlapping proton and neutron single-particle configurations [DeS53]. In particular the importance of the isoscalar attraction between the $\pi d_{5/2}$ and $\nu d_{3/2}$ orbitals had been identified in the oxygen, fluorine and neon isotopes [Tal62, Unn63]. Nestled below the emblematic Cathedral of Learning, the Pittsburgh cyclotron produced some remarkable contributions to nuclear structure. With a 15-MeV deuteron beam a study of (d,p) and (d,t) reactions on tin isotopes enabled to determine the spectroscopic factors of several single-particle orbitals, which for our present purpose we can define as normalisation factors that catch the overlap between the initial and final state [Coh61]. Introducing a simple pairing model to transform the occupation probabilities into single-particle energies, the $\nu g_{7/2}$ state could be firmly located in the lower reaches of the *gds* shell. Following up on this work, a detailed investigation of (d,p) and (d,t) reactions on strontium and zirconium isotopes showed an extraordinary drift of the same orbital to the very top of the shell [Coh62a]. Soon after Igal Talmi and Anthony Lane independently pointed out that between zirconium and tin the protons are stacked in the $\pi g_{9/2}$ orbital, which is the spin-orbit partner.

Examples in other mass regions were quickly uncovered [Coh62b]. From titanium to nickel protons pile up in $f_{7/2}$, provoking a downwards slant of the energy of the $f_{5/2}$ neutrons. We show in figure 1.1 the energy of the $5/2^-$ state with highest spectroscopic factor in the relevant (d,p) reaction above that of the main fragment of the $\nu p_{3/2}$ orbital. For ^{53}Ti, ^{53}Fe and ^{57}Ni the energy difference of the first known states with spins $5/2^-$ and $3/2^-$ is plotted as no spectroscopic factors are available. The addition of the first two $f_{7/2}$ protons induces an immediate effect, which then simmers down towards the end of the subshell. In ^{59}Ni the essence of $\nu f_{5/2}$ hovers at 341 keV above the $3/2^-$ ground state, while in ^{61}Ni this even reduces to 68 keV.

Likewise between cerium and lead protons amass in $h_{11/2}$, tugging down the $h_{9/2}$ neutrons. Once more (d,p) reaction data for ^{141}Ce, ^{143}Nd and ^{145}Sm reveal what happens before the $h_{11/2}$ protons fill in. The main fragment of the $\nu h_{9/2}$ orbital is situated at 1.4 MeV above the $7/2^-$, which by crude simplification we take to represent the $\nu f_{7/2}$ configuration. Because of strong deformation in the lanthanides the spectroscopic strengths are much fragmented and conclusions cannot be drawn reliably for

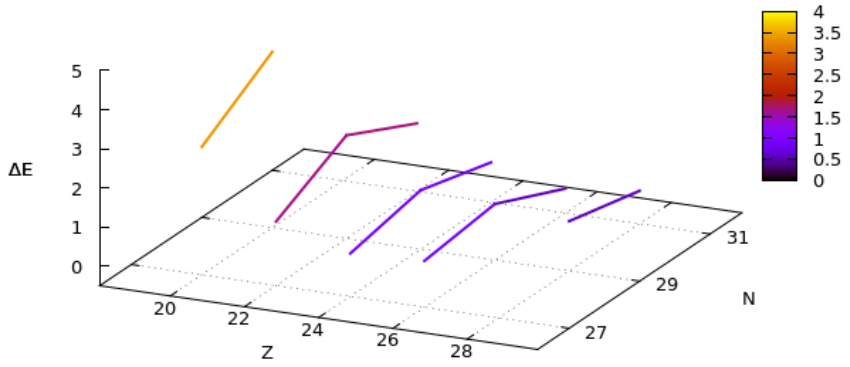

Figure 1.1: Energy differences of the $\nu f_{5/2}$ and $\nu p_{3/2}$ fragments of highest spectroscopic strength from ^{47}Ca to ^{59}Ni. When no spectroscopic factors are known the energy difference of the first states with spins $5/2^-$ and $3/2^-$ is given

$64 \leq Z \leq 76$. In platina and mercury, however, we arrive close enough to lead to recognise again the single-particle structures. Even though spin and parity assignments are tentative, in ^{171}Pt ($N = 93$) a $9/2^-$ state would lie 90 keV above the $7/2^-$ ground state. In ^{177}Pt ($N = 99$) the levels are better known and the spacing between the first $7/2^-$ and $9/2^-$ states equals 116 keV. In ^{175}Hg ($N = 95$) the ground state would revert to $7/2^-$ with a presumed $9/2^-$ level at 80 keV, which in ^{179}Hg ($N = 99$) would become 61 keV. Ignoring the eventual differences in pairing energy, the replete $\pi h_{11/2}$ configuration would thus render the $h_{9/2}$ and $f_{7/2}$ neutron orbitals nearly degenerate.

An energetic swing of the $h_{9/2}$ proton state was spotted in the gold ($Z = 79$) and thallium ($Z = 81$) isotopic chains [Goo77]. Reproduced in figure 1.2, it was treated as a self-consistent renormalisation of the spherical single-particle energies, by which was essentially meant that specific neutron orbitals act on specific proton orbitals through single-particle effects. Based on G-matrix calculations with the Reid soft-core potential that earlier had been applied to rare-earth nuclei from gadolinium to osmium but also had covered tin and lead, it was found that the $\nu h_{9/2}$ and $\nu i_{13/2}$ orbitals below $N = 114$ would better bind the $\pi h_{9/2}$ state than the $\nu f_{5/2} p_{3/2} p_{1/2}$ cluster does above $N = 114$. Because of the confounding $j_<$ and $j_>$ spin orientations that enter the game,

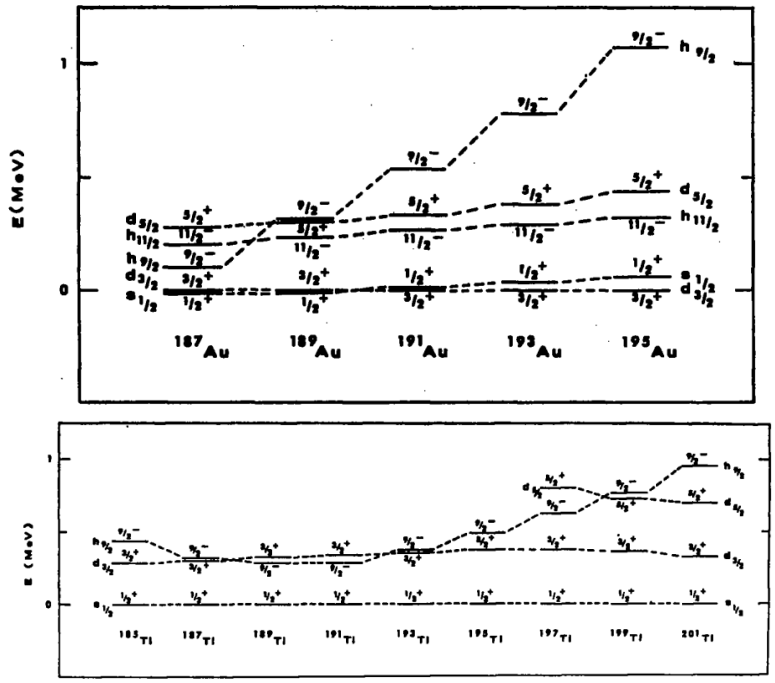

FIGURE 1.2: Selected states in odd gold and thallium isotopes. Taken from [Goo77]

the ℓ overlap of the orbitals would seem the essential feature. At the same time a clear distinction was made with an intruder state, which was defined as coming down in energy through collective effects instead.

Inch by inch a comprehensive framework throughout the nuclear chart came to the front that was expressed by Pedro Federman at Mexico and Stuart Pittel at Delaware whereby the residual proton-neutron interaction would align the nucleon spins and take on an isoscalar signature, similar as the force that rules the deuteron [Fed79]. When the protons and neutrons occupy orbits with comparable angular momentum, the interaction is enhanced and the $T = 0$ proton-neutron correlations would outweigh the $T = 1$ pairing contributions. In particular spin-orbit partner orbitals would assure the necessary geometrical overlap but many other combinations would equally do. Returning to neutron-rich zirconium, an increased number of $\nu g_{7/2}$ neutrons would start pulling protons across $Z = 40$ into $\pi g_{9/2}$. The protons in turn attract more neutrons into $\nu g_{7/2}$, polarising the nucleus. Deformation appears when this isoscalar residual interaction becomes stronger than the isovector component of the nuclear force, which instead restores the symmetry at the shell closures. In the lighter region from neon to

magnesium, the development of deformation was ascribed to the attraction between $d_{5/2}$ protons and neutrons that scatter into the $f_{7/2}$ state. At first it looks unexpected that both orbitals would be of the $j_>$ type, which for an isoscalar construction would imply that the orbital angular momenta are parallel oriented. As a matter of fact, short-range forces are commonly associated to opposite momenta. The interaction, however, would at the same time break open the $\nu d_{3/2}$ state below $N = 20$ and one cannot exclude that $j_< \leftrightarrow j'_>$ configurations also contribute. In heavy nuclei the situation is less clear since the large number of valence particles would always lend an advantage to the proton-neutron interactions over the pairing correlations.

Another anomaly was signalled at $N = 56$ in ^{94}Sr, where the first 2^+ energy does not rise the way it does in ^{96}Zr [Fed84]. From a comparison between ^{89}Y and ^{95}Y, the $p_{1/2}$ and $p_{3/2}$ proton states were seen to close in on each other by no less than 0.82 MeV, which the authors related to the $d_{5/2}$ neutron occupancy swelling from empty to full. This weakened spin-orbit splitting would lower the 2^+ energy in ^{94}Sr compared to ^{88}Sr, in as far as it corresponds to a $\pi p_{1/2}^{-1} p_{3/2}^{3}$ excitation. Of peculiar importance here is the association with the spin-orbit force that is brought to the fore, although it might also show that a possible $N = 56$ subshell closure in zirconium no longer holds as soon as one moves away from it.

The propensity of single-particle states to shift already in a spherical potential was further elaborated upon. Relying on a G-matrix interaction derived from the Reid soft-core potential as well as employing the Sussex force compiled by Elliott and colleagues a swath of examples was stitched together throughout the nuclear chart [Sor84]. For instance below $N = 114$ when neutrons are added in the high-spin $i_{13/2}$ orbital, the high-spin ghi proton states are predicted to fall. Above $N = 114$, neutrons assemble in the low-spin $p_{1/2}p_{3/2}f_{5/2}$ levels and the low-spin $sdpf$ proton configurations would slope down. As a result, the $Z = 82$ magicity for nuclei such as ^{192}Pt or ^{200}Rn would be cancelled. Likewise in palladium, xenon, samarium and ytterbium when neutrons gather in $s_{1/2}d_{3/2}f_{7/2}$, it would attract the πpdf levels. Similar conclusions were drawn for neutron levels as a function of proton occupancies. Particles of the same kind would feel the effect as well albeit to a smaller degree, confirming a relation that involves the quantum number ℓ but abandons an isoscalar $j_< \leftrightarrow j'_>$ effect.

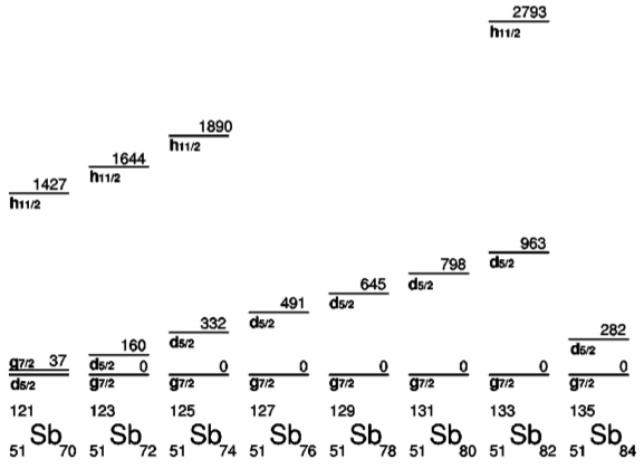

FIGURE 1.3: Selected experimentally observed states in odd antimony isotopes. Taken from [She02]

More recently moving levels have also been found near $Z = 50$ and $N = 82$. One proton beyond tin we meet antimony, for which we plot a state of affairs in figure 1.3. The $5/2^+$ level slowly rises from being the ground state in ^{121}Sb to 963 keV of excitation energy in ^{133}Sb, but in ^{135}Sb it sharply resets to 282 keV [She02]. The structure is interpreted as a $\pi d_{5/2}$ state, which would interact with $h_{11/2}d_{3/2}s_{1/2}$ neutrons below $N = 82$ and $f_{7/2}h_{9/2}$ ones above that. Among these $\nu h_{11/2}$ likely contains the key for pushing up $\pi d_{5/2}$ or by the same token pulling down $\pi g_{7/2}$. The effect across $N = 82$ is particularly pronounced but relating it to a specific configuration is not obvious. Theory that calls upon the G-matrix technique to construct a realistic interaction from the charge-dependent Bonn meson-exchange potential does not match the data well, unless the $\pi d_{5/2}$ position is manually marked down by 300 keV.

In the $N = 83$ isotones, migration of the $\nu h_{9/2}$ orbital relative to a ground state of $\nu f_{7/2}$ signature sets in after $Z = 64$ when protons rendezvous in the $h_{11/2}$ state [Bia10]. In ^{147}Gd ($Z = 64$) the relevant $9/2^-$ level is found at 1397 keV, while in ^{157}W it leisurely saunters at 318 keV. Shell-model calculations with a schematic spin-isospin exchange force reproduce the trend but not its magnitude. A tensor force is added explicitly but the improvement is not obvious, rather pointing to a predominance of the central component and hence an overlap of orbitals, the particular angular momenta of which matter less. Alternatively, the lack of clarity may be rooted in the inherent shortcoming

of comparing level energies with centroids of single-particle strengths.

The literature highlights the utmost difficulty to disentangle a definite single-particle from a broader collective behaviour. Rather than at $N = 114$, it had already been pointed out in the experimental work referred to above that the $\pi h_{9/2}$ energy in gold and thallium in fact reaches its minimum at $N = 108$, which had been explained by replacing the spherical shell-model orbitals by Nilsson ones [Goo77]. Once a deformed shell model is called in, however, it can by itself fully reproduce the evolution of the $\pi h_{9/2}$ state by turning it into an intruding oblate band head [Bou87].

Several years before, Ram Bansal and Bruce French at Rochester had identified the monopole component of the residual proton-neutron as the average energy that is weighted for spin and isospin [Ban64]. Apprehending its peculiar role in the shift of single-particle energies whilst likewise expanding on the idea of interacting proton and neutron orbitals in the origin of deformation, a schematic model was developed in a seminal paper on intruder states by Kris Heyde and the group at Ghent [Hey87]. A monopole correction was added to the pairing and proton-neutron quadrupole forces, thereby bringing together the microscopic insights by Federman and Pittel and the symmetry considerations from Elliott's theory. Particle-hole excitations across shells may be generated in odd nuclei from two particles and one hole (2p-1h), in even ones from two particles and two holes (2p-2h). The gain in pairing energy of such configurations is empirically determined from differences in binding energy. The monopole shift is written

$$\Delta E_M = 2 \sum_{j_\nu} \left(\langle j'_\pi j_\nu | V_{\pi\nu} | j'_\pi j_\nu \rangle - \langle j_\pi j_\nu | V_{\pi\nu} | j_\pi j_\nu \rangle \right) (2j_\nu + 1)\, v^2_{j_\nu} \tag{1.3}$$

for the case of two particles, here taken as protons, lifted from the j to the j' orbital with $V_{\pi\nu}$ denoting the residual interaction and v^2_j the occupation probability of an orbital. In the SU(3) model the quadrupole correlations become

$$\Delta E_Q \approx 4\kappa_0 \sqrt{\Omega_\pi - N_\pi}\, \sqrt{\Omega_\nu - N_\nu} \cdot N_\nu. \tag{1.4}$$

with κ_0 the normalised quadrupole strength, $\Omega = j + {}^1\!/_2$ the orbital degeneracy and N the number of valence pairs. Summing together the three contributions, the energy can be lowered by several MeV, as illustrated in figure 1.4. If the change in energy tends to overcome the shell gap, which may happen at midshell in medium and heavy mass

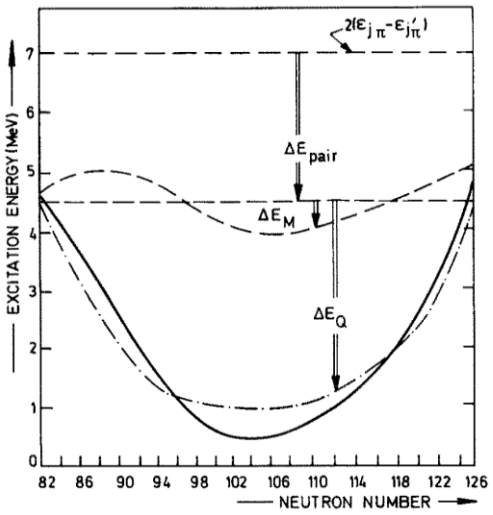

FIGURE 1.4: Contribution of a pairing force ΔE_{pair}, monopole ΔE_M and quadrupole ΔE_Q residual corrections to the excitation energy of a 0^+ intruder state in the lead isotopes. Taken from [Hey87]

regions, deformation sets in. Near shell closures instead, a competing shape called an intruder state can be found in the lower part of the level scheme and when its configuration is too different for much mixing to occur, the concept of shape coexistence is used [Hey83].[2] The delicate balance between monopole and quadrupole corrections was investigated in detail for 0^+ states in even-even zirconium, tin, gadolinium and lead.

As we hinted at earlier in our discussion on sodium and magnesium, instead of unravelling the nuclear interaction it is also plausible to probe the influence of the particle space. Indeed the prolate deformation that originally was framed in a Hartree-Fock scheme could also be understood in the shell model by extending the available set of states to the $\nu f_{7/2}$ level [Wat81, Sto83]. The spherical single-particle orbitals would move according to a similar formula as before, the energy ϵ_α of a state α being affected by the other full orbitals i through

$$\tilde{\epsilon}_\alpha = \epsilon_\alpha + \sum_i \langle \alpha i | V | \alpha i \rangle. \tag{1.5}$$

[2] Pondering upon the famous Hoyle state in ^{16}O, Haruhiko Morinaga already in 1956 advanced the idea that deformation appears at low energy in spherical isotopes [Mor56]. Ten years later the literature refers to the circumstance as nuclear coexistence [Bro66]

By combining Preedom-Wildenthal with Kuo-Brown matrix elements and allowing for excitations of neutrons across $N = 20$, the $\nu d_{3/2}$ and $\nu f_{7/2}$ orbitals become degenerate once sufficient neutrons pile up in the *sd* shell, the single-particle configurations mix into deformed states and the calculated ground-state masses are seen to agree much better with experiment. It offers an example of monopole migration in which neutrons act on neutrons but in which neither the overlap of the wave functions nor the relative spin orientation plays a clear role. As a matter of fact the $\nu f_{7/2}$ orbital dives for both $\nu d_{5/2}$ and $\nu d_{3/2}$ as it does for $\nu s_{1/2}$, while on the kin side $\pi d_{5/2}$, $\pi s_{1/2}$ and $\pi d_{3/2}$ are all attracted by all of the neutrons.

Building on this insight and limiting themselves to a one-liner abstract, Alfredo Poves and Joaquín Retamosa in Madrid were able some years later to reproduce the emergence of deformation and rotational structures at $N = 20$ in the even wider $\pi d_{5/2}\nu d_{3/2} f_{7/2} p_{3/2}$ model space [Pov87]. Chung-Wildenthal matrix elements were chosen for the *sd* segment and Kahana-Lee-Scott (KLS) ones for the *fp* part and the coupling of *sd* to *fp*, while the monopoles were modified by Eduardo Pasquini and Andrès Zuker in Strasbourg to improve the correspondence with local data. The *fp* configurations were shown to make their way into the *sd* shell, bringing about a rapid erosion of the $N = 20$ shell gap in neon, sodium, and magnesium. The paper concludes with an equally lapidary and vigorous statement that all the experimental data that were available at the time were reproduced in a consistent manner. Along the same lines also the β decay of ^{29}Na was ably interpreted, now adding a mass-dependent scaling factor to the universal *sd* interaction (USD) from Wildenthal [Bau87].

Nevertheless, it feels a bit abstruse that particle-hole neutron excitations alone would account for the deformation. The integration with the $T = 0$ proton-neutron interaction that we presented above was achieved back again at the American side of the Atlantic by Ernest Warburton, John Becker, and Alex Brown [War90]. Full *sdpf* shell-model calculations were now carried out, the dimensions of which ran up to 11000. With the Warburton-Becker-Millener-Brown (WBMB) interaction, which was assembled from the USD Hamiltonian by Wildenthal, an *fp* force by McGrory, and the Millener-Kurath potential to connect both, the ingredients that generate deformation in the region of neighbouring nuclei that is since known as the island of inversion were

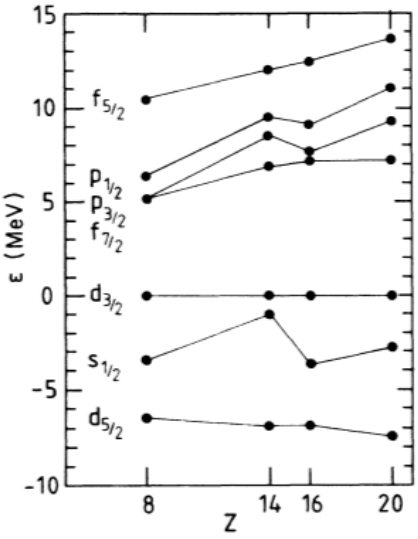

FIGURE 1.5: Neutron single-particle energies for the WBMB interaction. Taken from [War90]

described in depth. Plotted in figure 1.5, the $s_{1/2}$, $p_{3/2}$ and $p_{1/2}$ neutron single-particle energies show a curious attraction when protons huddle in $s_{1/2}$. Normalising instead to the $\nu s_{1/2}$ level, the $\nu f_{7/2}$ and $\nu f_{5/2}$ states evolve in a parallel fashion when first filling $\pi d_{5/2}$. After that, the $\nu f_{7/2}$ state bends off towards a tighter binding with $\pi d_{3/2}$, which however is not strong enough as to provoke the degeneracy of $\nu d_{3/2}$ and $\nu f_{7/2}$ that was suggested by Campi and his collaborators. Once neutrons are scattered across $N = 20$ they may share their presence between the nearby $\nu f_{7/2}$ and $\nu p_{3/2}$ states, for which indeed $\Delta\ell = 2$. The protons below $Z = 20$ develop collectivity as long as $\pi d_{5/2}$ and $\pi s_{1/2}$ are within reach of each other, in their turn enabling $\Delta\ell = 2$ correlations. This is the case for ^{30}Ne but no longer for ^{34}Si, thus marking the boundary of the island of inversion. Although the behaviour of the individual orbitals results from the best fit of the matrix elements, the numerical analysis that the authors perform reveals a deeper framework of neutron pairing and proton-neutron quadrupole interactions. Accordingly it links up with the interpretation that stands behind the low-lying 0^+ intruder states in tin and lead, thus referring to a common understanding of deformation throughout the nuclear chart.

The dissolution of the $N = 20$ magic number in the island of inversion, however, makes place for other lucky numbers. In extensive experimental work, several more new shell closures were observed. From mass measurements as well as nuclear spec-

troscopy, evidence was found for shell effects at 14 in ^{22}O [Thi00] and ^{34}Si [Bau89], 16 in ^{22}C [Pou86], ^{24}O [Oza00, Sta04], ^{36}S and ^{36}Ca [Doo07], 32 in ^{52}Ca [Wie13], and 34 in ^{54}Ca [Ste13].[3] Strides were also made on the theoretical side. The appearance of $Z = 14$ in ^{34}Si could be understood from the same Madrilene shell-model calculations that had before explained the disappearance of $N = 20$ [Bau89].

If one conjectures that in fact the distance between the $1d$ orbitals would widen, this would generate the new magic numbers at 14 and 16 at the cost of the one at 20. Elaborating on this and proposing that the same effect would act on the $1f$ and $2p$ pairs of states, such that it grows more pronounced for $1f$ than for $2p$, the gaps at 32 and 34 would be created. We sketch this point of view, centred on a spin-orbit force that is gaining in strength, in figure 1.6. The literature, nevertheless, is careful before it marks out a clear relation with the spin-orbit interaction. Indeed, a competing picture predicted that the nuclear potential far from stability would resemble a smooth and soft harmonic oscillator instead of the steeper Woods-Saxon shape [Dob94]. The feature was ascribed to an increased diffuseness of the neutron density, which in a relativistic mean-field (RMF) approximation of interacting Dirac nucleons is regulated by the isovector ρ meson. The slow derivative of the potential would naturally lead to a fading spin-orbit coupling and the resurgence of the harmonic magic numbers. The calculation relied on the widely used non-linear NL1 force [Rei86]. Elsewhere it was replaced with the NL-SH Lagrangian, which reproduced the neutron skin even better [Sha93].

Unfortunately neither the scheme of a stronger nor of a weaker spin-orbit interaction was really able to hold. For instance the positions of the proton $d_{5/2}$ and $d_{3/2}$ centroids in calcium revealed a curious behaviour, for which at first the spin-orbit force can be said to weaken before the trend suddenly inverts, as illustrated in figure 1.7 [Dol76]. Moreover it had already been noted by Bansal and French that the neutrons that fill the $f_{7/2}$ state do not interact with the $s_{1/2}$ protons as much as they do with the $d_{3/2}$ ones, pulling down the latter towards $\pi s_{1/2}$ [Ban64]. Taking both results together, for $Z = 14$ a new magic number appears but the evolution of the spin-orbit force seems at best erratic.

[3] The energy of the first excited state of ^{36}S was known since long but at the time it was not recognised as a sign of magicity [Oln71]

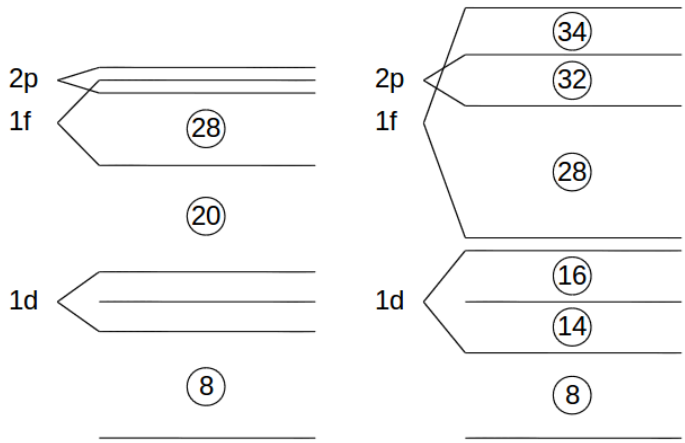

FIGURE 1.6: Evolution of shell-model orbitals if the spin-orbit interaction were to increase

1.2 Towards exotic nuclei

The magic number 28 possibly presents us with a more decisive case to arbitrate. For a strong spin-orbit interaction it would survive, while its disappearance would confirm the return to a harmonic oscillator. More RMF calculations, this time with the NL-SH formulation, confirmed deformation from silicium to calcium at $N = 28$ [Wer96]. This was comforted by the Coulomb excitation of the ^{40,42}S isotopes at $N = 24, 26$ performed at the National Superconducting Laboratory (NSCL) at East Lansing and corroborated by shell-model calculations that brought into play the USD Hamiltonian devised by Wildenthal in *sd* and an FPD6 force written by Richter for *fp*, with the cross-shell component taken from the WBMB set mentioned above [Sch96]. Also in ^{44}S squatting on $N = 28$ itself, deformation was acknowledged yet unlike its neighbours it would not be of a static but of a vibrational nature [Gla97].

A controversy developed as new shell-model calculations by Retamosa and collaborators, in which the *sd* shell was described by the USD interaction of Wildenthal, the *fp* one by a modified Kuo-Brown force KB', and the scattering between the shells according to the KLS transition elements introduced before, bore out the persistence of $N = 28$ [Ret97]. A brief report weighed in on the discussion to propose that the deformation in ^{44}S should be understood from the emergent proton magic number at $Z = 14$ and the related orbital degeneracy at $Z = 16$ that we discussed above, rather

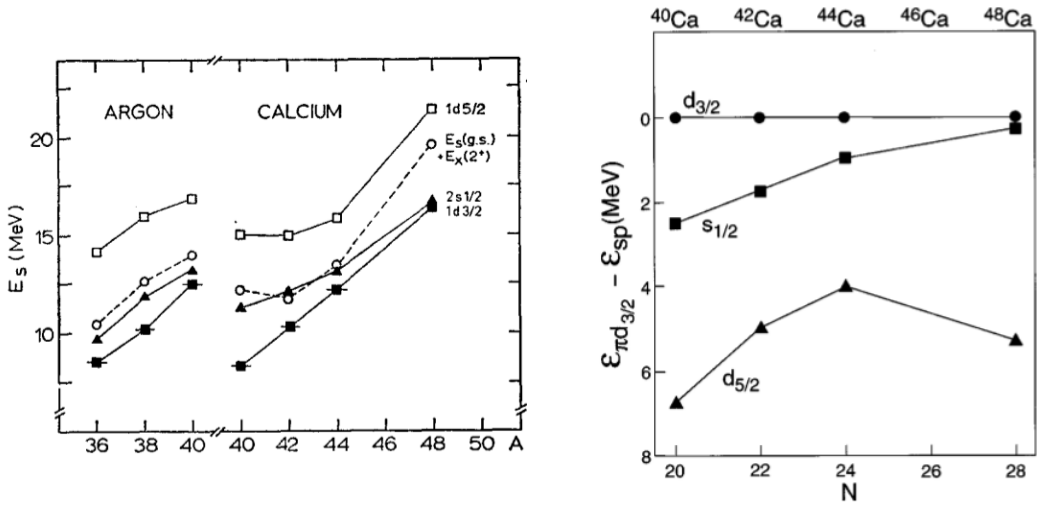

Figure 1.7: Proton single-particle energies in potassium isotopes defined as centroids of measured spectroscopic strength in Ca(d,τ)K pick-up reactions and plotted relative to the separation energy (left) and relative to the centroid of the $\pi d_{3/2}$ state (right). The left plot also contains values from Ar(d,τ)Cl, while the dashed line refers to the energy of a quadrupole phonon in the target. Taken from [Dol76] and [Cot98]

than any slipping of the $N = 28$ shell gap [Cot98].

For the ^{46}Ar nucleus at $N = 28$, a rather spherical shape had indeed been found in the experiment at NSCL [Sch96]. From the ^{46}Ar(d,p)^{47}Ar transfer reaction in inverse kinematics undertaken at the Grand Accélérateur National d'Ions Lourds (Ganil) at Caen a reduction in the spin-orbit splittings was established [Gau07]. Interestingly the variation in surface diffuseness, the main engine that drives the spin-orbit force, was deemed insufficient to explain the observation. Instead for the $\nu f_{7/2} f_{5/2}$ partner states the tensor force was called upon, which we referred to earlier but which was now singled out explicitly for a remarkable come-back [Ots05]. In short it postulated that after shedding the outer protons from the $d_{3/2}$ orbital, the residual proton-neutron force would slacken compared to the doubly magic reference at ^{48}Ca and release the $f_{7/2}$ neutrons upwards. The degeneracy of the $\pi s_{1/2}$ and $\pi d_{3/2}$ states portrayed in figure 1.7 would meanwhile deplete the former, creating a hole in the middle of the nucleus that would add a counteracting component to the $\nu p_{3/2} p_{1/2}$ separation [Tod04]. The combined effect would provoke a contraction of the $\nu f_{7/2} p_{3/2}$ shell gap that was quantified as 330(90) keV. With 4.47(9) MeV remaining, the closed character of the nucleus

would nonetheless not be compromised. Setting out from Retamosa's shell-model Hamiltonian, four specific matrix elements were adjusted to construct the SDPF-NR interaction for protons in the *sd* and neutrons in the *fp* orbitals [Num01]. Reproducing energies and spectroscopic factors, a narrowing of the gap by 362 keV was empirically computed with enticing comfort. Later on an excited 0_2^+ state was discovered at 2710 keV in ^{46}Ar and identified as a 2p-2h neutron structure by means of the same shell-model calculations [Dom03]. It was linked to the deformation in ^{44}S, where a 0_2^+ level was expected to come down in energy and strongly mix with the ground state.

While the magicity of $N = 28$ might linger in ^{46}Ar and yield to shape coexistence in ^{44}S, attention gathered on ^{42}Si. First of all Etienne Caurier at Strasbourg with collaborators revamped the SDPF-NR force, replacing the *fp* interaction KB' by the newer version KB3G that had been designed in Madrid [Cau04].[4] The corresponding SDPF-NR' result put the 2^+ state at 1.49 MeV without evidence for any particular deformation. Two experiments, however, arrived at opposite conclusions. At NSCL a small cross section for the two-proton knock-out reaction from ^{44}S into ^{42}Si was inferred from the low number of registered events, lending credibility to a local $Z = 14$ shell gap [Fri05]. Although the evidence was rather scant, a spherical shape was posited on grounds of the theoretical outcome of SDPF-NR. At Ganil a collapse of both $Z = 14$ and $N = 28$ was deduced from the γ spectroscopy of ^{41,43}P and ^{42}Si produced in secondary fragmentation [Bas07]. The low energy of 770(19) keV for the 2^+ state of ^{42}Si was explained from a compression of the proton and neutron orbitals once again due to the tensor force. More precisely, the full $f_{7/2}$ neutron orbital repels $\pi d_{5/2}$ and attracts $\pi d_{3/2}$, closing the distance between them and suppressing the proton gap. Peeling off the $d_{3/2}$ protons relieves the pull on $\nu f_{7/2}$ that exists in ^{48}Ca, restoring its propinquity to the *fp* shell. Because of the specific filling pattern in ^{42}Si, the tensor interaction is thus seen to counteract the spin-orbit splitting both for neutrons and protons. A lessened contribution from the spin-orbit force itself, however, cannot be excluded, as the latter equally depends on the nuclear density and thus it is affected by the filling and emptying of orbitals. The response of the tensor force moreover is not separated from that

[4] Whereas [Now09] asserts that SDPF-NR was defined in [Num01], which draws on KB' from [Pov81], close inspection reveals that [Bas07] cites to this purpose [Cau04], using KB3G from [Pov01]. Since [Num01] neither [Cau04] name their force, we shall designate the latter by SDPF-NR'

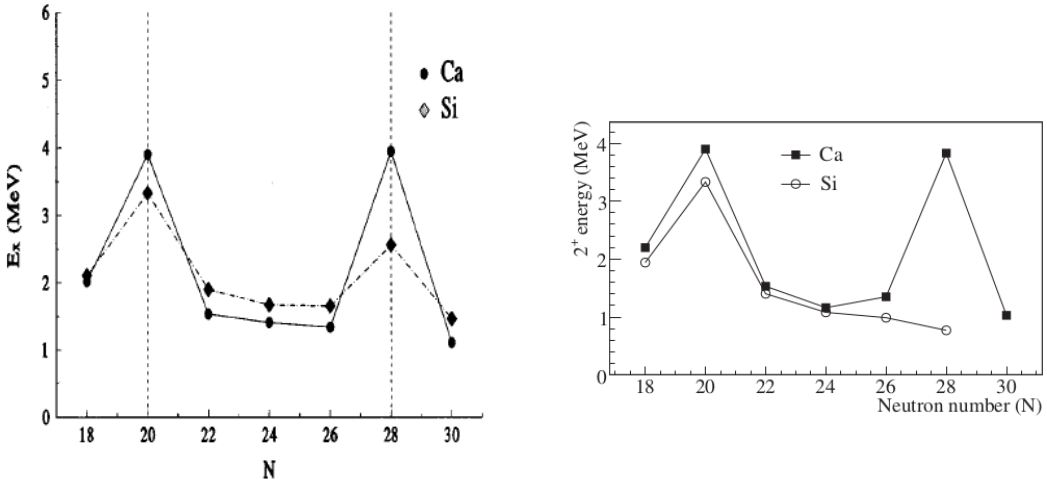

Figure 1.8: Evolution of 2_1^+ energies in calcium and silicon. The calculations are taken from [Ret97] (left), the experimental values from [Bas07] (right)

of particle-hole excitations that generate $\Delta j = 2$ quadrupole correlations. Unlike ^{46}Ar in which the shell gaps are too large to overcome, in ^{42}Si protons may jump from $d_{5/2}$ to $s_{1/2}$ and neutrons from $f_{7/2}$ to $p_{3/2}$, setting off collectivity through Elliott's SU(3) symmetry that we referred to above. In turn the matrix elements of the SDPF-NR' interaction could be tweaked till the calculation converged with the experiment, indicating ^{42}Si to spin as an oblate rotor with a quadrupole-deformation parameter β_2 close to -0.45.

If now $N = 28$ is seen to vanish in ^{42}Si, we can plot and compare the calculated and experimental energies of the first excited states in the calcium and silicon chains in figure 1.8. From these data it may seem strikingly evident that the tensor picture would prevail over the spin-orbit one, perhaps an insufficient but certainly a most meaningful facet of a complex and unfolding story. The image of ^{42}Si as a rotor has since been confirmed in proton knock-out reactions at the Radioactive Ion Beam Facility (RIBF) at Wakoshi outside Tokyo, adjusting the 2^+ excitation energy to 742(8) keV [Tak12].

Back in ^{44}S, the 0_2^+ microsecond isomer had meanwhile been discovered at Ganil at an excitation energy of 1365 keV [Gre05, For10]. Its decay rate was measured and interpreted as a proof of coexistence between the spherical configuration that it represents and a prolate ground state of $\beta_2 \approx 0.25$. A tensor force was not evoked but the deformation was understood from quadrupole correlations that again would

promote particles from $\pi d_{5/2}$ into $\pi s_{1/2}$ and from $\nu f_{7/2}$ into $\nu p_{3/2}$. The analysis was shouldered by shell-model calculations with the SDPF-U force, a delicately overhauled version of SDPF-NR by Frédéric Nowacki at Strasbourg and Alfredo Poves at Madrid [Now09]. Theoretically modulating the pairing contribution and empirically tuning the interaction parameters to separation energies and mass differences in the calcium isotopes, the 2^+ energy in ^{42}Si could be corrected from the earlier prediction of 1.49 to 0.82 MeV only.

From the evolving shapes that are apparent throughout the $N = 28$ isotones, apprehending the role of the spin-orbit interaction ultimately feels like reading tea leaves. Confusion only increases when we examine the ^{42}Al ($N = 29$) nucleus at the neutron drip-line [Bau07]. Observed in fragmentation of ^{48}Ca at NSCL, its existence was linked to the presence of an unpaired $d_{5/2}$ proton hole that would pull the $\nu p_{3/2}$ state enough down till it binds. A weakened spin-orbit splitting between the $\nu p_{3/2}$ and $\nu p_{1/2}$ orbitals was invoked to predict particle stability for the even heavier aluminium isotopes as it might bring $\nu p_{1/2}$ within reach, but this would eventually contradict the lowering of $\nu p_{3/2}$. In the ^{34}Si(d,p)^{35}Si transfer reaction at Ganil a decrease in the $\nu p_{3/2}p_{1/2}$ splitting was measured for ^{35}Si ($N = 21$) indeed [Bur14]. It was directly related to the removal of $d_{3/2}$ protons from ^{41}Ca and nicely reproduced both by the Michigan Three-Range Yukawa force from George Bertsch and colleagues and the KLS matrix elements inherent in the SDPF-U shell-model calculations, while the Next-to-Next-to-Next-to Leading Order chiral field theory (N^{3}LO) by David Entem and Ruprecht Machleidt from Idaho was called upon to hold the spin-orbit interaction fully responsible without any tensor contribution.

Because of the intrinsic spin dependence, it appears most difficult to disentangle tensor from spin-orbit effects and much as their fate far from stability is undecided at $N = 20$, likewise it remains obscure at $N = 28$. In view of this a decomposition of the nuclear force into its various contributions perhaps proves useful [Smi10]. Putting the knive into SDPF-U from $N = 8$ to $N = 20$, it exposes the role the central interaction plays in a steady ascent of the $\nu f_{5/2}$ orbital over several MeV of energy, counteracting the tensor component when filling the $\pi d_{5/2}$ state but reinforcing it when stuffing particles in $\pi d_{3/2}$. Likewise illustrated in figure 1.9, $\nu f_{7/2}$ would rise because of the central

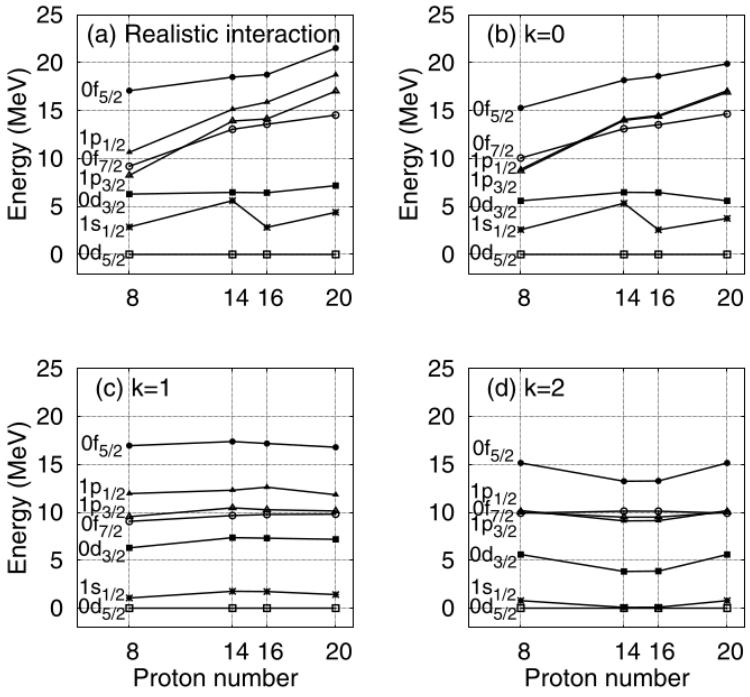

Figure 1.9: Single-particle energies for neutrons in the $N = 20$ isotones from oxygen to calcium with the SDPF-U interaction and decomposition in central ($k = 0$), vector ($k = 1$) and tensor components ($k = 2$). Taken from [Smi10]

interaction only, although the insensitivity of the tensor part is arguably due to the chosen normalisation to the position of $\nu d_{5/2}$, itself not free of correlations. For $\nu d_{3/2}$ the central force would curiously run against the tensor one. The vector interaction meanwhile remains flat but its importance would increase in heavier nuclei. A similar analysis for $Z = 20$ reveals a $\pi d_{5/2} d_{3/2}$ tensor attraction while packing particles into $\nu f_{7/2}$ from ^{40}Ca to ^{48}Ca. For cases where $\ell \neq \ell'$ the outcome is less clear. Instead of a single-parameter equation, we see a multifaceted picture coming to the fore in which one is faced with equivalent interpretations that may or may not involve the tensor force.

The renewed interest in the tensor force, however, was spurred by the work of the Tokyo group, who gauged it from a new angle and attached to an old concept a vivid and lucid image. We hark back to the turn of the century, when Takaharu Otsuka at Tokyo and colleagues introduced the technique of Quantum Monte-Carlo Diagonalisation to select relevant basis states for the Monte-Carlo shell model (MCSM) [Ots99].

Not to be confused with the Shell-Model Monte Carlo (SMMC) from Pasadena in which the Hamiltonian is decomposed into one-body operators [Joh92], the MCSM calculation restricts the diagonalisation to suitable subspaces of specific eigenstates to bring excited states within computational reach. Yutaka Utsuno also at Tokyo refined and expanded upon this scheme to gain insight in the role of intruder states in the formation of the island of inversion at $N = 20$ [Uts99]. The particles were allowed to roam in the *sd* shell and the $f_{7/2}$ and $p_{3/2}$ orbits around a ^{16}O core. The chosen SDPF interaction was composed of the USD, Kuo-Brown and Millener-Kurath forces for the *sd*, *fp* and cross-shell contributions respectively. Warburton's retuning of the $d_{3/2}f_{7/2}$ elements to better grasp the gap at the magic number 20 was included and a mass-dependent scaling factor was applied to all.

Recognising that the resulting calculations were to bind ^{26}O contrary to experiment, the authors proposed two adjustments to SDPF. Firstly, they intervened in the monopole terms. The algebraic decomposition of the interaction by Bansal and French that we referred to above had been generalised by Poves and Zuker, expressing how the single-particle energy of an orbit is modified by the occupation of all other valence orbitals [Pov81]. From the spin-averaged matrix element

$$V^T_{jj'} = \frac{\sum_J (2J+1)\langle jj'|V|jj'\rangle_{JT}}{\sum_J 2J+1} \tag{1.6}$$

one constructs the weighted sum and difference in isospin space

$$a_{jj'} = \frac{1}{4}(3V^1_{jj'} + V^0_{jj'}), \quad b_{jj'} = V^1_{jj'} - V^0_{jj'} \tag{1.7}$$

such that with the number operator n the interaction becomes

$$H^M_{jj'} = \sum_{i=j,j'} \left(\frac{a_{ii}}{2} n_i(n_i - 1) + \frac{b_{ii}}{2}(T_i^2 - \frac{3}{4}n_i) \right) + a_{jj'} n_j n_{j'} + b_{jj'} \boldsymbol{T}_j \cdot \boldsymbol{T}_{j'}. \tag{1.8}$$

For $V^1_{jj'} = V^0_{jj'} = V_{jj'}$ and $n_j = n_{j'} = 1$ the monopole term reduces to $H^M_{jj'} = V_{jj'}$, but for instance by adding one more particle to the j' state we readily find $H^M_{jj'} = V_{j'j'} + 2V_{jj'}$. If we set $n_j = 2$ and $n_{j'} = (2j_\nu + 1)\, v^2_{j_\nu}$, the recipe reproduces the monopole shift from Ghent that we presented before in equation 1.3. Through this formalism the $d_{5/2}d_{3/2}$ and $d_{5/2}f_{7/2}$ monopole elements were strengthened in an opposite manner in the isoscalar and the isovector channels, such that at stability the twist would cancel

out. A second mend to SDPF loosened the *sd* pairing interaction for $J = 0$ and $T = 1$ by 10%, such that the appearance of a magic number $N = 16$ in the exotic nucleus ^{24}O could finally be explained.

While deformation would hold together the subsequent neon isotopes up to $N = 24$, we recall that in stable ^{30}Si the $N = 20$ magic number stands firm instead. To spell out the transition and from a close investigation of the theoretical single-particle states that SDPF supplied, a strong attractive interaction between the $\pi d_{5/2}$ and $\nu d_{3/2}$ orbitals was proposed [Ots01a]. Removal of protons from $d_{5/2}$ along the $N = 16$ isotones from silicon to oxygen would relax this force and rise the energy of the $d_{3/2}$ neutrons, such the gap at $N = 20$ closes and a new one at $N = 16$ appears. The principle is illustrated in figure 1.10. The two-body interaction that steers the mechanism was rendered as a force that is invariant under rotations in the spin and isospin spaces,

$$V_{\sigma\tau} = \boldsymbol{\sigma}_1 \cdot \boldsymbol{\sigma}_2 \;\; \boldsymbol{\tau}_1 \cdot \boldsymbol{\tau}_2 \, f(r_{12}). \tag{1.9}$$

The inner products can be related to the Bartlett and Heisenberg exchange operators. By means of raising and lowering operators the expression is transformed as

$$\boldsymbol{\sigma}_1 \cdot \boldsymbol{\sigma}_2 = \frac{1}{2}(\sigma_{1+}\sigma_{2-} + \sigma_{1-}\sigma_{2+}) + \sigma_{10}\sigma_{20} \tag{1.10}$$

so indeed the vector operators cause spin and isospin to flip. The force will therefore link protons in $j_>$ and $j_<$ orbitals with neutrons in $j_<$ and $j_>$ states, respectively. To achieve the proper balance of the $T = 0$ and $T = 1$ contributions to the effect, the monopole components came under scrutiny. From the analytic formulae that were given, the strongest attraction was seen to arise between spin-flip partners in the isoscalar channel [Ots02]. The possibility of an additional tensor force was alluded to but not developed, although a pathway was put forward that links the spin-isospin terms to the action of the π and ρ mesons in the one-boson exchange potential. Interestingly and almost casually, a magic number was predicted at $N = 34$ from the upwards release of $\nu f_{5/2}$ induced by an empty $\pi f_{7/2}$ orbit in calcium, while erosion would slyly sap the gaps at $N = 82$ and $N = 126$.

In a successive pivotal paper, however, the spin-isospin force was unseated by the tensor interaction that was previously only hinted at [Ots05]. The concept drew its basic inspiration from the theory of meson exchange, following which the negative

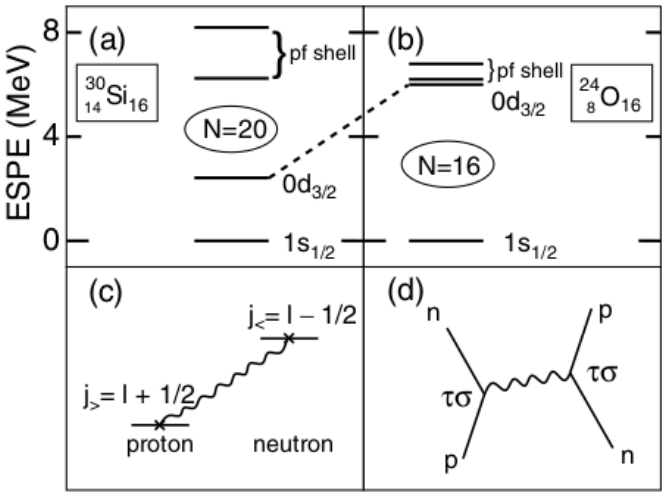

FIGURE 1.10: Single-particle energies for neutrons in ^{30}Si and ^{24}O with the SDPF interaction. The lower panels depict the interaction diagrammatically. Taken from [Ots01a]

intrinsic parity of the pion demands the particle be exchanged in a P wave that is not spherically symmetrical, hence the interaction becomes non-central and in particular spin dependent. For a ρ vector meson, the parity of which again is negative, a tensor component emerges in a more subtle manner when the P state is polarised perpendicularly to its motion. Abandoning the symmetry between spin and isospin, the adopted formalism therefore coupled the spins to a tensor of rank two so they match the spherical harmonics of second degree,

$$V_T = ([\boldsymbol{\sigma}_1 \times \boldsymbol{\sigma}_2]^{(2)} \cdot Y^{(2)})\,(\boldsymbol{\tau}_1 \cdot \boldsymbol{\tau}_2)\,f(r_{12}). \tag{1.11}$$

After some algebra the equation is shown to be equivalent to the more common expression 1.2 from Rarita and Schwinger that we presented above. With the reminder that $\boldsymbol{\sigma}_1 \cdot \boldsymbol{\sigma}_2 = 2S(S+1) - 3$, it is rapidly seen from the earlier formula that the force disappears for $S = 0$, so only if both intrinsic spins are parallel a tensor force crops up. When the orbital angular momenta of the two particles point in opposite directions, their relative momentum is high and the extent of their interaction well localised in space. On the other hand when they get in line, the relative wave function smears out along the course of motion. This was interpreted as a mutual attraction for the case of $j_< \leftrightarrow j'_>$ configurations and a repulsive response that is exerted by the $j_< \leftrightarrow j'_<$ and $j_> \leftrightarrow j'_>$ ones. The correlation being proportional to the radial overlap of the wave

functions, the purport of the monopole drift is most pronounced for $j \approx j'$.

The idea of a tensor interaction that is able to shift the single-particle levels was by no means new. Already early on Arnold Feingold had shown that the action of the tensor force in level splittings in ^{6,7}Li could be emulated by an intricate combination of central and spin-orbit forces [Fei56]. An attempt to separate out the tensor contribution in the $\pi p_{3/2} p_{1/2}$ spin-orbit splitting of ^{15}N was carried out some years after [Ter60]. A non-central interaction, comprising distinct spin-orbit and tensor parts, was called upon to model the position of the $\nu d_{5/2}$ level from ^{11}Be to ^{17}O [Mil75]. Quite explicitly, the tensor force was even invoked to explain how the narrowing and widening of the $\pi h_{11/2} h_{9/2}$ spin-orbit splitting swivels around at $N = 114$ in the gold and thallium isotopes as we described it above, but it fell off the radar perhaps because any clear relation with specific neutron orbitals could not be established [Goo78]. A concurrent theoretical paper nevertheless ventured into distinguishing the $2(2\ell + 1)$ spin-saturated shell closures, such as the magic numbers 20 and 40, from the spin-unsaturated ones, as 28 and 50 [Sch76]. The proton-neutron tensor component was held essential to create large proton spin-orbit splittings in ^{48}Ca and ^{90}Zr, since the spin-unsaturated $j_>$ neutrons would pull down $j'_>$ protons and push up $j'_<$ ones, which is rather opposite to the Tokyo way of thinking. In the region of ^{208}Pb relevant for gold and thallium, the presence of two spin-unsaturated levels, for protons as well as neutrons, rendered the underlying behaviour even harder to grasp.

The merit of the Tokyo group, however, resided in the systematic picture that was set up, focussing on the action of single-particle orbitals that stand in a peculiar relationship to each other and precluding an interpretation that would too quickly fall back on deformation or on the sole $T = 0$ proton-neutron interaction between spin-orbit partners discussed before. The attraction between the $\pi d_{5/2}$ and $\nu d_{3/2}$ orbitals at $N = 20$ could now seen as the expression of a wider scheme indeed. Removing $d_{5/2}$ protons from ^{30}Si relaxes the $d_{3/2}$ neutron orbital upwards and creates the $N = 16$ gap at the cost of $N = 20$ in ^{24}O [Sta04]. Working it out the other way and plugging a $d_{5/2}$ proton into ^{24}O would explain the existence of the fluorine isotopes beyond $N = 16$, as the extra particle allows them to bind additional $d_{3/2}$ neutrons unlike oxygen is able to. The occupancy of the $d_{5/2}$ proton orbital would still remain sufficiently low to keep

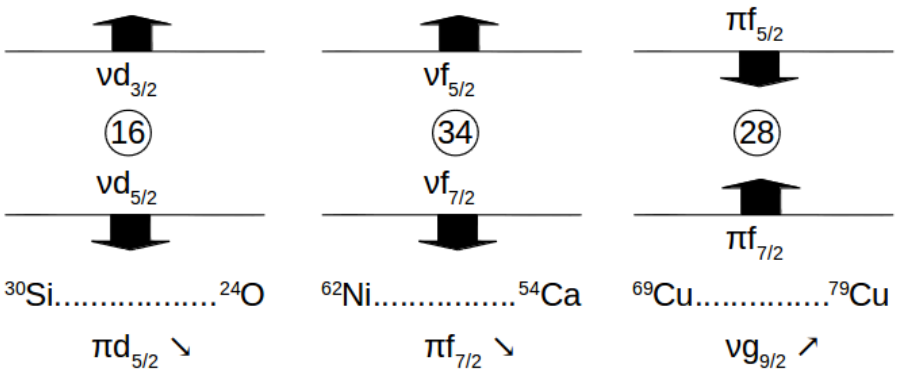

FIGURE 1.11: Evolution of the $N = 16$, $N = 34$ and $Z = 28$ shell-model gaps in the tensor paradigm when protons are removed from the $d_{5/2}$ and $f_{7/2}$ and neutrons added to the $g_{9/2}$ orbital, respectively

the $f_{7/2}$ neutron state down and allow the ^{31}F isotope to affirm its existence [Sak99]. Witnessing the occupancy of $\pi d_{5/2}$ swell further from ^{31}Na and ^{32}Mg to ^{34}Si and ^{36}S, the $\nu f_{7/2}$ state would finally be pushed out of the island of inversion and stand guard for a firm $N = 20$ shell gap at stability. Another example where the mechanism would come to the surface of the nuclear chart is given by the $N = 34$ gap in ^{54}Ca [Ste13]. The separation would open up when $f_{7/2}$ protons are skimmed off from ^{62}Ni, sending the $\nu f_{5/2}$ state upwards till it surpasses $\nu p_{1/2}$.

In spite of the demise of these magic strongholds, however, the concept of a shell model does not break down. The magicity would simply move elsewhere: 20 sees its place taken by a fierce duel between 14 and 16, 28 by a unsettled striving of 32 and 34. Of particular interest to the present work, the question stands stark as to what would happen to the next magic crossroad of $Z = 28$ and $N = 50$ at ^{78}Ni. As a matter of fact, in the neutron-rich copper isotopes beyond ^{69}Cu ($N = 40$) the $g_{9/2}$ neutron orbital is filled in triggering the $f_{5/2}$ proton state to dive down. If the tensor force will truly act in an opposite manner on the $\pi f_{7/2}$ orbital, the spin-orbit force would vanish and it would neatly close the $Z = 28$ shell gap in ^{79}Cu, as figure 1.11 may convince one of. This tantalising prospect may stir up fascinating expectations and we shall duly elaborate upon them in the following chapters. But to raise our story we first would like to invite the reader to a guided tour of the experimental copper scene.

Chapter 2

Experimental overview

In the present chapter we wish to report on the current status of our experimental knowledge of the neutron-rich copper isotopes. The ground state and the various low-spin levels first draw our attention. The relation between single-particle structure and collectivity will incite us to discuss shape coexistence. The odd-odd isotopes present a picture that is more compounded. We devote space and time to the impressive jump forward along $Z = 28$ towards exoticity that has been achieved in the last decade. We shall also comment on the standing of the other magic number in this region, $N = 50$, before combining all pieces in a description of ^{78}Ni.

2.1 The ground-state inversion in neutron-rich copper

According to the shell model, the ground-state of the neutron-rich copper isotopes ($Z = 29$) is provided by the $\pi p_{3/2}$ single-particle configuration. The easiest proton excitation is obtained by lifting the odd particle to the $\pi f_{5/2}$ orbital. It is this simple picture that was drawn upon when the β decay of the nickel isotopes beyond $N = 40$ was studied at Lisol, the on-line mass separator run by the university of Louvain at its site of Louvain-la-Neuve [Fra98]. A proton beam of 30 MeV of energy induced fission in two thin foils of uranium, which were suspended in a gas cell filled with argon. The reaction fragments were stopped and neutralised by collisions in the gas and channelled by its flow into the path of two lasers, the wavelengths of which were chosen to resonantly ionise the nickel mother nuclei. These were separated by mass in a magnetic field

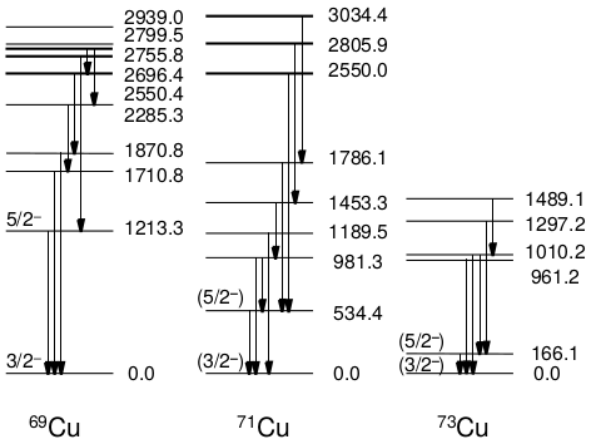

FIGURE 2.1: Simplified level schemes of ^{69,71,73}Cu after β decay. Taken from [Fra98]

and transported to a $\beta\gamma$ detection set-up of simple plastic scintillators and high-purity germanium crystals. The obtained level schemes are plotted in figure 2.1, in which ^{69}Cu served as a reference with respect to the existing literature [Run85, Bos88]. From the log ft values that were deduced it was inferred that the first excited state carries a spin and parity of $5/2^-$, its energy dashing down the hill. Whereas the $5/2^-$ level hovers at about 1 MeV in the lighter isotopes, it stalled at 534 keV in ^{71}Cu and tumbled to 166 keV in ^{73}Cu. An interpretation was advanced that traced the phenomenon to monopole migration, linked to the filling of the high-spin $\nu g_{9/2}$ orbital beyond $N = 40$.

In spite of the scarce incidence of distinct features close to magic numbers that flout anticipation, it took a decade before the copper isotopes were picked up for earnest study at Isolde at Geneva. Counting among the frontier laboratories in Europe with a long operational history and an exceptional experience, here we relate those endeavours in which a proton beam at 1.4 GeV of energy hit a thick target of uranium carbide, which was kept at a temperature of about 2000 °C. The thermal conditions favoured the rapid diffusion of the fission products out of the material towards a transfer tube, in which they were met with two laser beams that in this case resonantly ionised the copper atoms. After magnetic mass separation, the beam was sent to one of the many spectroscopy stations Isolde can boast of.

Nuclear orientation of an implanted sample of ^{71}Cu was thus achieved in a dilution refrigerator at temperatures down to 11 mK [Sto08]. By detecting the asymmetry of the β emission a low magnetic dipole moment was measured for its ground state, which

was partly imputed to the monopole action of the $g_{9/2}$ neutrons. A shell-model analysis with the GXPF1 Hamiltonian in the *fp* shell, drafted by Takaharu Otsuka at Tokyo and Michio Honma at Fukushima with colleagues as a follow-up to the SDPF force in the lighter nuclei [Ots01b, Hon02], was supplemented by a calculation in which the $f_{7/2}$ orbital was replaced by $g_{9/2}$ [Hon06]. Although the neutrons could freely stray in the latter, a mismatch with the experimental value persisted that prodded the need for equally embracing the proton excitations of the GXPF1 space.

Pressing towards the heavier isotopes, it appeared altogether within expectation that an inversion of the ground-state spin would take place near ^{75}Cu. The challenge did not fail to be taken up and was finally lifted in collinear laser spectroscopy also at Isolde [Fla09]. To understand how the spin is extracted in the measurement, we recall that the nuclear spin $\boldsymbol{I}$ couples to the atomic spin $\boldsymbol{J}$, which is expressed by introducing the quantum number $\boldsymbol{F} = \boldsymbol{I} + \boldsymbol{J}$. A hyperfine splitting of the atomic levels comes about for the various values of $\boldsymbol{F}$. The energies of the hyperfine components E_F are determined by two parameters A and B [Cas63],

$$E_F = \frac{K}{2}A + \frac{\frac{3}{4}K(K+1) - I(I+1)J(J+1)}{2I(2I-1)J(2J-1)}B \tag{2.1}$$

where

$$K = F(F+1) - I(I+1) - J(J+1) \tag{2.2}$$

and the hyperfine parameters are written as

$$\begin{aligned} A &= \frac{\mu B_e(0)}{IJ} \\ B &= eQ\frac{\partial^2 V_e}{\partial z^2}. \end{aligned} \tag{2.3}$$

The A parameter is proportional to the interaction between the magnetic dipole moment of the nucleus μ and the magnetic field that is provoked by the electrons at the centre of the nucleus $B_e(0)$. The B parameter describes the force that acts between the spectroscopic electric quadrupole moment of the nucleus Q and the electric field gradient that is generated by the electrons $\partial^2 V_e/\partial z^2$. Second-order effects such as the mixing of states with identical F are neglected. In the Collaps experiment that we discuss here, a shortened anagram for Collinear Laser Spectroscopy, the velocity of the arriving ion beam is tuned with an external voltage. The ions are neutralised and

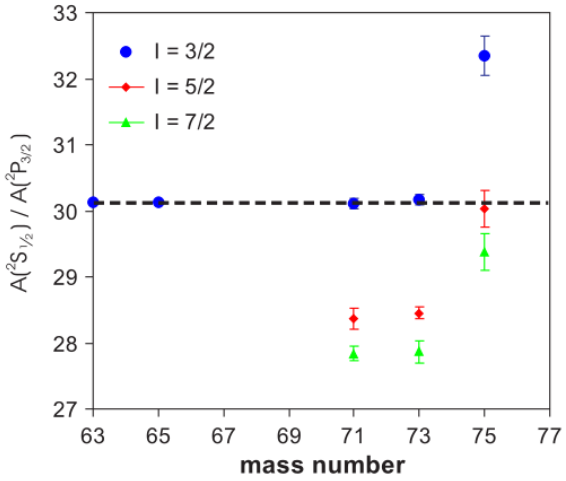

FIGURE 2.2: Ratio of atomic A factors for the ground and excited state in ^{71,73,75}Cu. Taken from [Fla09]

overlapped with laser light, for which a wavelength may be chosen that is different from the ionisation in the source in order to optimise the sensitivity to the spin and the electromagnetic moments of the nucleus rather than the production rate. If a resonance between the velocity of the ions and the wavelength of the laser is achieved the atoms absorb a quantum and decay shortly afterwards by emitting fluorescence photons, the intensity of which is recorded against the applied voltage.

Specifically the $4s\ ^2S_{1/2} \rightarrow 4p\ ^2P^o_{3/2}$ transition at 324.8 nm (30783.69 cm^{-1}) was selected to lift the copper isotopes out of their atomic ground state.[1] The A factors of the ground and excited state that are extracted from the fit of the hyperfine spectra depend on the choice of the nuclear spin I that is adopted. Shoving aside the hyperfine anomaly related to isotopic variations of the magnetic field as typically it is not larger than 10^4, the ratio of these two parameters nevertheless has to be constant throughout the isotopic chain. Assuming different possibilities for the value of I in ^{75}Cu, one found that only $I = 5/2$ fulfilled this condition and matched the known ratio of the lighter isotopes, as exposed in figure 2.2.

The magnetic dipole and electric quadrupole moments were comprehensively discussed in a subsequent paper [Vin10]. Shell-model calculations were carried out with the widely used jj44b and JUN45 forces, two realistic G-matrix interactions that were

[1] We give the wavelengths in air, the wave numbers in vacuum

steeped in the Bonn potential. The former of the two was developed by Alexander Lisetskiy and colleagues in Michigan and Darmstadt and evolved from the NR78 and jj44pna codes that we shall come across in sections 2.4 and 2.5 [Lis04]. The latter issued from the work by Honma at Fukushima with his collaborators, who previously had produced the SDPF and GXPF1 forces that occurred before in our text [Hon09]. Focussing on a ^{56}Ni core with $f_{5/2}pg_{9/2}$ valence orbitals wrapped around, both Hamiltonians were defined by parameters fitted to the local environment and therefore they were deemed appropriate to reflect the semi-magic nature of the $N = 40$ subshell gap. The measured magnetic moment of ^{75}Cu nicely agreed with the expectation for a $5/2^-$ state, whereas the deviating value for ^{73}Cu was not fully understood and was ascribed to the mixing of additional proton excitations into the wave function. The quadrupole moments were skillfully captured by the models, for which otherwise no particular increase in the collectivity beyond $N = 40$ was noticed. The analysis of the charge radii was published a number of years later and equally betrayed a subshell gap that only showed slim influence [Bis16].

Still at Isolde, the β decay of ^{77}Cu into ^{77}Zn was meanwhile scrutinised [Pat09]. By combining the pieces of information that the β-delayed neutron channel populates the 2^+ and 4^+ states in ^{76}Zn while the $\beta\gamma$ decay feeds levels that end up in more or less equal proportions on the presumedly $1/2^-$ isomeric state and $7/2^+$ ground state of ^{77}Zn, a $5/2^-$ assignment was favoured for the ground state of the copper isotope. The same conclusion was reached in a similar experiment at the Holifield separator at Oak Ridge soon after [Ily09]. For ^{79}Cu as well the Oak Ridge group suggested a $5/2^-$ ground state from the observation of a strong βn branch to the 2^+ excited level in ^{78}Zn [Win08].

Back again at Isolde, laser spectroscopy was carried out on ^{75,77}Cu directly in the ion source [Koe11]. Since in resonant laser ionisation for every chemical element the atomic transitions within the electron shells are distinct in energy, by tuning the wavelength of the laser that is irradiating the atom one can selectively excite and remove an electron from one element while another remains untouched. If now the bandwidth of the laser is sufficiently narrow, one becomes sensitive to the hyperfine interaction between the nuclear spin and the electron spin, which splits the atomic levels in a different manner for isotopes and isomers with different spin values. While the technique

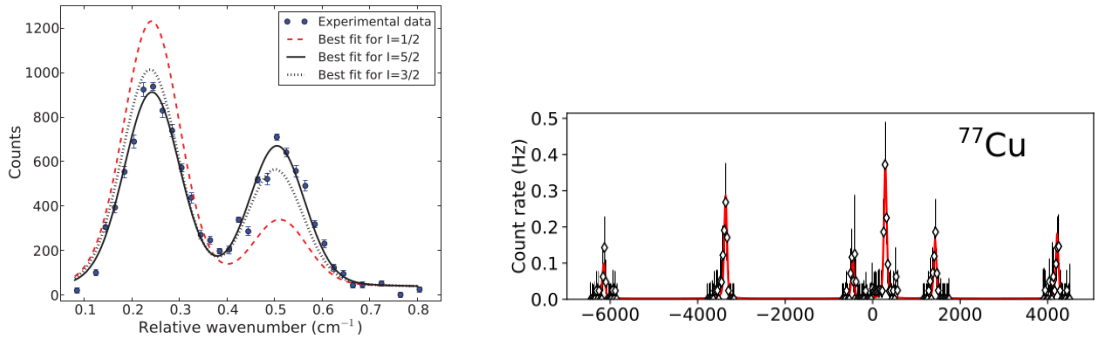

FIGURE 2.3: Hyperfine spectra for ^{77}Cu from intrasource laser spectroscopy relative to 30535.0 cm^{-1} (left) and collinear laser spectroscopy relative to the centroid frequency in MHz (right). Taken from [Koe11] and [DeG17]

in its early days suffered from an inferior resolution than what is routinely obtained in conventional collinear laser spectroscopy, being of the order of a sloppy 3.8 GHz compared to a sharp 75 MHz FWHM, it can operate at count rates as low as one atom per second. For the most exotic copper isotopes, intrasource spectroscopy therefore holds a competitive advantage.

The $4s\,^2S_{1/2} \rightarrow 4p\,^2P^o_{1/2}$ transition at 327.4 nm (30535.30 cm^{-1}) was now probed, followed by an excitation of 287.9 nm (34724.8 cm^{-1}) to the $3d^9 4s5s\,^2D_{3/2}$ auto-ionising state. Both for ^{75}Cu and ^{77}Cu a ground-state spin of 5/2 was deduced from the hyperfine spectra, an example of which we draw in the left panel of figure 2.3. Also for this measurement the magnetic moments were extracted, brought together with the values for the lighter isotopes in figure 2.4. Once again they fitted well with calculations by means of the jj44b and JUN45 interactions for a wave function that centred on the $\pi f_{5/2}$ single-particle state. The jump in the magnetic moment by 59% from ^{75}Cu to ^{77}Cu would point to the presence of particle-hole excitations across $Z = 28$, which the theoretical model spaces were not able to account for and not incidentally would be induced by the $g_{9/2}$ neutrons pushing the $f_{7/2}$ protons out of their orbits. It would provide an early signal of a possible reduction of the $Z = 28$ shell gap.

Six years later, the exotic copper isotopes finally came within reach of high-resolution collinear laser spectroscopy [DeG17]. With the Collinear Resonance Ionisation Spectroscopy (Cris) set-up at Isolde the hyperfine structure was investigated in the $4s^2S_{1/2} \rightarrow 3d^9 4s4p^4P^o_{3/2}$ electronic excitation at 249.2 nm (40114.01 cm^{-1}). A second

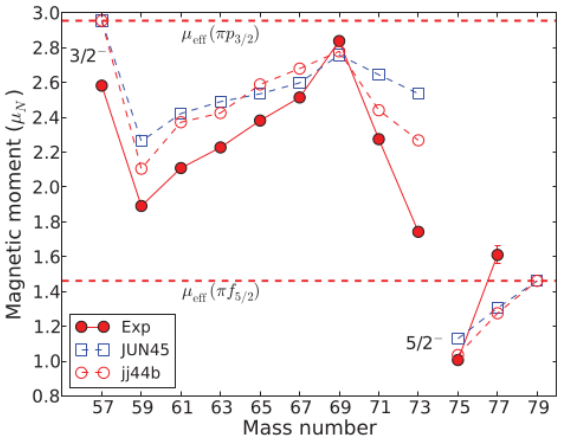

FIGURE 2.4: Magnetic moments of neutron-rich copper isotopes compared to calculations with the jj44b and JUN45 interactions. Taken from [Koe11]

laser at 314.2 nm (31813.27 cm^{-1}) to the $3d^9 4s4d\,^4P_{3/2}$ auto-ionising state was added, so unlike for Collaps the resonantly ionised particles could be detected directly. In due manner the spin and magnetic moment of ^{77}Cu were confirmed, the spectrum for which we present in the right panel of figure 2.3. Although the laser scheme was different and the hyperfine splitting cannot be compared directly with the one from the intrasource measurement, the resolution which with the peaks parade themselves is illustrative. In the spectrum on the left the axis spans 0.7 cm^{-1}, which swept over the second harmonic corresponds to a scanning range of 10.5 GHz in the first harmonic and matches the 10 GHz that are covered in the spectrum on the right. While the supporting shell-model calculations of the newer experiment rather stressed the survival of magicity, we may positively conclude that consensus exists today on the change of ground-state spin from $3/2^-$ to $5/2^-$ in the neutron-rich copper isotopes beyond $N = 44$.

2.2 The $5/2^-$ level

The sudden duck in energy of the first $5/2^-$ level in the copper isotopes prompts the question for more information on its nature. Since one-particle transfer experiments, in as far as the energy is chosen correctly, take place at the nuclear surface, they selectively populate or depopulate a single-particle state near the Fermi level. They allow to measure the extent to which the given configuration is present in the initial and fi-

	E_x (MeV)	J^π	(τ,d) [Bla65]	(τ,d) [Smi68]	(τ,d) [Bri76]	(τ,d) [Sch13]	(α,t) [Arm67]	(α,t) [Rou70]
^{63}Cu	0.962	$5/2^-$	1.98	1.76	1.92	1.94	2.40	–
^{65}Cu	1.116	$5/2^-$	1.56	–	1.14	1.49	2.28	1.95

TABLE 2.1: Spectroscopic factors for the first $5/2^-$ level in stripping reactions on nickel targets. The C^2S values as listed by [Bla65, Arm67] were multiplied by $2j+1$ with j the transferred angular momentum, while [Smi68, Bri76, Sch13, Rou70] quote as such $(2j+1)\,C^2S$

nal states of the nucleus by probing the single-particle content of the wave functions. In tables 2.1 and 2.2 we collect the stripping and pick-up reactions that lead to the neutron-rich ^{63,65,67,69}Cu isotopes. The nomenclature is defined as by convention with respect to the light particle.[2] The spectroscopic factor C^2S is here understood as the ratio of the experimental cross section to that obtained from a theoretical calculation, such as the Distorted-Wave Born Approximation (DWBA). It can be shown that S is essentially the overlap factor of the wave functions of the heavy constituents in the ingoing and outgoing channels of the reaction, while the Clebsch-Gordan coefficient C takes into account isospin. Although multiple definitions abound, C^2S should range from 0 to $2j+1$, with j the total angular momentum that is transferred.

The figures from stripping show the ease with which one can drop a particle in the $\pi f_{5/2}$ orbital, for which in an extreme shell model six empty places are available [Bla65, Smi68, Bri76, Sch13, Arm67, Rou70]. While the level carries about 30% of the strength, the spectroscopic factor is stronger still for the second $5/2^-$ state at 1412 keV in ^{63}Cu and 1623 keV in ^{65}Cu. The spectroscopic factors appear larger in (α,t) than in (τ,d), but this may dwell in the difficulty to model accurately the reaction mechanism in the early calculations.

Among these results we spend a bit more time on the systematic study that was undertaken with the split-pole spectrometer at the university of Yale and in which the single-particle centroids were extracted from the (τ,d) and (α,t) reactions on ^{58,60,62,64}Ni targets at 18 MeV and 38 MeV of beam energy, respectively [Sch13]. In figure 2.5 we

[2] Reviving an old practice, we denote the ^{3}He particle with τ

	E_x (MeV)	J^π	(d,τ) [Zei78]	(d,τ) [Han79]	(d,τ) [See91]	($\vec{\text{d}}$,τ) [Mai93]	(t,α) [Bac67]	($\vec{\text{t}}$, α) [Ajz81]
^{63}Cu	0.962	$5/2^-$	0.50	0.7	0.50	–	0.92	–
^{65}Cu	1.116	$5/2^-$	0.55	–	–	0.30	0.66	–
^{67}Cu	1.115	$5/2^-$	0.3	–	–	–	–	–
^{69}Cu	1.214	$5/2^-$	1.5	–	–	–	–	1.2

Table 2.2: Spectroscopic factors for the first $5/2^-$ level in pick-up reactions on zinc targets. In [Bac67] values for S are given but we assume C^2S is meant, while [Zei78, Han79, See91, Mai93, Ajz81] print C^2S

plot the spectroscopic factors in ^{63,65}Cu, from which the splitting of the $\pi f_{5/2}$ strength becomes clear immediately. It is noteworthy that also the transfer component with upper isospin was taken into account, to which end normalisation factors of 0.635 and 0.513 were applied to the $\ell = 1$ and $\ell = 3$ channels of the (τ,d) reaction. They are compared to the shell-model result from the GXPF1A G-matrix interaction, of which GXPF1 introduced above presents the precursor [Hon05]. Residing in the fp space and including the $f_{7/2}$ orbital, it bears witness to a qualitative understanding that is perhaps even more plausible than it is for its younger brother JUN45, also hailing from the Fukushima family of forces but with the $f_{5/2}pg_{9/2}$ set as active states. In figure 2.6 the centroids of the available single-particle orbitals are shown for the component of lower isospin, remarkably revealing how a distance develops between $\pi f_{5/2}$ and $\pi p_{3/2}$ after $N = 34$. While again the data draw better support from GXPF1A than from JUN45, the feature in fact translates into a gradually larger transfer strength to the $5/2^-_2$ rather than the $5/2^-_1$ state.

An interesting feature pops up in the (d,τ) and (t,α) pick-up reactions. The spectroscopic factors of the ground and excited states were measured by putting to use deuteron beams of 23.3 MeV at Argonne [Zei78] and 55 MeV at Groningen [Han79], and a triton beam of 13 MeV at Aldermaston [Bac67]. While one would not expect to touch upon much strength for the $\pi f_{5/2}$ particle state since it should essentially be unoccupied in the lighter isotopes, the obtained values of 0.3 to 0.92 in ^{63,65,67}Cu in-

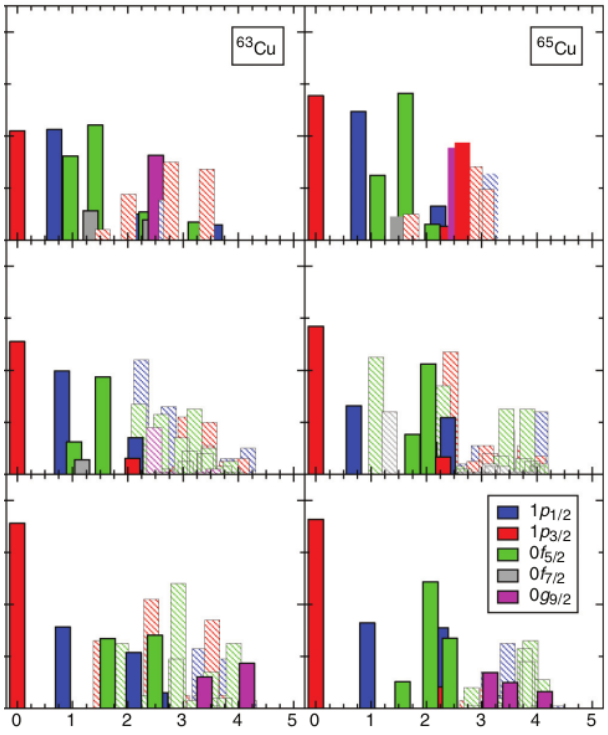

FIGURE 2.5: Spectroscopic strengths into ^{63,65}Cu obtained from (τ,d) for $\ell = 1, 3$ and (α,t) for $\ell = 4$ (top) compared to GXPF1A (middle) and JUN45 (bottom panels) shell-model calculations. The values are normalised such that an exhausted strength function would equal unity. Smaller fragments are multiplied by a factor of 10 and hatched. Taken from [Sch13]

dicate the presence of a certain amount of correlations stemming from this orbital in the ground states of the zinc nuclei. In ^{69}Cu a surprisingly large spectroscopic factor of 1.5 was found for the level at 1.214 MeV. Puzzled by the result and noting that the transfer reaction allows only to determine the orbital angular momentum ℓ rather than the total spin j, the article drew in the possibility of a $5/2^-$, $7/2^-$ doublet to explain the large value.

A subsequent transfer experiment took advantage of a polarised triton beam of 17 MeV at Los Alamos [Ajz81]. In this ^{70}Zn($\vec{t}, \alpha$)^{69}Cu reaction, the difference in cross section for angles to the left and to the right of the incoming beam was exploited to distinguish between $j = \ell - 1/2$ and $j = \ell + 1/2$ configurations. Indeed, assuming that the polarisation of the beam is directed upwards with respect to the plane that is spanned by the incoming and outgoing light particles and considering outgoing events to the left-hand side of the incoming beam, the angular momentum of the spinless α particle

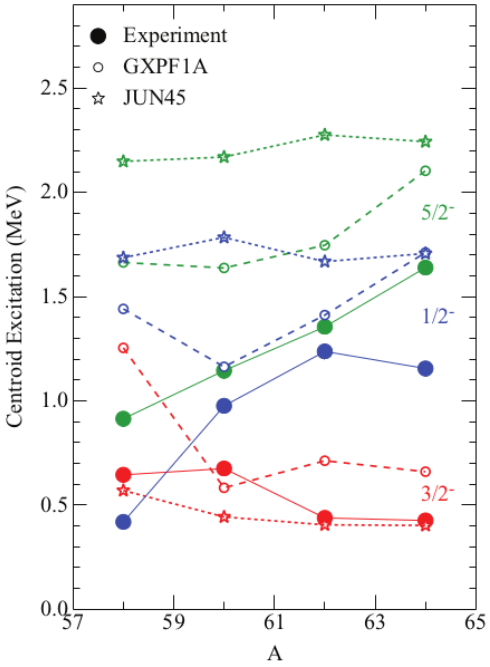

Figure 2.6: Energy centroids for the first three available proton single-particle orbitals in (τ,d) and (α,t) reactions on ^{58,60,62,64}Ni and corresponding GXPF1A and JUN45 shell-model calculations. Taken from [Sch13]

is pointing downwards, while the spin of the triton is most likely transferred to the nucleus in a parallel manner. As a result, the necessarily upwards angular momentum within the nucleus couples to the upwards intrinsic spin left by the triton to form an $\ell + 1/2$ state. With a lower probability, the triton spin is transferred in an antiparallel fashion and an $\ell - 1/2$ state is created. The analysing power $\boldsymbol{A}$ is then introduced as

$$\frac{d\sigma}{d\Omega} = \frac{d\sigma}{d\Omega}\bigg|_{P=0}\left(1 + \frac{3j_a}{j_a+1}\boldsymbol{P}\cdot\boldsymbol{A}\right) \tag{2.4}$$

with j_a the spin of the incoming light particle (m_a its magnetic quantum number) and $\boldsymbol{P}$ the polarisation vector oriented along an axis y such that $P_y = \langle m_a/j_a\rangle$ [Sat83]. With this definition we can now describe an overshoot of cross section to the left and a shortage of it to the right by choosing the sign of $\boldsymbol{A}$ to be positive for scattering to the left and negative for scattering to the right. One finds that the analysing power is related to the left-right asymmetry by

$$A_y = \frac{1}{P_y}\frac{j_a+1}{3j_a}\frac{(d\sigma/d\Omega)_L - (d\sigma/d\Omega)_R}{(d\sigma/d\Omega)_L + (d\sigma/d\Omega)_R}. \tag{2.5}$$

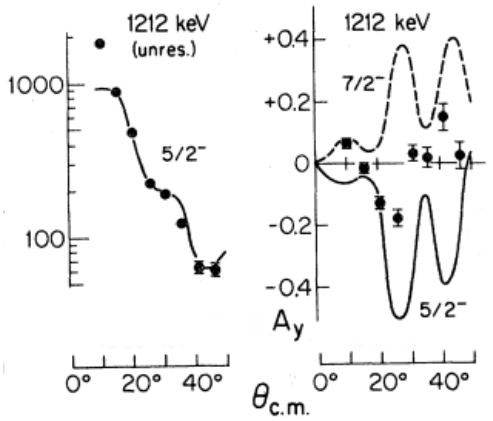

FIGURE 2.7: Angular distribution (left) and analysing power (right) for the level at 1212 keV in ^{70}Zn($\vec{t}, \alpha$)^{69}Cu. Taken from [Ajz81]

An average polarisation of $P_y = 0.73$ was attained in the experiment. The analysing powers for the ground state and the first excited state matched spin and parity values of $3/2^-$ and $1/2^-$, respectively. The asymmetry of the next level, here seen at 1212 keV, was not convincingly met by either a $5/2^-$ or a $7/2^-$ assumption and once again the hypothesis of a doublet was advanced. Upon examining in detail the data in figure 2.7, however, one may possibly dismiss the point at 10°, which unlike the measurements at other angles poorly coincides with the calculated angular distribution, and the one at 40°, for which the cross section and hence the statistics are low. The observed behaviour would in that instance rather agree with a $5/2^-$ signature. From high-resolution $\beta\gamma$ spectroscopy moreover, no indication for a doublet is apparent [Fra01]. Without it, the spectroscopic factor of $C^2S = 1.2$ for the 1212-keV level exposes a fairly large amount of $\pi f_{5/2}$ correlations in the ground state of ^{70}Zn.

The use of analysing powers to remove the ambiguity as to the total spin was again put to practise with a 52-MeV beam of polarised deuterons at Karlsruhe [Mai93]. Taking into account both stripping and pick-up and requiring that the summed spectroscopic strengths in both reactions be equal to the number of particles the orbital can hold, it was seen that the results for ^{65}Cu were to be renormalised by a factor of 0.70. The authors of an earlier related publication with unpolarised deuterons of 52 MeV to access ^{63}Cu at Jülich also had remedied the outcome of their measurement by normalising the strength function by truly 0.47 [See91]. We add that both experiments

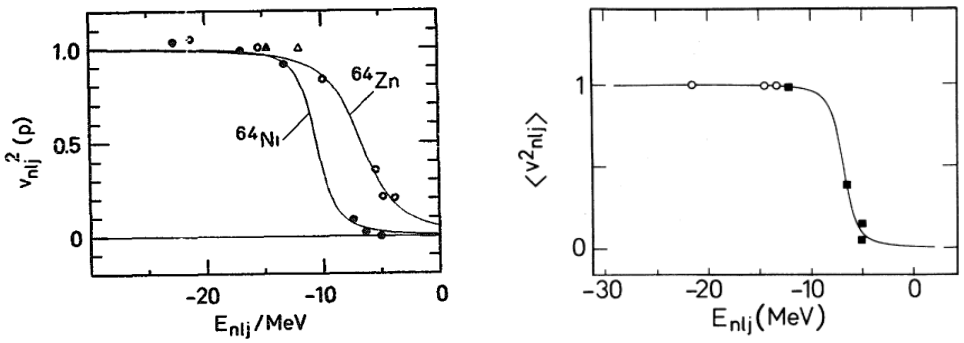

FIGURE 2.8: Fermi surface in ^{64}Ni (open) and ^{64}Zn (full symbols) (left) and ^{66}Zn (right) as derived from transfer reactions. The plots show the occupation probabilities of the $\pi d_{5/2}$, $d_{3/2}$, $s_{1/2}$, $f_{7/2}$, $p_{3/2}$, $p_{1/2}$ and $f_{5/2}$ orbitals as a function of their single-particle energy. Taken from [See91] and [Mai93]

yielded an interesting picture of the Fermi surface that we reproduce in figure 2.8 and that shows how after the renormalisation the occupancy of the $\pi f_{5/2}$ state remains consistent with what one expects. Incidentally it also illustrates how the proton wave functions start extending outwards as one draws away from the closed shell at $Z = 28$.

Besides the transfer work, we may glean information from the advent of a post-accelerated beam of ^{67,69,71,73}Cu at Isolde [Ste08]. After extraction from the ion source, the particles were bunched, charge bred and with an energy of 2.99 MeV per nucleon directed onto foils of ^{104}Pd and ^{120}Sn, in which Coulomb excitation occurred. Taking advantage of the Miniball γ array of eight cluster detectors assembled from three sixfold-segmented germanium crystals each and which surrounded the target in close geometry, the collected spectra revealed that in ^{67}Cu the $B(E2, 5/2^- \rightarrow 3/2^-)$ strength down to the ground state stood at 12.5(10) Weisskopf units while it tumbled down to values of 3.0(3), 3.9(5) and 4.4(5) in ^{69,71,73}Cu, respectively.[3] For easy reference in our discussion we summarise these and other numbers in table 2.3. The weak population of the $5/2^-$ level from $N = 40$ onwards pointed to a vanishing collectivity and was obviously related to the noted decrease in energy. Reaching beyond the transfer experiments for ^{67,69}Cu, it provided the first proof for the predominant single-particle

[3] For transitions with an initial spin J_i a spin factor $\frac{1}{2J_i+1}$ is to be taken care of, so for instance the value of $B(E2, 5/2^- \rightarrow 3/2^-)$ will be smaller by $^2/_3$ than the one for $B(E2, 3/2^- \rightarrow 5/2^-)$. The Weisskopf units express the strength relative to the single-particle estimate of a $L + {}^1/_2 \rightarrow {}^1/_2$ transition

	^{67}Cu		^{69}Cu		^{71}Cu		^{73}Cu	
	E_γ	$B(E2)$	E_γ	$B(E2)$	E_γ	$B(E2)$	E_γ	$B(E2)$
$1/2^-$	1170	14.0(13)	1096	10.4(10)	454	20.4(22)	135	23.1(21)
$5/2^-$	1115	12.5(10)	1214	3.0(3)	534	3.9(5)	166	4.4(5)
$7/2^-$	1670	3.0(5)	1871	4.6(7)	1190	10.7(12)	961	14.9(18)

TABLE 2.3: Energies in keV and $B(E2)$ values in Weisskopf units for the $1/2^-$, $5/2^-$ and $7/2^-$ transitions to the $3/2^-$ ground state in ^{67,69,71,73}Cu. Data taken from [Ste08]

character of this state in ^{71,73}Cu. It is, however, telltale that the energy slips in ^{71}Cu, while the downhill step in Coulomb excitation takes place two neutrons earlier. So it appears that the $N = 40$ subshell closure, which is reached in ^{69}Cu, confers the rigidity to the nucleus, whereas the $5/2^-$ energy would be affected by a very peculiar interaction with the $g_{9/2}$ neutrons, which indeed enter the scene in ^{71}Cu.

We end the discussion by comparing the situation in copper to that in the gallium chain, where one more pair of protons is present. Data are available from both transfer reactions and deep-inelastic collisions. As to the former, with a 26-MeV deuteron beam from the tandem accelerator at Orsay on a series of germanium targets, the excitation spectra of the gallium isotopes were reconstructed from the outgoing τ particles passing through a split-pole spectrometer [Rot78]. From ^{71}Ga to ^{73}Ga, the summed spectroscopic strength markedly increased for $\pi f_{5/2}$ whereas for $\pi p_{3/2}$ it decreased, as can be seen in figure 2.9. While $3/2^-$ remains the ground state, the energy of the first $5/2^-$ level moves down from 487 to 198 keV. The precedence of the $f_{5/2}$ proton orbital in the filling order above $N = 40$ was considered an anomaly and was imputed to a change in the nuclear shape at $N = 42$. It illustrates how a single-particle effect in copper would appear to express itself as collectivity in gallium. The hypothesis was corroborated in subsequent work in which two neutrons were transferred from a 17-MeV triton beam on targets of ^{69,71}Ga at the Q3D spectrometer at Los Alamos [Ver79]. From the distribution of the reaction components over several levels in ^{73}Ga, deformation was deduced to set in.

In the deep-inelastic work, a ^{76}Ge beam at 7 MeV per nucleon was shot on a ^{238}U

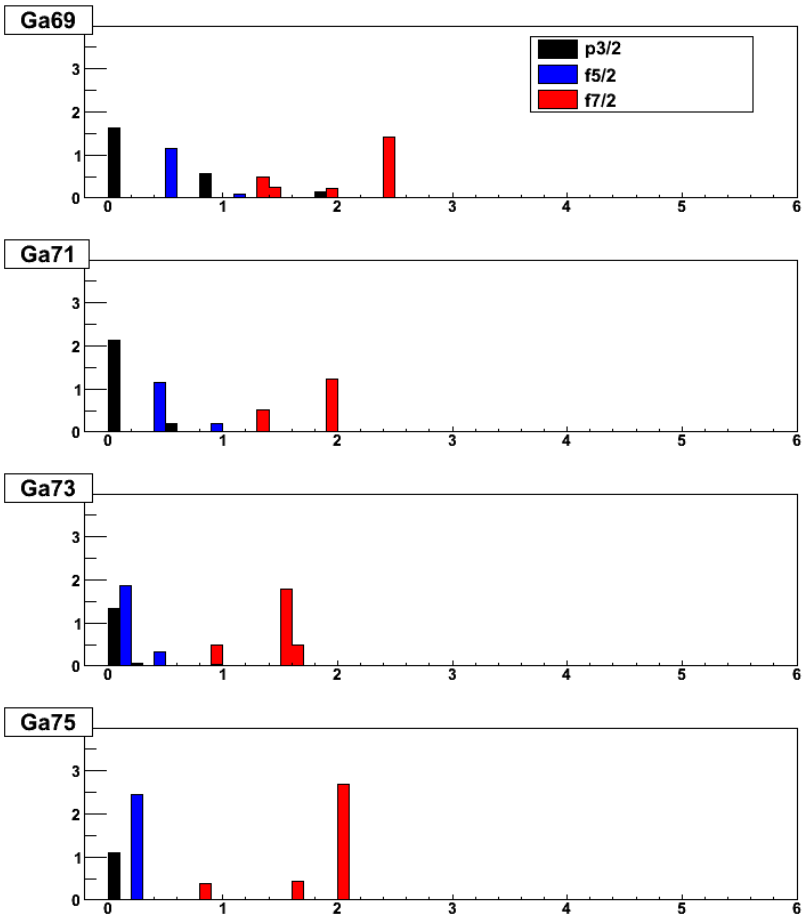

FIGURE 2.9: Strength functions for the $p_{3/2}$, $f_{5/2}$ and $f_{7/2}$ proton states measured in $^{A+1}$Ge(d,τ)^{A}Ga with $A = 69, 71, 73, 75$. Data taken from [Rot78]

target at Argonne [Ste09c]. The newly discovered states at high spin in ^{71,73,75,77}Ga were interpreted as built from a single proton around an even-even zinc core. The $7/2^-$ and $11/2^-$ yrast levels were related to the $3/2^-$ ground state and shown to follow the pattern of the 2^+ and 4^+ core excitations. The $9/2^-$ and $13/2^-$ states would stand atop the first $5/2^-$ one and obey an anologous $E2$ scheme. The $13/2^+$, $17/2^+$ and $21/2^+$ states of positive parity were linked to a proposed $9/2^+$ level but the similarity of their behaviour to the 2^+, 4^+ and 6^+ core states is not equally clear-cut. Quasiparticle configurations that couple to a phonon as well as three-quasiparticle structures were advanced that instead would accompany a transition to a γ-soft nucleus, in a like manner as it is seen in the lighter ^{65,67}Ga isotopes [Dan99]. While at the same time it provides a microscopic explanation for the earlier claims from the transfer experiment, the overall picture re-

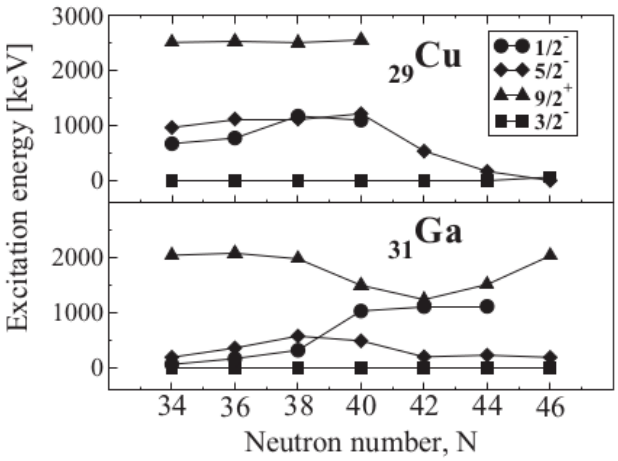

FIGURE 2.10: Energies of the lowest $1/2^-$, $3/2^-$, $5/2^-$ and $9/2^+$ levels in the odd copper (top) and gallium (bottom) isotopes. Taken from [Ste09c]

veals how collective bands arise above particular levels that themselves retain at least to some extent their single-particle nature. A comparison of relevant levels in the odd copper and gallium isotopes is shown in figure 2.10. From it one may appreciate the changing structure across $N = 40$, sharp in the case of copper, more gentle in the case of gallium.

Taking everything together, from stripping reactions we see a fragmented $\pi f_{5/2}$ strength in ^{63,65}Cu but from pick-up an increase in the $5/2_1$ spectroscopic factor is found for ^{69}Cu. Coulomb excitation corroborates this single-particle nature in ^{69}Cu, which then results in an outspoken decrease of the excitation energy in ^{71}Cu as observed in β decay. Transfer as well as and deep-inelastic reactions into gallium finally sketch a picture in which the single-particle states would couple to the core, from which then deformation duly develops.

2.3 The $7/2^-$ levels

Also for the $7/2^-$ states in the copper isotopes a rich bounty of information is available from the various transfer experiments we referred to above. The stripping results are compiled in table 2.4. A $7/2^-$ state appeared at 1.33 MeV in the ^{62}Ni(τ,d)^{63}Cu reaction at 22 MeV of ^{3}He [Bla65]. The spectroscopic factor of 0.46 was smaller than

	E_x (MeV)	J^π	(τ,d) [Bla65]	(τ,d) [Smi68]	(τ,d) [Bri76]	(τ,d) [Sch13]	(α,t) [Arm67]	(α,t) [Rou70]
^{63}Cu	1.327	$7/2^-$	0.46	0.57	0.64	0.90	0.80	–
^{65}Cu	1.482	$7/2^-$	0.43	–	0.32	0.73	0.56	0.55

Table 2.4: Spectroscopic factors for the first $7/2^-$ level in stripping reactions on nickel targets. The C^2S values listed by [Bla65, Arm67] were multiplied by $2j + 1$ with j the transferred angular momentum, while [Smi68, Bri76, Sch13, Rou70] directly quote $(2j + 1)\,C^2S$

the value of 0.80 extracted from the ^{62}Ni(α,t)^{63}Cu experiment at 26.7 MeV of ^{4}He [Arm67]. Other measurements enlarged the scattering further to 0.90 [Smi68, Bri76, Sch13, Rou70], while for the 1.48-MeV state in ^{65}Cu the number varied between 0.32 [Bri76] and 0.73 [Sch13], both in ^{64}Ni(τ,d)^{65}Cu at 18 MeV. It shows that the $\pi f_{7/2}$ orbital is not full but about half a particle can still be squeezed into a small cleft worn out by correlations, illustrating the shortcoming of the $Z = 28$ shell.

Data on pick-up is brought together in table 2.5. At the Rensselaer polytechnic in upstate New York, the ^{64}Zn(n,d)^{63}Cu proton pick-up reaction was examined with neutrons of 14 MeV [Wan65]. While the $5/2^-$ state was not populated, the generous spectroscopic factor of $S = 8(2)$ for the first $7/2^-$ state in the ^{63}Cu residue was understood in terms of an unfragmented $f_{7/2}^{-1}p^2$ proton-hole configuration.[4] Calculations in a particle-core scheme had foreseen that instead the state would be built from a 2^+ collective excitation coupled to the $3/2^-$ ground-state proton. While such a state likely exists, it would have to be looked for at a different energy.

As one can read from the table, the large spectroscopic factor is contradicted by later work. We note that in one instance the integral of the measured $\pi f_{7/2}$ strength function was normalised to 8 [Bac67] and recall that in two other cases normalisation factors were applied of 0.47 [See91] and 0.70 [Mai93].[5] In one experiment the spectroscopic factor for the $7/2_1^-$ state actually absorbed a $5/2^-$ component that could not be separated energetically [Han79]. The obtained values range from 0.67 to 2.7

[4] Unless we should separate out $C^2 = 5/6$, we assume that isospin was left aside and C^2S was meant
[5] We therefore deduce that C^2S should be read for S in [Bac67]

	E_x (MeV)	J^π	(n,d) [Wan65]	(d,τ) [Zei78]	(d,τ) [Han79]	(d,τ) [See91]	($\vec{d}$,τ) [Mai93]	(t,α) [Bac67]	($\vec{t}$, α) [Ajz81]
^{63}Cu	1.327	$7/2^-$	8(2)	1.5	1.4	1.08	–	1.61	–
^{65}Cu	1.482	$7/2^-$	–	1.2	–	–	0.67	0.89	–
^{67}Cu	1.670	$7/2^-$	–	0.90	–	–	–	–	–
^{69}Cu	1.711	$7/2^-$	–	2.7	–	–	–	–	1.8

TABLE 2.5: Spectroscopic factors for the first $7/2^-$ level in pick-up reactions on zinc targets. In [Wan65, Bac67] values for S are given but we assume C^2S is meant, while [Zei78, Han79, See91, Mai93, Ajz81] print C^2S. Error bars are included when published

throughout ^{63,65,67,69}Cu and are markedly smaller than the (n,d) result, pointing now to a considerable fragmentation of the $\pi f_{7/2}$ strength. The numbers indicate that one can remove one to two particles from the $\pi f_{7/2}$ orbital, which gives us the same measure of correlations that was observed in stripping.

In order to evaluate the contribution of higher excited states, we compile in figures 2.11 and 2.12 the strength functions for the $5/2^-$ and $7/2^-$ levels obtained in the various experiments. An amount of ambiguity persists in these plots, as some of the spin assignments are not confirmed and in particular a number of levels appears simultaneously as $5/2^-$ and $7/2^-$. From the stripping data we find that the second $5/2^-$ state draws most strength, as mentioned earlier in this text. The pick-up reactions confirm the fragmentation of the $\pi f_{7/2}$ strength over several states. Conversely the $7/2^-$ spectroscopic factors are weak in stripping but those for $5/2^-$ accessed in pick-up are not entirely negligible.

To avoid any misinterpretation induced by multiple spin assignments, we may follow the isotopic chain within one experimental context and so reproduce in figure 2.13 the strength functions from the most complete data set [Zei78]. Along $5/2^-$ and $7/2^-$, the figure includes also the $3/2^-$ ground state. For ^{63,65}Cu, the experimental $7/2^-$ centroids stand at 1.76 and 2.17 MeV. With only two levels of rather unequal intensity observed in ^{67,69}Cu, the centroid of the measured force tarries near 2 MeV. We conclude that both the $\pi f_{5/2}$ and $f_{7/2}$ centroids remain roughly at the same energy for

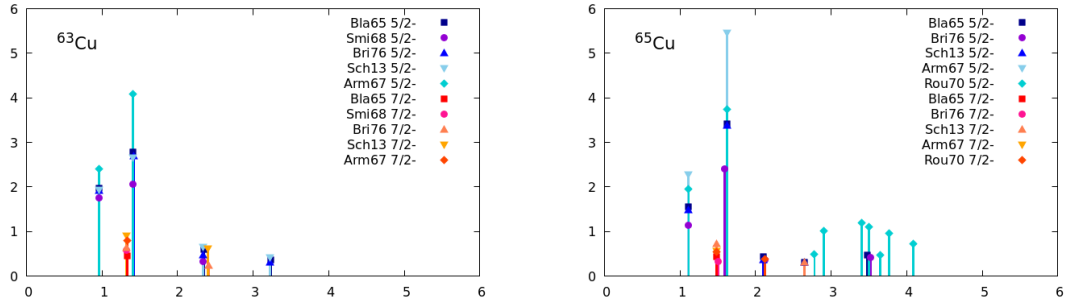

Figure 2.11: Spectroscopic factors of $5/2^-$ and $7/2^-$ levels in ^{63,65}Cu from stripping reactions on nickel targets. Data taken as indicated

$N \leq 40$.

At this point it is interesting to learn what happens when shifting two protons upwards. In the ^{70,72,74,76}Ge(d,τ)^{69,71,73,75}Ga reaction at 26 MeV already introduced above and illustrated in figure 2.9, it was seen that the $7/2^-$ centroid wavers between 1.5 and 1.9 MeV, while the one for the $5/2^-$ levels declines from 0.6 to 0.2 MeV [Rot78]. In as far as this may indicate an approximate contraction of the positions of the $\pi f_{5/2}$ and $\pi f_{7/2}$ single-particle orbitals, it might hint at a similar behaviour in the copper isotopes. Nevertheless, it is difficult to fathom whether a profound migration of the single-particle levels really takes place, since deformation will slowly set in for these $Z = 31$ nuclei and gradually erode the single-particle picture.

Stepping the proton staircase down again to $Z = 29$, new levels in the ^{71}Cu isotope were reported from the fragmentation of a ^{86}Kr beam on a nickel target, an experiment that took place at the Lise spectrometer at Ganil [Grz98]. A signature of $7/2^-$ was assigned to a state at 1189 keV, which was inserted in the $E2$ deexcitation band of a $19/2^-$ microsecond isomer itself situated at 2756 keV. The isomer was interpreted as a $\pi p_{3/2} \nu g^2_{9/2}$ structure, in fact the coupling of the $p_{3/2}$ copper ground-state proton to the 8^+ microsecond isomer in ^{70}Ni, which was seen at a comparable energy of 2870 keV [Pfü97].[6] The $E2$ cascade rolled down the spin sequence of the $\nu g^2_{9/2}$ pair.

In the same paper a level at 981 keV, the placement of which was not certain and for which no assignment of spin and parity could be given, appeared in the lower half of the level scheme. A collaboration at the Jaeri laboratory at Tokai soon after published

[6] The energy was soon corrected to 2860 keV [Bro98, Grz98]

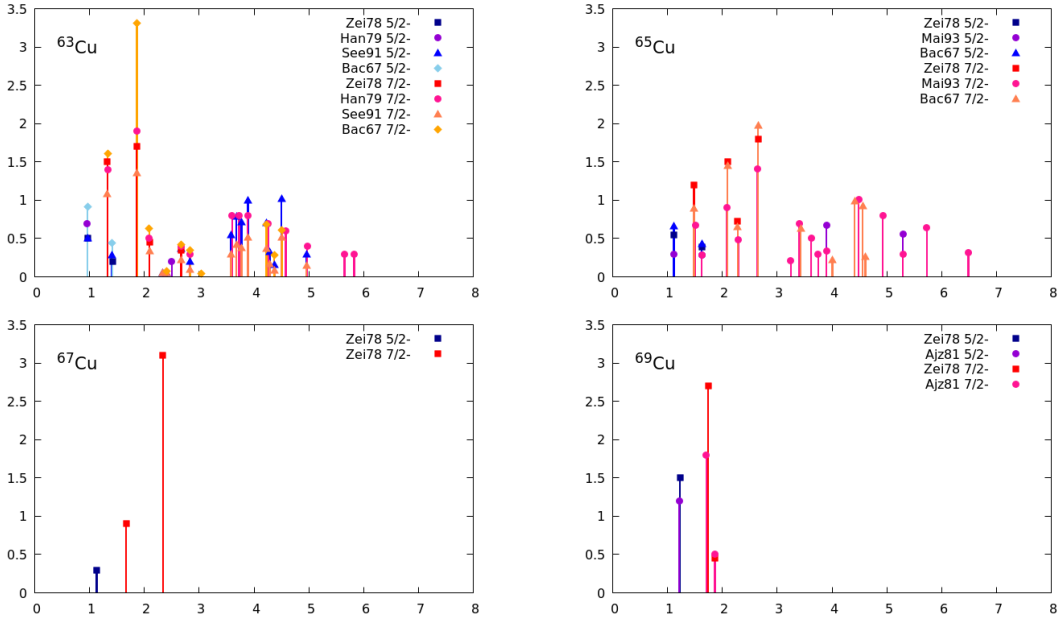

FIGURE 2.12: Spectroscopic factors of $5/2^-$ and $7/2^-$ levels in ^{63,65,67,69}Cu from pick-up reactions on zinc targets. Data taken as indicated

a diagram that was essentially identical for the deexcitation of the isomer but without any such 981-keV state [Ish98]. In the β decay of ^{71}Ni that we carried out at Lisol, γ rays both at 981 and 1189 keV were identified [Fra01]. Feeding percentages for the eponymous levels of 7.0% and 8.2% and log ft values of 5.9 and 5.8 respectively were deduced. Combining this observation with the similarity in the γ-decay pattern, a $7/2^-$ spin and parity was put forward also for the 981-keV level.

The first $7/2^-$ level in ^{69}Cu is situated at 1711 keV, while a second one turns up at 1871 keV. An outspoken decrease in the $7/2^-_1$ energy thus results by moving across $N = 40$ to ^{71}Cu. By analogy to the migration of the first $5/2^-$ state, a single-particle interpretation quickly popped up. This view was comforted through calculations with a particle-core coupling model (PCM) that proposed to identify the state at 981 keV in ^{71}Cu with the $f_{7/2}$ proton hole, on top of which a 2p-1h $\Delta j = 1$ band would squat [Oro00]. The article drew its inspiration from the occurrence of a similar structure that was recognised above the $7/2^-_1$ state in ^{69}Cu [Bro98, Ish00].[7] The single-particle

[7] The interpretation of excited levels in ^{69}Cu given in [Ish00] copies that of [Bro98] and is markedly different from the one that is based on the more limited data in the earlier publication [Ish97]

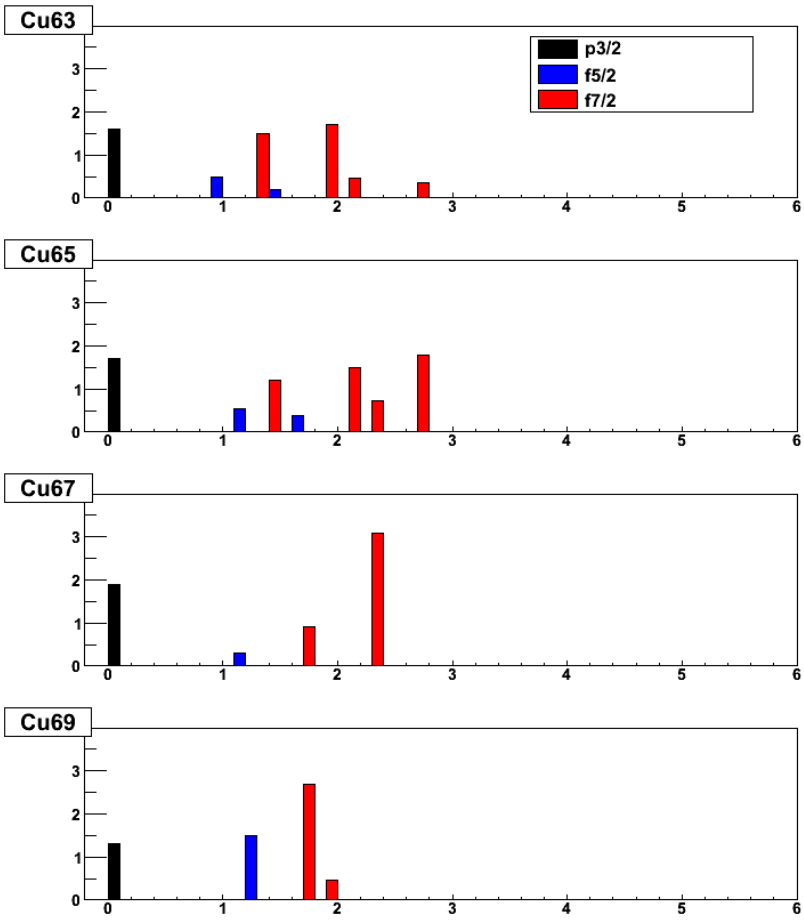

Figure 2.13: Strength functions for the $p_{3/2}$, $f_{5/2}$ and $f_{7/2}$ states measured in $^{A+1}$Zn(d,τ)^{A}Cu with $A = 63, 65, 67, 69$. Data taken from [Zei78]

wave function was subsequently inferred from the large spectroscopic factors that we gathered in table 2.5 for the ^{70}Zn(d,τ)^{69}Cu and ^{70}Zn($\vec{t}$, α)^{69}Cu reactions. The shell model concurred, sourced with the S3V' interaction contrived by Ioannis Sinatkas, Leonidas Skouras, Daniel Strottman, and John Vergados in Athens [Sin92] and adapted for the copper region by Hubert Grawe in Darmstadt [Gra99]. It could not reproduce two $7/2^-$ levels at low energy, from which it was deduced that one of them would lie outside the $f_{5/2}pg_{9/2}$ valence space, that is a $f_{7/2}$ proton hole state. If both the $\pi f_{7/2}$ hole and the $\pi f_{5/2}$ particle would indeed sneak closer to the Fermi surface, their spin-orbit gap would rapidly wane. To continue the story further, from the β-decay work at Lisol two candidates for $7/2^-$ states in ^{73}Cu lie at at 961 and 1010 keV.

As introduced in the previous paragraph, a number of years passed by during which

a copper beam was developed at Isolde for post-acceleration to moderate energies. The Coulomb excitation of ^{71}Cu immediately confirmed the collective nature of the 1189-keV level with a $B(E2, 7/2^- \rightarrow 3/2^-)$ intensity of 10.7(12) Weisskopf units [Ste08]. The 981-keV state was not seen, strengthening the hypothesis of a single-particle configuration that would have gone unobserved. At Argonne a little later, a deep-inelastic experiment took place with the Gammasphere germanium array in which both $7/2^-$ levels were visible [Ste09a]. The interpretation given in the earlier works was corroborated through shell-model calculations with a realistic interaction that was derived through G-matrix techniques from the Bonn boson-exchange potential in a $f_{5/2}pg_{9/2}$ model space by Morten Hjorth-Jensen from the Oslo group [Hjo95] and that incorporated modified monopoles from Nowacki in Strasbourg [Now96]. Only one $7/2^-$ state at 1.6 MeV was predicted with about 70% of the $\pi p_{3/2}\nu g^2_{9/2}$ configuration in its wave function, implying once again that the other $7/2^-$ level would derive from the $\pi f_{7/2}$ hole state.

The Coulomb excitation also showed a remarkable gain in collectivity in ^{71}Cu compared to its predecessors, the $E2$ strength being up from 3.0(5) at 1670 keV in ^{67}Cu and 4.6(7) at 1871 keV in ^{69}Cu while continuing to rise and reach 14.9(18) Weisskopf units at 961 keV in ^{73}Cu. This apparent contrast across the $N = 40$ divide deviates from the behaviour of the $5/2^-$ state, which is nicely illustrated in figure 2.14. It can be essentially related to the dropping energy of the $7/2^-$ excitation rather than a structural difference, as the spectroscopic factors for the states at 1670 and 1871 keV in the respective ^{68,70}Zn(d,τ)^{67,69}Cu reactions are small, indicating a collective component throughout. The nature of the $5/2^-$ excited state, on the other hand, turns predominantly into that of a single particle. At the same time the figure gives evidence how the collective $7/2^-$ state follows the trend of the 2^+ excitation in the nickel core. Looking in detail we see that the minimum of the quadrupole strength is situated at $N = 40$ in ^{68}Ni but at $N = 38$ in ^{67}Cu, implying that in the latter two neutrons would migrate into the $g_{9/2}$ subshell early on.

If one of both $7/2^-$ states indeed contains a proton hole then it can be argued that it should be favourably populated in a (d,τ) transfer reaction. Its lifetime would be short but possibly measurable with the Recoil-Distance Doppler-Shift (RDDS) technique

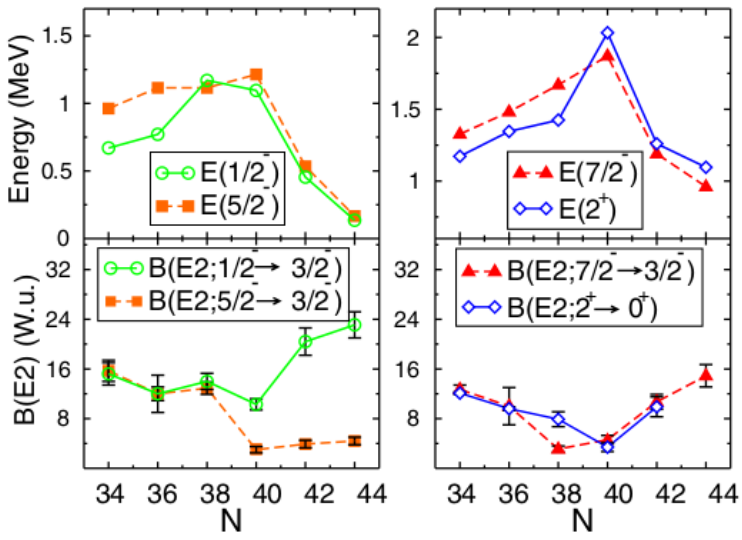

Figure 2.14: Energies and $B(E2)$ strengths of the $1/2^-$, $5/2^-$ and $7/2^-$ states in $^{63-73}$Cu. The systematics for the 2^+ core excitation in nickel are also plotted. Taken from [Ste08]

[Dew12]. This simple idea led to an experiment carried out at the Lise spectrometer at Ganil, the object of which were the states at 961 and 1010 keV in ^{73}Cu of likely spin and parity $7/2^-$. A beam of ^{74}Zn was produced in the fragmentation of a ^{76}Ge beam on a ^{9}Be foil at 60 MeV per nucleon. The secondary target, a disk of deuterated polyethylene of 35.5 mg/cm^2 thickness, was mounted in front of a ^{9}Be degrader of 51 mg/cm^2 in a plunger device developed through a collaboration between the universities of Cologne and Darmstadt. A variable distance was set between target and degrader, ranging from 0 to 20 mm with a precision of some 10 μm. The plunger was hemmed in by eight Exogam germanium detectors that were used for identification as well as the half-life measurement of the excited nuclear states. Further details of the experiment can be found in [Mou10].

Because of the different velocity of the recoiling nucleus in the target and in the degrader, the γ peaks are split in two components that each require their own Doppler correction. The half-life of a nuclear level is determined from the ratio of the γ rays emitted after the target to those emitted after the degrader. Every distance between target and degrader yields an independent measurement, systematic errors put aside, and can be related to the other members of the data set by an exponential function. In spite of this set-up the ^{73}Cu product nucleus was not observed in the experiment,

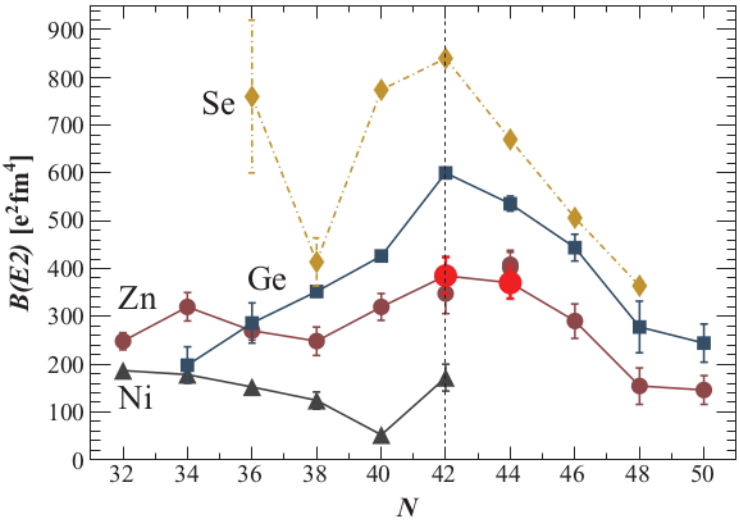

FIGURE 2.15: $B(E2, 2^+ \rightarrow 0^+)$ values for ^{72,74}Zn from the plunger experiment at Lise at Ganil drawn in red against the systematics of the surrounding region. Taken from [Nii12]

probably because of a low cross section for the pick-up reaction so statistics did not allow for a double-pronged γ ray to emerge beyond the background. The focus of the experiment shifted to the 2^+ excited state in ^{72,74}Zn that could be readily populated in inelastic scattering, with the subsequent analysis agreeing with previous results and centering on the appearance of γ softness at $N = 42$ [Nii12]. We use the opportunity to plot in figure 2.15 the systematics from nickel to selenium, displaying a persistent maximum of collectivity at $N = 42$. Yet alternatively one may also interpret the data as if the barycentre of the bell curve shifts to lighter N for heavier Z.

The excited states that are built on top of both $7/2^-$ levels in ^{71}Cu were also reported from an investigation with a ^{82}Se beam on a ^{238}U target at the Prisma large-acceptance spectrometer at the Legnaro laboratory [DeA12]. In ^{73}Cu the experiment confirmed the existence of the two levels at 961 and 1010 keV that had been seen before at Lisol in β decay and tentatively assigned $7/2^-$ from the similarity of the γ patterns. We wrote above that the one at 961 keV was populated in Coulomb excitation at Isolde. In ^{75}Cu two corresponding levels were likewise proposed at 767 and 888 keV.

Still more results were obtained from the deep-inelastic reaction of ^{76}Ge on ^{238}U at 577 MeV, again at the Prisma spectrometer at Legnaro [Sah15]. Here the same plunger that had been used at Lise at Ganil was surrounded by four modules of the state-of-

	Coulomb excitation		plunger	
	E_γ	$B(E2)$	E_γ	$B(E2)$
^{69}Cu	1871	4.6(7)	1711	0.09(4)
^{71}Cu	1189	10.7(12)	981	2.5(11)
^{73}Cu	961	14.9(18)	1132	1.1(6)

Table 2.6: Comparison of γ rays observed in the Coulomb excitation at Isolde and the plunger experiment at Legnaro deexciting a $7/2^-$ level to the $3/2^-$ ground state, except for the 1132-keV transition in ^{73}Cu that decays to the $5/2^-$ first excited state. Energies are given in keV and transition strengths in Weisskopf units. Data adapted from [Ste08, Sah15]

the-art Agata γ multidetector [Wie10], while the ^{238}U target was matched by a ^{93}Nb degrader foil. A half-life of 14(6) ps was fitted for the first $7/2^-$ level at 981 keV in ^{71}Cu, which corresponds to a $B(E2, 7/2^- \rightarrow 3/2^-)$ transition strength of 44(20) e^2fm^4 or 2.5(11) Weisskopf units. The large error bar reflects the dependence of the extracted value on the scattering of the data, which is inherent to plunger measurements that contain but a few points. Compiling this value in table 2.6 along with the preceding results from the Coulomb excitation at Isolde, namely a figure of 10.7(12) Weisskopf units for the second $7/2^-$ state at 1189 keV [Ste08], it appears to reinforce the interpretation put forth for both levels as a single-particle and a collective state, respectively. Surprisingly the authors did not concur and stated that the half-life they measured verily excluded a single-hole nature for the 981-keV level. Upon a first glance this seems upheld with difficulty in the nitid light of scrutiny, since 2.5 Weisskopf units would sensibly comply with the definition of being small. It also remains unclear why the 1189-keV transition was not seen, even though it was visible in the similar reactions mentioned above at Tokai, ^{76}Ge + ^{198}Pt at 635 MeV [Ish98], at Argonne, ^{64}Ni + ^{238}U at 430 MeV [Ste09a], and at Legnaro itself, ^{82}Se + ^{238}U at 515 MeV [DeA12].

As a matter of fact the identification of the 981-keV level with the $\pi f_{7/2}$ hole state would pose the challenge of it lying quite low in energy. So the article advanced shell-model calculations in a valence space of fp protons and $pf_{5/2}g_{9/2}d_{5/2}$ neutrons around a core of ^{48}Ca, under the acronym of its architects Silvia Lenzi, Frédéric Nowacki,

Alfredo Poves, and Kamila Sieja since gaining reputation as LNPS [Len10]. The interaction plugged together realistic two-body elements from several sources, that is an updated KB3G force by the precise name of KB3gr governing the *fp* subspace, Hjorth-Jensen's *G* matrix with an empirically adjusted monopole part called upon to describe the $\nu g_{9/2}$ orbital, and the phenomenological KLS parameters framing the $\nu d_{5/2}$ state. Two excited $7/2^-$ states were calculated, at 1115 and 1426 keV. They showed $B(E2)$ strengths to the $3/2^-$ ground state of 179 and 14.4 $e^2\text{fm}^4$, that is 10.2 and 0.8 Weisskopf units, and were respectively related to the experimental $7/2^-_2$ level at 1189 keV seen in Coulomb excitation and the $7/2^-_1$ one at 981 keV observed with the plunger. But the detailed composition that the wave functions revealed was particularly significant, for they linked the $7/2^-_2$ state to the $\pi p_{3/2} \times 2^+$ configuration with an amplitude that stood at 59%, while the $7/2^-_1$ level was traced back to the $\pi f_{5/2} \times 2^+$ coupling for which the amplitude reached 55%. A collective character was thereby inferred for both states but because of the structural mismatch a low transition rate would nevertheless result for the $7/2^-_1$ one.

The $7/2^-$ level at 1711 keV in ^{69}Cu was seen to decay to the $3/2^-$ ground state with a half-life of 26(11) ps, marking 1.5(6) $e^2\text{fm}^4$ or 0.09(4) Weisskopf units. The LNPS calculation produced two $7/2^-$ states at 1862 and 2186 keV, their configurations respectively led by 40% of $\pi p_{3/2} \times 2^+$ and 52% of $\pi f_{5/2} \times 2^+$. By comparing the theoretical $B(E2)$ values to the result from the Coulomb excitation, the former was held to correspond to the experimental level at 1871 keV that we described above. The second one was tied to the state at 1711 keV since the shell model imparts it a low transition strength, fitting with the long experimental half-life. As can be read from table 2.6, the $B(E2)$ values in ^{69}Cu are appreciably smaller than in ^{71}Cu, which was understood from the $N = 40$ subshell closure restricting the freedom of the neutrons.

Also the lifetime of the 1132-keV transition in ^{73}Cu was measured, deexciting the 1298-keV level to the $5/2^-$ first excited state at 166 keV. From the β decay at Lisol, a spin and parity of $7/2^-$ or $9/2^-$ had been suggested for the initial level. From the theoretical point of view, the LNPS analysis fixed two $7/2^-$ states at 937 and 1128 keV. The first one contains 45% of the $\pi p_{3/2} \times 2^+$ structure but surprisingly the second one sports a $\pi f_{7/2}$ occupancy of 6.4 out of a total of 8. The appearance of this proton hole

at a rather low energy instead of the expected $\pi f_{5/2} \times 2^+$ configuration would indicate a $Z = 28$ shell gap that becomes considerably weaker towards $N = 50$, ultimately precipitating the erosion of the magicity of ^{78}Ni. Experimentally the half-life of the 1298-keV level equalled 15(8) ps, translating into 20(11) e^2fm^4 or 1.1(6) Weisskopf units. The low value is consistent with the $\pi f_{7/2}$ hole configuration, be it that the shell model granted 0.001 Weisskopf units only. The $\pi p_{3/2} \times 2^+$ option cannot be ruled out from the plunger measurement itself, but from the earlier Coulomb excitation it can be assigned to the level at 961 keV. By consequence the $\pi f_{5/2} \times 2^+$ coupling is left for the state at 1010 keV. Interestingly, the absence of the γ rays at 961 and 1010 keV from our plunger spectra of ^{73}Cu at Lise at Ganil mentioned before [Mou10] now appears most meaningful, as it possibly points to a spectroscopic factor for either of these $7/2^-$ states that is lower than expected for a single-particle structure, while a plausible signal at 1132 keV instead could have been overlooked.

The limited purity of the 1010-keV level would moreover be responsible for γ-branching ratios that do not completely fit the picture, as they are fairly similar towards the $3/2^-$ ground state and the $5/2^-$ first excited state. For the 1298-keV level on the other hand they would signal the preference of the transformation of the $\pi f_{7/2}^{-1}(p_{3/2}f_{5/2})^2$ structure into $\pi f_{5/2}$ rather than into $\pi p_{3/2}$. Neither can one discard a different spin for the 1298-keV level, such as $9/2^-$. In this case the calculation would predict a strong transition to the $5/2^-$ first excited state, which however the plunger measurement did not confirm. Alternatively a $5/2^-$ assignment matching with a theoretical level at 1203 keV may be considered, for which a commodious transition rate of 0.63 Weisskopf units was computed. Actually agreeing quite well with the data, its wave function would then carry the $\pi f_{5/2} \times 2^+$ component for 22%.

It is important to notice that the plunger conditions of the experiment favoured slow transitions with low $B(E2)$ values only. While the Coulomb excitation probed the $\pi p_{3/2} \times 2^+ \rightarrow \pi p_{3/2}$ configurations, the plunger accessed the $\pi f_{5/2} \times 2^+ \rightarrow \pi p_{3/2}$ or $\pi f_{7/2}^{-1} \rightarrow \pi f_{5/2}$ ones. The complementarity is striking and instructive, yet a truly comprehensive approach that would measure all related states in a single experiment escapes us.

Stringing together all pieces of information, the hypothesis advanced by the PCM

calculations and the Coulomb excitation that the two $7/2^-$ states tentatively identified in the β decay would correspond to a phonon coupling of the ground state on the one hand and a $f_{7/2}$ proton hole on the other, proved too simple. While the uncertainties in the plunger measurement were perhaps too large to allow for a definite statement, the LNPS results rendered clear that a third $7/2^-$ state must exist, since the inversion of the $\pi p_{3/2}$ and $\pi f_{5/2}$ orbitals implies that the phonon couplings for both are to be found near in energy. Although the distinct nature of the three states might for a large part be obscured by mixing, other experimental approaches into the copper isotopes can disentangle these quantitatively. The transfer experiment we carried out and shall present in chapter 4 is geared to this question, but before we dive into the depth of the topic we first focus on the curious $1/2^-$ state.

2.4 The $1/2^-$ level

The first $1/2^-$ level in ^{69}Cu is situated at 1096 keV, its position nicely in line with the systematics of the lighter isotopes. Yet Coulomb excitation performed at Isolde found new states at energies of 454 keV in ^{71}Cu and 135 keV in ^{73}Cu, for which it exposed $B(E2, 1/2^- \rightarrow 3/2^-)$ strengths that stood surprisingly high at respectively 20.4(22) and 23.1(21) Weisskopf units against 10.4(10) in ^{69}Cu [Ste08]. Asserting its reputation as the tool of choice to unravel collective behaviour, the reaction mechanism branded the two fresh levels as low-lying collective modes that were assumed to carry a spin and parity of $1/2^-$. This was consistent with their absence in the analysis of the β decay at Lisol, where the $9/2^+$ ground states of ^{71,73}Ni would not easily induce their population. In a likewise manner the 1096-keV level was not recognised in the decay of ^{69}Ni [Fra01]. To be more precise, close inspection reveals that a weak transition at 1100 keV was visible in fact in the β-gated γ spectrum of ^{69}Cu, as well as a clear peak at 452 keV in that of ^{71}Cu. A deficiency in the energy calibration perhaps cannot be excluded, even though the two nuclei were studied extensively. These single γ rays, however, were rejected during the data evaluation for a different reason, namely because they could not be readily distinguished from contaminating lines introduced by doubly charged barium and lanthanum isotopes that were leaking through the separator

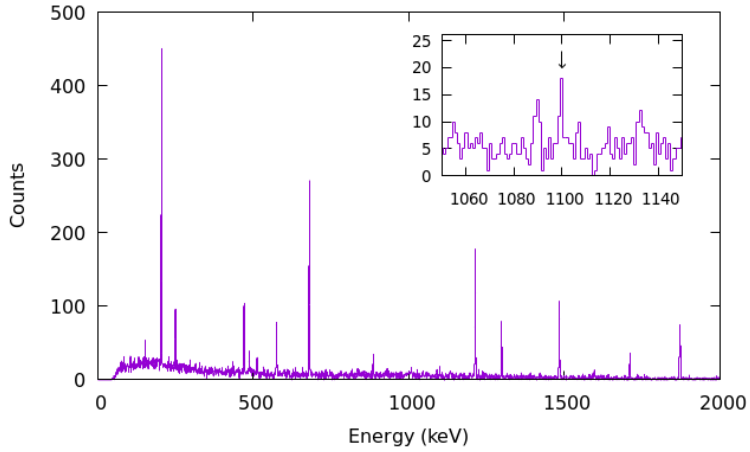

FIGURE 2.16: The β-gated γ spectrum at mass 69 at Lisol with the laser ion source resonant on nickel. The arrow in the inset indicates 1100 keV

at the same mass setting or implanted previously. The spectra are reproduced in figures 2.16 and 2.17. In ^{73}Cu the background fluctuations at low energy were too important to identify a possible peak at 135 keV, as can be seen in figure 2.18.

The strength of 10.4(10) Weisskopf units for the $1/2^-$ deexcitation in ^{69}Cu is a factor of three larger than that of 3.0(3) for the $5/2^-$ one, which is easily explained by the spin weight of $1/(2J_i + 1)$. It means there is no conspicuous onset of collectivity in this nucleus. Removing the spin factor for the values in ^{71}Cu on the other hand, an enhancement of 1.7 would be left that could be attributed to collective behaviour in the $1/2^-$ state. The deforming mode could be most easily understood as following from a $\pi p_{3/2} \times 2^+$ configuration. In the limit of a harmonic phonon, however, the multiplet rules established in literature predict the $5/2^-$ member to be lowest and the $1/2^-$ one to be highest in energy, with the order of the intermediate $3/2^-$ and $7/2^-$ states depending on the sign of the quadrupole moment [Paa81]. A $3/2^-$ level different from the ground state remains missing, while the observed $5/2^-$ level was tied to the $\pi f_{5/2}$ single-particle state, as discussed above. The candidates for $7/2^-$ configurations that were found at higher excitation energies might be deemed too far away to belong to the same structure. If a spin and parity of $5/2^-$ was assigned to the levels at 454 and 135 keV in ^{71}Cu and ^{73}Cu, respectively, it would indeed be acceptable that only these and no other multiplet members were seen. Because of the spin factor, their $B(E2)$ values would be three times smaller and they would no longer stick out as exceptionally high.

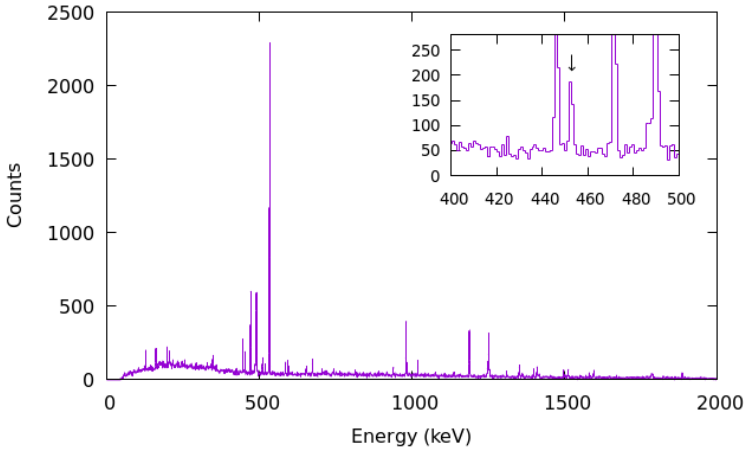

FIGURE 2.17: The β-gated γ spectrum at mass 71 at Lisol with the laser ion source resonant on nickel. The arrow in the inset indicates 452 keV

Of course then it becomes puzzling why a $5/2^-$ level would at most be weakly fed in the β decay of the $9/2^+$ ground state of nickel, which precisely was the main argument for the $1/2^-$ assignment. Although one should keep in mind that the multiplet rule may not be valid at low spin values, if it fails in ^{71,73}Cu it could rather imply that the wave function contains other significant components.

Added insight on the $1/2^-$ level came from the β disintegration of ^{71}Co into ^{71}Ni at NSCL, whick took place near the same time but was published with some years of delay [Raj12]. The parent nucleus was produced in the fragmentation of a ^{86}Kr beam on a ^{9}Be target at 140 MeV per nucleon and implanted in a stack of silicon detectors, upon which the emitted γ rays irradiated sixteen units of the Segmented Germanium Array (Sega) of high-purity detectors. Based on the systematics of nearby isotopes and the absence of coincidence relations with the most intense transition towards the ground state, two γ rays were tentatively assumed to feed a $1/2^-$ state in the nickel daughter at an energy of 499 keV. In figure 2.19 the reader can check out the argument that the spin difference with the $7/2^+$ and $9/2^+$ levels below forced the $1/2^-$ state to isomerise and undergo β decay. A 499-keV peak was even observed in the delayed γ spectrum but rather disturbingly it disappeared when background was subtracted and was further ignored. The data analysis was backed up by shell-model calculations from a collaboration between Michigan and Darmstadt [Lis04]. Dubbed as NR78, they dress a ^{56}Ni core with the $f_{5/2}pg_{9/2}$ orbitals through a realistic G-matrix interaction

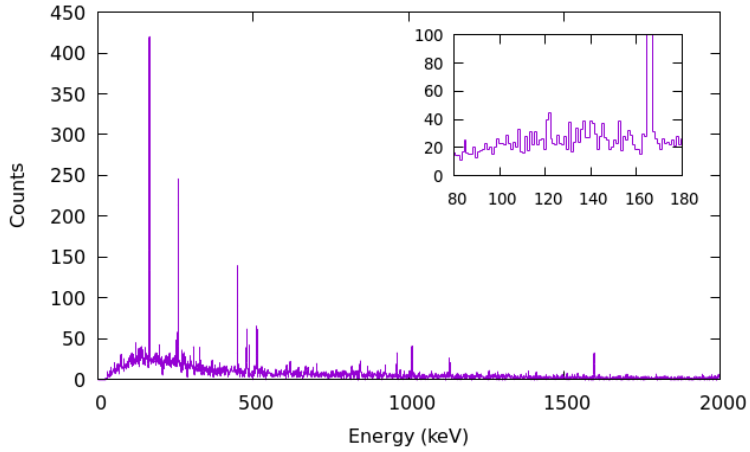

Figure 2.18: The β-gated γ spectrum at mass 73 at Lisol with the laser ion source resonant on nickel. The inset shows the region around 135 keV

that is rooted in the Bonn potential and adjusted for local features.[8] The level could be linked to the $\nu p_{1/2}$ single-particle hole with a reasonable purity of 60%, which would climb through the nickel chain from 400 keV in ^{69}Ni to 1300 keV in ^{77}Ni. Nonetheless in ^{73}Ni a similar $1/2^-$ state was not seen. The authors suggested that if indeed it rose in energy above a neighbouring $5/2^+$ state, it might γ decay but somehow escape detection. From the surprising statement we may surmise that the background conditions possibly remained an issue.

At Lisol we had measured the β decay of ^{71}Ni into ^{71}Cu before but the new information, which soon transpired from NSCL, incited to take a crisp look at it. Immediately it became clear that the isomer, the half-life of which was determined at 2.3(3) seconds, populates the $1/2^-$ level at 454 keV in ^{71}Cu [Ste09b]. The branching ratio amounts to 40(15)%, the larger share of 60(15)% finding shelter in the ground state. Nevertheless such a scenario may take the maven by surprise, as the Gamow-Teller strength is eight times larger for the $p_{1/2} \rightarrow p_{3/2}$ spin flip than it is for the $p_{1/2} \rightarrow p_{1/2}$ case [DeS74]. In ^{93}Tc, a nucleus with a closed neutron shell but 43 protons and therefore comparable to ^{71}Ni with its 43 neutrons, a $1/2^-$ isomer exists that as a matter of fact mainly decays to presumed $3/2^-$ states in ^{93}Mo. But if a single-particle state directly disintegrates into a collective one, the latter likely counts an overlapping component in its wave function

[8] The authors mention the charge-dependent Bonn potential whilst referring to [Lis04], which itself quotes the rather different Bonn-C potential

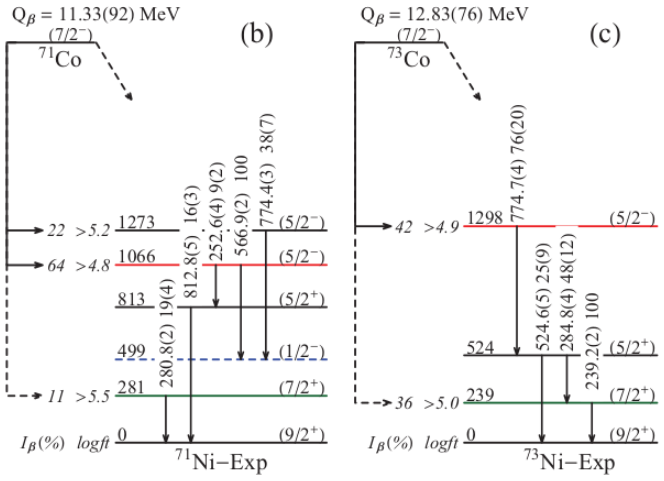

FIGURE 2.19: Experimental level schemes for ^{71,73}Ni in the β decay of ^{71,73}Co. Taken from [Raj12]

that enables the transition.

Several years before through independent work from β disintegration both at Lisol and NSCL an equivalent 3.5-second $1/2^-$ isomer had been established at 321 keV in ^{69}Ni [Mue99, Pri99]. Intriguingly, it populates by an amount of 74(9)% a 1298-keV level in ^{69}Cu that sports a spin and parity of $3/2^-$ rather than $1/2^-$. It is considered as a $\pi p_{3/2}\times 0^+_2$ configuration with a strong single-particle component, as a 1298-keV γ ray is absent in the Coulomb excitation. A remaining branch of 26(9)% proceeds to the $\pi p_{3/2}$ ground state. A structural change would thus appear to take place from ^{69}Cu to ^{71}Cu. In the former the 1298-keV level would capture an essential part of the $\nu p_{1/2} \rightarrow \pi p_{3/2}$ single-particle Gamow-Teller strength, while in the latter the 454-keV state would collect most of the feeding through the variety of components that hide in its wave function and tempt the same transforming neutron. Befitting a conundrum in which deformed and spherical states ostensibly occur together, a $\pi p_{3/2} \times 0^+_2$ configuration might still be available in ^{71}Cu, even if theoretical considerations such as the PCM calculations from section 2.3 would put it above 1 MeV [Oro00]. A sketch of the situation is presented in figure 2.20.

The Nilsson model was called upon to resolve the plot, as it is able to relate specific spin levels to primary single-particle structures. Assuming that the intrinsic angular momentum projected along the symmetry axis of the rotor, that is Ω, equals the total

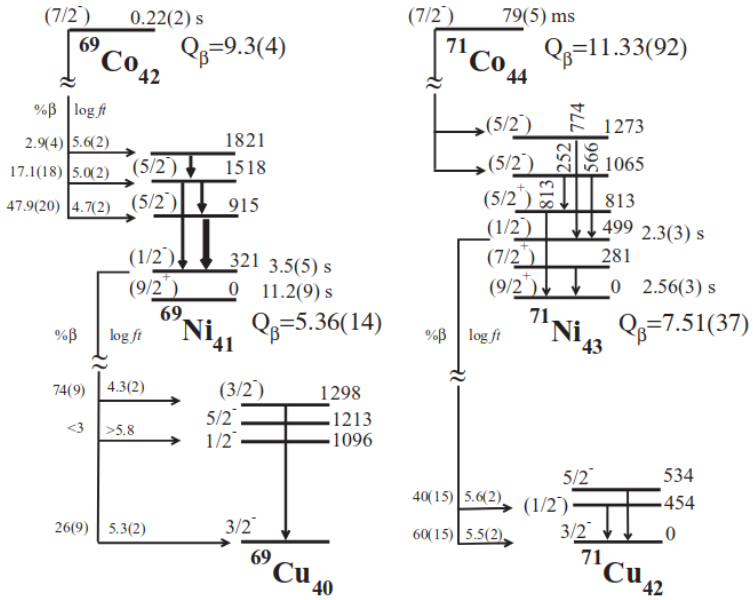

Figure 2.20: Simplified scheme for the β decay of ^{69,71}Co into ^{69,71}Ni and onwards into ^{69,71}Cu. Taken from [Ste09b]

angular momentum projected likewise, known as K, the $\Omega[Nn_z\Lambda] = 1/2^-[321]$ orbit as it is generated by prolate deformation from the $\pi p_{3/2}$ ground state of ^{71}Cu would underlie the 454-keV level [Ste09b]. One deduces a positive quadrupole deformation parameter ϵ_2 that does not exceed 0.23, as can be read from figure 2.21. From the β decay of ^{67}Fe at Lisol, a $1/2^-$ proton state lying at 492 keV in ^{67}Co meanwhile was tied in a similar fashion to the same $1/2^-[321]$ configuration with a prolate deformation of $0.25 \leq \epsilon_2 \leq 0.4$ [Pau08]. Loosely qualified as an intruder, the proton-neutron correlations that set off the deformation in this case would be induced by promoting a proton from the $\pi f_{7/2}$ to the $\pi p_{3/2}$ orbital across the shell gap, outlining a one-particle two-hole (1p-2h) excitation that effectively mimics the ground state of copper. Most of it depopulates by isomeric decay to the purportedly spherical $7/2^-$ ground state of ^{67}Co, the whereabouts of a fainter β branch being unknown.

By means of summary so far, while the $1/2^-$ state in ^{69}Cu contains a significant $\pi p_{1/2}$ single-particle component, in ^{71,73}Cu it sharply comes down in energy, appears to lose most of its single-particle content and acquires considerable collectivity. Since the Coulomb excitation did not give access to the shape of the nucleus, a careful formulation was retained in which single-particle and collective levels were suggested to

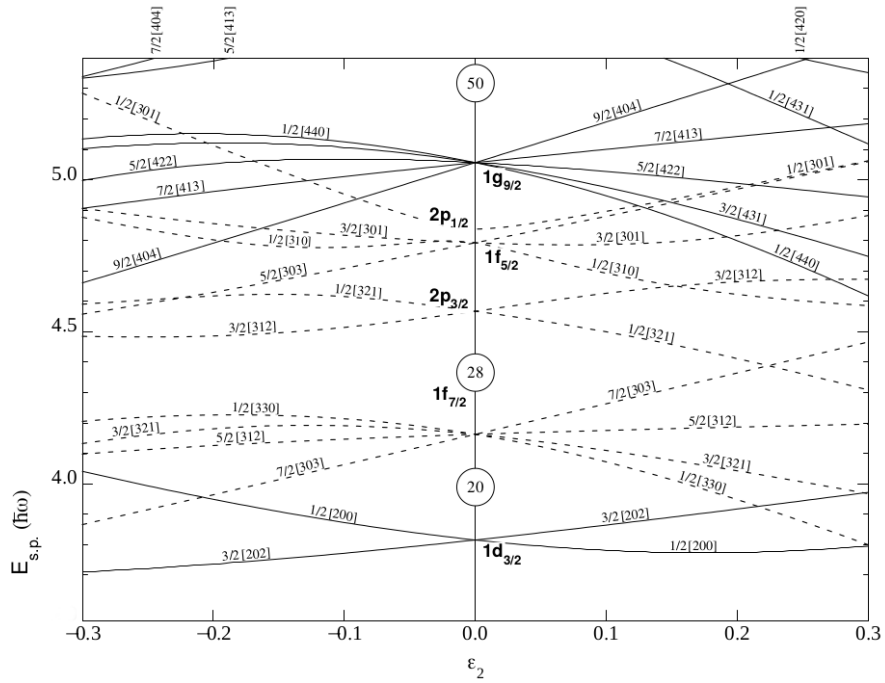

FIGURE 2.21: Nilsson diagram for selected proton states. Adapted from [Fir96]

coexist in an interplay. The $5/2^-$ and $7/2^-_1$ excited states descend in energy and would stay prominently single particle in nature, whereas the proper $\pi p_{1/2}$ orbital would be replaced by a deformed $1/2^-$ state that the Coulomb excitation preferentially populates. Once the $1/2^-$ structure is associated to the Nilsson orbital that derives from the $\pi p_{3/2}$ single-particle state, however, one can expand upon the idea and pull a string of thought that by default these nuclei are collective and that a fortiori the $3/2^-$ ground state must stem from the $3/2^-$[312] Nilsson complement, being deformed by a comparable design. Neither can one actually exclude that a $3/2^-$ assignment be envisaged for the 454-keV level in ^{71}Cu or the 135-keV one in ^{73}Cu themselves, in which case their remarkably large $B(E2)$ values would stoically drop by a factor of two. Until this possibility is discarded, the true nature of the deformation might lie covered in sphinx-like silence.

The laser spectroscopy of copper at Collaps at Isolde, which we mentioned before already, lifted a first tip of the veil as it did not disclose any distortion of the shape [Vin10]. But only when inspection moved on to ^{75}Cu, where we find ourselves in front of an equally intricate situation, did the cloak of fog recede. Information on low-

lying isomeric levels in this nucleus was obtained at the Lise spectrometer of Ganil in the fragmentation of a ^{86}Kr beam on a natural nickel target at 60.5 MeV per nucleon [Dau10]. Because of a weak coincidence signal between γ rays at 62 and 67 keV, these were placed above each other and two levels at 62 and 128 keV with respective half-lives of 370(40) and 170(15) ns were proposed. Spins and parities of $1/2^-$ and $3/2^-$ above a $5/2^-$ ground state were advanced for them, although the order was left open. Shell-model calculations were carried out with a Hamiltonian constructed by the groups in Madrid and Strasbourg in the $\pi fp\ \nu pf_{5/2}g_{9/2}$ space around a core of ^{48}Ca and pieced together out of fp two-body matrix elements from the KB3G force, $pg_{9/2}$ and $f_{5/2}g_{9/2}$ strips from work at Strasbourg, and a $f_{7/2}g_{9/2}$ fragment from the KLS collection. After some more tinkering of the $f_{7/2}f_{5/2}$ proton gap, they successfully predicted the ground-state spin inversion in ^{75}Cu. The $5/2^-$ ground state would retain a single-particle character, its $\pi f_{5/2}$ component standing at 65%. For the $3/2^-$ and $1/2^-$ states a purity was projected that amounted to 45% of $\pi p_{3/2}$ and 30% of $\pi p_{1/2}$, respectively. As to the details of the energy scheme itself, the model positioned the $3/2^-$ state at 179 keV and the $1/2^-$ one at a nearly identical energy of 181 keV. Yet perhaps more importantly, it put aside the need to fall back to the Nilsson scheme.

After an upgrade of the Lise spectrometer the experiment was repeated on a beryllium target [Pet16]. In the subsequent analysis with statistics that were now four times superior, the $\gamma\gamma$ coincidence relation reported before was not confirmed and instead two isomeric levels with improved half-lives of 310(8) and 149(5) ns were fixed at 62 and 66 keV. The isomeric nature was understood from the close energies and the suggested spins and parities were kept, still without settling on their sequence. Recalling the initial shell-model result, it obviously fits the spacing much better. Calculations with the competing jj44b and JUN45 interactions predict the $3/2^-$ state at around 100 keV but project the $1/2^-$ one between 500 and 1000 keV, as shown in figure 2.22. Whatever spin sequence is chosen the expected $B(E2, 3/2^- \rightarrow 5/2^-)$ transition strength underestimates the measured value, which can be explained by mixing with a $M1$ component. The $B(E2, 1/2^- \rightarrow 5/2^-)$ element is better modelled, but the deduced differences between both spin arrangements are too subtle to discriminate in a meaningful manner. In either case the $1/2^-$ state remains largely prone to deformation,

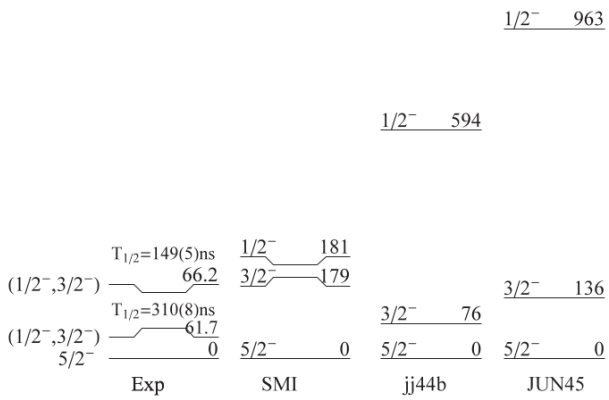

FIGURE 2.22: Experimental level scheme for ^{75}Cu compared to shell-model predictions from the Madrid-Strasbourg (labelled SMI), jj44b, and JUN45 interactions. Taken from [Pet16]

boasting a $B(E2)$ value to the ground state in excess of 16 Weisskopf units. Precisely a lack of collectivity may clarify why the energy of the $1/2^-$ state is not properly recovered with the jj44b and JUN45 forces.

The eventual measurement of the magnetic moment of the 66-keV level at RIBF keenly hit the charts [Ich19]. Fragmentation of a primary beam of ^{238}U on a beryllium target was followed by the removal of a proton from the selected secondary beam of ^{76}Zn on a chip of aluminium. The spin alignment that is inherent in the reaction mechanism was combined with an appropriate momentum setting of the Bigrips spectrometer to ensure that a significant fraction of 30% of it was preserved. By analysing the time-dependent oscillation in the angular distribution of the emitted γ radiation, the spin and parity was finally confined to $3/2^-$. The resulting magnetic moment obeyed the downwards trend of the $3/2^-$ states that we printed in figure 2.4. As there was no assessable spatial anisotropy in the experimental set-up for a $1/2^-$ state, the spin and magnetic moment of the latter could not be measured but its energy was hashed out at 62 keV. The data seemed well comprehended from the accompanying shell-model calculation with the A3DA-m Hamiltonian, a refinement by the Tokyo school of the A3DA force that we shall encounter in our next section and for which it now suffices to say that it acts in the $fpg_{9/2}d_{5/2}$ space [Tsu14]. Both the $1/2^-$ and $3/2^-$ states were interpreted as superpositions of a neutron excitation of the nickel core with a sole proton in the $\pi p_{1/2}$ respectively $\pi p_{3/2}$ orbital. While the statement appears somewhat oblivious to the common ordering of spin-orbit partners and the energy by which they

are separated, any deeper intricacies were blamed by the authors on admixtures in the wave functions.

The claim of a lingering single-particle character with a correlated core hidden beneath for the low-energy states in ^{75}Cu makes dawn a conclusion of a pervading tension between sphericity and deformation in the structure of the copper isotopes. It sounds, however, as a confusing enigma that the duality would already manifest itself within the individual states rather than across opposite ones. In the face of such democratic distribution of deformation, the burden may then even come the other way around and it is the energy drop of an abnormally pure $\pi f_{5/2}$ level that would be hardest to understand. At the very point when steady migration finally provokes a $5/2^-$ ground state in ^{75}Cu, the deformed $1/2^-$ level reaches its lowest excitation energy. One wonders if both would ever interact or instead the $1/2^-$ state would composedly turn upwards again as collectivity slowly dissipates on the way to $N = 50$. Warily seeking a better comprehension of the inner workings of collectivity, it seems therefore useful that we put our findings into a larger context.

2.5 Deformation and shape coexistence

We may attempt to gain an insight in the collectivity of the copper isotopes by gauging the behaviour of the underlying nickel core. Scanning through the range of accessible isotopes we expect that ^{68}Ni occupies a prominent spot, as the 40 neutrons it contains neatly add up to a subshell. The degree of magicity they lend to the nucleus, however, has proven controversial. The putative closure was foremost recognised from the occurence of a 0^+ first excited state at 1.77 MeV [Ber82]. Through a theoretical analysis with the density-dependent D1SA sibling from the family of forces created by Daniel Gogny at Bruyères-le-Châtel and refined for surface properties and pairing correlations, it was clarified as a shape isomer [Gir88]. The elevated energy of the 2^+ level at 2033 keV drew similarity to its valence mirror ^{90}Zr ($Z = 40$), where the numbers stand at 1761 and 2186 keV for the excited 0^+ and 2^+ states, respectively [Bro95]. More insight was gleaned from its β decay, however suggesting that the magic nature would not extend far and already the single proton in ^{69}Cu would polarise the core

[Mue99]. Also the decay of ^{68,70}Co stressed the importance of collective contributions in the wave functions of the ^{68,70}Ni daughters [Mue00].

The isotopes were next investigated at Ganil. While ^{68}Ni fragments were collected from the reaction of a primary beam of ^{70}Zn on a nickel target [Sor02], particles of ^{70}Ni along with a contamination of ^{74}Zn were produced from incoming ^{76}Ge on beryllium [Per06]. The species were transmitted through the Lise spectrometer before they hit a foil of ^{208}Pb, sustaining Coulomb excitation at average energies of 38 or 39 MeV per nucleon. The measurements were performed by photon and ion counting and normalised relative to the known figures for ^{70}Zn or ^{76}Ge. Upon examining the deduced $B(E2, 0^+ \rightarrow 2^+)$ transition probabilities, the low value of 270(60) e^2fm^4 or 16(4) Weisskopf units in ^{68}Ni jumped to 860(140) e^2fm^4 or 50(8) Weisskopf units in ^{70}Ni. The phenomenon was understood as a manifestation of superfluidity in ^{68}Ni, in which neutrons flow without hindrance into the $\nu g_{9/2}$ orbital across the $N = 40$ gap because of the energy they gain from the pairing force. The $g_{9/2}$ neutrons exert a tidal force on their underlying siblings and core polarisation is triggered in ^{70}Ni.

When pondering on the effect in detail, the two $g_{9/2}$ valence neutrons in ^{70}Ni would pull protons out of their $f_{7/2}$ orbit across $Z = 28$ because of a repulsion between the $\pi f_{7/2}$ and $\nu g_{9/2}$ single-particles states. Perceived as the counterpart of an attraction between $\pi f_{5/2}$ and $\nu g_{9/2}$, it was linked to the work on the tensor force by the Tokyo group that we kept on hold at the end of section 1.2. Here the idea bounced back as a versatile explanation for shell evolution in the nickel region and for the first time a tensor view was pinned to the monopole migration of the $\pi f_{5/2}$ state in copper. It is noteworthy that the shell-model predictions from the Madrid-Strasbourg Hamiltonian in its original version as developed for the description of ^{68}Ni could not keep pace with the rapid rise of collectivity in ^{70}Ni, but neither could a calculation with pairing and quadrupole forces in the Quasiparticle Random-Phase Approximation (QRPA). An overview of the scene is assembled in figure 2.23.[9]

We bring to the attention that the authors of the QRPA model promoted the idea that the apparent subshell closure at $N = 40$ might be provoked by the unhampered scattering of neutron pairs into the $g_{9/2}$ orbital of opposite parity [Lan03a]. The mech-

[9] In figure 2.15 the five times smaller quantity $B(E2, 2^+ \rightarrow 0^+)$ is given

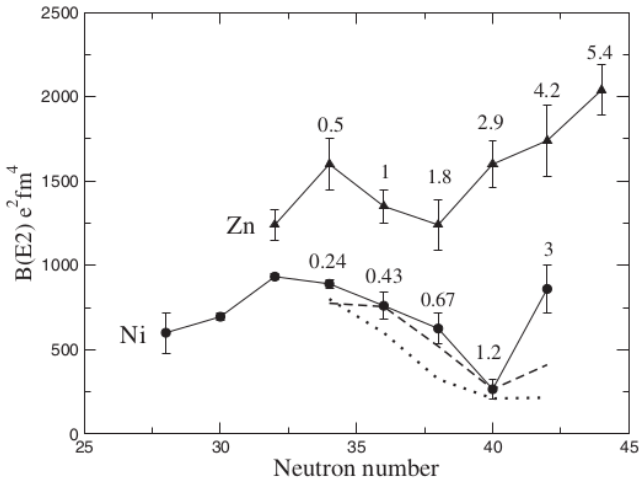

Figure 2.23: Experimental $B(E2, 0^+ \rightarrow 2^+)$ values from Coulomb excitation for the nickel and zinc isotopes compared to the shell-model prediction from the Madrid-Strasbourg interaction (dashed) and a QRPA model (dotted line). Taken from [Per06]

anism would supplant proton correlations and hence result in a low $B(E2)$ figure, while the energy gap would merely mirror the strength of the pairing force. The $\nu g_{9/2}$ orbital would still fill abruptly across $N = 40$ such that a sharp and sudden onset of monopole migration ensues, but the effect is accommodated with the absence of an appreciable impact on the mass surface as acknowledged from the Penning-trap measurements at Isolde and Jyväskylä [Gue07, Rah07]. The interpretation also patches up matters with the laser spectroscopy of the copper isotopes at Collaps at Isolde, where no particular polarisation of the core was apparent away from $N = 40$ [Vin10].

While for ^{74}Zn the transition rate of 2040(150) e^2fm^4 or 111(8) Weisskopf units fell not far from the systematics, as can be confirmed from figure 2.15, the high value that was obtained for ^{70}Ni prompted further investigation of the isotopic chain. Inelastic proton scattering by a ^{74}Ni beam off a liquid-hydrogen target took place at 81 MeV per nucleon at NSCL [Aoi10]. The experiment sought to determine the deformation length δ, which is defined as the product of the quadrupole-deformation parameter β_2 and the nuclear radius R and can be expressed by the formula

$$\delta = \frac{4\pi}{3ZeR}\sqrt{B(E2, 0^+ \rightarrow 2^+)} \tag{2.6}$$

with $R = 1.2A^{1/3}$ fm. Imagining the protons and the neutrons to move together, the result of 1.04(16) fm that was found corresponds to an upwards $B(E2)$ of 1230(380)

e^2fm^4 or 67(21) Weisskopf units. The strongly enhanced quadrupole correlation was explained by the weakening of the $Z = 28$ shell cleft due to the tensor interaction and simultaneous excitations of neutrons across the $N = 50$ divide, portending a loss of magicity in ^{78}Ni. The aforementioned shell-model calculations still could not tune to the right height of pitch but nevertheless drew a bit better on the muse of mime than those with the NR78 (jj44pna) force from the Michigan-Darmstadt team.[10]

As pleasing as it seemed, the spectacle was interrupted not so long after. The picture was diluted, not to say contradicted, by a series of experiments. We mentioned before in section 2.3 the deep-inelastic measurement on ^{71}Cu at Argonne [Ste09a]. The level scheme was extended with two newly found transitions atop the $19/2^-$ microsecond isomer at 2756 keV. The latter can be explained as the coupling of the $p_{3/2}$ ground-state proton to the analogous 8^+ isomer at 2860 keV in the ^{70}Ni core, generated from a stretched $g_{9/2}$ neutron pair. The γ transition of 2020 keV that stands above the copper isomer would contain the energy that is necessary to shuttle two neutrons between the fp and the $g_{9/2}$ orbitals, creating at the upper end $\pi p_{3/2}\, \nu(fp)^{-2} g^4_{9/2}$ configurations. It is a cogent observation that it concurs with the 2^+ energy of 2033 keV in ^{68}Ni. Up to the isomer, the semi-magic nickel core would persist before being broken, which pushes aside the idea of core polarisation at low energy that was inferred from the data at Ganil.

In the Coulomb excitation of ^{74}Ni, carried out at an energy of 96 MeV per nucleon at NSCL, a much smaller value for $B(E2, 0^+ \rightarrow 2^+)$ of 640(230) e^2fm^4 or 35(12) Weisskopf units was obtained [Mar14]. This could nonetheless be reconciled with the previous result from inelastic proton scattering. Using Aron Bernstein's relation for the ratio of the neutron and proton matrix elements in hadronic and electromagnetic transitions M_n/M_p and observing that with a proton probe the neutron distribution is scrutinised three times more intensely than the proton one [Ber81], the authors argued that the neutrons would take the lion's share in the large deformation length. The protons for their part would stick together in a rather rigid structure that brings about the low $B(E2)$ value seen in Coulomb excitation. The experimentally derived fraction M_n/M_p equalled 2.4(8), which was comforted by LNPS calculations that yielded

[10] When the literature refers to [Lis04] or [Lis05] without naming the interaction, from comparison with other articles we shall designate it by NR78 (jj44pna)

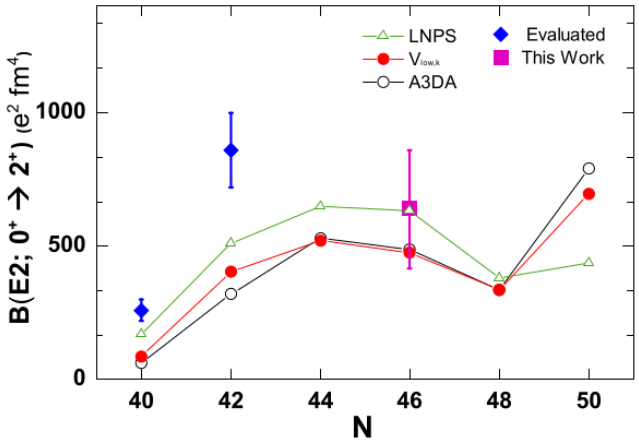

Figure 2.24: Experimental $B(E2, 0^+ \rightarrow 2^+)$ values from Coulomb excitation for the nickel isotopes compared to shell-model predictions from the LNPS, A3DA, and $V_{\mathrm{low}-k}$ interactions. Taken from [Mar14]

$M_n/M_p = 1.8$. It would mean that the neutron excitations decouple from the protons and the core polarisation that was perceived in ^{70}Ni peters out. Only when the neutron shell closes upon reaching $N = 50$, proton excitations would set in and the transition rate would rise again.

A marked increase of the $B(E2)$ value towards ^{78}Ni was even more evident in two other theoretical models that deserve attention. The A3DA force, first developed by Honma at Fukushima and revised by the group in Tokyo, combined the GXPF1A and JUN45 Hamiltonians with G-matrix elements from the N^{3}LO chiral interaction by Entem and Machleidt in order to span the $fpg_{9/2}d_{5/2}$ space [Shi12]. The calculation reproduced the experimental result for ^{74}Ni albeit at the lower limit of the experimental range. For ^{78}Ni, however, the collectivity would curiously surpass that of the entire subshell. A fresh addition to the stage came from the $V_{\mathrm{low}-k}$ interaction implemented in the $\pi f_{7/2}p_{3/2}\nu pf_{5/2}g_{9/2}d_{5/2}$ space by Luigi Coraggio and the group from Naples [Cor14]. Properly following a parabolic curve that also the other calculations set out till $N = 48$, once again an intriguing collapse of magicity seemed to lurk at $N = 50$. The numbers are summarised in figure 2.24.

Still at NSCL the excited states of ^{72}Ni were the subject of a lifetime measurement [Kol16]. After proton knock-out from ^{73}Cu on beryllium, the secondary beam arrived at a plunger with an energy of 102 MeV per nucleon. Determining the de-

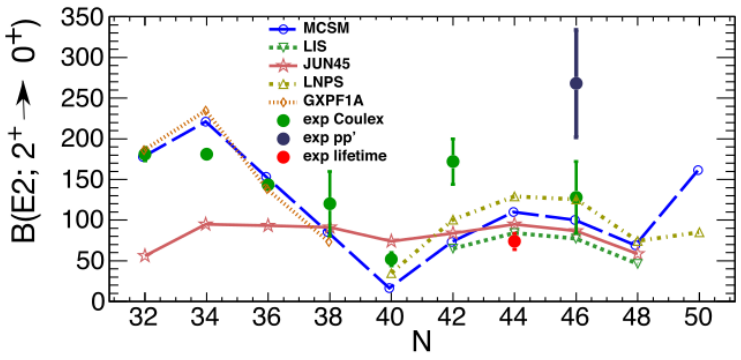

FIGURE 2.25: Experimental $B(E2, 2^+ \rightarrow 0^+)$ values from Coulomb excitation, inelastic proton scattering and lifetime measurements for nickel isotopes compared to shell-model predictions, among which MCSM refers to A3DA and LIS to NR78 (jj44pna). The (p,p') value for ^{74}Ni is misstated and should equal 246(76) e^2fm^4. Taken from [Kol16]

cay curve from two data points only, the RDDS technique yielded a $B(E2, 0^+ \rightarrow 2^+)$ value of 370(50) e^2fm^4 or 21(3) Weisskopf units with a surprisingly small error bar. Nonetheless the outcome was yet again lower than expected, lying at the lower end of the theoretical range of four different shell-model calculations that spanned the globe from Michigan-Darmstadt over Madrid-Strasbourg to Tokyo. If one requires a correct treatment of ^{68}Ni then credibility would be lent more easily to LNPS than to NR78 (jj44pna), JUN45, or A3DA, but the capricious spread of the data forced it to overshoot the transition rate in ^{72}Ni by the same factor of 1.7 as by which it undershot it in ^{70}Ni. The NR78 (jj44pna) solution systematically delivered weaker strengths that hence fitted ^{72}Ni better than ^{70}Ni, while A3DA prudently held the middle. Plotted in figure 2.25, the compiled results present a riddle that perhaps illustrates the difficulty to perform these measurements accurately and the theoretical balancing act that it may set off.

But the mystery could be unfolding. While rather aiming at dipole strengths, the Coulomb excitation of a beam of ^{70}Ni at 260 MeV per nucleon on a secondary gold target at RIBF occasioned a new measurement of the $B(E2, 0^+ \rightarrow 2^+)$ value in this nucleus, yielding 428(210) e^2fm^4 or 25(12) Weisskopf units, half the amount of the earlier result [Wie18]. Even with the large error bar, it brought the number much closer to the theoretically expected parabola. Deformation lengths were obtained at RIBF from the scattering of ^{72}Ni at an average energy of 238 MeV per nucleon and ^{74}Ni at 231 MeV

per nucleon in a thick target of liquid hydrogen [Cor18]. They were extracted from the measured (p,p') cross sections by means of coupled-channel reaction calculations that involved a pool of parameters, in particular the KD02 global potential of Koning and Delaroche. Unlike the figures from Coulomb excitation they included the contribution from the neutrons in the nucleus and so the extracted nuclear deformation β_2 exceeded the electromagnetic quantities by 15 to 30%. As it is visible in figure 2.26, this made ^{74}Ni end up within the error bars from the earlier scattering experiment. For ^{76,80}Zn, however, the (p,p') data fell below those that were reported for Coulomb excitation, perhaps hinting at unobserved feeding contributions or limitations in the reaction model.

The light shed by theory did not penetrate far. While not comparing directly to the scattering outcome, $B(E2)$ computations within a QRPA approach with the Gogny D1M interaction surpassed the value from Coulomb excitation for ^{72}Ni by 20% but for ^{74}Ni plodded 25% below. The LNPS interaction produced numbers that roughly offered the same conclusions as for QRPA, straying 60% above for ^{72}Ni and 15% below for ^{74}Ni.[11] Invoking the Jeukenne-Lejeune-Mahaux folding model, the ratio M_n/M_p could be determined by combining the input from theory and experiment and was found to top N/Z, indicating that neutrons would dominate the collectivity while protons would retain the magicity.

Relativistic Coulomb excitation of ^{74}Ni with the Euroball-Riken Cluster Array (Eurica) of 84 encapsulated germanium crystals arranged in twelve cryostats at RIBF joined the hustle [Got20]. The extracted result was consistent with the two previous figures from inelastic proton scattering and touched the upper range of the error bar of the equivalent measurement at intermediate energy. It thus left room once again for the original claim of core polarisation, whereas any clear parabolic behaviour of the $B(E2)$ strength would remain compromised. For its theoretical context the article drew upon the PMMU Hamiltonian by Kazunari Kaneko at Fukuoka and collaborators [Kan14]. The abbreviation refers to the recipe of pairing, multipole, and monopole terms with which a universal description of all mass regions is aimed at. Moderate agreement was achieved, albeit better than what the Parthenopean $V_{\mathrm{low}-k}$ interaction delivered.

[11] The article refers to the frame of the interaction as the Large-Scale Shell Model (LSSM), a tag which however we shall reserve for the newer version that appears in [Tan19]

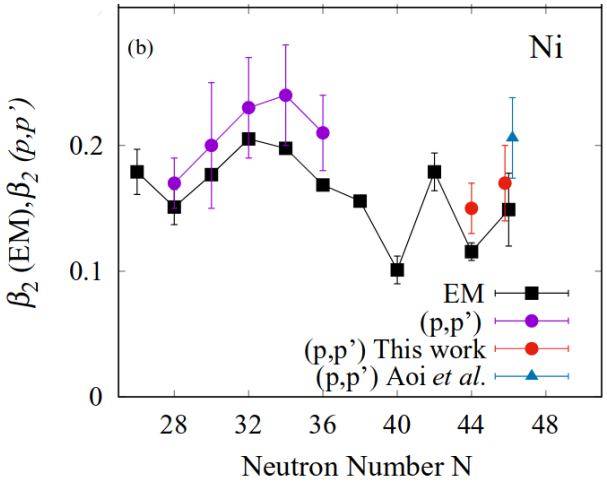

FIGURE 2.26: Experimental β_2 deformation parameters from electromagnetic probes and inelastic proton scattering for the nickel isotopes. Taken from [Cor18]

We may also wish to take a look at the excited 0^+ states in the nickel isotopes. First we dwell on ^{68}Ni, which as we mentioned above procures intensive interest from the pivotal 0^+ state it harbours at 1.77(3) MeV [Ber82]. The momentous result, which we show in figure 2.27, was established from the angular distribution in the (^{14}C,^{16}O) reaction at 72 MeV measured with a 180° magnetic spectrometer at the tandem accelerator at Orsay. It was immediately recognised that a semi-magic nucleus was being explored, the first 2^+ level presenting itself only at 2.20(3) MeV. Drawing a parallel to ^{90}Zr at $Z = 40$, the gain in pairing energy by lifting two particles into the $g_{9/2}$ neutron orbital was deemed at the origin of the inversion in the conventional level ordering. A Hartree-Fock-Bogoliubov calculation confirmed the presence of a deformed minimum at $\beta_2 = 0.4$ lying next to the spherical ground state.

A possible third 0^+ state is located at 2511 keV and was populated in the β decay of ^{68}Co at Lisol [Mue00]. A claim for a 0^+ level at 2202 keV was advanced through an experiment with a ^{238}U beam on a ^{70}Zn target at 6.33 MeV per nucleon carried out at Ganil [Dij12]. The assertion was reinforced by the prediction of a 2p-2h intruder configuration, specifically $\pi f_{7/2}^{-2}$, at an energy of precisely 2202 keV [Pau10]. The concordance was astonishing, since the estimate relied on simple arithmetics and was only meant to be accurate within 100 keV.

The level, however, was not seen in the reverse experiment with a beam of ^{70}Zn

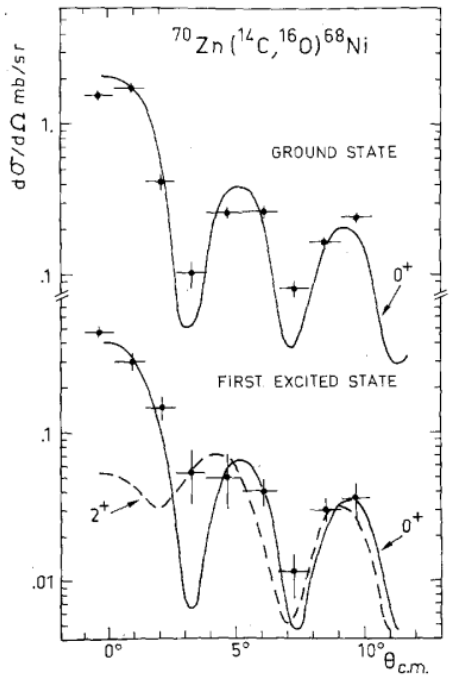

Figure 2.27: Angular distributions of the ground state and first excited state at 1.77 MeV in the ^{68}Zn(^{14}C,^{16}O)^{68}Ni reaction. Taken from [Ber82]

at 6.14 to 6.29 MeV per nucleon on targets of ^{197}Au, ^{208}Pb and ^{238}U at Argonne soon after [Chi12]. The 0^+ assignment for the state at 2511 keV on the other hand was confirmed, the $\gamma\gamma$ angular correlation of which is reproduced in figure 2.28 and depended crucially on a single data point. The confusion in the Ganil measurement can possibly be ascribed to an insufficient resolution of the mass and charge identification of the Vamos spectrometer at that time.

The interest in ^{68}Ni did not subside. At NSCL a beam of ^{70}Ni, itself produced in the fragmentation of ^{82}Se on beryllium, was directed onto a secondary chip of the same material [Rec13]. The two-neutron knock-out reaction at an average energy of 75 MeV per nucleon was carefully puzzled out and the energy of the second 0^+ state was brushed down from 1770(30) to 1603.5(3) keV. Oddly enough the intensity relations in the level scheme were taken from earlier work by the same group [Chi12] but differed from it, as can be checked from figure 2.29. The context and corollary for placing the 1139-keV ray below and not above the one at 662 keV, which fixed the energy of the 0^+_2 state, remained plausible nonetheless. The paper abundantly compared the result to shell-model calculations based on the jj44pna, jj44b, JUN45, LNPS and

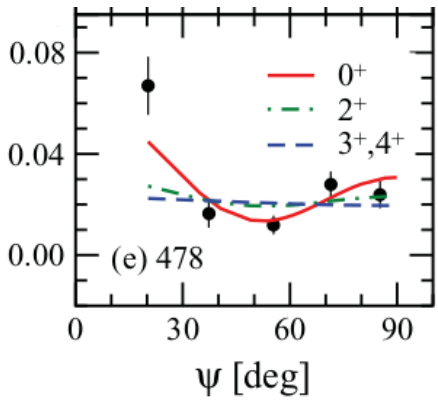

FIGURE 2.28: Angular correlation of the 478-keV γ ray deexciting the 0^+ level at 2511 keV in ^{68}Ni. Taken from [Chi12]

A3DA interactions, where we recognise jj44pna as a variant nomenclature for NR78. The outcome for the first three of these was rather similar, however unable to foresee within their $f_{5/2}pg_{9/2}$ model space a third 0^+ state below 3.5 MeV. Only the larger πfp $\nu pf_{5/2}g_{9/2}d_{5/2}$ and $fpg_{9/2}d_{5/2}$ bases of LNPS respectively A3DA managed to do so.

The analysis concluded that extensive configuration mixing, in which several neutrons are lifted from the $pf_{5/2}$ orbitals to the $g_{9/2}$ one across $N = 40$, would be prevalent even in the ground state. Collectivity would be induced and from the measured transition rates three distinct structures in the nucleus transpired, corresponding to each of the 0^+ states. Although the deformation was not experimentally determined, the calculations professed that the ground state would contain a closed neutron configuration for more than 30% joined to an equal amount of the $\nu g_{9/2}^2$ excitation, the 0_2^+ would mainly be triggered by the elevation of two neutrons, and the 0_3^+ owe its arrival to the promotion of two protons. While the different sources of deformation would provide the frame for multiple shape coexistence, they would also help to clarify the seemingly conflicting results from the Coulomb excitation that we attested to above, as various states would bear various amounts of neutron or proton collectivity.

A next experiment at NSCL focussed on the decay of the 0_2^+ state by internal conversion [Suc14a]. A sample of ^{68}Co was produced in the fragmentation of a ^{76}Ge beam and implanted in a double-sided germanium strip detector. Its β decay fed the excited 0_2^+ state in ^{68}Ni, the half-life of which in turn was refined to 268(12) ns and its energy put at 1605(3) keV. From the measured $E0$ transition strength to the ground

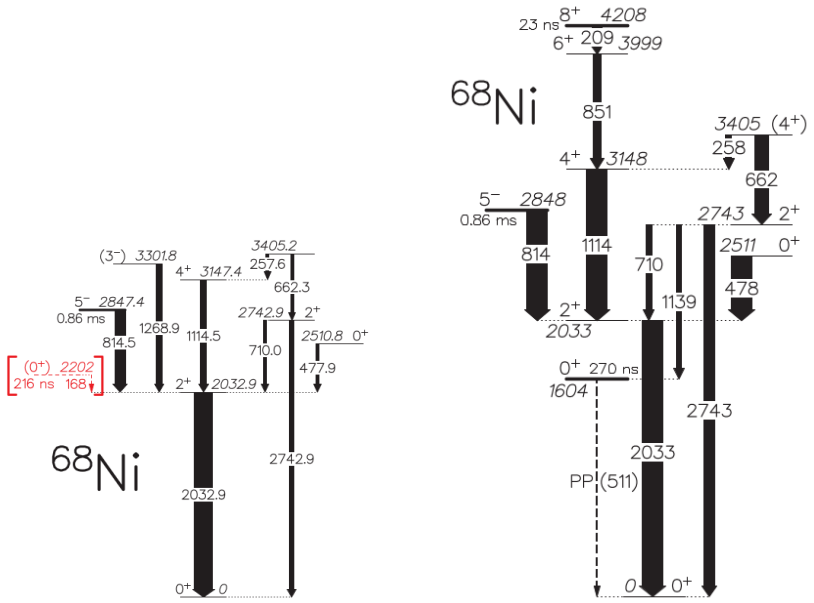

Figure 2.29: Partial level schemes of ^{68}Ni where the width of the arrows represents the intensities of the transitions according to [Chi12] (left) and [Rec13] (right)

state a difference of mean-square charge radii between the ground state and the isomer of 0.15 fm^2 was inferred, which is of the order of the increase in charge radius between two neighbouring isotopes. On this occasion the A3DA results were reported upon in depth, putting forth a potential-energy surface that is illustrated in figure 2.30 and contains three minima. It supported the interpretation in which a spherical ground state and an oblate excited 0^+_2 state coexist, while the 0^+_3 configuration for its part was predicted to take on a prolate shape.

Some difficulties persist, however. Considering that the neutron effective charge is generally smaller than the proton one, it is surprising that the $E0$ strength in ^{68}Ni is larger than in its proton counterpart ^{90}Zr, that is $\rho^2(E0) = 7.6(4)\,10^{-3}$ compared to $3.46(14)\,10^{-3}$. Moreover it is stated that the 0^+_1 and 0^+_2 states strongly mix and indeed the minimum in the potential energy is not very deep. Back in section 1.1 we defined shape coexistence as the occurrence within the same nucleus of distinct shapes with little interference among them. Relative to a spherical ground state the deformed excited states come down in energy because of the quadrupole correlations that ensue when protons and neutrons are excited across shell gaps, a phenomenon known as intruder states.

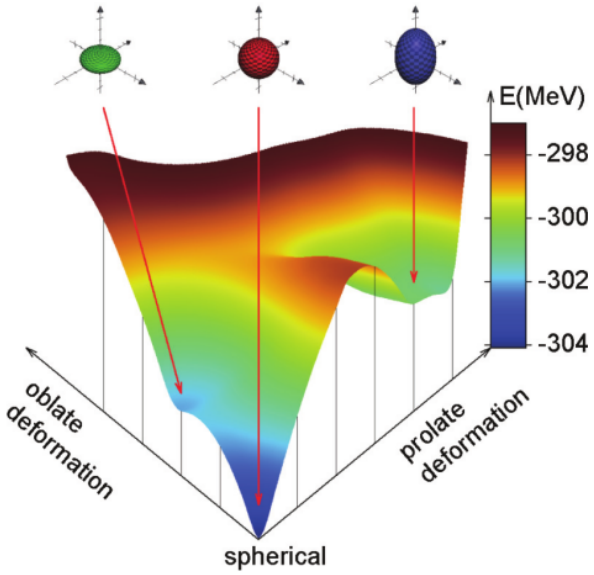

FIGURE 2.30: Potential-energy surface of ^{68}Ni calculated with the A3DA interaction. Taken from [Suc14a]

The topic was revisited by the Tokyo shell-model group with an updated version of the A3DA Hamiltonian, which we have already hinted at in the previous section and which was denoted A3DA-m [Tsu14]. The literature gives no details on the precise alterations that it encompassed but conceptually it introduced the notions of type-I and type-II shell evolution. The former describes the change in single-particle energies as a function of a varying number of protons or neutrons, while the latter refers to any such change that depends on the particular configuration within the same nucleus, such as the deformation that is induced by particle-hole excitations. As neutrons are added in the $\nu g_{9/2}$ subshell to ^{68}Ni, the gap between the $\pi f_{7/2}$ and $\pi f_{5/2}$ states narrows, flaunting a famous example of type-I behaviour. In exactly the same manner, as neutrons are promoted into the $\nu g_{9/2}$ orbital creating states at higher excitation energy in the ^{68}Ni nucleus itself, the very proton gap is reduced and the nascent deformation is stabilised. This type-II effect is dramatically demonstrated in figure 2.31, where for the 0^+_3 state four neutrons would be excited into $\nu g_{9/2}$ that in turn let more than two protons slip out of $\pi f_{7/2}$ across $Z = 28$. As a result the 0^+_3 state is deeply mired in a prolate minimum with $\beta_2 \approx 0.4$ at 2.9 MeV above the spherical ground state. The 0^+_2 state sports an oblate appearance with $\beta_2 \approx -0.2$ at an energy of 1.6 MeV. Although in figure 2.30 the

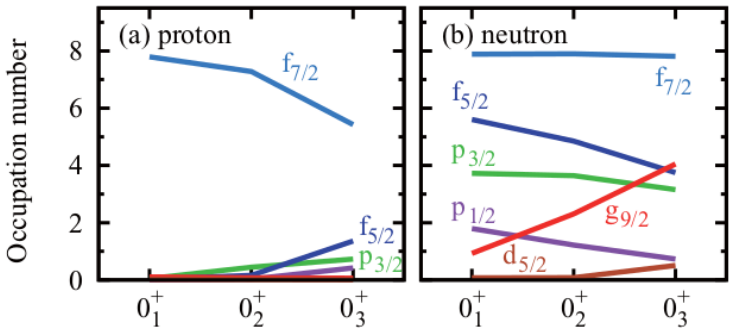

Figure 2.31: Occupation numbers of proton and neutron orbitals for 0^+ states in ^{68}Ni with the A3DA-m interaction. Taken from [Tsu14]

potential passageway from 0^+_2 to 0^+_1 runs low enough to overcome, mixing is prevented by the antisymmetrisation of the wave functions. Tellingly it is the monopole part of the tensor interaction rather than the proton-neutron quadrupole force that brings about the modification of the orbital energies such that particle-hole excitations set in more rapidly and deformation emerges.

At Isolde ^{68}Ni was populated in the β decay of ^{68}Mn as it passes through ^{68m}Co [Fla15]. The excited 0^+ states were now fixed at 1603.6(6) and 2511.1(2) keV with a half-life of 235(23) ns for the former, while the level scheme was sorted out in greater detail. Also at NSCL ^{68}Ni was produced following the β decay of ^{68m}Co, this time from an initial sample of ^{68}Fe [Cri16]. The half-lives of the 0^+_2 and 0^+_3 states were determined as 268(12) and 0.57(5) ns respectively. From figure 2.32 one can read that for the shorter one the agreement appeared to be superior with LNPS than with A3DA. Concurrently the fair transition rate of 39.0(34) e^2fm^4 or 2.4(2) Weisskopf units from 0^+_3 to 2^+_1 would draw the prolate and oblate structures closer together, indicating a certain degree of mixing. Likewise intertwined wave functions were recognised for the 0^+_1 and 0^+_2 levels, their mixing angle given by the relation $\cos^2\theta = 0.74$ or $\theta = 31°$. This translated into a difference of mean-square charge radii of 0.17(2) fm^2, in line with the earlier result. It lends to same conclusion as we reached before, namely that the claim by the authors that shape coexistence is firmly established runs rather contrary to the distilled picture in which the distinct characters of the 0^+ states would be diluted. It would cast its shadow on the potential surface plotted in figure 2.30, rivetting the argument on the role of the tensor force within the theoretical model.

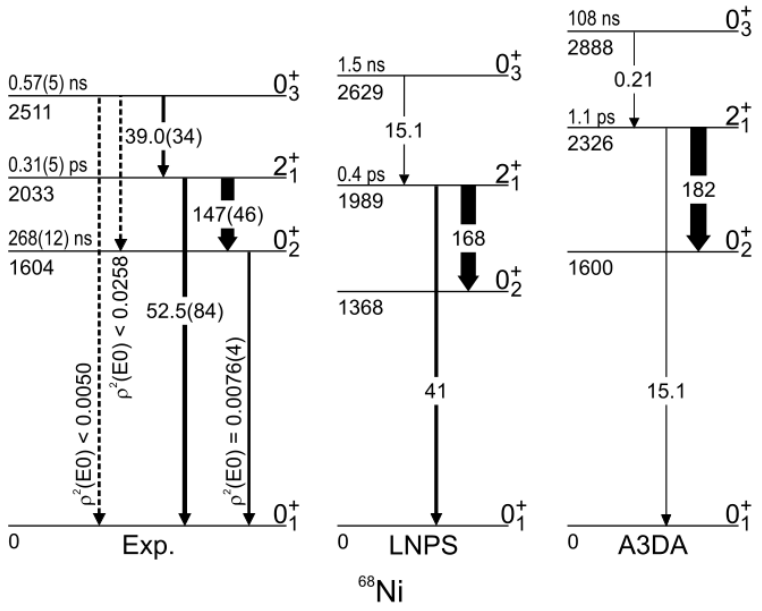

FIGURE 2.32: Half-lives and transition strengths in ^{68}Ni compared to LNPS and A3DA calculations. Taken from [Cri16]

Another quite interesting experiment took place at Isolde, in which a radioactive beam of ^{66}Ni at an energy of 2.6 MeV per nucleon was directed onto a titanium foil implanted with radioactive tritium [Fla19]. By transferring two neutrons onto the incoming projectiles several states in ^{68}Ni were accessed, the spin and parity of which could be assigned from the characteristic angular distribution of the escaping protons. Insight into their structure was gleaned from the cross section of the reaction, writing it as a coherent superposition of contributions from individual single-particle states with expansion coefficients that are known as two-nucleon amplitudes (TNA). Relying on shell-model calculations with the A3DA-m force, the ground state of ^{66}Ni would be built from neutrons in $p_{3/2}$, $f_{5/2}$, $p_{1/2}$ and $g_{9/2}$, which is illustrated in figure 2.33. In the final states of ^{68}Ni the same single-particle components are present. For the 0_1^+ ground state the $\nu p_{1/2}$ contribution swells, although the transfer amplitude remains large in all four channels. The wave function of the 0_2^+ level contains a boosted share of $\nu g_{9/2}$. Only the TNA for the $\nu g_{9/2}$ pair, however, appears to be significant and a cross section is obtained that counts ten times less.

It strikes an awkward tune that the TNA for the $\nu p_{3/2}$ and $\nu f_{5/2}$ pairs when transferred into 0_2^+ are severely suppressed, as the occupation of these orbitals does not

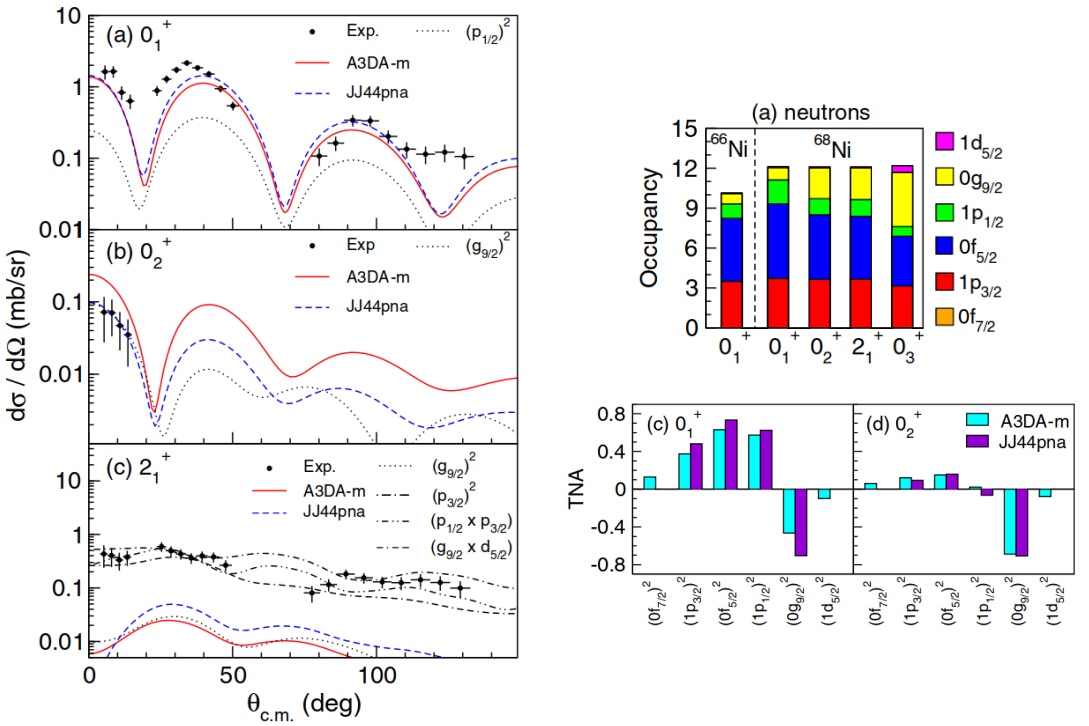

Figure 2.33: Angular distributions for the $0^+_{1,2}$ and 2^+_1 final states in the ^{66}Ni(t,p)^{68}Ni reaction (left). Neutron occupation numbers for selected states in ^{66,68}Ni (top right) and TNA for the $0^+_{1,2}$ final states (bottom right) calculated with the A3DA-m interaction. Taken from [Fla19]

change much from 0^+_1 to 0^+_2. Perhaps the low beam velocity compared to the excitation energy of 1621(28) keV might take its toll and the reaction to the excited state survives essentially because of the much stronger $\nu g_{9/2}$ component in the final state. Although the deformation was not measured directly, the wave function was pried into, from which shape coexistence could be inferred. For the transfer channel to the 2^+ level, however, the theory curiously overestimated the cross section by a factor of ten. The jj44pna interaction, which does not include the $d_{5/2}$ orbital, was equally investigated but yielded a likewise outcome throughout. It would imply that the snag is not related to the size of the model space.

Back at NSCL, in ^{70}Ni shape coexistence was posited based on the observation in the β decay of ^{70}Co of an excited 0^+ state at 1567 keV [Pro15]. From comparison with the A3DA calculation, in which the oblate minimum could not differentiate itself much from the ground state, it was preferentially identified as the prolate structure and thereby would confirm the sharp decrease in energy of more than 900 keV from ^{68}Ni

to ^{70}Ni that was put forward by the theory. It remains unfortunate that once again the deformation could not be measured. Subsequent work managed to extract a half-life of 1.65 ns for the 0^+_2 state and a lower limit for its transition rate to the 2^+_1 level of 58 e^2fm^4 or 3.4 Weisskopf units [Cri16]. The A3DA force anticipated figures of 7.1 ns and 29 e^2fm^4 or 1.7 Weisskopf units, while sadly no results from LNPS were available. In a similar fashion as for the case of ^{68}Ni discussed above, a higher degree of mixing seems present than shape coexistence might warrant.

Also RIBF climbed the boards with the β decay of ^{70}Fe, focussing on type-II shell evolution in the structure of ^{70}Co [Mor17]. In passing we note that the quoted A3DA predictions for ^{70}Ni included above the 0^+_2 prolate state at 1.5 MeV with $\beta_2 > 0.2$, although not accessed experimentally and not further commented upon, an oblate 0^+_3 level at 2.2 MeV with $\beta_2 \approx -0.13$. At RIBF it was also possible to press on to ^{72}Ni, where several candidates for excited 0^+ states populated in the β decay of ^{72m}Co do exist but lack confirmation [Mor16a]. While nothing on excited 0^+ states is known so far in ^{74}Ni, again at RIBF a tentative 0^+ level was catalogued at 2995 keV in ^{76}Ni [Söd15].

Awaiting more data towards ^{78}Ni, we surmise that if the nickel isotopes contain competing structures at nearby energies, deformation must readily surface in their neighbours. Indeed it was shown to set in quickly for the iron isotopes ($Z = 26$) at $N = 40$. At Isolde the 2^+ energies of ^{64,66}Fe were determined from the β decay of laser-ionised manganese [Han99]. Situated at 746 and 574 keV, respectively, they slanted down from the 800-keV bar observed in the preceding isotopes and provided an early indication for collectivity in the region. The effect was linked to a strong interaction between the $\pi f_{7/2}$ and $\nu g_{9/2}$ orbitals. Whereas the standard tensor mechanism would predict a repulsion, the authors however proposed an attraction instead that would lower the $\nu g_{9/2}$ state. As a matter of fact the behaviour seemed similar to what was seen in zinc or germanium, which we illustrate in figure 2.34. A close look reveals that actually the sag sets in two neutrons before. It suggests that the propensity for deformation is dominated by the overlap with $\nu g_{9/2}$, which would be larger for $\pi f_{7/2}$ than for $\pi p_{3/2} f_{5/2}$.

Continuing further below, chromium isotopes ($Z = 24$) were populated in the β

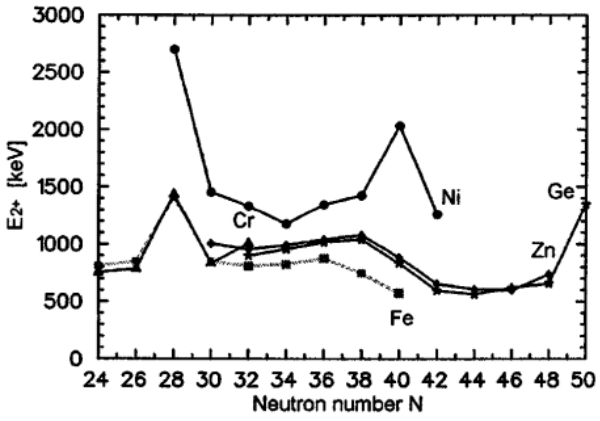

Figure 2.34: Systematics of the first 2^+ energies in the even-even chromium to germanium isotopes. Taken from [Han99]

decay of vanadium, the latter produced from a ^{76}Ge beam on a ^{58}Ni target and selected in the Lise spectrometer at Ganil [Sor03]. Timid 2^+ energies of 646 and 446 keV were spotted for ^{60,62}Cr, from which a strong deformation of $\beta_2 \approx 0.3$ could be inferred. By comparing to the well-known island of inversion at $N = 20$, the importance of the quadrupole force in generating collectivity was recognised. More precisely in the scheme of quasi-SU(3) symmetry proposed by the Strasbourg team, a spin-orbit splitting that is suitably strong pushes the $f_{7/2}p_{3/2}$ orbits to the bottom of the *fp* shell [Zuk95]. In the *gds* shell above, the same would happen for the $g_{9/2}d_{5/2}$ sequence. The interaction is thereupon restricted to the subspaces of these two orbitals, which stand to each other in a $\Delta j = 2$ relationship. The approach harks back to the original SU(3) scheme devised by Elliott and discussed in section 1.1, but the spin quantum number is now absorbed into the mathematical formalism by replacing the orbital momentum ℓ by the total momentum j. Applying the image to the neutron integument, collectivity is generated at $N = 20$ for the former and at $N = 40$ for the latter pair of orbitals both through the monopole and quadrupole terms of the interaction.

For this reason the $\Delta j = 2$ $\nu g_{9/2}$ and $\nu d_{5/2}$ orbitals were included in a dedicated interaction in the $\pi fp\ \nu pf_{5/2}g_{9/2}d_{5/2}$ domain, to which end the Madrid-Strasbourg calculations presented before were supplemented with the relevant two-body matrix elements from Hjorth-Jensen's realistic *G*-matrix force. The shell model showed how the $f_{5/2}$ neutrons are swiftly pulled down by the $f_{7/2}$ protons, while the $d_{5/2}$ ones

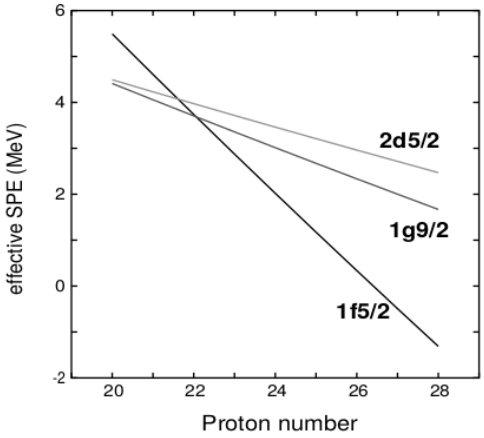

FIGURE 2.35: Evolution of neutron single-particle energies at $N = 40$ from the Madrid-Strasbourg interaction. Taken from [Sor03]

steadily flee the Fermi surface, a behaviour we reprint in figure 2.35. This would leave the $N = 40$ cleft closed in calcium where they are absent and tear it open in nickel where the proton orbital gains full occupancy. Midway in chromium and iron the $\nu g_{9/2}$ level would be enough degenerate with the $\nu f_{5/2}$ and $\nu d_{5/2}$ ones to clear the way for quadrupole correlations. The trend reminds the reader of the tensor analysis, in which the attractive $j_<$ and $j'_>$ orbitals set the rule, and explicit reference was paid to the work by the Tokyo group. By firstly triggering the drift of the $\nu f_{5/2}$ single-particle energy, the tensor point of view might even prepare the path of the quasi-SU(3) model, in which the converging $\nu g_{9/2}$ and $\nu d_{5/2}$ orbitals finally drive the deformation. Digging into the details though, the attempt to reconcile both interpretations might prove hard to hold as none of the $j_>$ orbitals is actually repelled with respect to the baseline, so it remains unclear whether both mechanisms can really be related to each other.

At NSCL from the inelastic scattering of fragmentation beams on a beryllium target it was found that the first excited 2^+ state in ^{64}Cr keeps a low pitch at 420 keV [Gad10]. In the β-decay study of ^{64}V also at NSCL some years later the energy was refined to 430 keV [Suc14b]. The first article mentioned the projected shell model (PSM), developed by Kenji Hara in Munich and focussing on high-spin states [Har95]. Pointing out the influence of the $\nu g_{9/2}$ orbital at low as well as at high spin, it performed fairly well for chromium and iron [Sun09]. Also shell-model calculations were presented that were carried out in the fp space with the GXPF1A code, but at $N = 40$ these did not match

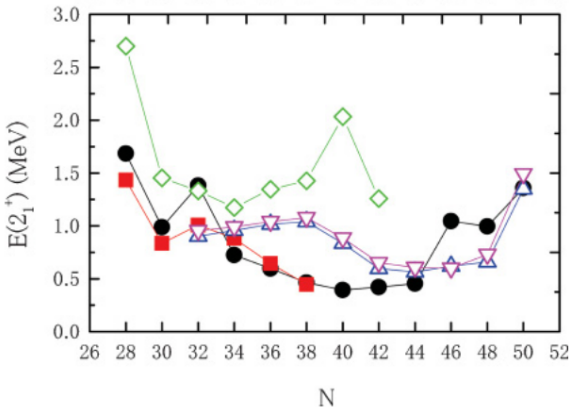

Figure 2.36: Calculated (black) and experimental (red) 2^+ energies in even-even chromium isotopes along with experimental values in nickel (green), zinc (purple), and germanium (blue). The experimental data point from [Gad10] is not shown but fits the calculation. Taken from [Kan08]

the data well. The model space was thereupon expanded with the $\nu g_{9/2}$ state and an early version of the PMMU Hamiltonian from Fukuoka was implemented [Kan08]. It incorporated monopole correction terms that were empirically adjusted without regard to the relative orientation of the orbitals but instead chosen such that the $p_{3/2}$, $f_{5/2}$ and $g_{9/2}$ single-particle energies become nearly degenerate at $N = 40$. Strong closures appeared at $N = 28$ and 32 in chromium but towards $N = 40$ the behaviour was markedly better, with figure 2.36 showing how deformation takes shape on either side of ^{68}Ni. This hinted that there might be no need to include the $\nu d_{5/2}$ particles near $N = 40$, unlike the view that is advocated by quasi-SU(3).

Meanwhile lifetime measurements of 2^+ states with the RDDS method at the Vamos beam line at Ganil confirmed the collectivity in ^{64}Fe, demonstrating a sharp increase in its $B(E2, 2^+ \rightarrow 0^+)$ value from 214(26) in ^{62}Fe to 470^{+210}_{-110} e^2 fm^4 in ^{64}Fe, that is a jump from 15 to 31 Weisskopf units [Lju10]. While large-scale shell-model calculations in the $\pi fp\ \nu fpg_{9/2}d_{5/2}$ space as well as a mean-field model based on the Gogny D1S surface-optimised force met with limited success, the authors brought to the fore the idea of a new island of inversion. Ultimately this provided the basis for putting together the LNPS Hamiltonian, which we have cited in our text before but upon the roots of which we stumble here [Len10]. With the microscopic origin of the deepen-

ing deformation in iron and below as one of its chief motivations, the LNPS interaction pulled under the spotlight the quasi-SU(3) symmetry that we evoked above. Drawing a precise parallel to the region of $N = 20$ near ^{32}Mg, the pattern generates deformation through the action of the quadrupole force. The essential ingredient is the presence of orbitals that stand in a $\Delta j = 2$ relationship to each other, that is $\nu p_{3/2} f_{7/2}$ for $N = 20$ and $\nu g_{9/2} d_{5/2}$ for $N = 40$. With protons confined to the fp shell while neutrons roam the $p f_{5/2} g_{9/2} d_{5/2}$ orbitals, deformation naturally emanates from the computation in a region that is centred on ^{64}Cr.

How the distribution of orbitals came along is a different question, though. From figure 2.37, which in fact represents a development of figure 2.35, one assesses that the $\nu f_{5/2}$ and $\nu g_{9/2}$ particles benefit from a reduced repulsion as protons are removed from the $f_{7/2}$ orbital. But one also sees that the $\nu f_{7/2}$ spin-orbit partner evolves in a parallel fashion, which stands orthogonal to the tensor idea. The same observation is obtained for the $\nu p_{3/2} p_{1/2}$ orbitals, except for an unattended strong attraction between the $p_{3/2}$ neutrons and the $p_{3/2}$ protons for $28 \leq Z \leq 32$. A likewise effect appeared for the $s_{1/2}$ neutrons against the $s_{1/2}$ protons for $14 \leq Z \leq 16$, so a simple overlap of wave functions may contribute to the trend. As to the quasi-SU(3) partners, LNPS assumed an identical behaviour of the $\nu g_{9/2} d_{5/2}$ spacing in nickel as is known from zirconium. Estimating the $N = 50$ gap in ^{78}Ni at 5 MeV, this put the energy difference in ^{68}Ni at 2 MeV, effectively bridging the cleft and setting off quadrupole correlations across it.

Let us now cross $N = 40$. Once more at NSCL, a 2^+ energy of 517 keV was measured in the ^{68}Fe nucleus, created in one and two-proton knock-out reactions on cobalt and nickel isotopes [Adr08]. From the β decay of manganese residues collected after the fragmentation of a ^{86}Kr beam at Ganil, the energy was corrected to 522 keV [Dau11]. Beyond-mean-field calculations with a five-dimensional collective Hamiltonian (5DCH) and the Gogny D1S force as well as the PSM referred to above converged in their description of the deformation, linking it to low-lying $\nu g_{9/2}^2$ configurations. In ^{70}Fe a 2^+ energy of 483 keV was uncovered from the β decay of implanted ^{70}Mn fission fragments at RIBF [Ben15]. A shell-model approach based on the $V_{\mathrm{low}-k}$ interaction from the Naples group indicated an ever growing deformation, which was traced to the $\nu d_{5/2} g_{9/2}$ quadrupole correlations as well as the monopole force between $\pi f_{7/2}$ and

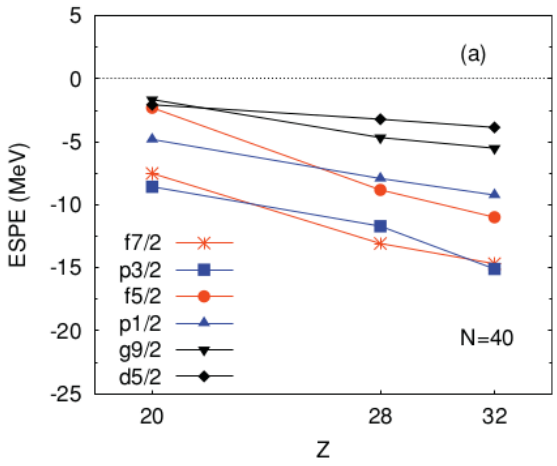

Figure 2.37: Evolution of neutron single-particle energies at $N = 40$ from the LNPS interaction. Taken from [Len10]

$\nu f_{5/2}$, in line with the LNPS work.

The Seastar campaign, standing for Shell Evolution and Search for Two-Plus Energies at RIBF, was launched in an attempt to coordinate several experimental efforts towards the most exotic nuclei available to date. It focussed on proton knock-out of fission fragments on a thick liquid-hydrogen target embedded in the Magic Numbers Off Stability vertex tracker (Minos), selecting the entrance and exit channels in the Bigrips and Zerodegree spectrometers respectively. In-flight γ spectroscopy was achieved with the upgraded Detector Array for Low Intensity radiation (Dali-2) mounted around Minos and composed of 186 NaI(Tl) scintillator crystals for a total photopeak efficiency of 26% at 1 MeV. One of the first results was the confirmation of the 2^+ energy of ^{70}Fe at 480 keV [San15]. In the same bustle the excitation was seen to slowly climb to 520 keV in ^{72}Fe, while in ^{66}Cr the contraction carried on at a lazy pace to 386 keV. So the trend of low 2^+_1 energies appeared to persist along with a growing number of neutrons up to $N = 46$. To better grasp the sense of the numbers we bring them together in figure 2.38, where on the scale that is chosen a rather flat behaviour is discernable for $N \geq 38$ in chromium and $N \geq 40$ for iron. The monopoles of the LNPS force were overhauled and the pairing elements corrected in the $\pi fp\ \nu f_{5/2}p_{1/2}g_{9/2}d_{5/2}$ valence space. From the improved interaction called LNPS-m, exquisite agreement with the data was reaped in all cases. A reasonably constant deformation of the 2^+ state was calculated

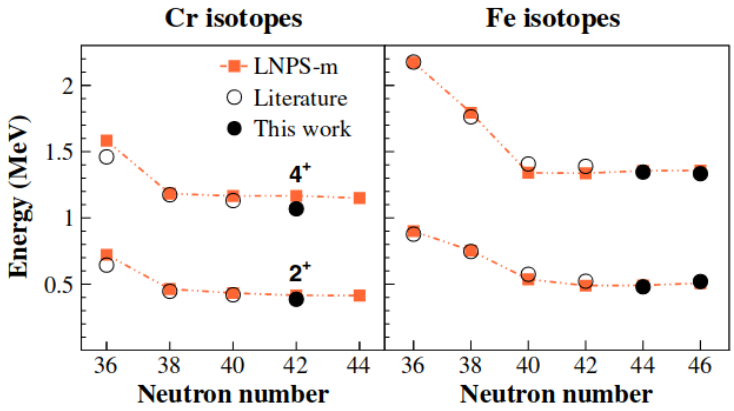

FIGURE 2.38: Experimental 2^+ and 4^+ energies compared to LNPS-m calculations for chromium (left) and iron (right) isotopes. Taken from [San15]

of $0.30 \leq \beta_2 \leq 0.33$ for $^{62-68}$Cr and $0.24 \leq \beta_2 \leq 0.30$ for $^{66-72}$Fe.

Yet a new bud of the Madrid-Strasbourg code superseding LNPS-m was meanwhile put in place [Now16]. Baptised PFSDG-U, it operated in the complete harmonic πfp νsdg realm, by which virtue it naturally included excitations across both the $Z = 28$ and $N = 50$ gaps. Crafting its two-body matrix elements through G-matrix skills from the charge-dependent Bonn potential, the monopole part was touched up and the single-particle energies amended, partly weaving in the values from the JUN45 Hamiltonian. From figure 2.39 we observe that the $\nu g_{9/2}g_{7/2}$ and $\nu d_{5/2}d_{3/2}$ orbitals move in parallel fashion as the $\pi f_{7/2}$ occupation varies, so any reference to a tensor relation would be absent. From the figure we also read that by increasing the neutron number towards $N = 50$, sphericity would not be restored in chromium. Instead the local deformation would morph into yet another island of inversion, the emergence of which would thus manifest an almost regular feature throughout the nuclear chart. Moreover, the known island around ^{64}Cr at $N = 40$ would blend into the newly discovered one around ^{74}Cr at $N = 50$, in which β_2 was set to reach 0.39. Swapping the relevant orbitals for their counterparts in the oscillator shell below, a striking analogy with the evolution from ^{32}Mg at $N = 20$ to ^{40}Mg at $N = 28$ was laid bare. But the impact of PFSDG-U proved even broader, as the real scoop of the exercise swung back to ^{78}Ni, for which a first excited 0^+_2 level at 2.65 MeV was anticipated. Shape coexistence crystallised on the tip of the tongue.

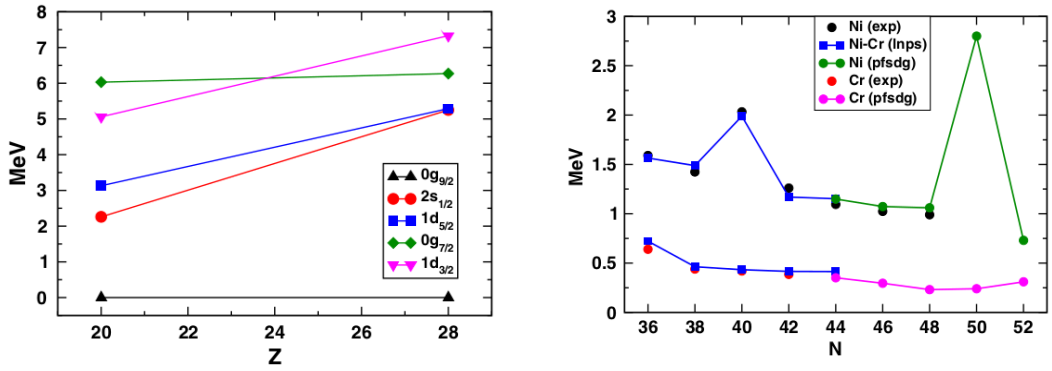

Figure 2.39: Evolution of neutron single-particle energies at $N = 50$ from the PFSDG-U interaction (left) and experimental 2^+ energies compared to LNPS and PFSDG-U calculations for chromium and iron isotopes (right). Taken from [Now16]

2.6 The odd-odd isotopes

Heeding the eagerness of the reader to inquire about the art of magicity, we nonetheless postpone its pursuit and branch off the straight path for a useful excursion into the odd-odd copper isotopes. Their microscopic structure is defined by a single proton beyond $Z = 28$ and an unpaired neutron in the $\nu g_{9/2}$ orbital. In spite of the change in parity a neutron is easily tempted to wander across $N = 40$ and leave a $\nu p_{1/2}$ hole behind because of the greater gain in pairing force that is obtained. Indeed for a schematic surface δ interaction, the energy stored in a 0^+ pair where the particles carry an angular momentum j is proportional to $2j + 1$ so one profits from a factor of five in a $\nu g^2_{9/2}$ configuration compared to $\nu p^2_{1/2}$ [Bru77]. The sole $p_{1/2}$ neutron then combines with the $p_{3/2}$ proton to create a 1^+, 2^+ doublet, while the 3^-, 4^-, 5^-, and 6^- constituents of the $\pi p_{3/2} \nu g_{9/2}$ coupling are to be found at higher energy. If the level ordering among these arrangements gives rise to spin gaps, isomers are likely to appear.

With this picture in mind the β disintegration of ^{68,70}Ni into ^{68,70}Cu was investigated at Lisol along with the study of the ^{69,71,73}Cu isotopes that we have reported on before. Since ^{68}Cu holds a body of only 39 neutrons, the $\nu p_{1/2} \pi p_{3/2}$ configuration unsurprisingly delivered a 1^+ ground state with its likely 2^+ excited complement at an energy of 84 keV above. At 721 keV the promotion of the neutron into the $g_{9/2}$ orbital is known to produce an isomer with a presumed signature of 6^-. It was not observed as the β decay from the 0^+ nickel mother nucleus bypassed it. The 758-keV ray detected in co-

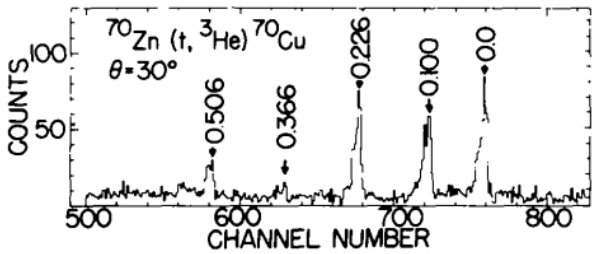

FIGURE 2.40: Spectrum of the ^{70}Zn(t,τ)^{70}Cu reaction with excitations energies labelled in MeV. Taken from [She77]

incidence with the 84-keV transition was interpreted as a low-spin state that attracted a small branch of direct β feeding but standing lonesome never reached publication [Fra99]. Most of the decay strength in fact immediately proceeded to the ground state, as it would require not more than a plain allowed Gamow-Teller conversion from a $p_{1/2}$ neutron to a $p_{3/2}$ proton.

Once we cross the $N = 40$ barrier and come upon the ^{70}Cu nucleus, however, matters become interesting. A transfer experiment with a 24-MeV triton beam from the three-stage accelerator at Los Alamos populated five of its levels through the ^{70}Zn(t,τ) reaction [She77]. The three strongest peaks emerging in the focal plane of the Q3D spectrometer, shown in figure 2.40, were interpreted as members of the high-spin multiplet. From a careful consideration of energy systematics in the neighbouring zinc isotopes the authors cautiously pointed out that the peak designated with 0.0 may not have been the ground state but that a low-spin doublet could have gone undetected a few hundred keV lower, thereby presenting a structure similar as in ^{68}Cu.

The low-spin doublet was uncovered at Lisol. With a spacing of 78 keV, the 1^+ level was put below the 2^+ excited state so as to conform with the significant β-decay branch towards the 0^+ ground state of ^{70}Zn recorded in the literature [Taf71]. It stands for the same Gamow-Teller transmutation as in ^{68}Ni. The Lisol data also contained γ rays that were attributed to the high-spin structure, in particular a sequence of 127 and 140-keV transitions matching two of the energy differences assessed in the transfer reaction. Unfortunately the partial level schemes could not be related to each other. The only available piece of information on their connection came from the known β decay of ^{70}Cu, in which a difference of 140(80) keV had been determined between

the endpoint energies of the isomers in the Kurie plots [Rei75]. While in that study the high-spin isomer had been placed above the low-spin ground state with the said amount, for the clarity of our narration we should stress that this value is not to be confused with the energy of 140 keV established from the transfer reaction within the high-spin multiplet itself.

When it turns hard to disentangle isomeric states with γ spectroscopy, intrasource laser spectroscopy offers a powerful tool. We have dwelled on it in detail already in section 2.1 when evaluating the ground-state spin of ^{75,77}Cu but the principle had actually been pioneered at Gatchina near Saint Petersburg more than twenty years earlier [Mis87]. Indeed it had been noticed that by scanning the wavelength of the laser that was used in a resonant ionisation scheme in the ion source it was possible to discriminate the isomeric states in ^{141}Sm and ^{164}Tm. Once the laser linewidth was adequate, which equalled 3 GHz for the isotopes of ytterbium, it became feasible to extract nuclear charge radii and electromagnetic moments from the centroids and shapes of the measured hyperfine structures [Alk92]. At Isolde, the method was first applied to the silver isotopes because of their large intrinsic hyperfine splitting, where even with a royal resolution of 12 GHz the ^{107m}Ag isomer could be separated out [Fed00].

Despite the smaller splitting for lower masses, intrasource spectroscopy was soon put to use at Isolde to elucidate the structure of the ^{68}Cu and ^{70}Cu isotopes. Within a two-step scheme a first laser scanned a narrow region around 327.4 nm while a second one at 287.9 nm resonantly ionised the particle. For ^{68}Cu, we illustrate in figure 2.41 the ability it bore to select one isomer against another [Koe00a]. The intrinsic bandwidth of the scanning transition amounted to 1.2 GHz but was broadened by the Doppler effect in the hot ionisation cavity to 3.8 GHz. In the experiment on ^{70}Cu, with the same laser sequence the level schemes for the $\beta\gamma$ decay of either isomer were sorted out and the magnetic moments deduced [Koe00b]. The spin and parity assignments of 1^+ for the ground state and $(3\text{-}6)^-$ for the isomer were copied from the literature, as the accuracy of the data did not allow for a more precise statement.

The magnetic moments of ^{68,70}Cu were analysed with greater care in a next publication [Wei02]. The adopted assignments of 1^+ for ^{68g}Cu and 6^- for ^{68m}Cu complied with the literature. In figure 2.42 we plot the spectra recorded for ^{70}Cu. The fits

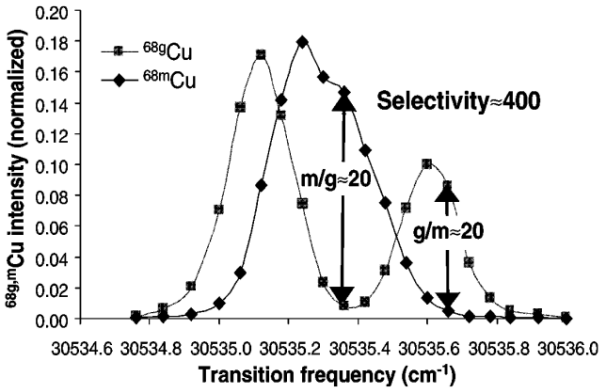

FIGURE 2.41: Yield of ^{68m,g}Cu as a function of the wave number of the first-step of the laser ionisation scheme. Taken from [Koe00a]

comprised four transitions, since the total electron spin in the atomic lower and upper levels equalled $^1/_2$ so both states split in two. From the figure we discern the intensity variations of specific γ transitions in the upper and middle panel or eventually the β-decay yield in the lower panel as a function of the laser wavelength, which brought irrefutable evidence for the existence of a third isomer in this nucleus. This time the spins could be constrained from consideration of Nordheim's rule as modified by Max Brennan and Aron Bernstein, stipulating that in the $\pi p_{3/2}\nu g_{9/2}$ multiplet the outer values of 3^- and 6^- would come lowest in energy [Bre60]. Vladimir Paar's parabola for a residual proton-neutron quadrupole interaction then awarded 6^- to the lower one of these, leaving 3^- for the isomer above so as to maximise the spin gap between them [Paa79]. Both were connected by a 101-keV $M3$ isomeric transition, while an $M2$ isomeric transition at 141 keV linked the 3^- isomer to the stil higher-lying long-lived 1^+ state. Unlike ^{68}Cu the ground state therefore no longer corresponded to the $\pi p_{3/2}\nu p_{1/2}$ configuration but to a member of the $\pi p_{3/2}\nu g_{9/2}$ multiplet. Empirical calculations of the magnetic moment based on single-particle estimates confirmed the spin values.

The new findings invited a critical review of the β-decay data that had been gathered at Lisol [Van04a]. In a lengthy and exhaustive paper an extended level scheme was presented for ^{70}Cu, which we reproduce in figure 2.43. It featured six additional transitions at 101, 126.5, 141, 233, 957, and 1152 keV.[12] Among these the line at 126.5

[12] Throughout this text we have chosen to quote γ energies with a precision not better than 1 keV. Here we make an exception to differentiate the 126.5-keV transition from the one at 127 keV

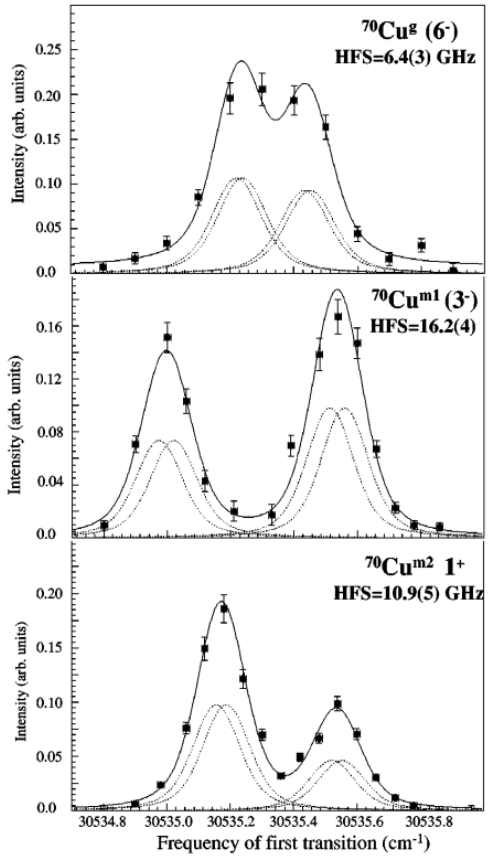

Figure 2.42: Yield of ^{70m1,m2,g}Cu as a function of the wave number of the first step of the laser ionisation scheme. Taken from [Wei02]

keV was hypothetical, as its coincidence relations were indistinguishable from those of the 127-keV transition. Its energy fitted the level diagram but otherwise its relative intensity of $\dagger_\gamma = 4(3)$ reduced its relevance. The γ ray at 233 keV with $\dagger_\gamma = 2(1)$ had been recognised before but omitted at the time. Its placement now forced the peak at 386 keV living elsewhere in the scheme to be treated as a perfect doublet and reincarnate in immediate coincidence with the 233-keV ray, where it provided a pathway parallel to the 618-keV crossover transition. The 957-keV line with $\dagger_\gamma = 3(2)$ had been considered too faint and rejected in the earlier analysis while the 1152-keV one with $\dagger_\gamma = 6(3)$ had not been identified.

Of greater significance were the transitions at 101 and 141 keV, which we already mentioned above and were discovered in the β decay of ^{70}Cu to ^{70}Zn at Isolde. They notably appeared in the unconditioned γ spectrum but vanished when a $\beta\gamma$ coincidence

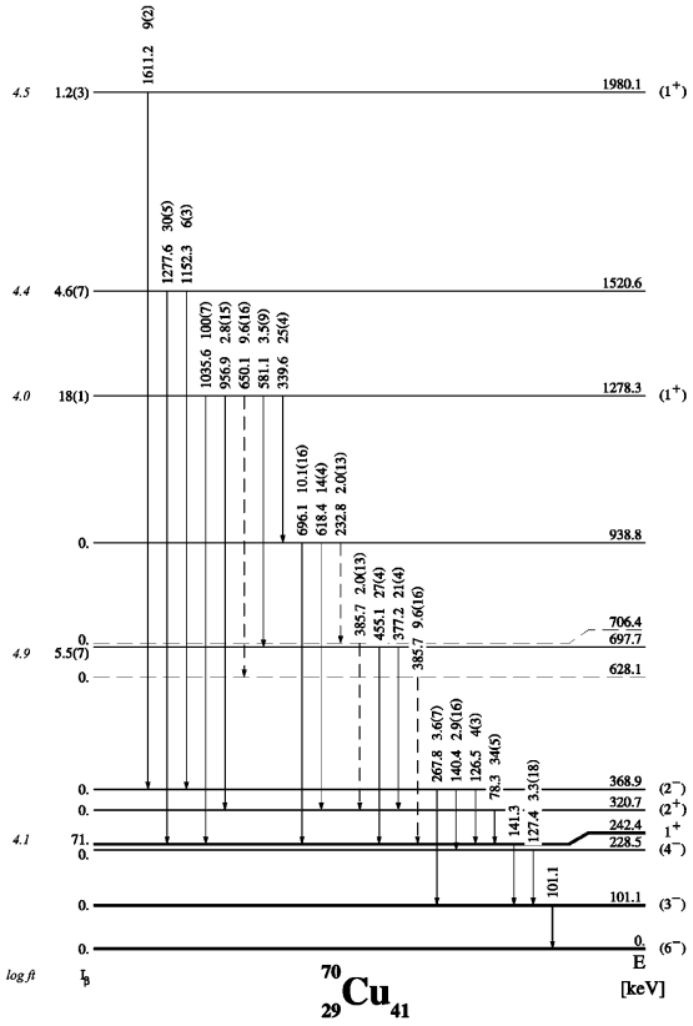

FIGURE 2.43: Level scheme of ^{70}Cu in the β decay of ^{70}Ni. Taken from [Van04a]

was imposed. The further clue to their origin lay in their response to the laser signal, which behaved in the same manner as the middle and bottom panels of figure 2.42. Being triggered by resonant laser ionisation but without the subsequent emission of a β electron, they were ascertained as isomeric transitions out of respectively the 3^- and the 1^+ long-lived states. For that very reason it had not been possible to detect them with the β-decay set-up at Lisol for the isomeric half-lives of respectively 33 s and 6.6 s had pushed them outside the acquisition window.

The lack of coincidences for the isomeric transitions implied that one long-lived state decayed directly into the other without passing through intermediate levels. From the observation that the sum 1152 + 268 keV in the high-spin scheme matched the

energy 1278 + 141 keV in the low-spin scheme, the 1^+ state could be fixed at 141 keV above the 3^- one. The latter would then transform by the 101-keV transition to the 6^- ground state below, for which a half-life of 45 s was measured. Recalling the transfer data in figure 2.40 also the level at 229 keV was believed to belong to the high-spin multiplet and a signature of 4^- was proposed. This was actually in agreement with a local shell-model calculation undertaken to help sort out the interpretation of the $19/2^-$ microsecond isomer in ^{71}Cu in an experiment that we have commented upon earlier [Ish98]. The residual interaction was calibrated by attributing four of the five peaks in the transfer spectrum to the multiplet, even if the the original article had claimed this for three of the states only. The weakest one at 366 keV was reasonably ignored and from systematics the remaining levels at 0, 100, 226, and 506 keV were assumed to carry the spins and parities of 6^-, 3^-, 4^-, and 5^-, respectively.

The experimental results were backed up by the shell model. Hjorth-Jensen's realistic G-matrix interaction with Nowacki's monopoles in the $f_{5/2}pg_{9/2}$ valence space, already introduced before in our text in section 2.3, generated the high-spin structure in the proper order but inverted the two low-spin levels. For each of these states it predicted a fair purity of the wave function of 49 to 59%. The 1^+ level at 1980 keV in the upper part of the level diagram drew quite some ink as it carried a weak but definite decay branch that the calculations could not place. The associated 1611-keV ray is to a certain extent the analog of the 758-keV transition that we mentioned above in the discussion of ^{68}Cu. Finally also the magnetic moments were computed, which proved excellent for the 6^- and 3^- isomers but some 20% too large for the 1^+ one.

The presence of the third isomer was confirmed soon after by mass measurements at the Isoltrap spectrometer at Isolde [Van04b]. As before the fission products of interest were resonantly ionised by laser light but now they were transported to a Penning trap, in which their movement was confined by a combination of electric and magnetic fields. For the purpose of our text we limit ourselves to the external magnetic field B. When the associated cyclotron frequency ω_c matched the mass m of the ion with charge q according to the simple formula $\omega_c = qB/m$, the ion absorbed energy from the field and upon extraction from the trap a minimum appeared in the time of flight. This resonance was explored as a function of the laser wavelength, for which we know

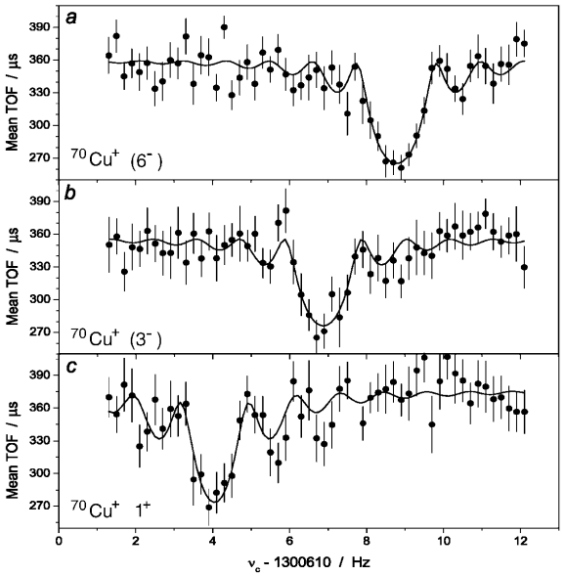

FIGURE 2.44: Mass resonances of ^{70}Cu isomers. Taken from [Van04b]

that specific settings would enhance indivual isomers. The recorded spectra are pictured in figure 2.44. With a resolving power of the cyclotron frequency better than 10^6, mass differences of 101(3) and 242(3) keV could be determined, perfectly fitting the $\beta\gamma$ data.

After all, the ground state of ^{70}Cu had been correctly identified in the transfer experiment, while the Kurie plots from the β disintegration of copper had found the right energy difference between the two isomers but strangely swapped the states. Unlike in ^{68}Cu the high-spin structure had not been missed when the β decay of nickel was examined by the writer of this text in his early career but it had taken intrasource spectroscopy to solve the puzzle by positing a third isomer and mass measurements to close a debate that had spanned nearly thirty years. Throughout the entire work a single-particle model around a semi-magic core of ^{68}Ni had proven particularly successful to interpret the appearance and the behaviour of the isomers, in line with the scheme that was outlined in the beginning of this section.

Some questions nonetheless persisted. From a single-particle point of view, the 141-keV transition transformed a $p_{1/2}$ neutron into a $g_{9/2}$ one. The $6j$ symbol that pops up in the expression for the reduced matrix element only exists for an operator of order 4 [Hey94]. The expected half-life for an $M4$ transition, however, exceeded the

measured value by six orders of magnitude. An important admixture of other components in the wave function therefore brought the lifetime down. It became evident that one was hitting the limits of the single-particle model, which seemed even more clear in ^{68}Cu where the equivalent 693-keV transition deexcited the 3^- state at 777 keV to arrive at the 2^+ level at 84 keV within mere 2.4 ns.

For the level at 369 keV, which was weakly observed in the transfer reaction and not regarded as part of the high-spin multiplet, a spin and parity of 2^- was surmised. At low excitation energy only the $\pi f_{5/2}\nu g_{9/2}$ coupling would produce such a level, but its subsequent decay by means of the 126.5-keV transition to the $\pi p_{3/2}\nu p_{1/2}$ structure would involve a two-step process that once more revealed a considerable mixing with other configurations.[13] It may explain why the calculations struggled with its energy and put it more than 1 MeV higher.

As selective laser ionisation made it possible to tune the isomeric content of a radioactive beam, the opportunity to trigger Coulomb excitation from specific spin states was quickly grasped at Isolde [Ste07]. The 6^- isomer in ^{68,70}Cu was post-accelerated to 2.83 MeV per nucleon and shot onto a target of ^{120}Sn, around which the Miniball γ detector was mounted. An $E2$ transition lifted the isomer to the 4^- level, from where it fell back to the 3^- one, proceeding further to the ground state in the case of ^{68}Cu but being isomeric as discussed before for ^{70}Cu. While a most commendable experimental feat in itself, not so much novel insight could be gleaned from it. The shell-model calculations that relied on the quoted realistic interaction with modified monopoles were tweaked by Nadezda Smirnova at Ghent in order to account better for the sharp behaviour of the $5/2^-$ states in the odd isotopes and the anomalous energy of the 2^- level in ^{70}Cu. The theoretical $B(E2, 6^- \rightarrow 4^-)$ strength remained flat at about 40 e^2 fm^4 or 2.3 Weisskopf units, whereas the experiment appeared to expose a resolute drop from 68(6) e^2 fm^4 in ^{68}Cu to 41(5) e^2 fm^4 in ^{70}Cu, that is 4.1(4) to 2.4(3) Weisskopf units. The need for additional excitations in ^{68}Cu could be mended by increasing the neutron effective charge from $e_\nu = 0.5e$ to $1.0e$ whilst keeping the proton charge at $e_\pi = 1.5e$, suggesting that the solidness of the $N = 40$ subshell in ^{70}Cu would rapidly fade.

[13] At some point in the article also the 4^- state at 229 keV is assigned to the $\pi f_{5/2}\nu g_{9/2}$ multiplet. Earlier in their text the confused authors, among whom the reader's guidance, concur that it rather belongs to $\pi p_{3/2}\nu g_{9/2}$

Coulomb excitation of the 3^- isomer somewhat watered down these conclusions [Rap11]. Again at Isolde and with an energy of 2.85 MeV per nucleon on a target of ^{120}Sn, transitions from the 3^- and 6^- initial states to the 4^- and 5^- final states within the high-spin multiplet of ^{70}Cu gave a broader base to evaluate the interdependence of the various matrix elements. The earlier $B(E2, 6^- \rightarrow 4^-)$ value for ^{68}Cu was revised to 77(8) e^2 fm^4 and a number of 69(9) e^2 fm^4 was extracted for ^{70}Cu, which made for a recession from 4.7(5) to 4.0(5) Weisskopf units only and dimmed a potential effect across $N = 40$. The 5^- state meanwhile could be placed more precisely at 511 keV. The shell model with the aforementioned realistic interaction modified twice but now plugging in vigorous effective charges of $e_\pi = 1.9e$ and $e_\nu = 0.9e$ nicely matched the measurement, which we illustrate in figure 2.45. The LNPS force in a larger $\pi fp\ \nu p f_{5/2} g_{9/2} d_{5/2}$ model space but with regular effective charges of $e_\pi = 1.5e$ and $e_\nu = 0.5e$ also achieved agreement. By way of exercise and rather than redressing the charge parameters, the $d_{5/2}$ neutron orbital was amputated from among the valence partners, which resulted in a visibly degraded performance. It vividly proved that neutron excitations across $N = 50$ are an essential element to understand the properties of these nuclei, notably validating the idea of quasi-SU(3) symmetry between the $\nu g_{9/2}$ and $\nu d_{5/2}$ states with $\Delta j = 2$ that runs through the Strasbourg thinking. It would then only have been a matter of dotting the i and crossing the t for LNPS not to miss the ground state by 20 keV.

The high-spin multiplet in ^{72}Cu was seen at the Lise spectrometer at Ganil in two fragmentation experiments. At first in the reaction of ^{86}Kr on nickel a short-lived 1.76-μs isomer was found at 270 keV, for which a spin and parity of 4^- was proposed [Grz98]. When the isotope was produced from a beam of ^{76}Ge on beryllium, the lifetimes of several states could be measured with fast BaF_2 scintillators [Mac01a]. Combined with an appreciation of typical Weisskopf transition strengths in neighbouring nuclei a multipolarity sequence of $E2 - M1 - E1$ was deduced for the γ deexcitation of the isomer. Deliberating among the same multiplet configurations as for ^{68,70}Cu, this led the authors to fix in reverse order the ground state as 2^+, infer for the two intermediate levels 3^- and 4^-, and reassign the isomer itself as 6^-. With a straightforward γ pathway to decay, long-lived states like in ^{70}Cu would naturally disappear.

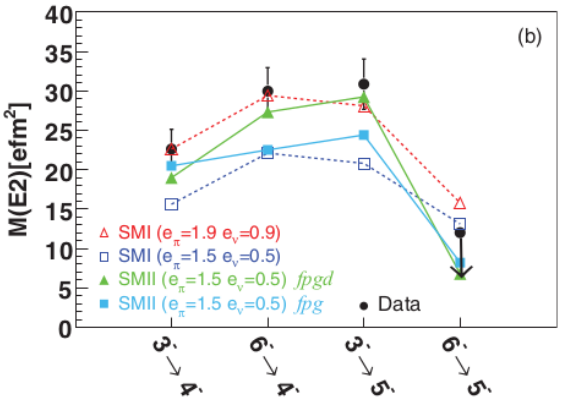

Figure 2.45: Experimental $E2$ matrix elements in ^{70}Cu compared to shell-model calculations with Hjorth-Jensen's realistic interaction as modified by Nowacki and Smirnova (labelled SMI) and the LNPS force (labelled SMII). Taken from [Rap11]

Also in the original β-decay campaign at Lisol ^{72}Cu was part of the game even though the low-spin doublet was provisionally spotted in two states at 376 and 470 keV, interconnected by an intense ray of 94 keV in much a analogue fashion as the 78-keV line in ^{70}Cu. Because of the modest statistics the case was revisited and completed upon some years later [Tho06]. Compared to the earlier analysis the new scheme curiously omitted the 470-keV transition but more significantly it confirmed that except for the 3^- state only low-spin levels were populated. However, with the 2^+ member of the $\pi p_{3/2}\nu p_{1/2}$ coupling now invested in its role of ground state and the first candidate for a 1^+ level appearing at 376 keV, a bizarre distortion of the low-spin doublet ensued. The shell model still based on the same realistic interaction with modified monopoles from Strasbourg and further improvements from Ghent was of no avail, as from figure 2.46 we read that it put the 3^- level lowest of all and predicted the first positive parity states at about 400 keV. The single-particle approach seemed valid, as the purity of the wave functions in the multiplets ranged from 45 to 64%. Standing four particles away from ^{68}Ni, it was nonetheless realised that the various quasiparticle constructions offered many possibilities and therefore the article left open the option that the ground state would rather relate to a different 2^- structure, built from 33% of $\pi f_{5/2}\nu g^3_{9/2}$ with 19% of $\pi p_{3/2}\nu g^3_{9/2}$. Such a solution suggested that the reordering of the proton orbitals that was so prominent in the odd-even isotopes would in the odd-odd ones outweigh the variation in neutron configurations.

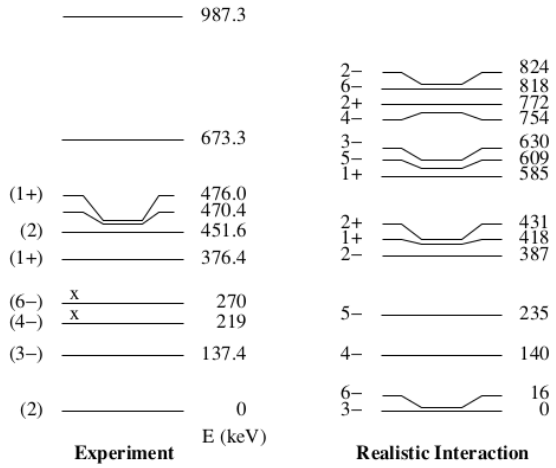

FIGURE 2.46: Experimental levels in ^{72}Cu compared to shell-model calculations with Hjorth-Jensen's realistic interaction as modified by Nowacki and Smirnova. Taken from [Tho06]

More ground-state spins of copper isotopes were constrained from the β-decay patterns into their zinc daughters that were observed at Isolde [Van05]. For ^{74}Cu, a spin of 2 or 3 was consistent with the data, for ^{76}Cu, a value of 3 or 4. In ^{78}Cu, it would rise to 4 or 5. No indications for isomers were spotted. The shell model, once again formulated with the familiar realistic interaction and its modified monopoles but without the adjustments from Ghent, featured little success in describing the ground-state spins in the middle of the neutron shell but performed better for ^{70}Cu and ^{78}Cu. We print these theoretical level schemes in figure 2.47.

Collinear laser spectroscopy on ^{72}Cu and ^{74}Cu at Collaps at Isolde brought light [Fla10]. With the same laser transition of 324.8 nm and the same analysis algorithm of ratios of A factors that we presented for ^{75}Cu in section 2.1, a spin of 2 emerged for the ground state of both isotopes. From the negative magnetic moment that was measured, a negative parity pierced through. Calculations with the jj44b and JUN45 shell-model forces were put forth, which evidenced that indeed the best agreement with experiment was obtained for the $\pi f_{5/2}\nu g_{9/2}^{2n+1}$ configuration. The prominence of the $f_{5/2}$ proton orbital already at $N = 43$ was thereby affirmed. While also the quadrupole moments were reasonably well reproduced, the position of the ground states on the other hand could not be distilled from the algebra, as the reader may judge from figure 2.48. Especially for ^{72}Cu the $\pi f_{5/2}$ single-particle energy did not seem to fall into place

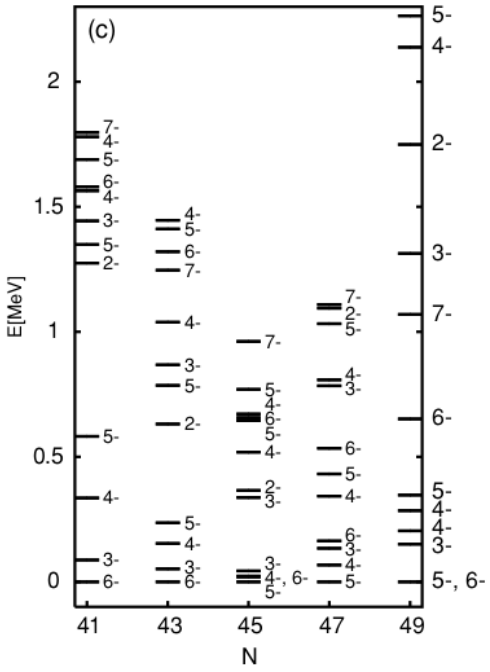

Figure 2.47: Shell-model calculations for neutron-rich copper isotopes with Hjorth-Jensen's realistic interaction as modified by Nowacki. Taken from [Van05]

in JUN45, where it was a stronger contributor to the second 2^- state than to the first one. Thanks to its resolution, the same work also improved on the magnetic moments of ^{68,70}Cu from intrasource spectroscopy [Vin10].

It is not easy to reconcile a 2^- ground state for ^{72}Cu with the $E2 - M1 - E1$ γ cascade out of the isomer that we described above. Most likely the Weisskopf single-particle estimates were too rigid and cannot be upheld, shoving a glob of quicksand under the multipolarities. If we recall the Paar parabola, one should find the 3^- and 6^- states at the lower end and the 4^- and 5^- ones at the upper end of the spectrum, which as a matter of fact we can see from figures 2.46 and 2.47. The calculations from figure 2.48 do not contradict this, but neither do they assist in a straighforward identification of the isomer.

The observation of a γ ray of 166 keV in the β disintegration of ^{74}Ni at Lisol, which was likewise the energy of the most intense transition in the level scheme of ^{75}Cu, prompted speculation of βn decay for this nucleus. Initially this was thrown cold water upon by the high probability P_n of 30(8)% that was inferred, calling for a much

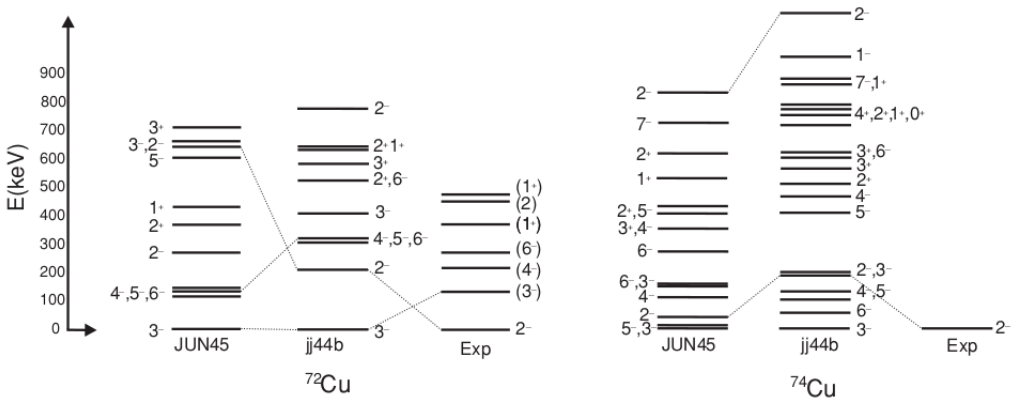

FIGURE 2.48: Experimental level schemes of ^{72,74}Cu compared to shell-model calculations with the jj44b and JUN45 interactions. Taken from [Fla10]

more dominant process than the theoretical predictions available at the time would foretell [Fra98]. The issue of delayed neutron emission was explored in a dedicated effort at the Holifield facility [Win09]. In a peculiar development, instead of selecting the particles by resonant laser ionisation like at Lisol and Isolde they were first mass separated and then energised in a tandem accelerator to 225 MeV such that their atomic number could be figured out from the energy loss in an ionisation chamber. Neutron branching ratios of 7.2(5)% for ^{76}Cu, 30.0(27)% for ^{77}Cu, and 65(8)% for ^{78}Cu were determined, which could be reasonably accounted for in a continuum-QRPA model for spherical nuclei designed by Ivan Borzov [Bor05]. The agreement became even better if the theory forced the $f_{5/2}$ proton orbital to take up the ground state in the copper isotopes.

The interest in P_n values soon spread to NSCL where Nero was called upon, a genuine Neutron Emission Ratio Observer [Hos10]. Nero's judgment was an upper limit of 7.2% for ^{76}Cu and neutron-emission probabilities of 31(4)% for ^{77}Cu, 44(5)% for ^{78}Cu, and 72(12)% for ^{79}Cu, as displayed in figure 2.49. The discrepancy for ^{78}Cu was boldly discounted on behalf of the deficiencies of γ-ray spectroscopy. Calculations were formulated in a global QRPA framework written over many years by Peter Moeller and his colleagues, taking as input the nuclear masses from the literature compilations when they were available and from the Finite-Range Droplet Model (FRDM) in case they were experimentally unknown [Moe03]. In spite of a marked tendency of the authors towards their own model, the global QRPA was outdone by the continuum

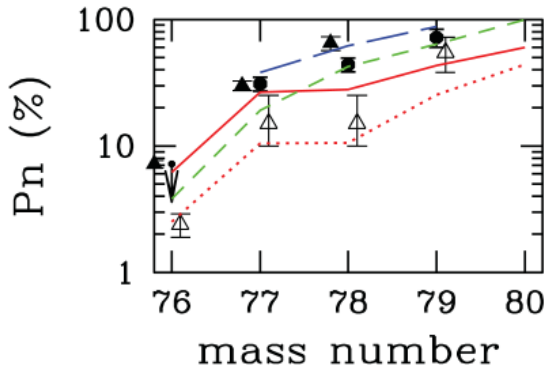

Figure 2.49: Neutron-emission probabilities for copper isotopes from NSCL (black circles) and Holifield (black triangles) compared to literature data (open triangles) and calculations from global QRPA (red solid and dotted lines), continuum QRPA (green), and the jj44b interaction (blue). Taken from [Hos10]

QRPA referred to before, the latter diplomatically holding the middle ground between the NSCL and the Holifield data. The revised lower value for ^{78}Cu nevertheless relaxed the need for the proton orbitals to be fixed in the updated continuum computations. An attempt at understanding the neutron branching ratios from the jj44b shell-model interaction proved an excellent proposition, even if the Gamow-Teller operator had to be quenched by a factor of 0.37 instead of the more common value of 0.7 or 0.75.[14] The deviation was traced to the $\pi f_{7/2}$ orbital that was absent from the valence space and as it turned out could not be ignored in evaluating the β decay.

The β decay records from Holifield initially suggested a spin and parity of 4^- or 5^- for the ground state of ^{78}Cu [Win08]. A subsequent analysis exposed the feeding towards levels of higher spin in the ^{78}Zn daughter and inclined towards a 6^- assignment [Gro09]. The deduction was nonetheless superseded by 5^- once again when a direct decay branch to the 4^+ state was recognised [Kor12]. A $\pi f_{5/2}\nu g_{9/2}^{-1}$ configuration was proposed, in line with the level ordering that was meanwhile established for the proton orbitals in the odd isotopes. The Paar parabola flips over for a particle-hole structure and in the present case predicts 5 as the lowest multiplet member, while the simpler coupling rule of Brennan and Bernstein would give $j_\pi + j_\nu - 1 = 6$.

Crossing the Atlantic eastwards again, the ever improving production rates at Isol-

[14] The article listed the JJ4B interaction, which elsewhere the literature styles as jj44b

de tempted laser spectroscopy to take aim at ^{78}Cu. The intrasource experiment on ^{75,77}Cu that we devoted time to in section 2.1 did collect a nice signal for ^{78}Cu but could not achieve enough resolution for a meaningful conclusion to be drawn [Koe11]. Collinear spectroscopy at Cris churned out the complete isotopic chain from ^{73}Cu to ^{78}Cu [DeG17]. With an excitation step of 249.2 nm and an ionisation step of 314.2 nm a signature of 3^- was set for ^{76}Cu but notwithstanding the fair quality of the spectrum a range of 4 to 7 was left open for ^{78}Cu. Whereas consensus exists for the spin of former isotope, the latter thus remains conjectural at 5^-.

With the evidence gathered from spin sequences and electromagnetic moments throughout the entire family of odd-odd neighbours, the various multiplets that we came across bear testimony to the conclusion that while the neutron rapidly leaves behind the $p_{1/2}$ state to venture out into $g_{9/2}$, the proton for its part gradually deserts the $p_{3/2}$ orbital to find shelter in $f_{5/2}$. The remarkable power of the single-particle model to penetrate and dissect the nuclear structure from ^{68}Cu up to ^{78}Cu pays worthy tribute to the persistence of a solid nickel core.

2.7 The breakthrough to ^{78}Ni

In section 2.5 we learnt that the deformation that is observed in copper could not be satisfactorily traced back to the possible polarisation of the nickel core, while several questions remained as to the $B(E2)$ behaviour of the latter. Suspended between a single-particle model and an insight of shape coexistence in ^{68}Ni, we stumbled upon the island of inversion centred on ^{64}Cr. The recognition of a novel island that homes in on ^{74}Cr rises the expectation that we would steer towards shape coexistence also in ^{78}Ni. But the nucleus has been hard to reach.

Before any spectroscopy of ^{78}Ni became feasible, its existence was confirmed at the Gesellschaft für Schwerionenforschung (GSI) at Darmstadt [Eng95]. A beam of ^{238}U at 750 MeV per nucleon was directed onto a beryllium target. Among the fission fragments, which were separated in the FRS spectrometer and identified from their magnetic rigidity, time-of-flight and energy deposit, ^{78}Ni was observed. We reproduce in figure 2.50 the three counts of ^{78}Ni collected after 132 hours or 5.5 days of

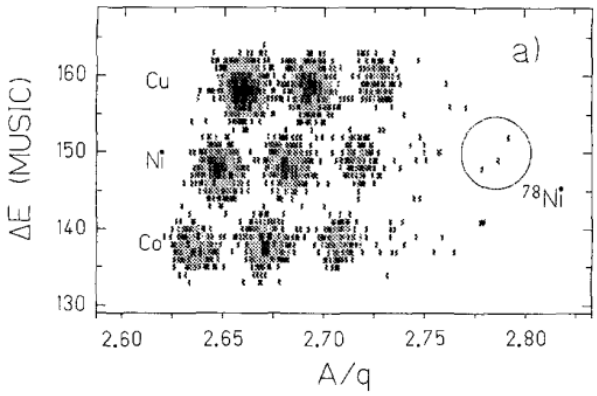

Figure 2.50: Identification plot of the experiment in which ^{78}Ni was observed for the first time. Taken from [Eng95]

irradiation, which made for a cross section of 0.3(2) nb.

At NSCL ten years later, ^{78}Ni could be selected among the fragmentation residues of ^{86}Kr at 140 MeV per nucleon on a beryllium target [Hos05]. The eleven events registered in 104 hours stand for a much lower cross section in this process of 0.02(1) pb. The half-life was measured as 110^{+100}_{-60} ms, which in fact fits well the value of 160 ms that had been projected from the measurement of the lighter isotopes at Louvain [Fra99]. In figure 2.51 we draw it along with the theoretical predictions from the global QRPA with FRDM masses discussed before [Moe03] and the Extended Thomas-Fermi method with Strutinsky Integral (ETFSI), an earlier version of the continuum QRPA also mentioned in the previous paragraph [Bor03].[15] While both computations were in reasonable agreement with the data, a development by John Pearson in which the shell gaps were quenched (ETFSI-Q) performed even better [Pea96]. A separate approach that incorporated the Hartree-Fock-Bogoliubov formalism and attempted to employ the Skyrme SkO' interaction throughout but for a finite-range force in the proton-neutron particle-particle channel was lauded as a fully self-consistent QRPA [Eng99]. It was outdone nonetheless by a shell-model calculation by Karlheinz Langanke and Gabriel Martínez-Pinedo, essentially based on Hjorth-Jensen's realistic *G*-matrix interaction [Lan03b].

The upgrade of the RIBF facility in 2006 allowed for the advent of high-energy

[15] The older models labelled Moeller-97 and Borzov-97 figured in the plot do not include first-forbidden transitions

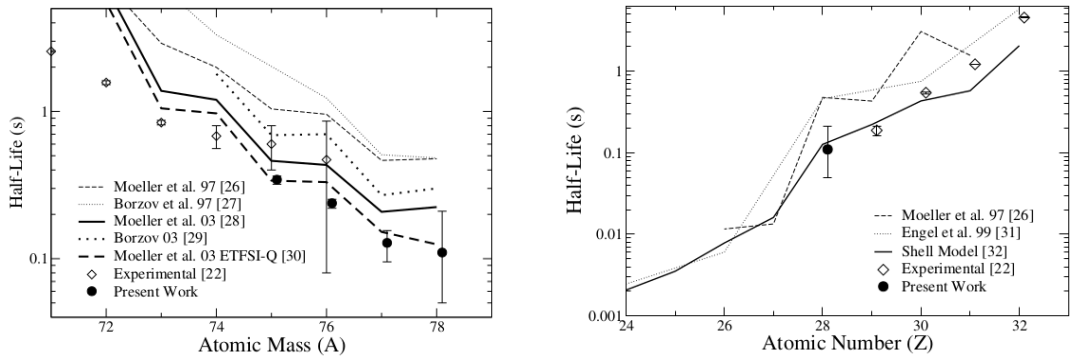

FIGURE 2.51: Half-lives of nickel isotopes (left) and $N = 50$ isotones (right) compared to theoretical predictions. The Engel-99 set includes values for even Z only. Taken from [Hos05]

high-intensity beams of ^{238}U. By the end of 2009, 1 pnA of ^{238}U was reached, the threshold of 10 pnA was crossed in 2012 and 100 pnA was set to become available in 2021. At an energy of 345 MeV per nucleon the beam fissions in flight upon passing through a thick beryllium target. The products are identified in the Bigrips separator from their energy loss, time of flight and magnetic rigidity. During the experimental campaign of 2012-13 the particles were transmitted through the Zerodegree spectrometer and implanted in the Wide-range Active Silicon-strip stopper Array for Beta and Ion detection (Wasabi), a multilayer stack of double-sided silicon-strip counters installed at the final focal plane. This served as β trigger for the collection of γ rays in the Eurica ensemble introduced already above. Illustrating the scope of the endeavour, the nuclear chart was swiftly extended with the ^{80,81,82}Ni and ^{83}Cu isotopes [Sum17]. The β decay half-lives of ^{76,77}Co, ^{79,80}Ni and ^{81}Cu were readily measured, while the ones for $^{72-75}$Co, $^{74-78}$Ni and $^{78-80}$Cu were improved upon [Xu14]. For ^{78}Ni, $1.2\,10^4$ events were accumulated during 13 days of 5 pnA of ^{238}U beam and its half-life was corrected to 122.2(5.1) ms.

Theoretical backing again came from the global QRPA with FRDM masses, although it predicted a staggering along the proton number that was not seen in experiment, as one can read from figure 2.52. Also depicted are the results from the mass formula that was designed by Hiroyuki Koura, Takahiro Tachibana, Masahiro Uno, and Masami Yamada (denoted KTUY) [Kou05] married with a second-generation gross theory of β decay likewise by Tachibana (GT2) [Tac95]. In this work the staggering

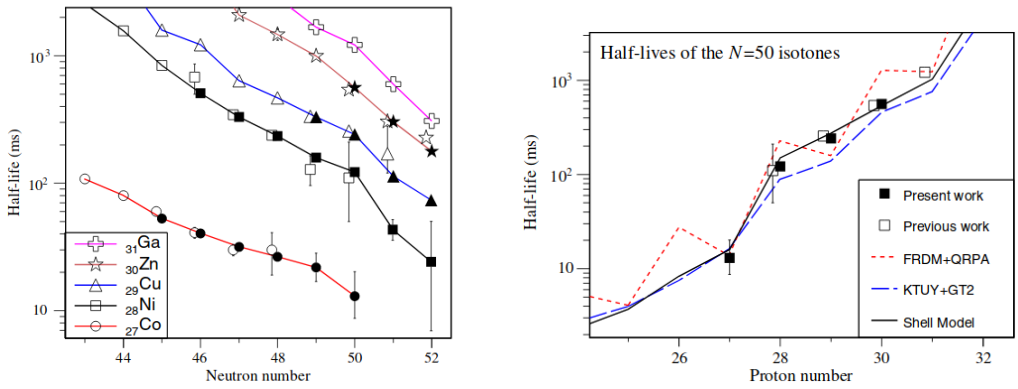

Figure 2.52: Half-lives of isotopes from cobalt to gallium (left) and $N = 50$ isotones compared to theoretical predictions (right). Taken from [Xu14]

was reduced and the calculated values ran closer to the data points. The shell model tried its chance with the Madrid-Strasbourg interaction, to which was added a formalism for β decay with matrix elements that were renormalised by factors ranging from 0.38 to 1.266 [Zhi13]. It reproduced quite accurately the measurement, in particular the discontinuity at ^{78}Ni, which was interpretated as an indication for the magicity of this nucleus. In hindsight the same observation can be made for the NSCL experiment, where unlike the gross theories the shell model indeed foresaw a kink in the half-lives. With the knowledge specifically of ^{77}Co, it was now possible to confirm this.

A shift of slope was also visible in the isotopic chains plotted in figure 2.52. For ^{79,80}Ni the half-lives turned out to be shorter than what one may deduce from extrapolation, which would imply that the first neutrons outside the $N = 50$ shell would be appreciably less bound than those inside the shell, increasing the Q_β value and hence the β-decay rate. Compared to their ^{76,77}Co counterparts the half-lives of the nickel isotopes remain long, which would relate to a Q_β value that is high for cobalt as the $\pi f_{7/2}$ orbital is properly closed in the nickel daughter, while for the decay of nickel the created proton is neatly put in the next shell in copper corresponding to a lower Q_β value. The former statement adds evidence to the survival of the $N = 50$ gap, the latter indicates that also the $Z = 28$ one is quite well sealed. The simultaneous reinforcement of both closures constitutes an example of what is known as the mutual support of magicities, an outstanding facet of nuclear structure that was ascertained before in ^{208}Pb [Zel83].

In a next series of experiments the Eurica campaign delivered a wealth of high-resolution γ spectroscopy, exploring the neighbourhood of ^{78}Ni. Among this we cite the β decay of ^{76}Co into ^{76}Ni, which populated a possible 0_2^+ level at 2995 keV and which we have commented upon earlier in our text [Söd15]. Here we would like to point out the location of its 2_1^+ level at 990 keV, a slight readjustment of the energy of 992 keV that had been reported earlier in this isotope following the fragmentation of a ^{86}Kr beam at NSCL [Maz05]. In ^{74}Ni the state is situated at 1024 keV, established from the same NSCL data set in the β decay of ^{74}Co. The steadiness of the energy was reproduced by realistic shell-model computations with the S3V' and NR78 forces. We put on record that the latter is seen to perform better.

It is worth advertising that the RIBF experiment confirmed the presence in ^{76}Ni of an 8^+ isomer at 2418 keV with a half-life of 548(3) ns, originally identified in the same work from NSCL at 2420 keV with a half-life of 590^{+180}_{-110} ns and where already it decayed in a seemingly standard manner through the 6^+ and 4^+ levels to the 2^+ state. The search for it nevertheless had been a long-standing issue, since an analogous state had been found in ^{70}Ni but in spite of much effort never so in ^{72,74}Ni [Grz98, Ish02, Saw03, Maz05]. To understand its behaviour, the concept of seniority was put to use, a property of a nuclear system defined as the number of protons or neutrons that are not paired to a total angular momentum of 0^+. Within the jj-coupling scheme, it helps to sort out the nucleon configurations of a single j shell by means of only two quantum numbers, the total angular momentum J and the seniority υ. Applied to the $\nu g_{9/2}$ orbital, it explains the existence of a 6^+ ($\upsilon = 4$) state, which the S3V' interaction situates 300 keV above the 6^+ ($\upsilon = 2$) one [Gra02]. If conceivably its position would be lowered, as it happens in the NR78 (jj44pna) code, a second deexcitation channel would be unlocked that prevents the appearance of an 8^+ ($\upsilon = 2$) isomer in ^{72,74}Ni [Lis04]. Obviously such analysis depends crucially on a correct identification of the 8^+ level, which for ^{72}Ni was for some time a subject of controversy between attempts from the Gammasphere array at Argonne [Chi11] and the Eurica set-up at RIBF [Mor16a]. The latter raised the energy to 2778 keV, indeed squeezing in two 6^+ states just below.

Also the β decay of ^{74}Co into ^{74}Ni was revisited at Eurica [Mor18]. The level scheme was extended and the calculations expanded beyond NR78 (jj44pna) with the

SCI, A3DA-m, and 2+5 models. The first one of these is an empirical interaction in which the weight of $\nu g^2_{9/2}$ excitations was linearly interpolated between ^{70}Ni and ^{76}Ni [Van14]. The meaning of the SCI acronym is not shared with the readers of the article but its theoretical foundations centre on the conservation of seniority.[16] The A3DA-m force we discussed before, while the arcane 2+5 insignia was conferred to the realistic calculation with the charge-dependent Bonn potential that above we classified as the $V_{\mathrm{low}-k}$ interaction from Naples. The outcome of this wizard's box was somewhat disenchanting. While satisfactory for the 2^+_1 energies, none of the available tools was able to grasp the peculiar pattern of the intensity ratios. Since these are intrinsically linked to the seniorities of the states, one is led to concede that their respective structures still escape theory.

Removing a particle instead of creating one, the knock-out of a proton from ^{77}Cu to ^{76}Ni during the Seastar experiments brought in an interesting piece of information [Ele19]. Supported by LNPS calculations, three states were populated with comparable cross sections at energies from 3.4 to 4.1 MeV and assigned to the $\pi f^{-1}_{7/2} f_{5/2}$ multiplet. While naturally the hole strength spread into several final states, it indicated a rough energy where the $\pi f_{7/2}$ orbital could be expected.

Turning our attention to copper itself, the β decay of ^{77}Ni showed the existence in ^{77}Cu of transitions up to 3 MeV [Sah17a]. We illustrate the rich and featureful spectrum gleaned from Eurica in figure 2.53. The level scheme that was constructed from the recorded $\gamma\gamma$ coincidence relations extended up to 4 MeV of energy and is revealed in figure 2.54. The first excited state takes residence at 293 keV. Alike the $5/2^-$ ground state its spin and parity of $3/2^-$ was assigned from a shell-model calculation with the A3DA-m force. The monopole component provided for a tensor attraction of the $\pi f_{5/2}$ state to the eight neutrons in the $g_{9/2}$ orbital, pushing the $5/2^-$ configuration down to the ground state. The matrix elements proved not strong enough to do so in ^{75}Cu, which is clearly perceivable from the single-particle energies printed in figure 2.55. However, once the higher-order multipole terms were included the inversion could be readily reached at $N = 46$ in accordance with experiment.

In order to get a quantified handle on the single-particle content of the levels, the

[16] In the article on the ^{72}Ni experiment at Argonne an earlier version appears as Pairing, Seniority, and Quasispin algebra (PSQ) [Chi11]

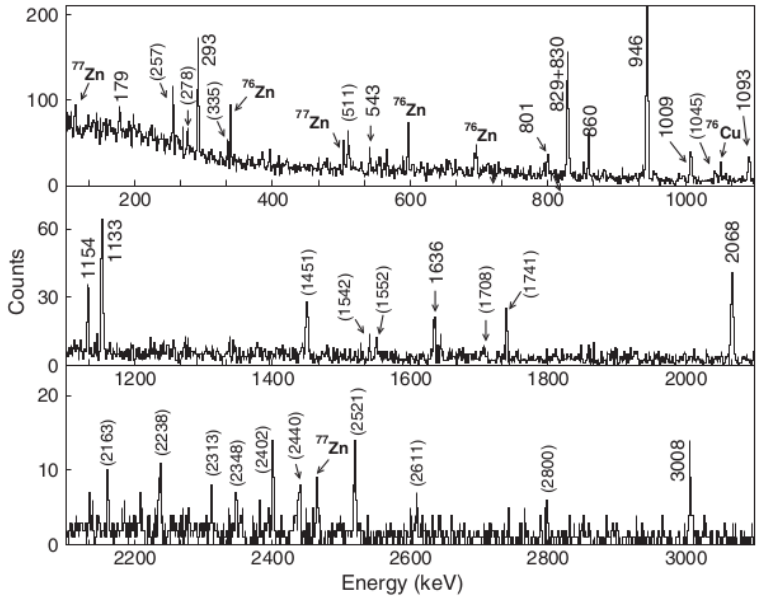

FIGURE 2.53: Spectrum of γ transitions in ^{77}Cu after β decay of ^{77}Ni. Those that carry an energy label were assigned to ^{77}Cu. Taken from [Sah17a]

concept of spectroscopic factors was imported from reaction theory. It differs from the experimental log ft value by freezing the neutrons and instead expresses the overlap between an initial wave function in a closed ^{76}Ni core, to which an external proton must be joined, and a final proton state in the ^{77}Cu daughter nucleus. Essentially formulating the probability of a particle-core excitation, it tallied up to 0.64 for the $5/2^-$ ground state and 0.62 for the $3/2^-$ excited one and confirmed the single-particle nature of both.

In ^{75}Cu the computed spectroscopic factor for the $5/2^-$ state only reached 0.46. Interestingly when a 2^+ excitation in the ^{74}Ni core was generated the overlap integral amounted to a rather large value of 0.24.[17] For a 2^+ excitation in the ^{76}Ni isotope a corresponding spectroscopic factor of 0.18 was found in the ^{77}Cu system. The smaller share of collectivity in ^{77}Cu would in all likelihood be brought about by the lesser number of $g_{9/2}$ neutron holes.

To fathom the structure of the next states, it is useful to bear in mind the selectivity of the feeding mechanism. The β decay from the $9/2^+$ ground state of ^{77}Ni is not ex-

[17] The uncommon notion of several spectroscopic factors for a single state can still be understood as the probability that a given configuration contributes to the contents of the wave function

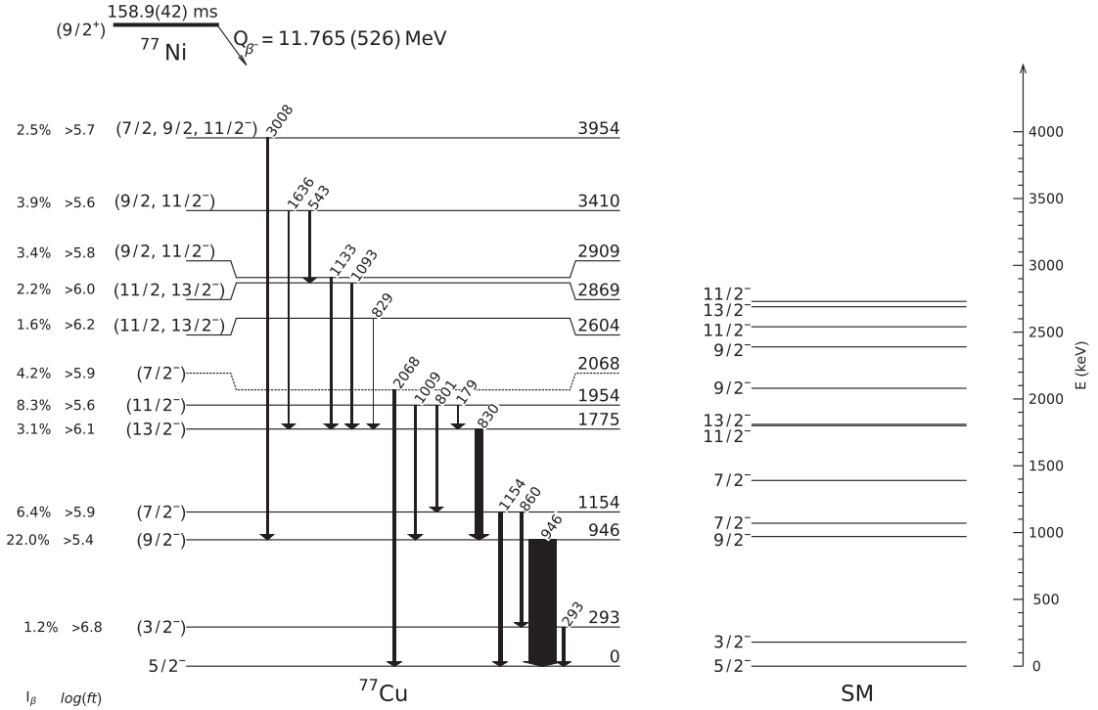

Figure 2.54: Level scheme of ^{77}Cu after β decay of ^{77}Ni along with the theoretical prediction from the A3DA-m interaction. Taken from [Sah17a]

pected to access levels of low spin. Based on the log ft values, the intense transition at 946 keV that guides most of the γ deexcitations to the $5/2^-$ ground state was therefore proposed to correspond to the $9/2^-$ member of the $\pi f_{5/2} \times 2^+$ multiplet, calculated at almost the same energy with a spectroscopic factor of 0.70. The neighbouring level at 1154 keV could match the $7/2^-$ state anticipated just above, the configuration of which would be given by a superposition of $\pi f_{5/2} \times 2^+$ and $\pi p_{3/2} \times 2^+$ with spectroscopic factors of 0.19 and 0.51 respectively. These weakly coupled configurations naturally appear near 1 MeV, as we recall from above that the 2^+ state in ^{76}Ni had been found at an energy of 990 keV.

The upper part of the scheme presents us with a series of presumed $7/2^-$, $9/2^-$, $11/2^-$ and $13/2^-$ levels. The spins were constrained from the $\gamma\gamma$ relations as well as the log ft values. In particular the $13/2^-$ state at 1775 keV was associated with the $\pi f_{5/2} \times 4^+$ structure, supported by a spectroscopic factor of 0.48. For the $11/2^-$ level at 1954 keV a $\pi p_{3/2} \times 4^+$ coupling with a spectroscopic factor of 0.30 was put forward. The 4^+ energy in ^{76}Ni is located at 1920 keV [Söd15]. Nevertheless, since the Q_β

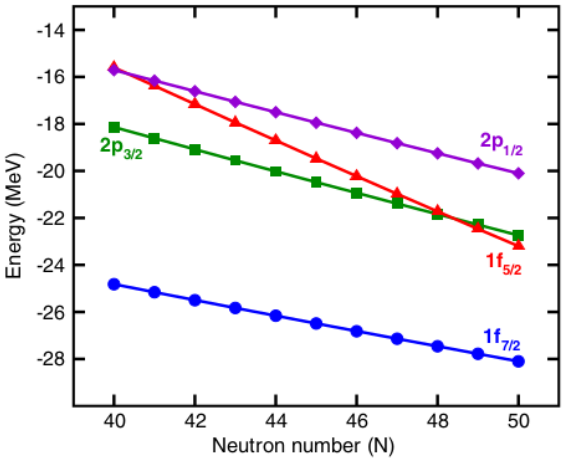

FIGURE 2.55: Evolution of proton single-particle energies in nickel isotopes from the A3DA-m interaction. Taken from [Sah17a]

energy totalled a stern 11.8 MeV the β feeding may actually have come in far higher than what was measured, so the extracted log ft values are to be read as lower limits and the mooted spins treated with some caution.

Yet one level stood out among these, as it decayed directly to the ground state earning it a $7/2^-$ tag. This 2068-keV level could represent the remaining high-spin member among the two mentioned multiplets, that is the second $7/2^-$ level resulting from the mixing of the $\pi p_{3/2} \times 2^+$ and $\pi f_{5/2} \times 2^+$ structures. But the authors chose a different path and instead held up the level as a candidate for the $\pi f_{7/2}$ hole, albeit calculated at a notably lower energy of 1389 keV.[18] With a purity of the wave function no less than 74%, the hypothesis carries considerable consequence for the size of the $Z = 28$ gap. The existence of the suggested state, however, hinges on the absence of a coincidence relation for the eponymous γ ray, for which a faint coincidence with the 946-keV transition was discarded as statistically unconvincing. Even so, it is not obvious that a hole state would be easily accessed in β decay, in which a proton is soundly created.

While the A3DA-m interaction allowed for a fair understanding of the main features of the level scheme, it significantly split the spectrum in a sequence of single-particle structures below an energy of 0.3 MeV and a regime of states that are weakly

[18] Since a $\pi f_{7/2}$ hole in copper can be thought of as a $\pi f_{7/2}$ particle coupled to the $\pi f_{7/2}^{-2}(p_{3/2}f_{5/2})^2$ core excitation in nickel, the authors actually link the level to the $\pi f_{7/2} \times 0_2^+$ configuration

coupled to core excitations from 0.9 MeV onwards. Such behaviour is only possible if the $Z = 28$ gap is sufficiently strong, since this creates a space for single-particle excitations to proceed within the valence shell before the nickel core is broken. If the level at 2068 keV would effectively embrace the $\pi f_{7/2}$ hole, it would constitute a curious exception to this.

The fact that the $\pi p_{1/2}$ single-particle state is missing from the act should not trouble us, since likely a $1/2^-$ state is not fed in the β decay from the $9/2^+$ ground state of ^{77}Ni. Nonetheless if a neutron would jump from the $p_{1/2}$ orbital into the $g_{9/2}$ one then a $1/2^-$ long-lived state could appear in ^{77}Ni, similar to what happens in ^{71}Ni. Just like we described in section 2.4, the spin difference with the ground state would trigger β decay of the isomer by transforming the $p_{1/2}$ neutron into a $p_{1/2}$ proton. If a fraction of the isomeric population would survive during the transport of the beam through the Bigrips and Zerodegree spectrometers, the time of flight for which measured some 500 ns, perhaps its deexcitation could be recovered as one of the γ rays that were not placed in the level scheme but that would proceed down to the $3/2^-$ or $5/2^-$ lowest states. For instance the lines at 1045 or 1451 keV might be candidates. From the theoretical side, the first two $1/2^-$ states were calculated at 547 keV and 1143 keV [Sah17b]. However, only the former of these contains a modest contribution of 20% stemming from $\pi p_{1/2}$. Instead both are members of the core-coupling multiplets and contain 70% of one particle in $\pi f_{5/2}$ and $\pi p_{3/2}$, respectively, emboldened by the 2^+ excitation of ^{76}Ni. It remains at any rate surprising that the calculation would put the $\pi p_{1/2}$ single-particle state higher up, farther away from the Fermi surface than $\pi f_{7/2}$. We cannot but conclude that the state is heavily fragmented, which would merely remind us of the collectivity of the $1/2^-$ state in ^{67,69,71,73}Cu that had been noticed in Coulomb excitation at Isolde [Ste08].

Supplementary hints to the structure of ^{77}Cu came from an experiment that had taken place at RIBF in 2011 but was only published several years later [Vaj18]. With the Bigrips spectrometer centered on heavier ^{80}Zn, proton knock-out in a thick beryllium target was used to produce ^{77}Cu from a component of ^{78}Zn in the incoming beam. The simple but quintessential spectrum recorded with the Dali-2 detector array of NaI(Tl) crystals and pictured in figure 2.56 showed just three transitions. The lack

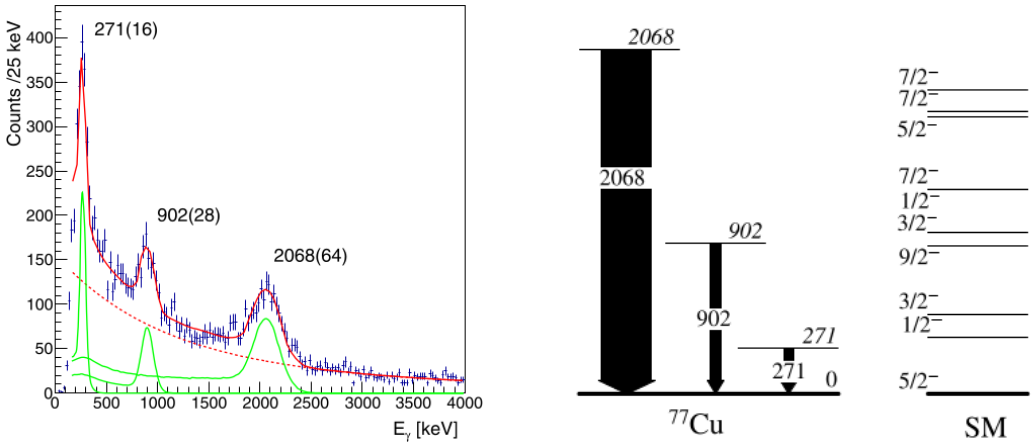

FIGURE 2.56: Spectrum of γ transitions in ^{77}Cu after knock-out from ^{78}Zn (left) and level scheme along with the theoretical prediction from the LNPS interaction (right). Taken from [Vaj18]

of $\gamma\gamma$ coincidences led to a level scheme that was equally simple, as can be seen in the second panel of the same figure. A shell-model study with the LNPS Hamiltonian in the $\pi fp\ \nu p f_{5/2}g_{9/2}d_{5/2}$ domain was duly performed.

Upon comparison, the first excited state at 271(16) keV was assigned a spin and parity of $3/2^-$ and probably matches the $3/2^-$ level at 293(1) keV from the β decay, the energy difference lying just outside the error bar. A $1/2^-$ possibility offered by the shell model was rejected since it was believed the removal of a proton would mainly populate the $\pi f_{7/2}$ hole and the subsequent γ deexcitation of a $7/2^-$ level would readily bypass a $1/2^-$ state. The line at 902(28) keV strayed 1.6 σ apart from the known 946(1)-keV transition. From the calculation a spin and parity of $3/2^-$ or $9/2^-$ could be advanced, both generated by the $\pi f_{5/2} \times 2^+$ coupling and at least for the latter spin consistent with the earlier observation. Since a 2^+ core excitation is likely not present in the ground state of ^{78}Zn, the multiplet member must be populated in the knock-out reaction by a stepwise mechanism. The third γ peak rose from the spectrum at 2068(64) keV, confirming the transition that had been surmised in the β decay at exactly the same energy. In as far as it was not fed from above by γ rays that went undetected but was directly populated in the knock-out reaction, it strengthened much the argument for a $f_{7/2}$ proton hole state.

Also spectroscopic factors were provided by the theory, here normalised to $2j+1$.

While for the ground state the factor reached only 1.5, for the $3/2^-$ level it stood disappointingly small at 0.2. The remaining fractions were not localised but possibly were absorbed in the multiplet states. The $7/2^-$ state ran off with a precious spectroscopic factor of 3.5, providing quantification for its nature as a proton hole. Three more fragments of the $\pi f_{7/2}$ distribution with an integrated weight of 2.9 popped up between 3 and 4 MeV, indicating that additional feeding may arrive at higher energies. The spread of the strength function over several levels is a noteworthy asset of the model that is less present in the A3DA-m calculation mentioned above.

Figure 2.57 combines the experimental data for the $3/2^-$ and $5/2^-$ states from β decay, laser spectroscopy and γ spectroscopy with that for the $7/2^-$ states from transfer reactions. For the latter the authors limited themselves to the first level, even if in particular for ^{71}Cu the centroid of the strength had been determined to lie higher. The present results for ^{77}Cu are included and theoretical single-particle energies for $\pi f_{5/2}$ and $\pi f_{7/2}$ relative to $\pi p_{3/2}$ from the $\pi + \rho$ meson exchange force are plotted alongside. While perhaps not the most recent calculation, this model drew its merit from simulating with relative ease the tensor interaction in the nucleus, which enjoyed renewed interest and which we dwelled upon in section 1.2 [Ots05]. The deviation from the theoretical energies was largest for the $7/2^-$ levels, implying that these are rather fragmented states for which a proper treatment of the centroid should be taken into account. Unless this is done, no conclusion on the evolution of the shell gap should probably be aimed at and the assessment by the authors as to the insensitivity to the isospin seems somewhat precipitous. As to the $5/2^-$ levels their single-particle nature appeared to be established with more certainty. In conclusion the $Z = 28$ gap defined by the $\pi f_{5/2} f_{7/2}$ spin-orbit splitting would shrink considerably from 4 MeV at $N = 40$ to 1.6 MeV at $N = 48$, binding more vigorously the $f_{5/2}$ protons at the cost of the $f_{7/2}$ ones. While the energy for this would be paid for by the tensor force through the action of the $g_{9/2}$ neutrons, the authors wrote that nevertheless the gap would not be reduced enough as to threaten the preservation of magicity in ^{78}Ni.

We may now shortly come back to the measurement of the magnetic moment of ^{75}Cu at RIBF that we presented in section 2.4 [Ich19]. Next to an appreciation of the $3/2^-$ and $1/2^-$ excited states, the article included a discussion of the ground-state inver-

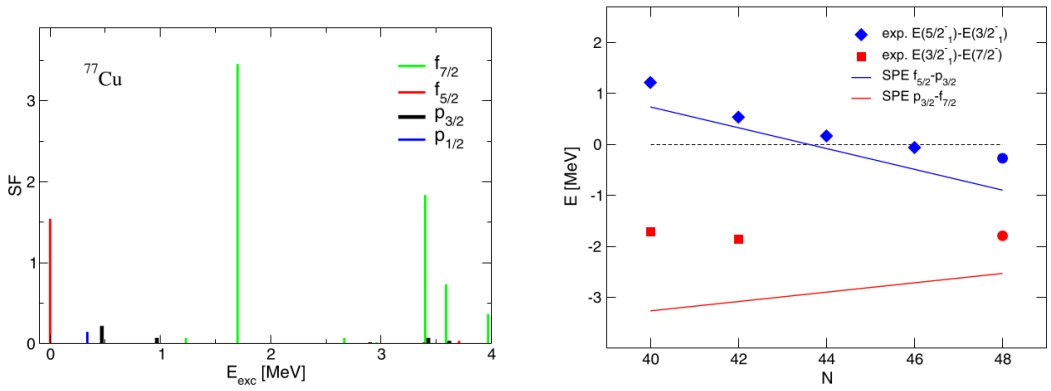

FIGURE 2.57: Spectroscopic factors in ^{77}Cu after knock-out from ^{78}Zn calculated with the LNPS interaction (left) and experimental energy differences for $3/2^-$, $5/2^-$ and $7/2^-$ states in copper isotopes compared to proton single-particle energy differences in nickel isotopes from the $\pi + \rho$ tensor force (right). Taken from [Vaj18]

sion in copper that drew on the A3DA-m shell-model force. It decomposed the $\pi f_{5/2}$ single-particle energy into a monopole term and a contribution from the excitation of the nickel core, in which neutrons in the $g_{9/2}$ orbital couple to a spin and parity of 2^+. The energy shift of the $5/2^-$ state survived this operation, basically because the 2^+ level from ^{72}Ni to ^{76}Ni remains at a fairly constant elevation of 1 MeV, although the precise position where it crossed the $3/2^-$ ground state was moved from $N = 48$ to $N = 46$. The energy evolution reproduced in figure 2.58 is not essentially different from what was shown in figure 2.55, where we explained how an earlier crossing of the orbitals could be achieved by adding higher-order multipoles. The lesson we retain is that in a refined treatment, the $5/2^-$ level can no longer be considered as a pure single-particle state but a significant fraction of its wave function derives from a $\pi f_{5/2} \times 2^+$ perturbation. The potential-energy surfaces that are pictured in figure 2.59 expose a prolate deformation in both the $5/2^-$ and $3/2^-$ states of ^{75}Cu that are mixed to such an extent as to turn them nearly indistinguishable. While at the same time the figure underscores that the underlying ^{74}Ni nucleus is not free from deformation either, the authors nonetheless insisted that the potential wells were not particularly deep in the middle of the neutron subshell and that sphericity would rapidly return to ^{78}Ni.

Still part of the Eurica series, the β decay of ^{75}Ni to ^{75}Cu was published only later on [Bel20]. Its level structure is completed and a $\Delta j = 1$ intruder band is posited, the

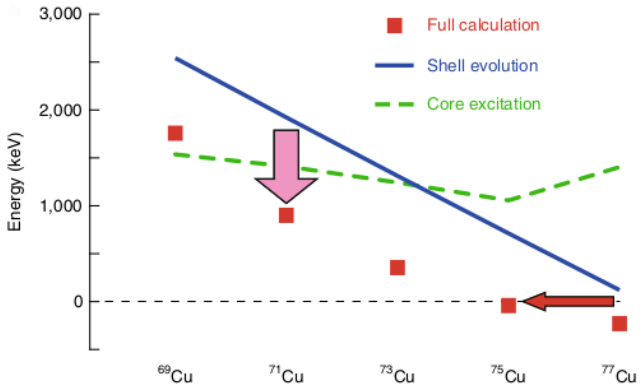

Figure 2.58: Decomposition of the $\pi f_{5/2}$ single-particle energy for copper isotopes calculated with the A3DA-m interaction. Taken from [Ich19]

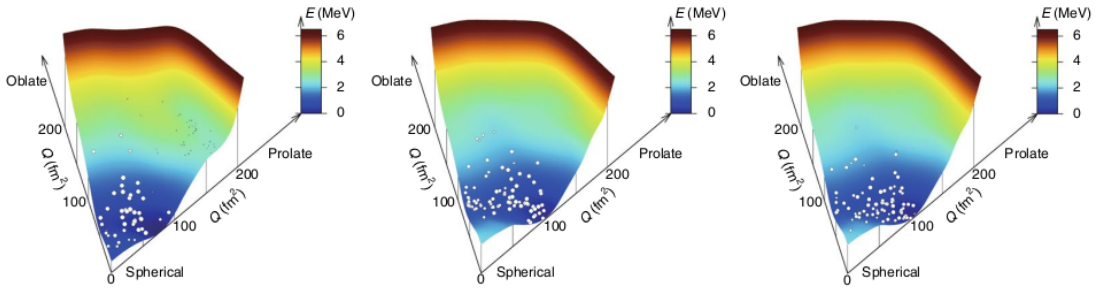

Figure 2.59: Potential-energy surfaces for the ground state of ^{74}Ni (left), the $5/2^-$ ground state (middle) and the $3/2^-$ excited state of ^{75}Cu (right) calculated with the A3DA-m interaction. Taken from [Ich19]

$7/2^-$ head of which would run through the copper chain in an analogous way to the 0^+_2 states in the nickel cores. The idea originates in the early interpretation that was given for the 1711 keV level in ^{69}Cu as a $\pi f_{7/2}$ hole [Bro98, Ish00] and picked up in the PCM calculations [Oro00]. Supported by an A3DA-m analysis, the remaining states were neatly classified into $\pi p_{3/2} \times 0^+, 2^+, 4^+$ and $\pi f_{5/2} \times 0^+, 2^+, 4^+$ configurations, regularly spaced by two units of angular momentum. While the clarity displayed by figure 2.60 certainly seduces, it brings an important part of the $\pi f_{7/2}$ hole strength down to just 1 MeV of excitation energy in ^{71,73}Cu. It climbs to 1484 keV in ^{75}Cu, well above the first tentative $7/2^-$ state that is experimentally seen at 950 keV. At 1680 keV a third candidate for a $7/2^-$ level, left out from the figure, would belong to the band built on the $\pi f_{5/2}$ particle. Reflecting on what we wrote at the end of section 2.3, any such

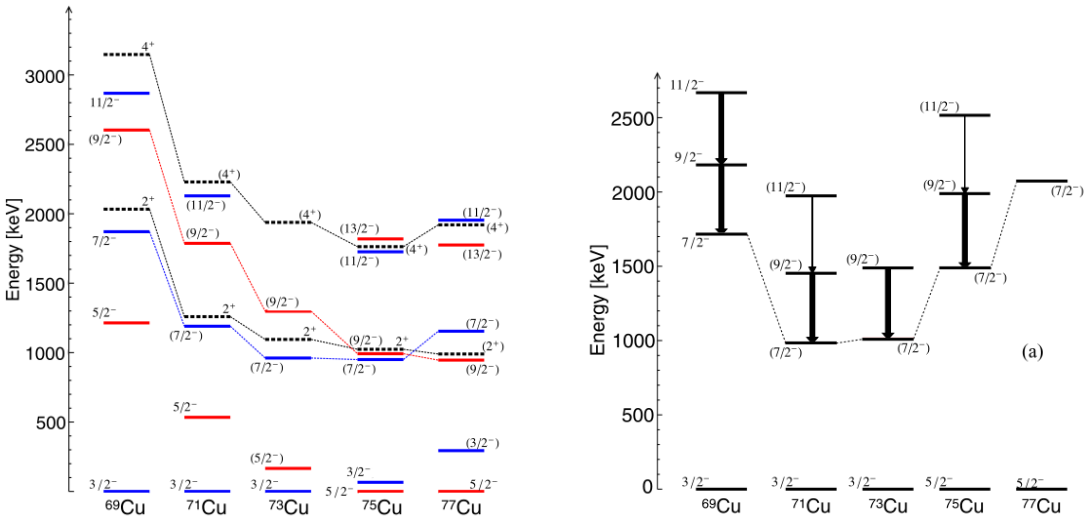

FIGURE 2.60: Systematics of particle-core coupling states from the $\pi p_{3/2} \times 0^+, 2^+, 4^+$ (blue) and $\pi f_{5/2} \times 0^+, 2^+, 4^+$ configurations (red) along with corresponding levels in the nickel cores (dashed) (left) and of intruder states (right) in the odd copper isotopes. Taken from [Bel20]

view will have to withstand the probe of proton pick-up, an issue that we postpone till chapter 4. We note in passing that for the $1/2^-$ state at 62 keV the theoretical wave function is scattered over many components but is expected to steeply raise its energy towards $N = 50$.

2.8 Sailing along $N = 50$

Not only RIBF was drawn into the quest for tackling the neutron-rich nickel region. Most other laboratories, however, committed themselves to heavier elements first as nickel is notoriously hard to extract from the target in conventional isotope separation on-line because of its chemical properties. So exploring a bit farther around the corner, they readily came upon $N = 50$, the other magic number of interest for the understanding of ^{78}Ni. Winding back several years and setting out at $Z = 35$, a $3/2^-$ ground-state spin and parity was deduced for the $N = 50$ nucleus ^{85}Br from the angular distribution in the ^{86}Kr(d,τ)^{85}Br transfer reaction realised at the Crocker cyclotron at Davis [May72]. As it indicated that the $\pi f_{5/2}$ orbital filled before the $\pi p_{3/2}$ one, a $5/2^-$ ground state therefore could be conjectured for ^{83}As at $Z = 33$ and ^{81}Ga at $Z = 31$.

To verify the hypothesis, the β decay of ^{83}Ge into ^{83}As was examined with a simple set-up of two germanium detectors at the Tristan isotope separator at Brookhaven [Win88]. From systematics the first excited state at 307 keV was presumed to carry a spin and parity of $3/2^-$ and linked to a $\pi p_{3/2}$ wave function above the $\pi f_{5/2}$ ground state. The $\pi p_{1/2}$ strength instead would be fragmented, a feature that is reminiscent of our discussion of the copper isotopes. Because the flurry of levels in the lower half of the scheme could be reasonably accounted for by a shell-model calculation with a new set of empirical two-body matrix elements that two of the authors, Xiangdong Ji and Hobson Wildenthal, just had prepared at Drexel university [Ji88], it was explicitly stated that no intruder configurations had to be invoked. The topic did not attract attention for many years, till ^{83}As was spotted again in the heavy-ion reaction of a ^{18}O beam on a ^{208}Pb target at the Vivitron facility in Strasbourg [Por11]. The γ decay of the 307-keV state was not observed, even if the Euroball germanium array that sought for it was assembled from the impressive number of 15 cluster detectors of seven closely-packed large-volume crystals each, 26 clover detectors of four smaller crystals each, and 30 single-crystal detectors. The yrast cascades typical for a high-spin fusion-fission experiment would indeed bypass it, indirectly confirming the assignments from the β decay.

As to ^{81}Ga, the $5/2^-$ spin and parity could be derived from the feeding pattern in its β decay to ^{81}Ge, measured at the Osiris separator at Studsvik [Hof81]. The $1/2^+$ and $5/2^+$ states at respectively 679 and 711 keV in ^{81}Ge were recognised as intruder states. Excited states in ^{81}Ga were identified in the β decay of ^{81}Zn, produced in deuteron-induced fission of ^{238}U at the Parrne mass separator at Orsay [Ver07]. For the first of these states at an energy of 351 keV a spin and parity of $3/2^-$ was suggested, which could be retrieved by the shell model with the jj44b force at a somewhat lower position as a $\pi p_{3/2} f_{5/2}^2$ configuration. The ground state was affirmed as rather pure with 75% of the $\pi f_{5/2}^3$ structure. From the extrapolation of the computations, a doubly magic ^{78}Ni nucleus was projected. We add that the authors invested a dedicated effort in a modified Ji-Wildenthal interaction for ^{81}Ga, which however did no longer reproduce the $5/2^-$ ground-state spin of ^{83}As that occurred in the original work by Ji and Wildenthal as well as for the jj44b Hamiltonian.

Collinear laser spectroscopy of gallium took place at Collaps at Isolde [Che10]. In ^{75,77}Ga the $3/2^-$ ground states were ascribed to a $\pi p_{3/2} f_{5/2}^2$ wave function. In ^{79}Ga, however, the measured magnetic and quadrupole moments imposed that the same $3/2^-$ spin would stem from a ground state in which the $\pi f_{5/2}^3$ component would prevail. Experimentally the inversion of the $p_{3/2}$ and $f_{5/2}$ proton orbitals thus appeared accomplished in quite a comparable manner as for copper, even if the spin values did not directly correspond to a single-particle orbital but ought to be understood from a construction of three quasiparticles. While clarifying the moments, the jj44b and JUN45 Hamiltonians that were called upon backtracked as to the level ordering. Sticking to a $\pi p_{3/2} f_{5/2}^2$ picture of the ground state, both put the correct configuration several hundreds of keV too high. In ^{81}Ga, a spin of $5/2^-$ was found in line with the β-decay work. Having reached $N = 50$, the protons would rearrange within the orbital and settle for a single-particle scheme, which now the calculations had no difficulty to certify.

With the successive isotope chains closing in on $N = 50$, it became possible to probe the neutron parameters themselves. A radioactive beam of ^{79}Zn was post-accelerated to 2.83 MeV per nucleon at Isolde [Orl15]. Sent onto a target of deuterated polyethylene, protons emitted from the ^{78}Zn(d,p)^{79}Zn transfer reaction were registered in the T-Rex array of segmented silicon telescopes while γ rays were collected in eight triple-cluster germanium detectors of the Miniball set-up. A level at 983 keV above the $9/2^+$ ground state was populated but as one may assess from figure 2.61 the angular distribution showed almost no variation. From the adopted correspondence with a $\ell = 2$ angular distribution calculated by means of DWBA a spin and parity of $5/2^+$ was assigned, which with a spectroscopic factor of 0.38(5) would be spawned by the $\nu d_{5/2}$ single-particle state.[19] While a second transition at 441 keV clambered above this level, a third line at 236 keV could not be placed for the lack of a proper coincidence relation and instead was deduced to decay into an isomer. From the proton spectrum it was nevertheless possible to reconstruct its excitation energy as 1100(150) keV. Because of the underlying background the angular distribution could not be extracted easily but from a combined fit in a broader energy range a transferred momentum compatible with $\ell = 0$ and a spectroscopic factor of 0.41(3) were put forward, quali-

[19] In this work the spectroscopic factors appear to be normalised to 1

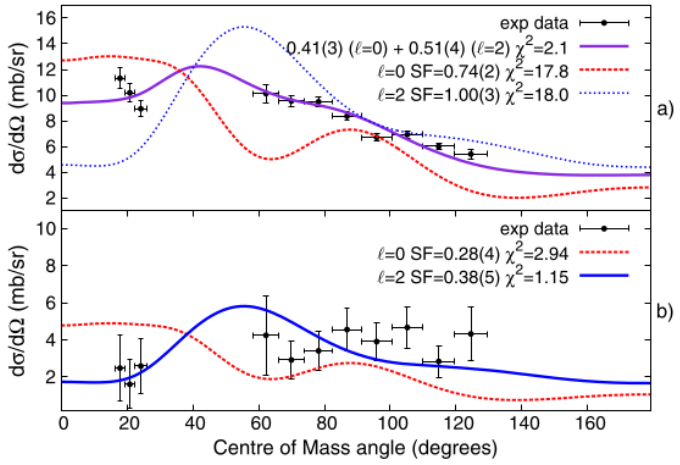

Figure 2.61: Proton angular distributions in the ^{78}Zn(d,p)^{79}Zn reaction for an excitation energy of 0.85 to 1.55 MeV (top) and requiring an additional coincidence with the 983-keV γ transition (bottom) compared to DWBA calculations. Taken from [Orl15]

fying the isomer as a $1/2^+$ state with a $\nu g_{9/2}^{-2} s_{1/2}$ structure. In spite of the rather limited evidence from the experiment, the $N = 50$ gap was declared as robust.

Laser spectroscopy still at Collaps confirmed the existence of the $1/2^+$ isomer [Yan16]. A sharp increase in the mean squared charge radius by 0.204(6) fm^2 was interpreted as a neutron excitation from the $g_{9/2}$ to the $s_{1/2}$ orbital that would develop into a halo-like structure, albeit diluted from mixing with a $\nu g_{9/2}^{-2} d_{5/2}$ contribution coupled to a collateral phonon to account for the spin. Descending the $N = 49$ isotones from ^{87}Sr to ^{79}Zn, the systematics compiled in figure 2.62 demonstrate a sequence of 1p-2h intruder states that falls below 1 MeV in ^{83}Se, after which the trend would turn over and one would witness a decrease in deformation of the $1/2^+$ state as its wave function would gradually change content from $\nu g_{9/2}^{-2} d_{5/2} \times 2^+$ to $\nu g_{9/2}^{-2} s_{1/2}$. Above the near-spherical ground state of ^{79}Zn a spherical $\nu s_{1/2}$ intruder would stand, with an increase in radius that is large enough to justify the measured isomer shift and redeem the credit of establishing the first sign of shape coexistence near ^{78}Ni.

The energy of the isomer was determined soon after through γ spectroscopy at RIBF, fixing it at 943 keV [Del16]. The aptness of the PFSDG-U interaction written in the wake of shape coexistence was illustrated by its magnetic moment [Wra17]. The experimental g factors, defined as the dimensionless ratio $g = \mu/I$, are summarised

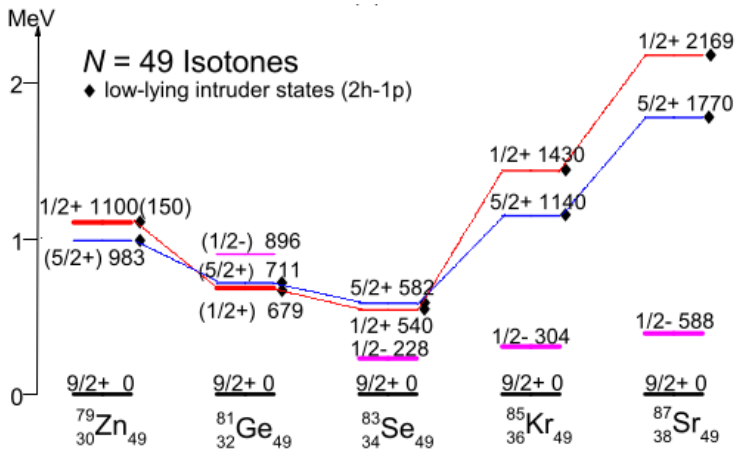

FIGURE 2.62: Systematics of the first $1/2^-$, $1/2^+$, $5/2^+$ and $9/2^+$ levels in the $N = 49$ isotones. Taken from [Yan16]

across the zinc isotopes in figure 2.63, in which also sundry calculated results are gathered. As usual for jj44b and JUN45 the spin gyromagnetic ratios g_s were reduced by a factor 0.7 from the free values and effective charges of $e_\pi = 1.5e$ and $e_\nu = 1.1e$ were taken. For A3DA-m, LNPS-m, and PFSDG-U no scaling of the g factor was judged necessary and the effective charges were set at $e_\pi = 1.31e$ and $e_\nu = 0.46e$.[20] The plot strikingly testifies how the $1/2^+$ isomer in ^{79}Zn knocked out all theories except for PFSDG-U. If we evaluate the respective model spaces, $f_{5/2}pg_{9/2}$ for jj44b and JUN45, $fpg_{9/2}d_{5/2}$ for A3DA-m, $\pi fp\ \nu f_{5/2}p_{1/2}g_{9/2}d_{5/2}$ for LNPS-m, and $\pi fp\ \nu sdg$ for PFSDG-U, the inclusion of the $\nu s_{1/2}$ orbital in the latter was clearly instrumental for a correct computation.[21] The satisfactory agreement for the high-spin ground states, in particular for those interactions that did not allow for cross-shell excitations, otherwise provided an indication that the magicity of ^{78}Ni would be upheld both for protons and neutrons. On the other hand we might keep in mind that the PFSDG-U work would not follow up on the $1/2^-$ and $5/2^-$ states in the lighter isotopes, for which the νfp orbits are essential ingredients.

We shall pick up on shape coexistence in the next section but for now remain in the

[20] While the authors explicitly refer to [Len10], where a polarisation charge of 0.5 is adopted such that $e_\pi = 1.5e$ and $e_\nu = 0.5e$, we do find the quoted numbers in the LNPS calculations of [Cor18]

[21] Although the LNPS-m domain is defined in the paper as $\pi fpg_{9/2}d_{5/2}\ \nu pf_{5/2}g_{9/2}d_{5/2}$, we write the one that is quoted by [San15], the difference likely being irrelevant

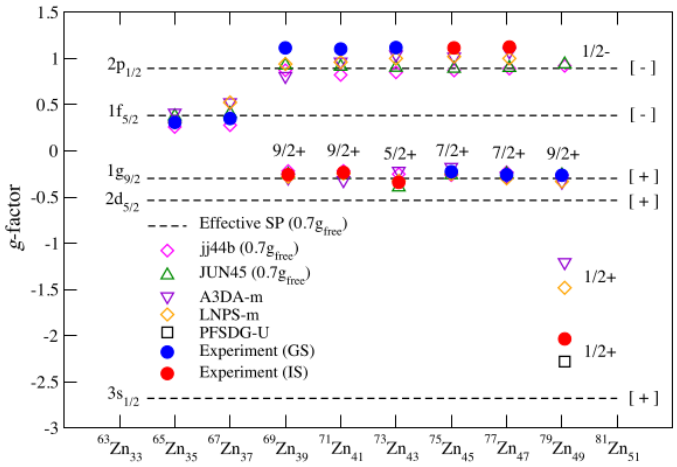

Figure 2.63: Experimental g factors of ground and isomeric states in zinc isotopes compared to theoretical expectations. Taken from [Wra17]

zinc chain. The mean squared charge radii were investigated at the Collaps laser line as well and like elsewhere on the nuclear chart displayed a typical odd-even staggering, which extended up to ^{79}Zn [Xie19]. Introducing the differential quantity

$$\Delta^{(3)}\langle r^2\rangle = \langle r_A^2\rangle - \frac{1}{2}(\langle r_{A-1}^2\rangle + \langle r_{A+1}^2\rangle), \tag{2.7}$$

which is positive if the charge radius is bigger and negative if it is smaller than the local average, we observe from figure 2.64 that the isotopes with an odd neutron are smaller than their neighbours with an even number of neutrons. The reason resides in a mechanism known as blocking, through which the odd neutron prevents the scattering of fellow neutron pairs into higher orbitals. By virtue of their mutual interaction also the protons are left in their lowest energy states and hence the charge radius is minimal. Upon closer look, however, the odd-even behaviour proved more delicate to interpret, for it became anomalous in ^{71}Zn. The 41 neutrons produced an exceptionally large radius, as the single $g_{9/2}$ neutron appears to draw more of its kin across the $N = 40$ gap because of the corresponding gain in pairing energy. Once again the protons would then walk the path opened by the neutrons. Conversely the neighbouring ^{70,72}Zn isotopes could be stunted, as a $g_{9/2}^2$ neutron excitation without a catalyst would require an expensive change in parity for two particles. Calculations with the A3DA-m interaction comforted the conclusions, albeit the inversion being stronger even in theory than in experiment. The article incidentally included a second version of the A3DA-m

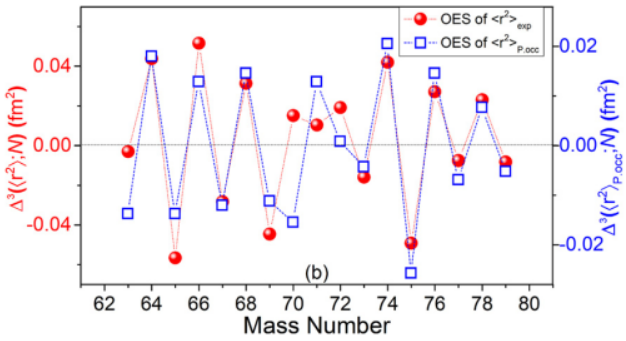

FIGURE 2.64: Odd-even staggering of zinc isotopes (red) compared to calculations with the A3DA-m interaction (blue). Taken from [Xie19]

force in an enlarged $pfsdg$ valence space, hitting back at the $1/2^+$ isomer in ^{79}Zn with a prediction for its magnetic moment that was accurate to 3%.

The copper isotopes were next to fall victim to Isolde. We discussed in detail in section 2.1 how both intrasource and collinear laser spectroscopy had constrained the ground-state wave function of ^{75,77}Cu. In section 2.6 laser experiments scrutinised and provided spin assignments for several odd-odd isotopes. Having acquired more luggage throughout this paragraph on the $N = 50$ gauge, we may now elaborate on the experiment that took place at Cris and explore the importance of the valence orbitals for the JUN45, A3DA-m and PFSDG-U interactions specifically [DeG17]. While the three models now all applied the same fine tuning of the magnetic dipole moment, that is spin gyromagnetic ratios g_s quenched by a coefficient of 0.75 and orbital g_l factors of 1.1 for protons and -0.1 for neutrons, we recall that for the electric quadrupole moments effective charges were chosen of $e_\pi = 1.5e$ and $e_\nu = 1.1e$ in JUN45 but $e_\pi = 1.31e$ and $e_\nu = 0.46e$ in A3DA-m and PFSDG-U. From figure 2.65 it can be read that for JUN45 its $f_{5/2}pg_{9/2}$ model space indeed was not sufficiently large to accurately describe the measurements.[22] Accordingly the better performance for A3DA-m was traced to its inclusion of the $f_{7/2}$ orbital below and $d_{5/2}$ one above. It also appeared that the PFSDG-U force did not derive clear benefit from adopting the even wider scope of $\pi fp\ \nu sdg$ to let the neutrons freely flow into the upper orbitals, as the agreement with the experimental data did not improve further. Indeed the quasi-SU(3) symmetry

[22] Somewhat surprisingly the values for JUN45 from [DeG17] in figure 2.65 do not precisely match those from [Koe11] in figure 2.4

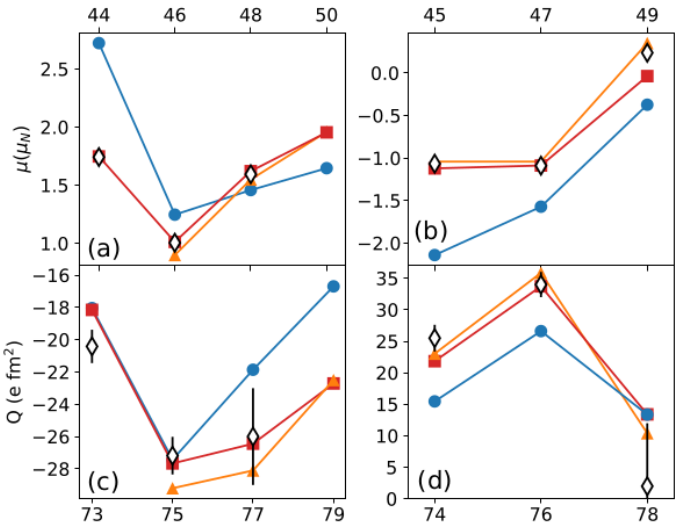

Figure 2.65: Magnetic moments (top) and electric quadrupole moments (bottom) of neutron-rich copper isotopes compared to calculations with the JUN45 (blue), A3DA-m (red) and PFSDG-U (orange) interactions as a function of N (top axis) and A (bottom axis). Taken from [DeG17]

between the $\Delta j = 2$ $\nu g_{9/2} d_{5/2}$ states, a basic tenet underlying the model, did not require the superfluous $\nu s_{1/2} d_{3/2} g_{7/2}$ orbitals. For the quadrupole moment of ^{75}Cu one even notices a deterioration, adding caution as to the complexity of this quantity.

The mean squared charge radii from the Cris experiment were published some years later, allowing for fresh light to be shone on them [DeG20]. The odd-even staggering $\Delta^{(3)}r$ here was defined for the charge radii themselves but with an opposite sign, so for the smaller odd isotopes the number turns positive. The reader can be convinced of the regular pattern in figure 2.66. Intriguingly, however, the staggering faded away as one neared the $N = 50$ closure. Through careful inspection a correlation with the infamous change in the ground-state spin was discerned. The dynamics of the neutron field that polarises the proton distribution would be inhibited and the odd-even tango interrupted when the solitary proton stumbles from $p_{3/2}$ into $f_{5/2}$, the quantum state that governs the copper ground state from $N = 46$ on.

The Density-Functional Theory (DFT), into which Witek Nazarewicz at Michigan and Paul-Gerhard Reinhard at Erlangen incorporated the parametrisations proposed by Sergey Fayans in Moscow, largely reproduced the absolute values of the radii. Zoom-

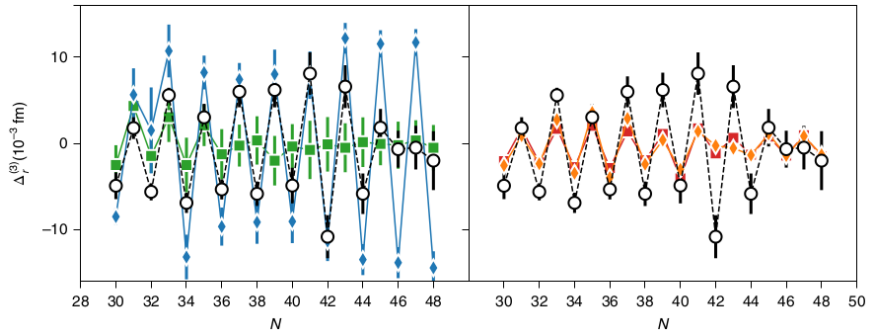

FIGURE 2.66: Odd-even staggering of copper isotopes compared to calculations with the Fy(std) (green) and Fy(Δr) (blue) DFT (left) and the EM 1.8/2.0 (orange) and PWA (red) VS-IMSRG parametrisations (right). Taken from [DeG20]

ing in, the Fy(std) functional underestimated the amplitude of the odd-even variation whereas the Fy(Δr) one followed it more closely. Both, however, failed to account for the spin inversion at $N = 46$, visibly a step too far for the current theoretical tools. The Valence-Space In-Medium Similarity Renormalisation Group (VS-IMSRG), its chaldean denomination hiding the respective contributions from a shell-model diagonalisation in the valence space and an ab-initio renormalisation technique, was put to use by Jason Holt and his collaborators at Vancouver with a choice of two chiral interactions. The EM 1.8/2.0 potential embodies a refinement of the N^{3}LO force from Entem and Machleidt, the numerals referring to the cut-off momentum Λ and the three-nucleon cut-off momentum Λ_{3NF}. The second one labelled PWA was constrained from the partial-wave analysis of proton-proton and proton-neutron scattering. Both forces fared well at the $N = 28$ and $N = 50$ shell closures but missed the finer features, almost forlorn at the strong staggering in $^{68-73}$Cu and showing little sensitivity to the switching proton orbitals beyond.

Among the results from Isolde we should not forget to mention the mass measurement of ^{79}Cu at Isoltrap [Wel17]. At a rate of barely two ions per microcoulomb the superior accuracy of the Penning traps quickly shoved aside previous work with an analysing dipole magnet at Holifield [Hau06]. Challenged by a meagre yield of $6\,10^{-3}$ events per second and at low resolution the latter had been honestly qualified by the authors themselves as opportunistic but nonetheless had left an anomalous entry in the literature. Instead in the new experiment, a smooth continuation of the mass surface

was evidenced. Although the hallmark of magicity is most commonly obtained from the behaviour of the mass surface across a gap rather than its mere extension before it, the authors anticipated the ^{78}Ni neighbour to be doubly magic from the skillful performance of shell-model calculations with the PFSDG-U force. While the comparison with the JUN45 predictions was perhaps not decisive without passing the threshold of $N = 50$, its treatment of particle-hole excitations in an appropriate model space certainly put it at an advantage.

2.9 An anchor of nuclear structure

Looking for a spot to drop our anchor in a sea of experimental striving, we recall our discussion from section 2.5 where with firm guidance the PFSDG-U interaction had put us back on the nickel track. We wrote that it postulated a first excited 0_2^+ level at an energy of 2.65 MeV in ^{78}Ni, steering attention to the phenomenon of shape coexistence [Now16]. At the same time two 2^+ states were situated at 2.88 and 3.15 MeV, respectively. The 0_2^+ and 2_1^+ levels would belong to a prolate 2p-2h intruder band with $\beta_2 \approx 0.3$, while the 2_2^+ state would be built from a 1p-1h configuration. The deformation originated from enhanced quadrupole correlations in specific subspaces. Next to the quasi-SU(3) symmetry that we introduced before, the concept of pseudo-SU(3) symmetry was called upon. It pertains to the coherence of all levels within a given oscillator shell except for the one with the highest total momentum, that is the $\nu p_{3/2} p_{1/2} f_{5/2}$ set below $N = 40$ and the $\nu s_{1/2} d_{5/2} d_{3/2} g_{7/2}$ group above $N = 50$. Quasi-SU(3) symmetry then relates to the degeneracy of the remaining orbital with a $\Delta j = 2$ partner orbital within the same primary shell, for instance of $\nu g_{9/2}$ with $\nu d_{5/2}$ above $N = 40$, setting the scene for $\nu g_{9/2}^{-2n} d_{5/2}^{2n}$ quadrupole correlations to take their turns. Closer to $N = 50$ the matter is slightly different, as collectivity might already be generated by the sole quadrupole moment of an open $\nu g_{9/2}$ orbital. The potential-energy surface for ^{78}Ni is pictured in figure 2.67, where next to the spherical ground state we identify an oblate minimum at $\beta_2 \approx 0.3$. In the previous section we passed under the spotlight the appearance of an isomer in ^{79}Zn and explained it as a first token of shape coexistence in the region, pressing the salience of PFSDG-U.

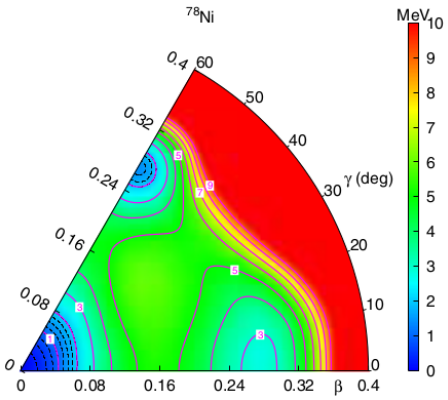

FIGURE 2.67: Potential-energy surface for ^{78}Ni from the PFSDG-U interaction. Taken from [Now16]

So expectations were high and minds were tuned when ^{78}Ni finally came within sight of in-beam γ spectroscopy at RIBF. Hoisting the flag of Seastar again and taking advantage of an intensity of 12 pnA of primary beam of ^{238}U hitting at 345 MeV per nucleon a solid piece of beryllium, 5 particles of ^{79}Cu and 290 of ^{80}Zn were produced per second [Tan19]. Identified and selected in the Bigrips spectrometer, the secondary projectiles at 250 to 280 MeV per nucleon induced (p,2p) and (p,3p) knock-out reactions in a thick target of liquid hydrogen. The escaping protons were recorded and their vertex reconstructed in the Minos time-projection chamber surrounding the cryogenic tube while the associated prompt γ rays were registered in the Dali-2 array of 186 NaI(Tl) scintillator crystals. The outgoing heavy fragment was tagged in the Zerodegree spectrometer. Surprisingly the γ spectra from the two specified reaction channels proved strikingly different. Plotted in figure 2.68, a keen candidate for the first 2^+ energy lay at 2600 keV in one spectrum but at 2910 keV in the other. Either value seemed high enough for ^{78}Ni to be invested as doubly magic at last, a major celebration for a much weathered and challenged shell model, but the circumstances undeniably pointed at the population of adjacent separate structures. Coincidence spectra were constructed and albeit low in statistics the data did not display any transition in common, as we can learn from figure 2.69. Even if a possible deformation could not be determined directly, it was tempting to infer the detection of a low-lying parallel band and eventually the emergence of shape coexistence.

New data provoke new theories. Already whilst awaiting the publication of the

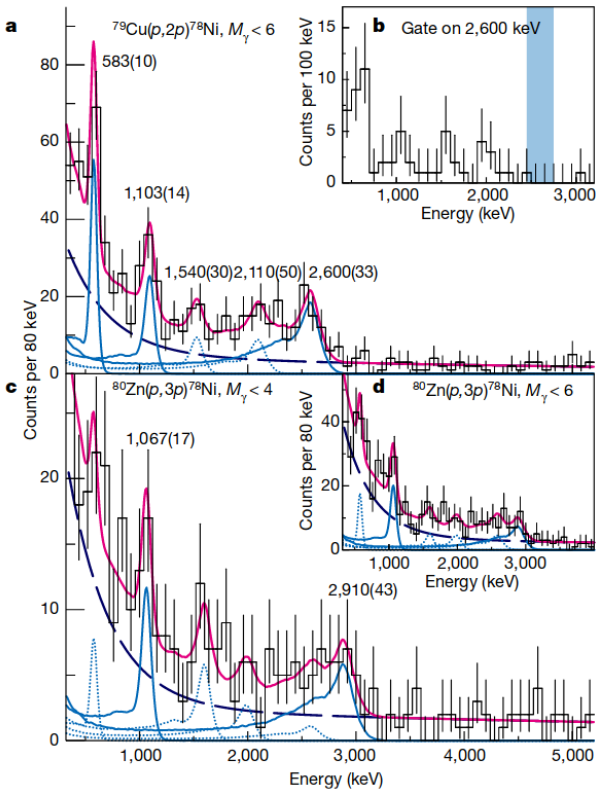

Figure 2.68: The γ spectrum of ^{78}Ni in the ^{79}Cu(p,2p) (top) and ^{80}Zn(p,3p) (bottom) reactions. Taken from [Tan19]

data, Gaute Hagen and collaborators at Tennessee refined the Coupled-Cluster (CC) technique and built on the EM 1.8/2.0 chiral force introduced before to establish a correlation between the energy of the first 2^+ state in ^{48}Ca and in ^{78}Ni [Hag16]. Anticipating the experimental result they evoked for ^{78}Ni an energy comprised between 2.1 and 3.1 MeV. An overview of the 2^+ energies in the nickel chain together with the Coupled-Cluster results is brought together in figure 2.70 with the value for ^{78}Ni added to figure 2.69. In this work, however, shape coexistence was absent from the horizon like a mirage lost.

Next on stage we welcome back VS-IMSRG. Developed in an international effort between Darmstadt, Michigan, and Tokyo, with fresh input from Ohio it had computed a range of ground-state energies up to ^{78}Ni some years earlier [Her14]. Overhauled at Vancouver, here it posited a core of ^{60}Ca that is girded by the $\pi fp\ \nu sdg$ valence orbitals and injected into this space the same EM 1.8/2.0 interaction as for the Coupled-Cluster

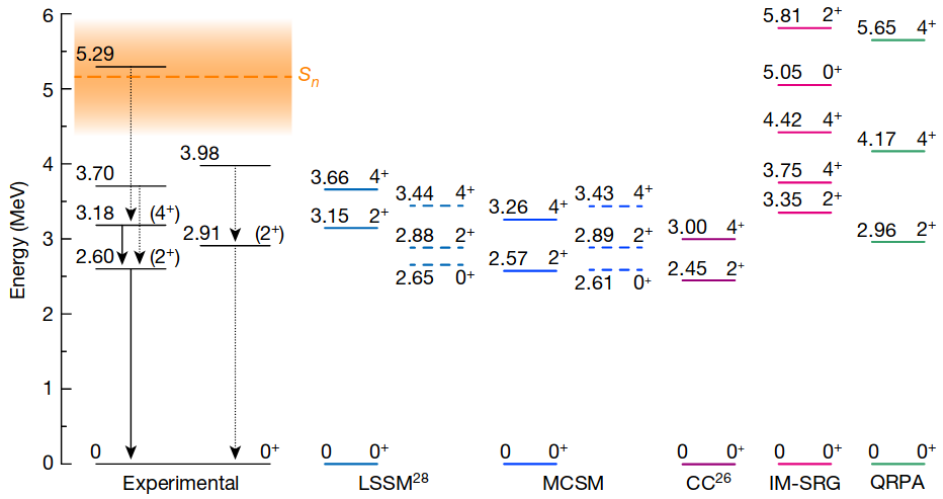

FIGURE 2.69: Experimental level scheme of ^{78}Ni compared to the LSSM, MCSM, CC, VS-IMSRG and QRPA theoretical models. Taken from [Tan19]

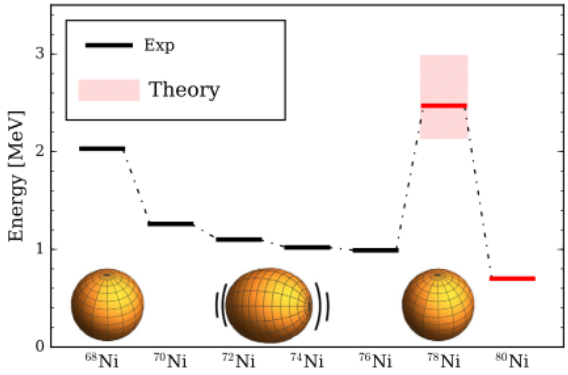

FIGURE 2.70: Experimental 2^+ energies in neutron-rich nickel isotopes (black) compared to CC calculations with the EM 1.8/2.0 interaction (red). Taken from [Hag16]

calculations. It then delved into the box of ab-initio mastery and pulled out a 2^+ energy of 3.35 MeV, as can be read from figure 2.69. The figure stood rather high, because unfortunately particle-hole excitations were truncated at low order. Neither was there in the model any mention of shape coexistence, the second 2^+ state at 5.81 MeV checking in as spherical.

Meanwhile a QRPA treatment was undertaken by Sophie Péru at Arpajon that incorporated the Gogny D1S interaction, a force in which the surface energy of the nucleus is adjusted to arrive at a correct description of fission barriers [Per14]. In figure 2.71 we present its projected 2^+ energy for ^{78}Ni just above 3 MeV. The figure also

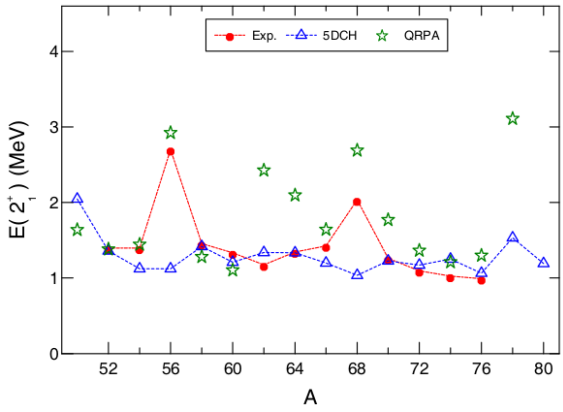

Figure 2.71: Experimental 2^+ energies in nickel isotopes (red) compared to 5DCH (blue) and QRPA (green) calculations with the D1S interaction. Taken from [Per14]

includes an evaluation of the D1S force with the 5DCH formalism. As can be read from the plot, both performed awkwardly for particular isotopes but much better for other ones. Notably at magic numbers the QRPA scheme appeared more adequate than 5DCH, so it was the more obvious choice when the computations were evaluated anew when the experimental value was made public. This time the D1M interaction was embraced, which instead endeavours to accurately fit the equation of state of neutron matter as well as to provide a universal mass model. The updated calculation put the 2^+ state at 2.96 MeV, hitting not far off the mark but with a balance of 65% of neutron excitations from $g_{9/2}$ to $d_{5/2}$ and 28% of proton promotions from $f_{7/2}$ to $f_{5/2}$ it did not uncover competing forms.

Scanning the horizon for shape coexistence to appear, the MCSM approach turned up. Although in principle tagging a technique, the label was adopted to designate the broader strand of shell-model codes formulated by the Tokyo group. The valence domain was enlarged to the entire *fpsdg* realm and an expanded A3DA-m force was moved into gear. We exemplified above in section 2.5 how the model contained the keys for generating shape coexistence in ^{68}Ni, but whereas originally it only had computed a spherical structure for ^{78}Ni just below 3 MeV, it now was able to produce two 2^+ states at 2.57 and 2.89 MeV. The second one would belong to a prolate deformed band with $\beta_2 \approx 0.3$ lurking atop the 0^+_2 state at 2.61 MeV. Looking from close by the size of the valence space seemed critical, since without the $\nu s_{1/2} d_{3/2} g_{7/2}$ orbitals the 2^+

energies drifted upwards to 2.89 and 4.72 MeV. The structural discord between both bands became evident from the number of particle-hole excitations that they involved. For the spherical stretch this amounted to 0.5 for protons and 1 for neutrons, while the deformed sequence scored 2.5 both for protons and neutrons.

The PFSDG-U force from Strasbourg, with which we opened this section, was granted a larger scope by gluing it together at the $N = 44$ neutron midshell with the LNPS matrix elements. Covering the complete region of interest, the new framework was given the generic name of Large-Scale Shell Model (LSSM). The resulting 2^+ levels that we reported above deviated from the A3DA-m calculation not so much in energy as in their nature. As a matter of fact the spherical state conformed not to the 2^+_1 but to the 2^+_2 mark, which was dominated by a 1p-1h excitation. Sitting 270 keV lower, the 2^+_1 prolate intruder counted 2.5 particle-hole contributions, again whirring at $\beta_2 \approx 0.3$. In both the MCSM and LSSM models, shape coexistence was thus definitely sparked even if experimentally one could not readily assess which 2^+ state was spherical or deformed. If nevertheless the 0^+_2 intruder band head, located at 2.61 MeV for MCSM and at 2.65 MeV for LSSM, would stay on a downwards trajectory beyond $N = 50$, magicity would quickly melt away.

In order to appreciate the pathway of the knock-out process to arrive in the different structures, it is instructive to examine the spectroscopic factors that the calculations supplied for the (p,2p) channel. Taken as measures for the probability of an initial configuration to appear in the content of the final wave function, they were multiplied with single-particle cross sections obtained from the Distorted-Wave Impulse Approximation (DWIA) designed by Kazuyuki Ogata and collaborators at Osaka to yield partial cross sections to individual levels [Wak17]. There is a degree of inconsistency in the approach as the spectroscopic factor is determined by matching the experimental level with a theoretical one that most often sits at a different energy, while the DWIA cross section is calculated for a single-particle state at the very energy of the experimental level. However, as the energy dependence of the cross sections is rather weak, the error is small. We digest the cumulative partial cross sections in figure 2.72.

Apart from knock-out of a $f_{5/2}$ proton to the ground state, it appeared that the strength for removing a more deeply hidden $\pi f_{7/2}$ particle was situated above 4 MeV.

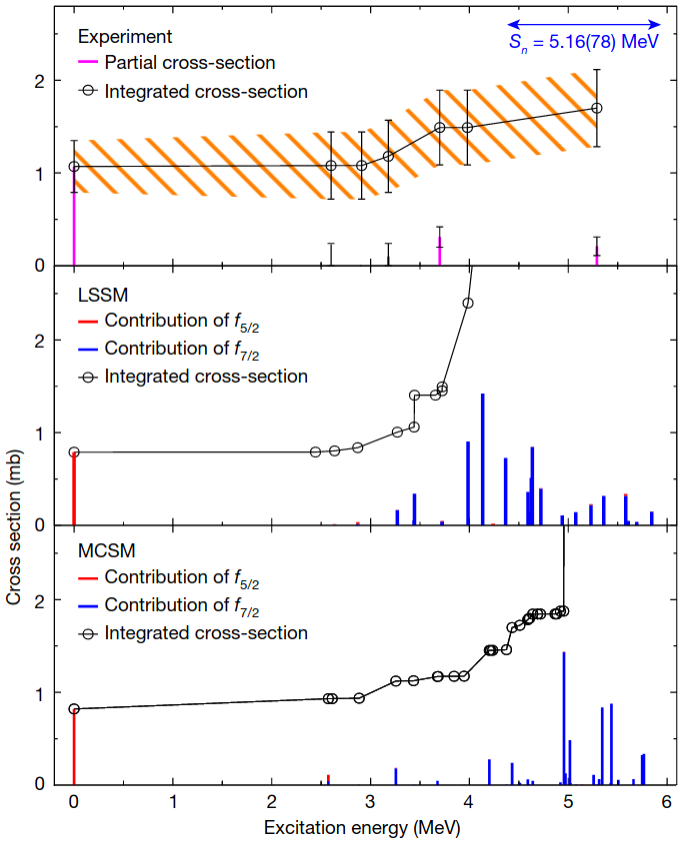

Figure 2.72: Experimental cumulative partial cross sections for ^{78}Ni in the ^{79}Cu(p,2p) reaction (top) compared to the LSSM (middle) and MCSM (bottom) theoretical models. Taken from [Tan19]

Importantly it was also fairly fragmented, for LSSM even more so than for MCSM. It meant that the reaction would create a hole at high energy distributed over many quasiparticle states rather than accessing either of the 2^+ levels directly. Since the γ spectrum was well accounted for by fitting the response functions of the identified transitions, the nucleus would deexcite through a swarm smaller of γ rays that each on its own remained below the detection threshold. While the reaction model did not cover the (p,3p) mechanism, one might expect that the ejection of a pair of protons would privilege the ground state as well as 2p-2h structures as final configurations. Whether the latter would commit to deformation could not be confirmed, as the lack of agreement in the theoretical overlap functions for two nucleons between zinc and nickel cautioned against it.

The first γ spectroscopy of ^{78}Ni brought many clues but it seems early to call it a day. Walking through a wealth of experimental data in the preceding sections of this chapter, we found arguments that favoured the weakening as well as the persistence of the shell gaps in ^{78}Ni. Among the former, perhaps most convincingly a new island of inversion was brought to the surface [San15]. As to its survival as a doubly magic icon, we may cite the visibility of single-particle structures in the level scheme of ^{77}Cu [Sah17a, Vaj18], the regular behaviour of electromagnetic moments from laser spectroscopy [DeG17], or the mass measurement of ^{79}Cu [Wel17]. Holding a middle way, shape coexistence came out of the woods in ^{79}Zn [Yan16] and ^{78}Ni itself [Tan19]. The interpretations we gave often rested on a latticework of specific facets determined by individual orbitals that alternate with collective phenomena. But rivalling theoretical views as to the deeper origins endured. A drifting monopole component of the tensor force was put forward, perhaps at times hard to distinguish from a failing spin-orbit potential. The action of pairing and quadrupole forces in quasi-SU(3) and pseudo-SU(3) symmetry schemes showed its strength, whereas the prospects that chiral forces offer were briefly highlighted. While we round up our overview of the experimental data here, we now touch land and seek to explore more carefully these theories.

Chapter 3

Theoretical endeavour

In the first chapter of our text we passed in review some key elements of the physics of the *sd* shell. We were left undecided as to the precise mechanism within the nuclear force that unsettles the magic numbers 20 and 28. As our discussion progressed, we moved from lighter to medium masses to arrive at the *fp* orbitals, which carried our interest in the previous chapter. For their theoretical description we shall start from the particle-core coupling model, which aims at a schematic view of individual single-particle states that are weakly coupled to the vibrations of an underlying core. Next we shall attempt to understand the evolution of such states from more complete calculations with elaborate nuclear Hamiltonians in the shell model. We shall then extend this insight to the interpretation of shape coexistence, a central guest in the wider plots of nuclear structure.

3.1 The particle-core coupling model

Since the copper isotopes present us with a lonesome proton outside a supposedly closed nickel nucleus, it is legitimate to attempt a description that couples the outlying particle to the inner core. Originally proposed by Aage Bohr and Ben Mottelson the technique knows many emanations, of which the Particle-Core Coupling Model (PCM) written by Kris Heyde and Pieter Brussaard at Utrecht is one example [Hey67, Oro00]. The core is allowed to generate up to three quadrupole and two octupole vibrations, to which a single particle with energy ϵ_j is added. The 0_2^+ excitation is simulated by

the superposition of two phonons. Also the 2p-1h configuration is considered, which by virtue of the additional proton pair can be treated as a hole etched into a core of zinc and bring into play the collective excitations of zinc. The interaction between the single particle or the hole and the phonon of multipole order λ is formulated as the product of a coupling strength ξ_λ, the phonon energy $\hbar\omega_\lambda$, and a spherical harmonic function $Y_{\lambda\mu}$. As it is independent of the specific nature of the particle or the hole, the model is essentially defined by the set of parameters ϵ_j, $\hbar\omega_\lambda$ and ξ_λ. Where possible they are extracted from experimental data but extrapolated otherwise.

The PCM finds the first $5/2^-$ state in ^{69}Cu at 1161 keV and predicts it to come down to 683 keV in ^{71}Cu and 211 keV in ^{73}Cu. While the agreement is most satisfactory, it is not so much of a surprise as it is directly related to the choice of $\epsilon_{f_{5/2}}$, which is shown in figure 3.1 and drops from 0.90 MeV in ^{69}Cu to -0.30 MeV in ^{73}Cu. The crossing of the $p_{3/2}$ and $f_{5/2}$ proton orbitals is thereby effectively imposed at $N = 44$. Two $7/2^-$ states are calculated, revealing themselves as $\pi p^2_{3/2} f^{-1}_{7/2}$ and $\pi p_{3/2} \times 2^+$ structures. Hovering high at 1.6 and 1.9 MeV in ^{69}Cu, they reduce their mutual distance to 0.1 MeV and fall to an energy of 1.1 MeV in ^{71,73}Cu. Their parametrisation deserves a diligent examination, for which figure 3.2 may be helpful. On one hand an unperturbed 2p-1h excitation is injected as surrogate input for the position of the $\pi f_{7/2}$ single-particle state. Within the present scheme it captures the $Z = 28$ gap, except for the pairing gain among the two $\pi p_{3/2}$ particles. On the other hand the $\pi p_{3/2}$ orbital serves as our reference and its energy is put to zero, so the excitation of the second $7/2^-$ level is solely determined by the core phonon and its coupling strength. Upon fine tuning it turns out that a static quadrupole moment for the 2^+ phonon must be retrieved from the PCM toolbox, which is not uncommon but experimentally hard to verify. It is more worrisome perhaps that the coupling parameter drives the response of the nickel body away from the 2p-1h structure on either side of ^{69}Cu, curiously washing out the effect of the $N = 40$ subshell closure. Diagonalisation produces two $7/2^-$ states that converge towards each other and decrease in energy.

Thanks to the many parameters in the model, the calculated $7/2^-$ states closely follow the experimental data. The lowest of both confronts us with a $f_{7/2}$ proton orbital that tumbles down across $N = 40$ and lies much lower than one might expect from a

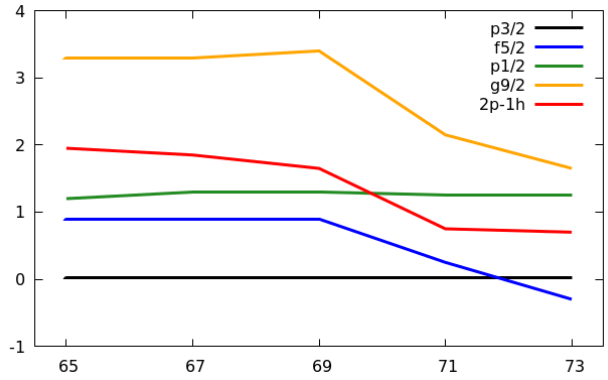

FIGURE 3.1: Single-particle and 2p-1h energies for neutron-rich copper isotopes in the PCM. Data taken from [Oro00]

magic shell gap. Moreover stirring up the zinc core, which the 2p-1h configuration naturally relates to, a $\Delta j = 1$ excited band is set into motion. A sequence of γ rays is indeed discernable in the experimental spectrum of ^{69}Cu above the $7/2^-_1$ state at 1711 keV [Bro98, Ish00]. For the latter a large spectroscopic factor is measured in proton pick-up reactions as discussed before and listed in table 2.5, from which the band can indeed be classified as constructed atop a proton hole rather than through neutron excitations. It is then proposed that in ^{71}Cu the $7/2^-_1$ level at 981 keV would likewise relate to the $\pi f_{7/2}$ hole and support an excited band. In ^{73}Cu, the 2p-1h tag is furtively attached to the $7/2^-_2$ level at 1010 keV. To prove these statements, however, spectroscopic factors would be needed.

With a seemingly satisfactory view of the $5/2^-$ and $7/2^-$ states, the model proceeds to evaluate the other states. Along the ideas of Federman and Pittel referred to in the early pages of our text, one may foresee a shift in energy to happen for the $\pi g_{9/2}$ orbital as much as for the $\pi f_{5/2}$ one, since the spatial overlap with the $\nu g_{9/2}$ particles would be more than sizeable. The PCM pushes $\epsilon_{g_{9/2}}$ down the hill and projects a monopole migration from 2.4 MeV in ^{69}Cu to 1.5 MeV in ^{73}Cu. Unfortunately the experimental spin assignments are tentative at best at these excitation energies. In ^{69}Cu a level at 2551 keV might match [Ish97]. In ^{71}Cu the state at 1786 keV was assigned a spin and parity of $9/2^+$, even if it would turn the 1252-keV transition to the $5/2^-$ state at 534 keV into an accelerated $M2$ transition that is not straightforward to explain [Ish98]. The picture that is spurred of a downsloping $\pi g_{9/2}$ orbital parallel to the $\pi f_{5/2}$ state

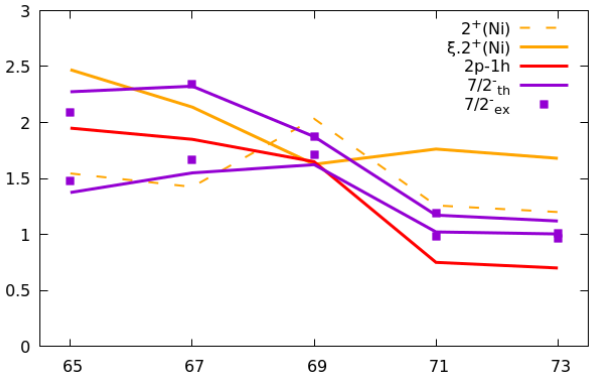

FIGURE 3.2: Quadrupole vibrations in the nickel core before and after multiplication by the PCM coupling strength ξ, unperturbed 2p-1h energies, and diagonalised $7/2^-$ energies for neutron-rich copper isotopes in the PCM compared to experimentally proposed $7/2^-$ levels. Data taken from [Oro00]

would lead so far as to create a shell gap for $Z = 34$ at $N = 50$, as one can gather from figure 3.3. Soon after, however, the signature of the 1786-keV level was revised by the reader's host as $7/2^-$ or $9/2^-$ and the lowest candidate for a $9/2^+$ spin and parity put at 2806 keV instead [Fra01]. For ^{73}Cu the latter experimental work suggested a level with $9/2^+$ spin and parity at 2385 keV, so the story quickly unwinds and little evidence seems left for a migration of the $\pi g_{9/2}$ orbit.

The absence of an attraction between the $\pi g_{9/2}$ and $\nu g_{9/2}$ particles appears to rule out the spatial overlap of the concerned orbitals as the main and decisive feature of monopole movement. The universality of the phenomenon is visibly refuted, although we should remain cautious and not link too hastily observed quantum states to underlying single-particle energies when a quantitative assessment for instance through spectroscopic factors is not available. Nevertheless, it may still be possible that in a similar manner as for the 2p-1h configurations in copper the even-even particle-hole excitations across $Z = 28$ in iron, nickel, and zinc come down in energy. They would account for the emergence of low-lying 0^+ states in these isotopes, throwing a hint at shape coexistence that would be induced by $\pi f_{7/2}$ holes. Several 0^+ states are indeed noticed in the region but when we encountered them in section 2.5, we wrote that neutrons contribute to them at least in equal parts. An illustrative example for ^{68}Ni was given in figure 2.31.

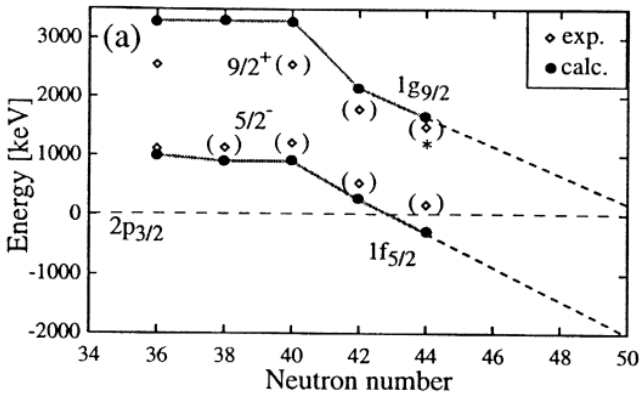

FIGURE 3.3: Extrapolation of $\pi f_{5/2}$ and $\pi g_{9/2}$ single-particle energies for neutron-rich copper isotopes in the PCM compared to experimental $5/2^-$ and $9/2^+$ states. For ^{71,73}Cu the $9/2^+$ assignments are unconfirmed. Taken from [Oro00]

As to the $\pi p_{1/2}$ state, it takes permanent residence just above 1 MeV. A $1/2^-$ state close below the first $5/2^-$ level is produced by coupling the $3/2^-$ ground state to the 2^+ phonon and is wrapped in collectivity. The PCM would provide an elegant explanation for the experimental data but within its relatively simple frame it is obviously not bothered by the more subtle considerations that were advanced for this level in section 2.4.

The PCM offered a straightforward solution to describe excitations across the $Z = 28$ shell gap at a time that most shell-model calculations still ran in valence spaces that were too limited to rouse them. Its predictive power, however, is held in balance by a broad range of parameters that cannot be constrained easily. Since basically the output only walks as far as the input gives it leeway, the model cannot determine by itself if monopole migration actually occurs. While it nicely reproduces the experimental drift of the $5/2^-$ level, its assessment of the $7/2^-$ and $9/2^+$ states appears as speculative. On the positive side, the possibility in itself of reproducing many of the established features of the copper isotopes proves the validity of the ^{68}Ni core. The abrupt energy shifts at $N = 40$ are present without any phonon at work, underscoring a sharply defined occupation of the $\nu g_{9/2}$ orbital that is close to zero for $N \leq 40$ and hence a well pronounced subshell.

As a distant relative to the PCM we wish to address briefly the QRPA. Unlike the shell model, it replaces protons and neutrons by quasiparticles that arrange in super-

fluid pairs and is particulary well suited for the description of deformation in heavy nuclei with open shells. Although effective nuclear forces act on harmonic wavefunctions in a self-consistent manner, the absence of the familiar quantum numbers might reduce the insight in the underlying structure. For instance the $N = 40$ subshell gap in ^{68}Ni discussed in section 2.5 is probed with a schematic model that incorporates a pairing, a quadrupole, and a hybrid quadrupole pairing force [Lan03a]. The computed modest $B(E2)$ value matches well the measurement, identifying the 2^+ state as a neutron excitation. A complementary SMMC calculation underlines that the actual proton strength lies much higher, while the apparent rigidity of the nucleus is more easily explained by the change in parity across $N = 40$ rather than an energy difference that is to be bridged. The expectation for ^{70}Ni for this reason remains equally low, which however experiment does not confirm. Pictured in figure 2.23, we pondered upon the puzzle at length in section 2.5 [Per06].

For the half-life of ^{78}Ni several QRPA models try their chance [Hos05, Xu14]. In section 2.7 we presented a global QRPA calculation by Peter Moeller and colleagues [Moe03], the ETFSI code by Ivan Borzov [Bor03], the ETFSI-Q variant by the group of John Pearson [Pea96], as well as a Skyrme version by Jonathan Engel and coworkers [Eng99]. The global QRPA and the continuum QRPA [Bor05] find a useful application to the P_n values of the neutron-rich copper isotopes that we dwelled on in section 2.6 [Win09, Hos10]. More results for the nickel chain are obtained with the Gogny D1S interaction by Sophie Péru [Per14], while the QRPA calculations for the $E2$ transition strengths of ^{72,74}Ni in section 2.5 [Cor18] and the 2^+ energy of ^{78}Ni in section 2.9 [Tan19] rely on the D1M force.

Much sophistication enters into the many manifestations of nuclear superfluidity, such as the proton-neutron relativistic quasiparticle random-phase approximation abbreviated as pn-RQRPA [Nik05]. The β-decay half-lives are calculated with the DD-ME1* density-dependent meson-exchange interaction between particles and holes, which next to the *sigma* and ρ mesons includes an additional tensor term for the ω meson, whereas the Gogny D1S force binds particles. They are nonetheless overestimated by a factor of 600 for ^{70}Ni down to eight for ^{78}Ni. The ground state swaps spin from $3/2^-$ to $5/2^-$ in ^{75}Cu, allowing the spectrum of ^{79}Cu to display a $3/2^-$ state at 870

keV.

The proton-neutron relativistic quasiparticle time-blocking approximation, denoted pn-RQTBA, further develops the pn-RQRPA based on a fundamental nucleon-nucleon interaction that exchanges π and ρ mesons and subsequently couples the quasiparticles to phonons [Rob16]. The theoretical strength is severely fragmented with a larger part of it arriving in the Q_β window, as a result of which the predicted half-lives of the nickel isotopes now approach the experimental values within a factor of two.

3.2 Monopole migration

The displacement of specific levels in the shell model due to the filling of opposite orbitals was observed from early times on. We wrote in section 1.1 that it was ascribed by Federman and Pittel to the spatial overlap of the respective proton and neutron wave functions and striking examples were found throughout the nuclear chart. When the first experimental results on the level structure of the neutron-rich copper isotopes beyond $N = 40$ came out, theoretical work would be embarked upon from different springheads and it is no surprise that the idea was picked up again.

An extreme single-particle interpretation indeed identified the first $5/2^-$ level in ^{69,71,73}Cu as the $\pi f_{5/2}$ orbital, the slump of which was connected to the growing occupation of the $\nu g_{9/2}$ state. Qualified as the monopole migration of an $\ell - 1/2$ orbital due to the interaction with an $\ell' + 1/2$ partner orbital where $\ell \approx \ell'$, the energy shift ΔE_M of for instance a proton orbital with angular momentum j_π is obtained from the spin-averaged matrix element of the residual proton-neutron interaction $V_{\pi\nu}$ multiplied by the number of particles present in the interacting neutron orbitals with angular momentum j_ν,

$$\Delta E_M = \sum_{j_\nu} \overline{\langle j_\pi j_\nu | V_{\pi\nu} | j_\pi j_\nu \rangle} \, (2j_\nu + 1) \, v^2_{j_\nu}, \tag{3.1}$$

with $v^2_{j_\nu}$ the occupancy of the neutron state. The expression is shown to reduce to [DeS63]

$$\Delta E_M = \sum_{j_\nu} F^{(00)0} \, (2j_\nu + 1) \, v^2_{j_\nu} \tag{3.2}$$

with $F^{(00)0}$ the zeroth-order Slater integral,

$$F^{(00)0} = \int \left|R_{n_\pi l_\pi}(r_\pi) R_{n_\nu l_\nu}(r_\nu)\right|^2 w_{00,0}(r_\pi, r_\nu)\, \mathrm{d}r_\pi \mathrm{d}r_\nu. \tag{3.3}$$

The factors $R_{n_\pi l_\pi}(r_\pi)$ and $R_{n_\nu l_\nu}(r_\nu)$ respectively symbolise the radial proton and neutron wave functions and $w_{00,0}(r_\pi, r_\nu)$ the monopole coefficient of the residual interaction. It is defined by the expansion

$$V_{\pi\nu} = \sum_{s_\pi s_\nu k_\pi k_\nu, r} w_{s_\pi s_\nu k_\pi k_\nu, r}(r_\pi, r_\nu)\, (\boldsymbol{T}^{(s_\pi k_\pi) r}(\pi) \cdot \boldsymbol{T}^{(s_\nu k_\nu) r}(\nu)), \tag{3.4}$$

in which the irreducible tensor operators $\boldsymbol{T}^{(s_\pi k_\pi) r}(\pi)$ and $\boldsymbol{T}^{(s_\nu k_\nu) r}(\nu)$ of order r are composed of spin tensors of order s_π and s_ν and angular momentum tensors of order k_π and k_ν. Combining all elements, we put to the record that the monopole movement depends on the occupancy of the valence orbitals, the radial overlap of the proton and neutron wave functions, and the monopole strength of the residual proton-neutron interaction. It is the latter parameter that confers its name to the effect, while it is the Slater integral of radial wave functions that explains the attraction between orbitals with similar angular momentum.

At Ghent the formalism was applied to a zero-range δ interaction with a spin-exchange term [Smi04]. As illustrated in figure 3.4, it successfully brings forth a downsloping behaviour for the $f_{5/2}$ proton orbit. A ground-state inversion is not achieved, however, while also the $\pi g_{9/2}$ state sneaks down. With only two parameters to modulate, the strengths V_0 of the δ force and α of the spin-exchange part, the evolution is indeed gradual and not as steep as experimentally ascertained. The choice of 400 MeV fm^3 for V_0 is copied from an earlier study of the tin nuclei, whereas the value of 0.1 for α is of small interest since the monopole interaction the way it is formulated here remains independent of the spin.[1] Since a closed core of ^{56}Ni is assumed for the calculations, the $\pi f_{7/2}$ hole falls outside the model space and its whereabouts cannot be assessed. Because of the insensitivity of the model to the spin orientation, one expects it to obey an identical trend as the $\pi f_{5/2}$ spin-orbit partner, just like the $\pi p_{1/2}$ particle that mirrors the $\pi p_{3/2}$ ground state.

[1] One can proof that the matrix elements of a residual interaction vanish unless $s_\pi = s_\nu$ [DeS63]. The statement is then hidden in the indices of the Slater integral, (00) standing for (sk) hence $s = 0$

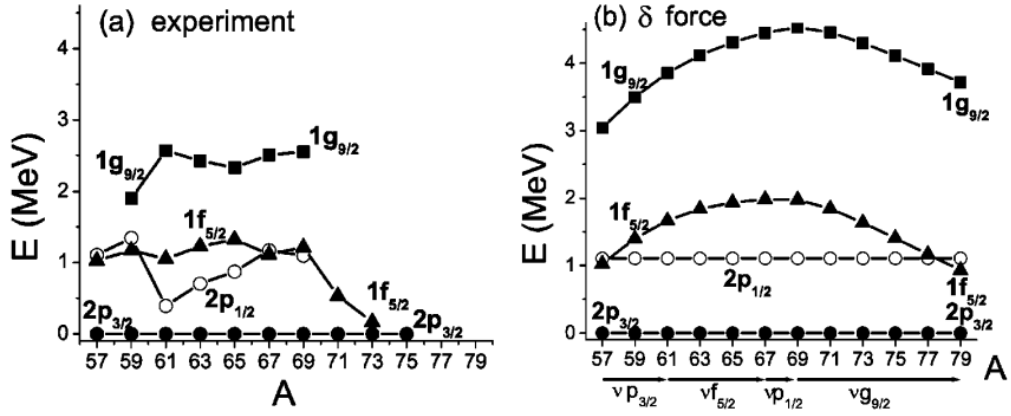

FIGURE 3.4: Experimental centroids (left) and theoretical single-particle energies with a δ interaction (right) for the odd copper isotopes. Taken from [Smi04]

To overcome the limitations of the schematic δ force, Hjorth-Jensen's realistic interaction was explored [Hjo95]. Since it is not straighforward to derive the nucleon-nucleon potential directly from quantum chromodynamics, a meson theory is often embraced. Limited to the exchange of one boson, its parameters are the coupling constants of the π, η, ρ, ω, σ, and δ resonances and their cut-off values at short distances. This makes up a set of 13 parameters that is fixed from scattering experiments at low energy. Among the several available nucleon-nucleon potentials, the Bonn potential is chosen. Its tensor interaction, which results from a finely tuned balance between an attractive contribution from the pseudoscalar π meson and a repulsive part from the vector ρ meson, is weaker than for instance in the Paris or the Reid potentials. It is compensated for by a stronger central or spin-orbit force. The G matrix that was introduced by Keith Brueckner at Bloomington back in 1954 provides the technical means to compute the Hamiltonian in the nuclear medium, which forms the basis for the shell-model calculations acting in a valence space of $p_{3/2}f_{5/2}p_{1/2}g_{9/2}$ orbitals around a ^{56}Ni core. The monopole terms controlling the single-particle energies are subsequently modified following work by Nowacki, constraining them by a fit as complete as possible along the $Z = 28$ and $N = 50$ chains [Now96].

From figure 3.5 we observe that a $5/2^-$ ground state is now foretold in ^{79}Cu, while a parabolic behaviour between $N = 40$ and $N = 50$ shines through for the $1/2^-$ level and no clear tendency is evident for the $9/2^+$ one. The calculated spectroscopic fac-

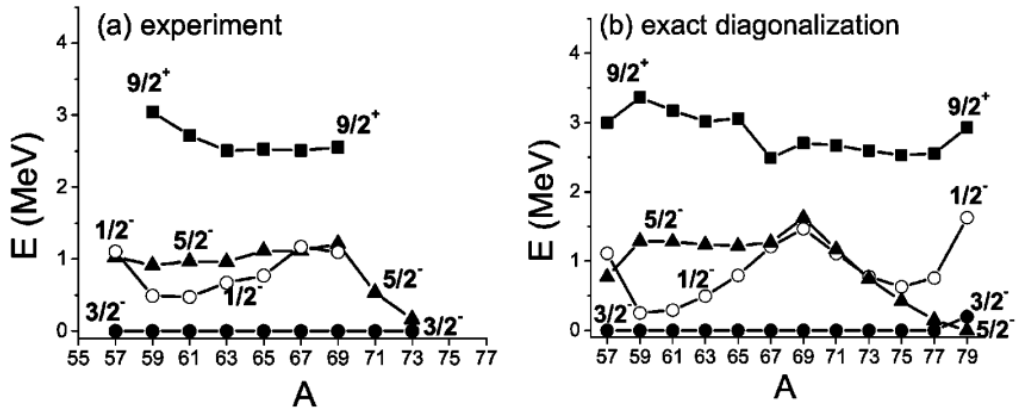

FIGURE 3.5: Lowest levels for a given spin from experiment (left) and from the shell model with a realistic G-matrix interaction (right) for the odd copper isotopes. Taken from [Smi04]

tors for dumping a proton onto a nickel nucleus exceed 75% in the case of the $3/2^-$ state and reduce to 50% for the $1/2^-$ one, indicating a sizable degree of purity in the wave functions. The $5/2^-$ level on the other hand exhibits a mixed character in ^{69,71}Cu with the $9/2^+$ state even more strongly so, implying a predominance of different components. The findings run contrary to the idea of a $5/2^-$ single-particle configuration accompanied by a $1/2^-$ collective mode as we fancied it from experiment.

The G-matrix calculations were comprehensively relied upon for the interpretation of the level schemes of the odd-odd copper isotopes in section 2.6 [Van04a, Van05, Tho06]. They were extended to reproduce the $E2$ transition strengths measured at Isolde described in sections 2.2 and 2.6 [Ste07, Ste08] as well as the γ spectroscopy of ^{71}Cu at Argonne mentioned in section 2.3 [Ste09a]. The electromagnetic quantities are computed with effective charges of $e_\pi = 1.5e$ and $e_\nu = 0.5e$ and spin gyromagnetic ratios g_s quenched by a standard weight of 0.7. From figure 3.6 we learn that the agreement for the deexcitation values in the odd isotopes is sometimes off by a factor of six and the isotopic trends are not recovered. We are visibly left with a picture of the nucleus that is much too rigid, since the $\pi f_{7/2}$ state is not part of the model space and the $7/2^-$ level can only be generated through a grit of collectivity. Figure 2.45 reminds us that the situation was decidedly improved upon when the details of the interaction underwent further modifications at the hands of the group at Ghent and in particular the limitations of the model space were compensated for by increasing the

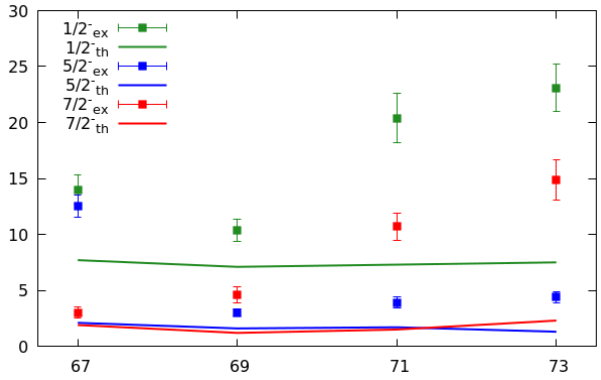

Figure 3.6: Measured $B(E2)$ values in Weisskopf units for the $1/2^-$, $5/2^-$ and $7/2^-$ transitions to the $3/2^-$ ground state in ^{67,69,71,73}Cu compared to shell-model predictions from a realistic G-matrix interaction. Data taken from [Ste08]

effective charges to $e_\pi = 1.9e$ and $e_\nu = 0.9e$ [Rap11]. For the finer influence of these adjustments on the level schemes, we may refer the reader to a close comparison of figures 2.46 and 2.47.

3.3 Realistic interactions

In the absence of a closed formula for the nuclear strong force the landscape of shell-model interactions is naturally vast and one can eagerly indulge amidst an extensive literature. Nevertheless mindful of the scope of our text, we propose laces tied a visit to Athens, where the S3V interaction offers a rewarding viewpoint [Sin92]. Coined together by Sinatkas, Skouras, Strottman, and Vergados from the original set of Sussex matrix elements for nucleon-nucleon scattering, it applies a correction up to second order to account for the nuclear medium. It then deftly takes in hand a core of ^{100}Sn from which it plucks out particles, the available hole space consisting of the $g_{9/2}pf_{5/2}$ orbitals. Since information on the relevant single-hole energies in ^{99}In and ^{99}Sn is experimentally beyond reach, they are extracted from a fit to the energy spectra of the $N = 50$ isotones from ^{94}Ru down to ^{87}Rb.

Even though the subject of the paper revolves around nuclei for which $A \approx 90$, the single-particle energies in ^{79}Cu are derived for the sake of reference. We print them in table 3.1 along with the values from the empirical interaction that Ji and Wildenthal

	$\pi f_{5/2}$	$\pi p_{3/2}$	$\pi p_{1/2}$	$\pi g_{9/2}$
Ji and Wildenthal	0	1.15	2.56	7.27
S3V	0	2.20	3.39	4.89
S3V'	0	1.34	3.33	3.61
Hjorth-Jensen	0	0.30	1.77	3.01
NR78 (jj44pna)	0	1.50	2.90	7.43

TABLE 3.1: Proton single-particle energies for ^{79}Cu from the interactions by Ji and Wildenthal, S3V, S3V', by Hjorth-Jensen as modified by Nowacki, and NR78 (jj44pna). Data taken from [Ji88, Sin92, Dau00, Lis04]

drew up some years earlier at Drexel university and that the reader may remember from our discussion of ^{83}As in section 2.8 [Ji88]. In their force a ^{78}Ni core is encircled instead by proton particles picked from the $f_{5/2}pg_{9/2}$ valence space. While the single-particle energies are at first computed from a Bardeen-Cooper-Schrieffer formalism and the two-body matrix elements are expressed following Schiffer and True through a linear combination of two central Yukawa functions, they are improved upon by an iterative fit to a large selection of experimental levels in the $N = 50$ isotones from ^{82}Ge to ^{96}Pd. Both the Ji and Wildenthal and S3V interactions foretell a $5/2^-$ ground-state spin and parity, with the $\pi f_{5/2}$ orbital bound tighter by 1 MeV relative to the $\pi p_{1/2}$ and $\pi p_{3/2}$ states in the latter. The low position of the $f_{5/2}$ proton orbit is ascribed by Ji and Wildenthal to the action of the $f_{5/2}$ to $g_{9/2}$ neutron orbitals, the ground state of ^{80}Zn harbouring the $\pi f_{5/2}^2$ configuration to 80% [Ji89].

Whereas at this point the energy spectrum of ^{79}Cu remains speculative, the level schemes produced by the realistic S3V force nicely agree with the observed ones down to strontium ($Z = 38$). Straying farther below, however, the performance quickly worsens. For its first application to the nickel region a core of ^{56}Ni is therefore chosen, surrounded by neutrons that are selected from the $f_{5/2}pg_{9/2}$ model space and the single-particle energies of which are adjusted to local data in $^{64-68}$Ni [Paw94]. To the extent that the energies are essentially shifted as a function of shell occupancy, they simulate the action of the monopole part to steer the evolution of the mean field. The

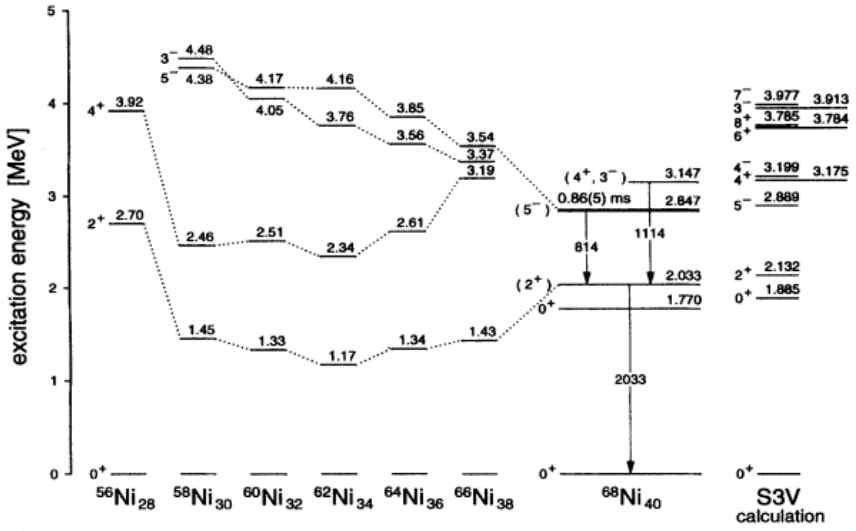

Figure 3.7: Experimental level scheme of ^{68}Ni along systematics of the preceding isotopes and compared to a modified S3V calculation. Taken from [Bro95]

resulting comparison with experiment up to ^{67}Ni appears reasonable but it is not more convincing than what is found from a competing calculation with a schematic surface δ interaction, leaving doubt to linger as to the actual aptness of the single-particle energies. Also the model space arguably presents an issue, as it does not allow for proton excitations of the core. In ^{68}Ni the first excited 2^+ state is obtained 100 keV higher than the measured value of 2033 keV, altogether an able success that we illustrate in figure 3.7 [Bro95]. The excitation energies of newly found levels in ^{69,70}Ni are likewise computed and compared to the results from Hjorth-Jensen's force, although now the authors rather express their dissatisfaction with both [Grz98].

The interaction was tailored afresh by Grawe at Darmstadt, enlarging the valence space to protons and neutrons from the $f_{5/2}pg_{9/2}$ orbitals but treating either fluid independently [Gra99]. The single-particle energies are fixed in ^{69}Ni from the γ spectroscopy at Ganil [Grz98] and in ^{69,71,73}Cu from our β decay at Lisol [Fra98]. In the guise of S3V', the model is put to use for the description of ^{78}Zn [Dau00]. The level structure is reproduced with fair accuracy, while effective charges that are kept at $e_\pi = 1.5e$ and $e_\nu = 0.5e$ yield an outcome that matches well the observed transition strengths. The single-particle spectrum of ^{79}Cu is summarised in table 3.1, where also the prediction from Hjorth-Jensen's interaction with modified monopoles quoted in the

same work is listed for comparison. The absence of theoretical convergence will perhaps not surprise but at least one concludes that the data grant considerable flexibility to the various models and their fitting procedures, as they all manage to accommodate in a broad sense the same experimental level schemes in spite of different choices of parameters.

Although the single-particle energies are shaken up again, notably introducing a degeneracy of the $\pi f_{5/2}$ and $\pi p_{3/2}$ states for $N > 40$, the S3V' force being grafted onto the copper isotopes naturally honours many of the features that we noticed in sections 2.1 to 2.3 [Fra01]. The calculated level diagrams up to ^{79}Cu are displayed in figure 3.8. The dropping $5/2^-$ state correctly becomes the ground state in ^{75}Cu, while the $3/2^-$ configuration climbs to more than 1 MeV in ^{79}Cu. The first $7/2^-$ level in ^{71}Cu comes out near 1.5 MeV with the next one at 1.8 MeV. We recall that experimentally two $7/2^-$ levels are identified below 1.2 MeV, which led to the hypothesis that one of these would correspond to the $\pi f_{7/2}$ hole state as the model is not equipped with it. A $9/2^+$ level resolutely rises from 1.8 MeV in ^{71}Cu to 3.6 MeV in ^{79}Cu, in which a candidate could be recognised for the $g_{9/2}$ proton structure. In the image that lingers the monopole migration of the $\pi g_{9/2}$ orbital is indeed proportional to the overlap of its wave function but it may nevertheless be cancelled by residual interactions that are ignored by the S3V' force and that could mask the observed effect. Although omitted from the figure, we also find back a $1/2^-$ level at low excitation energy in the theoretical level schemes. In ^{71}Cu it sits above the $5/2^-$ state at 0.6 MeV and after passing a minimum at 0.4 MeV in ^{73}Cu it makes it way up to 0.8 MeV in ^{77}Cu, whereas experiment sees it even lower. Moving to ^{72}Ni, the interaction cannot explain the disappearance of the 8^+ seniority isomer, which we commented upon in section 2.7 [Gra02]. It shows up one more time for the level schemes of ^{74,76}Ni before being dismissed by more recent theories [Maz05].

Our next stride therefore brings us to the work of Lisetskiy and colleagues in Michigan, which the NR78 force calls home [Lis04]. An apparent alias for what is known in later publications as jj44pna, it settles for a core of ^{56}Ni enclosed by the $f_{5/2}pg_{9/2}$ space of orbitals. The two-body matrix elements are deduced from a realistic G matrix that is dictated by the Bonn potential. The single-particle energies are pulled into place from

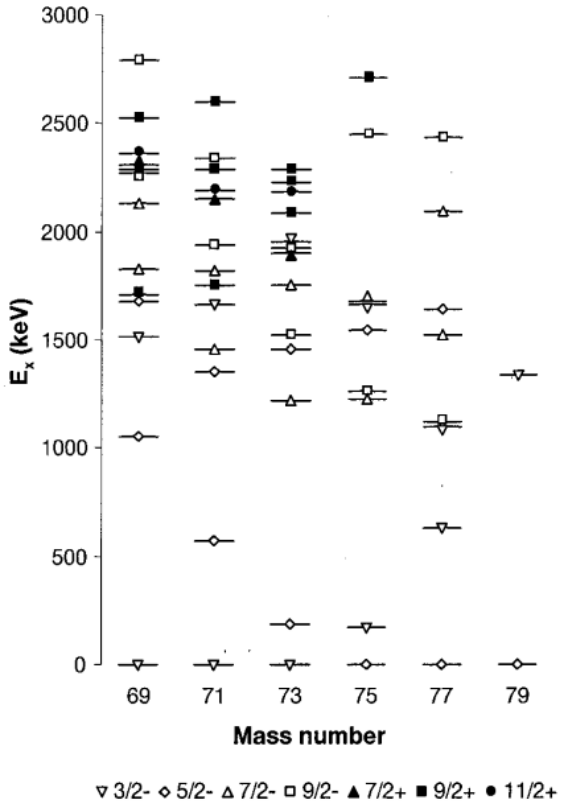

Figure 3.8: Theoretical level schemes of neutron-rich copper isotopes with the S3V' interaction. Taken from [Fra01]

a fit to available data in ^{57}Ni to ^{78}Ni for the neutrons and ^{79}Cu to ^{100}Sn for the protons. Curiously they encompass a theoretical Hartree-Fock value for the binding energy of ^{78}Ni. Since the proton and neutron subspaces are kept separated, only isovector matrix elements are computed. From table 3.1 we ascertain that the obtained Hamiltonian once again puts the $f_{5/2}$ proton orbit below the $p_{3/2}$ one in ^{79}Cu. The effect is explicitly tied to the strong monopole interaction with the $g_{9/2}$ neutrons as evidenced from the β decay at Lisol, pointed at by the spin-flip that occurs between the $\pi f_{5/2}\nu g_{9/2}$ and $\pi p_{3/2}\nu g_{9/2}$ configurations. Thanks to the particular emphasis that is given to the correct value of the $\nu g^2_{9/2}$ matrix element for $J = 2^+$ the known 2^+ energies in the even nickel isotopes are accurately reproduced, although the article stops short of giving a prediction for ^{78}Ni. In the ^{72,74}Ni isotopes the calculation finds two 6^+ states below the 8^+ one, explaining the disappearance of the seniority isomer in these isotopes that we dwelled upon in section 2.7 [Maz05].

Whereas the determination of the deformation length of ^{74}Ni reported in section 2.5 seems to expose the limits of the model, for which rather large effective charges of $e_\pi = 2.0e$ and $e_\nu = 1.0e$ are envisioned [Aoi10], the $B(E2)$ value in ^{72}Ni comes out nicely [Kol16]. Recalling figure 2.25, however, we keep in mind that the data are subject to some controversy. The interaction offers deeper insight into the excited states of ^{68}Ni [Rec13, Fla19], but the picture it delivers of the intensity balances governed by the seniority rules in ^{74}Ni does not convince, as recounted in section 2.7 [Mor18]. In the odd nickel isotopes, it successfully helps to elucidate the $\nu p_{1/2}$ single-particle character of the $1/2^-$ isomer in ^{71}Ni, a puzzle we unravelled in 2.4 [Raj12].

Meanwhile the proton-neutron matrix elements were filled in, adjusting the isoscalar monopoles of the G-matrix interaction to experimental levels in the odd copper isotopes [Lis05]. The first attempt at forecasting the structure of copper suggests a premature $5/2^-$ ground state in ^{73}Cu already, beyond which the $3/2^-$ state steeply rises upwards to reach its single-particle energy of 1.5 MeV in ^{79}Cu. Soon after this shortcoming was remedied and a new scion by the name of jj44b saw the light, which now is optimised to a wide range of data in nuclei from nickel to zinc with $48 \leq N \leq 50$. It quickly bears fruit, shouldering the observed level scheme of ^{81}Ga whilst accounting for the proper $5/2^-$ ground state in ^{83}As, a topic we discussed in section 2.8 [Ver07]. We find a revised plot for the copper isotopes in figure 3.9, with the ground-state spin inversion taking place in ^{75}Cu and the $3/2^-$ level at an excitation energy of 391 keV in ^{79}Cu [Fla09]. Also the $1/2^-$ level draws the attention, parabolically running through the isotope series. In a fashion that is similar to S3V' its energy remains rather high and it veers up once it passes ^{73}Cu. With a standard reduction of the spin gyromagnetic ratios g_s by a factor of 0.7, the calculation moreover struggles with the ground-state magnetic moment of ^{73}Cu. The authors guess a relation, since a lower $\pi p_{1/2}$ single-particle energy would induce a $\pi p_{1/2} \times 2^+$ component in the ground-state wave function that could bring the magnetic moment in line with the experiment. For ^{75}Cu the theoretical and measured magnetic moments converge, the wave function leaning into $\pi f_{5/2}$ configurations that tally up to 90%.

The laser spectroscopy of copper covered in sections 2.1 and 2.6 invited further calculations of the electromagnetic moments. Conventional spin gyromagnetic ratios

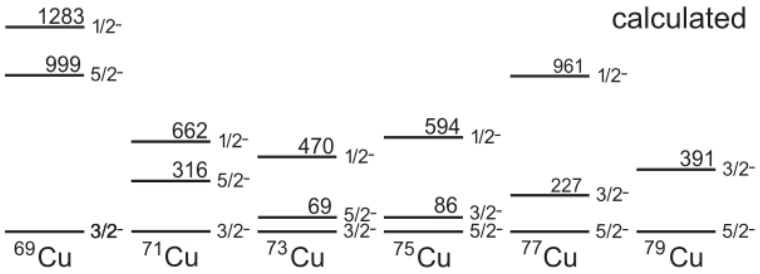

Figure 3.9: Theoretical level schemes of neutron-rich odd copper isotopes with the jj44b interaction. Taken from [Fla09]

g_s of 0.7 times the free ones are plugged in, whereas the effective charges slightly oscillate from $e_\pi = 1.4e$ and $e_\nu = 1.0e$ by one author [Fla10] to respectively $1.5e$ and $1.1e$ by the next [Vin10], stressing the dependence on subtleties in the model. The earlier conjecture on the low single-particle energy of the $\pi p_{1/2}$ state is abandoned and the suspicion is raised that proton disruptions across the $Z = 28$ gap, which logically fall outside the valence space, play an important role instead. The interaction fails to catch the sharp increase in the magnetic moment of ^{77}Cu apparent from figure 2.4, a fact that is likewise attributed to the unphysical stiffness of the proton core [Koe11]. With respect to the odd-odd isotopes, the comparison between theoretical and experimental moments confirms the presence of the $\pi f_{5/2}$ orbital in the ground states of ^{72,74}Cu. The corresponding level schemes, collected in figure 2.48, are met with less satisfaction. For gallium the effective charges are kept at $e_\pi = 1.5e$ and $e_\nu = 1.1e$ [Che10]. As we stated in section 2.8, the predictions miss the $\pi f_{5/2}^3$ ground state in ^{79}Ga but mark it right in ^{81}Ga, revealing a difficulty to correctly accommodate the orbital ordering in more complex multiparticle configurations.

The γ spectroscopy of ^{75}Cu, which we peered into in section 2.4, as well tends to refute the single-particle nature of the $1/2^-$ state [Pet16]. The transition rates underscore collectivity and again bring up the boundaries imposed by the valence space. Interestingly the neutron-branching ratios in the βn decay of $^{76-79}$Cu detailed in section 2.6 are restored if the Gamow-Teller strength is attenuated by a factor of 0.37, the uncommon severity of which is once more imputed to the absence of $f_{7/2}$ proton excitations from the model [Hos10]. Gathering the evidence from the different corners, we cannot ignore that the $f_{7/2}$ protons in the core are consistently perturbed, a tenet that is

possibly linked to the available $g_{9/2}$ neutrons.

In an optimistic attempt at bibliographical exhaustion we add that we mentioned the jj44b Hamiltonian in passing with regard to ^{68}Ni in section 2.5 [Rec13] and in the context of ^{79}Zn in section 2.8 [Wra17].

In more recent approaches the G matrix is replaced by a somewhat different technique in which the troublesome repulsion of the nucleon-nucleon force at high momentum is integrated out, resulting in a $V_{\mathrm{low}-k}$ interaction that is free of any mass dependence [Bog02]. With a cut-off parameter Λ of 2.6 fm^{-1}, the charge-dependent Bonn potential is renormalised and in the $\pi f_{7/2}p_{3/2}$ $\nu pf_{5/2}g_{9/2}$ model space the team from Naples successfully managed to generate the $N = 40$ subshell closure in ^{68}Ni as well as the island of inversion around ^{64}Cr [Cor14]. Adding the $\nu d_{5/2}$ orbital allows to extend the calculations to the heavier chromium isotopes. Although one may deem the force unfit for the description of copper because of the omission of the $\pi f_{5/2}$ state, in ^{78}Ni it proposes the first 2^+ energy at 2.6 MeV, close to experiment.

In our text we came across the $V_{\mathrm{low}-k}$ model in section 2.5, where it compared favourably to the experimental $B(E2)$ value from the Coulomb excitation of the ^{74}Ni isotope [Mar14]. Figure 2.24 moreover shows that the core of ^{78}Ni would be broken rather easily, as the calculation foresees the possibility that a proton is lifted from $f_{7/2}$ to $p_{3/2}$ and a sudden increase in the $E2$ transition rate is predicted. The effective charges are computed consistently and vary from one single-particle excitation to another, ranging from 1.22 to 1.42 for protons and 0.35 to 0.61 for neutrons. The interaction also appears in our discussion of ^{70}Fe [Ben15]. In section 2.7 we bumped into ^{74}Ni again, striving to sort out the seniority of its excited states [Mor18] as well as its Coulomb excitation [Got20].

3.4 The impact of the tensor force

Continuing our overview of shell-model approaches, time has come to travel east to Japan. We presented in section 1.2 the SDPF force elaborated by Utsuno at Tokyo and colleagues, a remarkable outcome of which is the prediction for new magic numbers to appear at $N = 16$ and $N = 34$ [Uts99]. As calculations move into the intermediate

mass region of the nuclear chart, it is replaced by the GXPF1 interaction assembled by Otsuka at Tokyo and Honma at Fukushima with their colleagues [Ots01b, Hon02]. Aiming at a description of the entire *fp* shell, it relies once again on a realistic *G* matrix that is derived from the Bonn potential, while the single-particle energies and two-body matrix elements are further determined from carefully chosen binding and level energies in isotopes from ^{47}Ca to ^{66}Ni and ^{65}Ge. As $N = 40$ is not crossed, an extension with the $g_{9/2}$ orbital at the cost of suppressing the $f_{7/2}$ one is attempted [Hon06]. The ambition however hits a snag, as we recounted in section 2.1 that the limited success in calculating the magnetic moment of ^{71}Cu is taken as evidence that the proton excitations cannot be simply left out [Sto08].

A modified version called GXPF1A is meanwhile introduced, in which five isovector matrix elements are shifted by up to 0.5 MeV [Hon05]. Four of these imply the $p_{1/2}$ and $f_{5/2}$ orbitals, narrowing their distance at $N = 34$. In our text we encountered GXPF1A in section 2.2 when evaluating transfer reactions on stable nickel isotopes and found partial agreement with the data, with figure 2.6 indeed displaying a reduced energy spacing for the $\pi p_{1/2}$ and $\pi f_{5/2}$ states at $N = 34$ [Sch13]. In section 2.5 we commented upon an unsuccessful effort to reproduce the observed collectivity of ^{64}Cr at $N = 40$, but since the $\nu g_{9/2}$ state is not included in the model space perhaps one is asking for the moon [Gad10].

As the reader may recall from section 1.2 it was meanwhile realised that the spin-isospin force, which had been called upon to motivate the magic numbers at $N = 16$ and $N = 34$ [Ots01a], did not fulfil its promise to explain the facets of nuclear evolution and upon riper thought a tensor interaction of second rank was held up [Ots05]. Although the tensor force is a natural ingredient of the meson exchange that the *G* matrix is based upon and it is implicitly present in phenomenologically fitted shell-model Hamiltonians, diligent exertion to express it distinctively was spent by the Tokyo group. The renewed framework stipulates that an attraction exists between the unlike orbitals $j_<$ and $j'_>$ and a repulsion between the like orbitals $j_<$ and $j'_<$ or $j_>$ and $j'_>$. Since the tensor interaction is different from zero only when the spins of both particles add up to 1, it is the orientation of the orbital angular momenta that truly matters. When the orbital momenta are anti-aligned to each other, an image comes about in

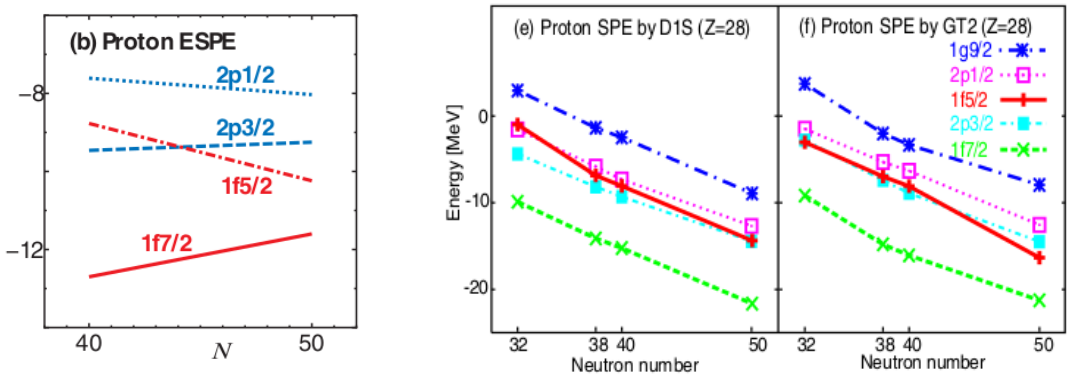

FIGURE 3.10: Evolution of proton single-particle energies in nickel isotopes from a $\pi + \rho$ tensor force (left), the D1S model (middle), and the GT2 interaction (right). Taken from [Ots05] and [Ots06]

which the relative wave function of both particles is well localised and an attraction results that is analogous to the case of the deuteron. As soon as they align the relative wave function is spread out and repulsion dominates.

Focussing on the monopole action only, the related energy drifts can be spelled out with various assumptions for the deeper origin of the tensor force. At longer distances the triplet-even nucleon-nucleon potential ($S = 1$, L even) behaves similarly for the Michigan Three-Range Yukawa, the Argonne V8', and the standard G-matrix theories as it does for a simple $\pi + \rho$ meson-exchange model with short-range cut-off, so for convenience the latter is taken. Setting out from the effective single-particle energies that GXPF1 prescribes for ^{68}Ni, the swift downsloping $\pi f_{5/2}$ state from $N = 40$ to $N = 50$ marks a trend that is counterbalanced by the opposite tendency of the $\pi f_{7/2}$ spin-orbit partner. This is shown in the leftmost panel of figure 3.10, where also a smaller reduction is visible for the $\pi p_{3/2} p_{1/2}$ orbitals. If confirmed by experiment, the accumulating $g_{9/2}$ neutrons would inexorably precipitate a closure of the $Z = 28$ shell gap towards ^{78}Ni. The article on the γ spectroscopy of ^{77}Cu that we came upon in section 2.7 indeed took support from the $\pi + \rho$ model to address this claim [Vaj18].

Stepping aside from the shell model for a while, we can explore how a tensor force is accommodated in the mean field. To that end the Gogny-type GT2 force was devised, comprising a central as well as a tensor part [Ots06]. The central component is cut to the Gogny D1S interaction, which contains the spin and isospin exchange

operators yet otherwise stands tensorless. The contributions of the exchange operators are kept in equilibrium in a manner that is opposite between GT2 and D1S. Also the sign of the spin-orbit force is reversed but the triplet-even potentials are equivalent, for GT2 actually moving closer to single-pion instead of $\pi + \rho$ exchange. Gaussian functions are taken for the radial dependence throughout, even if for the tensor term of GT2 this may not be fully appropriate. The spin-isospin structure of the tensor force still obeys equation 1.11. The evolution of the single-particle energies for nickel in the GT2 and D1S models is compared in the middle and right-hand panels of figure 3.10. While for D1S only the $\pi f_{5/2}$ orbital seems sensitive to the quantum numbers of the neutron matter, the GT2 force exerts an attraction on $\pi f_{5/2}$ and a repulsion on $\pi f_{7/2}$ and $\pi g_{9/2}$ once the $\nu g_{9/2}$ particles arrive beyond $N = 40$. Before $N = 38$ we witness the complementary action, gentle courtesy of $\nu f_{5/2}$.

In order to frame correctly the tensor contribution to the structure of systems above $N = 40$, we still must insist on an interaction that extends to the $g_{9/2}$ orbital. Ruminating the knot of GXPF1 over again, the JUN45 force finally answers to this request [Hon09]. Sticking to the common path, a G-matrix interaction is spun from the Bonn potential that now lives in the $f_{5/2}pg_{9/2}$ space around a core of ^{56}Ni. It is refined by fitting 45 linear combinations of the single-particle energies and two-body matrix elements to experimental binding and excitation values spanning $63 \leq A \leq 96$. Significantly the nickel and copper isotopes are excluded from the procedure this time in order to mitigate the ripples of proton excitations from the omitted $f_{7/2}$ orbital into the data set, while deformed nuclei for which $Z > 33$ and $N < 46$ are likewise ignored.

Although one would not expect JUN45 to perform particularly well for nickel and copper, they present the first isotopic chains to be examined. From figure 3.11 we ascertain the crossing of the $f_{5/2}$ and $p_{3/2}$ proton energies at $N = 48$, while the corresponding spin levels pass each other already at $N = 46$ in ^{75}Cu. However as we anticipated, the collective character of the experimental $1/2^-$ level escapes the model. A weak tensor effect can be presumed from the slope of the $\pi g_{9/2}$ single-particle energy but is not reflected in the calculated level positions, betraying a more complex wave function. As a matter of fact it elucidates the projected yet unobserved migration of this level when we discussed the PCM in section 3.1. A more detailed view of the

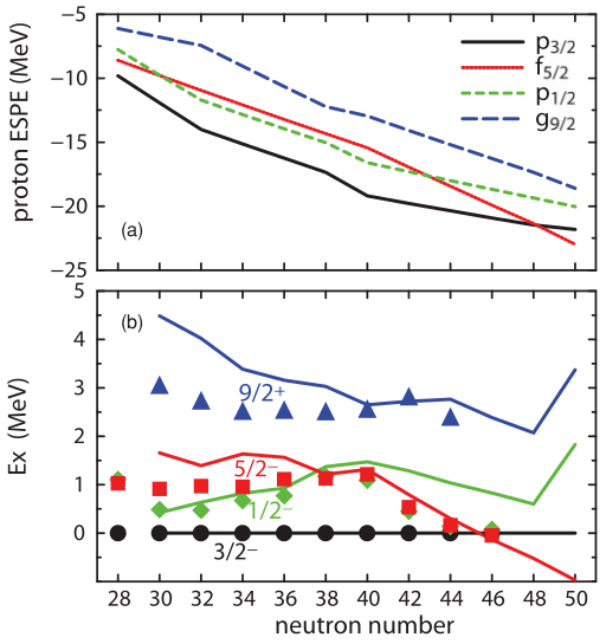

FIGURE 3.11: Theoretical proton single-particle energies (top) and experimental level energies of the lowest $3/2^-$, $1/2^-$, $5/2^-$, and $9/2^+$ spin states compared to predictions (bottom) from the JUN45 interaction in the copper isotopes. Taken from [Hon09]

levels of the ^{71,73,75}Cu isotopes is given in figure 3.12, offering an occasion to oppose JUN45 to the predictions from the jj44b force. We recall that the fitting procedure of the latter explicitly comprises data from nickel to zinc, so its relative accuracy bears no secret. In figure 3.13 a slightly zoological outcome for the nickel isotopes is plotted. While a problem persists for the 2^+ state at $N = 34$, we see that beyond $N = 40$ the magic element remains a challenge.

Nonetheless the JUN45 Hamiltonian proved popular, as the literature can attest to. With spin gyromagnetic ratios g_s normalised by a factor of 0.7 and effective charges of $e_\pi = 1.5e$ and $e_\nu = 1.1e$ the interaction works out pleasantly for the electromagnetic moments of neutron-rich copper, among which the magnetic moment of the single-particle ground state of ^{75}Cu presented in section 2.1 [Vin10]. It stumbles when proton excitations of the core step in, like for ^{73}Cu but also for ^{77}Cu as compiled in figure 2.4 [Koe11]. Proceeding to the odd-odd isotopes from section 2.6, ^{72}Cu turns out to be troublesome nucleus, the wave functions of which do not match the experimental level ordering as illustrated in figure 2.48 [Fla10]. Higher up this honour befits ^{79}Ga,

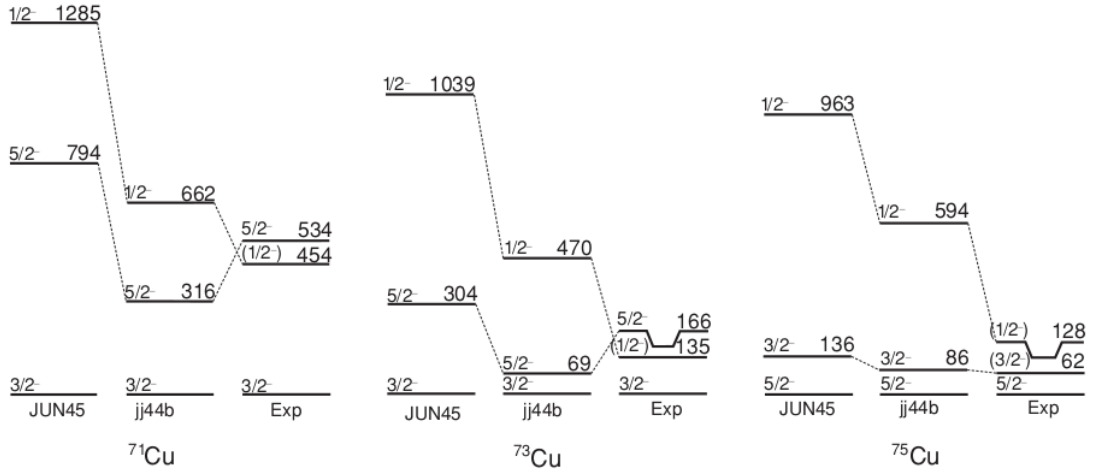

Figure 3.12: Experimental level schemes of ^{71,73,75}Cu compared to shell-model calculations with the jj44b and JUN45 interactions. Taken from [Fla10]

in which the theoretical state with the correct ground-state magnetic moment lies over 300 keV upwards and for which we refer to section 2.8 [Che10]. In ^{79}Zn it shares the fate of jj44b, openly confirming that the single-particle configuration of the observed isomer lies outside its valence domain [Wra17]. When copper comes back to the attention for a systematic investigation of its isotopic chain, JUN45 is heartlessly overtaken by the more recent theories pictured in figure 2.65 [DeG17]. The mass measurement of ^{79}Cu still features a fair comparison, which is justified since we do not pass $N = 50$ [Wel17].

The limitations of the model space are felt when we survey the transfer reactions from nickel into copper in section 2.2 [Sch13]. For the same reason in section 2.4 the $5/2^-$ ground state of ^{75}Cu is more easily sorted out than the deformed $1/2^-$ state, which is immediately visible in figure 2.22 [Pet16]. In section 2.5 its restricted base explains the flat performance in the Coulomb excitation of nickel [Kol16] whilst overlooking the 0^+_3 state in ^{68}Ni [Rec13].

Returning to the rather conceptual work, in the meantime the monopole-based universal interaction V_{MU} is proposed [Ots10]. Seeking to reduce the nuclear potential to those features that seem fundamental to comprehend shell evolutions in their wider context, it is composed of a Gaussian central force that simulates the global behaviour of GXPF1A and a $\pi + \rho$ tensor interaction that is specific to the quantum numbers of

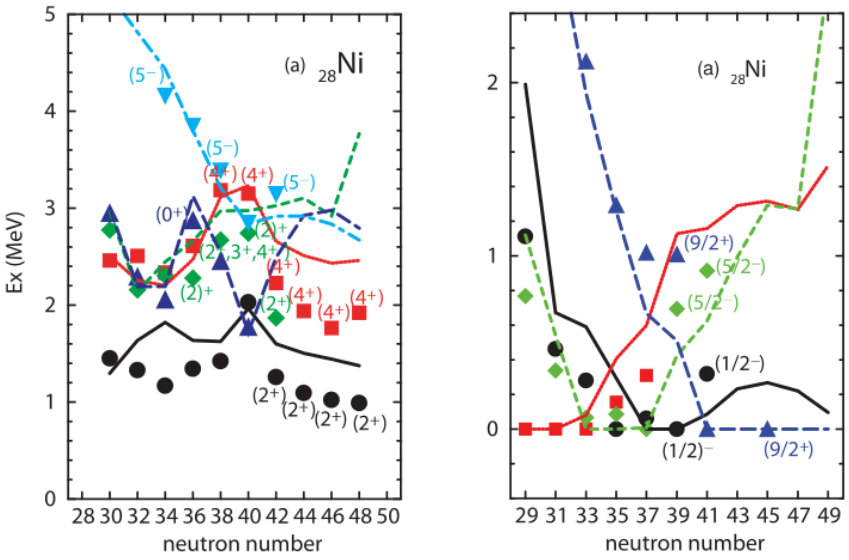

FIGURE 3.13: Experimental level energies compared to predictions from the JUN45 interaction for the even (left) and odd nickel (right) isotopes. Taken from [Hon09]

the involved orbitals. Underlining the robustness of the scheme, it is indicated that short-range correlations and effects of the nuclear medium do not influence appreciably the tensor monopoles, a phenomenon that is known as renormalisation persistence [Tsu11]. Their action is absorbed by the central potential, since the renormalisation is essentially driven by the distance between the nucleons. The resulting prediction for the nickel isotopes is shown in figure 3.14 and resembles that of the GT2 force in figure 3.14 more than that of the JUN45 one in figure 3.11, the crossing of the $p_{3/2}$ and $f_{5/2}$ orbitals occurring at $N = 45$.

An offspring of the V_{MU} force is found in the work by Kaneko from Fukuoka and colleagues. At first a sum of schematic pairing, quadrupole and octupole forces is carefully steered with locally chosen monopole corrections to describe the neutron-rich chromium isotopes around $N = 40$ [Kan08]. The monopole part is replaced with the V_{MU} set of parameters, which are viewed as universally valid [Kan14]. The updated PMMU interaction of pairing, multipole and unified monopole components alternatively operates in the pf and $pf_{5/2}g_{9/2}$ spaces but oddly predicts a higher excitation energy of the 2^+ state in ^{66}Ni than in ^{68}Ni. Nonetheless it was espoused in section 2.5 when we related the Coulomb excitation of ^{74}Ni [Got20] and also appeared in the clarification of the low 2^+ energy of ^{64}Cr [Gad10].

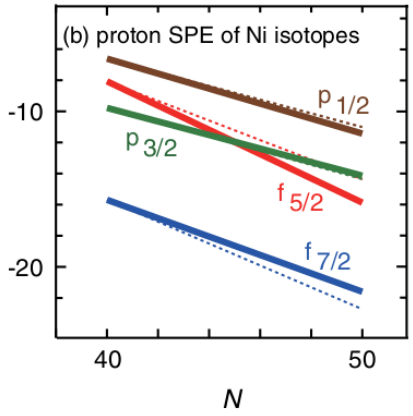

Figure 3.14: Evolution of proton single-particle energies in nickel isotopes from the V_{MU} interaction. Taken from [Ots10]

With the constant goal to surmount the shortcomings of the model space, the Tokyo group picked up Honma's A3DA force, which is formulated in the $fpg_{9/2}d_{5/2}$ realm around a ^{40}Ca inert core [Shi12]. It gathers its two-body matrix elements from the GXPF1A Hamiltonian for the fp shell, JUN45 when the $f_{5/2}pg_{9/2}$ orbitals couple to $g_{9/2}$, and a G matrix that is inspired by the N^{3}LO chiral interaction from Entem and Machleidt for the remainder. The single-particle energies and the monopole components are modified to match a range of forecasts from GXPF1A and JUN45 as well as, somewhat unexpectedly, Woods-Saxon single-particle energies in stable semi-magic nuclei. A last touch of phenomenological adjustment to experimental data near $N \approx 40$ is added. The single-particle energies obtained for nickel are drawn in the left panel of figure 3.15 and indeed follow those of JUN45 in figure 3.11. Interestingly the $\pi f_{5/2}$ and $\pi g_{9/2}$ states abandon their migration after passing $N = 50$. The 2^+ energies in the even nickel isotopes in the right panel of the figure comply with experiment in a far stricter manner than they did in figure 3.13. While the interaction tightly handles the case of $N = 34$, the first excited 2^+ state of ^{78}Ni would serenely stand just below 3 MeV of energy.

In spite of the reasonably high excitation energy that is foreseen for ^{78}Ni, a surprising result of the A3DA interaction lies in the corresponding $B(E2)$ value, a peculiarity we mentioned in section 2.5. Looking back at figures 2.24 and 2.25, we find for ^{72,74}Ni a behaviour of the theoretical transition strength that is more regular than ex-

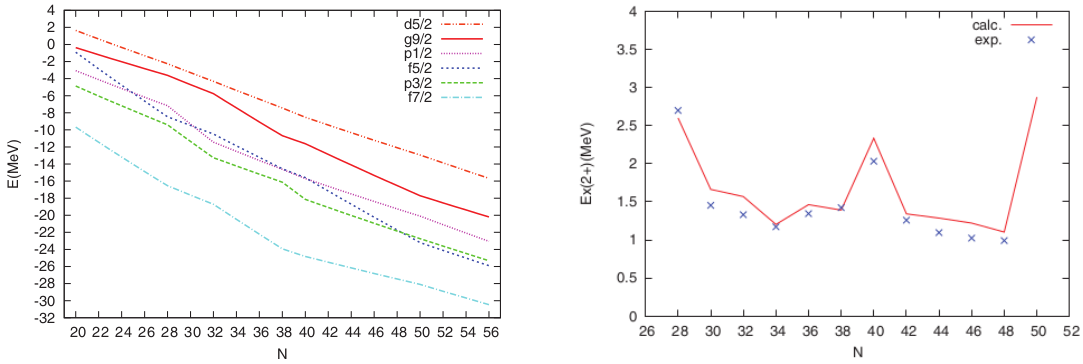

FIGURE 3.15: Evolution of proton single-particle energies in nickel isotopes from the A3DA interaction (left) and experimental 2^+ energies in nickel isotopes compared to A3DA calculations (right). Taken from [Shi12]

periment purports [Mar14, Kol16]. Keeping throughout the chain the effective charges at $e_\pi = 1.5e$ and $e_\nu = 0.5e$, a minimum ensues in ^{76}Ni followed by a jump of 50% in ^{78}Ni. Even as it respects both the $Z = 28$ and $N = 50$ shell gaps, the calculation as a matter of fact produces a sudden surge of neutron excitations across $N = 50$ in the latter isotope, which is left unexplained. In the beginning of the subshell in ^{68}Ni the model successfully computes three 0^+ states with distinct spherical, oblate and prolate shapes, exhibiting their full colour in figure 2.30 [Rec13, Suc14a]. The lifetime of the 0^+_3 level, however, is overestimated by two orders of magnitude [Cri16]. Moving to ^{70}Ni, the oblate minimum flows into the ground state while the prolate shape develops deeper [Pro15]. The discrepancy for its half-life is reduced to a factor of four. A prediction for an oblate 0^+_3 state in ^{70}Ni reappears in a later publication but its origin is not disclosed [Mor17].[2]

The small revisions that are applied to the A3DA Hamiltonian during its learning curve earn it the label A3DA-m. Although it is not clearly stated when it sheds its skin, following other authors we fix it at the introduction of type-I and type-II shell evolution by Yusuke Tsunoda still in Tokyo [Tsu14]. The denomination of type I is reserved for those tensor forces that are generated by particles in different nuclear systems along an isotopic or an isotonic chain. They are characterised by a $j_< \leftrightarrow j'_>$ attraction be-

[2] While both articles [Pro15] and [Mor17] refer explicitly to A3DA and print the same 0^+_2 and 4^+_1 energies in the theoretical level schemes, they oddly differ for the 2^+_1 and 2^+_2 energies

tween protons and neutrons and correspond to the pattern that we encountered along the copper isotopes. But the tensor paradigm can also be provoked by an internal redistribution of particles following a change in configuration within the same nucleus, notably by virtue of particle-hole excitations. When the particles are excited into an orbital that exerts a tensor force on an orbital of the opposite kind of particle such that both orbitals are brought closer to the Fermi surface, the behaviour is referred to as type II. If for instance neutrons flow into a $\nu j'_>$ state such that a $\pi j_< \leftrightarrow \nu j'_>$ tensor attraction is induced, a positive feedback loop is triggered till a new equilibrium is found. Because of the many particle-hole configurations that become involved, deformation is a likely outcome. The mechanism imitates the symmetry-breaking Jahn-Teller distortion famous in chemistry and solid-state physics, in which the degeneracy of an electron configuration is lifted and the ion or molecule resolves into a deformed state of lower energy [Ots10].

Type-II shell evolution forms the grounds on which the occurrence of the different coexisting shapes in ^{68}Ni is explained. The microscopic cradle that generates the deformation is traced back to the tensor force, inducing correlations between the $f_{5/2}$ and $f_{7/2}$ proton orbitals on one side and the $g_{9/2}$ neutron orbital on the other side that strengthen the local minima in the potential-energy surface. Shape coexistence between spherical and strongly deformed patterns is manifested by the three 0^+ states that have repeatedly taken centre stage in section 2.5. Above the spherical ground state, the 0^+_2 state lies oblate at 1.6 MeV with a deformation parameter $\beta_2 \approx -0.2$. Schematically it counts two neutrons that cross the $N = 40$ gap into the $\nu g_{9/2}$ orbital. The 0^+_3 state stands prolate at 2.9 MeV with $\beta_2 \approx 0.4$. It holds a balance of two proton holes in $\pi f_{7/2}$ and four neutrons particles in $\nu g_{9/2}$. In figure 2.31 the reciprocal excitation of protons and neutrons mutually reinforcing each other is especially clear for the 0^+_3 state. The A3DA-m interaction also enables to disentangle the various contributions to the wave functions that play a subtle role in the two-neutron transfer reaction from ^{66}Ni into ^{68}Ni [Fla19]. In ^{74,76}Ni a more complex image of triaxiality develops, although a proper description of the seniority configurations of ^{74}Ni that we passed upon in section 2.7 remains a challenge [Mor18]. The ^{78}Ni nucleus on the other hand would settle in a single spherical minimum amidst vanishing shape coexistence. The

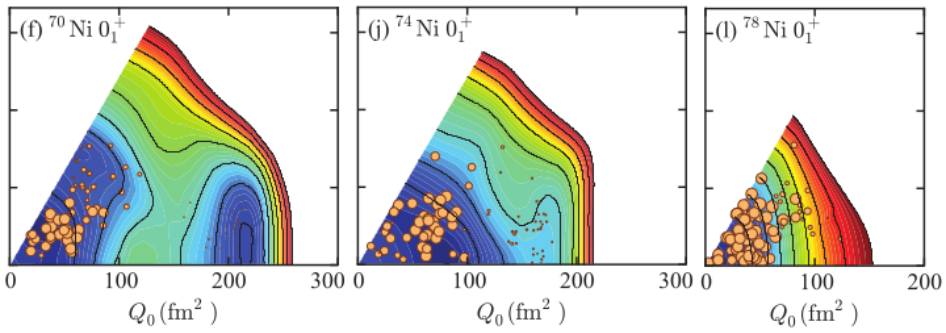

FIGURE 3.16: Potential-energy surfaces for ^{70,74,78}Ni from the A3DA-m interaction. Taken from [Tsu14]

minimum of its potential-energy surface is noticeably flat, as shown in figure 3.16.

A slightly sophisticated view arises for ^{75}Cu, which we can compile from sections 2.4 and 2.7 [Ich19]. We learnt that the mixing between the $5/2^-$ ground state and the $3/2^-$ excited state produces two equivalent prolate states, visualised in figure 2.59. Together with the $1/2^-$ level that is energetically sandwiched between, they would contain a collective core excitation with a more or less distinct single-particle component. The equal treatment of the three levels is somewhat quizzical and while it clarifies the monopole migration of the $\pi f_{5/2}$ and $\pi p_{3/2}$ single-particle states proceeding undisturbed on top of the core, it perhaps obscures the dynamics of the $1/2^-$ state not really responding to any tensor leverage. The A3DA-m contributes prominently to the interpretation of the level scheme of ^{77}Cu still in section 2.7, underscoring the single-particle nature of the $5/2^-$ and $3/2^-$ levels but at the same time bringing forth a solid fraction of 74% of the $\pi f_{7/2}$ hole strength at a low energy of 1.4 MeV [Sah17a]. The $p_{1/2}$ state on the other hand is fragmented. The single-particle energies in figure 2.55 present a close-up view that basically coincides with the wider picture from A3DA in figure 3.15, surmising a nearly constant $Z = 28$ gap albeit defined by different orbitals in $N = 50$ than in $N = 40$.

Since ^{79}Cu bears peculiar interest in our work, in table 3.2 we list the finer facets of its theoretical structure. The ground state carries a spin and parity of $5/2^-$, above which the first excited state at 0.29 MeV sports a $3/2^-$ signature. The purities of the respective $\pi f_{5/2}$ and $\pi p_{3/2}$ wave functions are calculated at respectively 76 and 75%. A $1/2^-$ level appears next at an energy of 1.95 MeV, for which the dominant $\pi p_{1/2}$ configuration

E_x (MeV)	J^π	leading	second	third
0	$5/2^-$	76% $\pi f_{5/2}$		
0.29	$3/2^-$	75% $\pi p_{3/2}$		
1.96	$1/2^-$	49% $\pi p_{1/2}$	13% $\pi f_{5/2}\nu d_{5/2}$	10% $\pi f_{7/2}^{-1} p_{3/2} f_{5/2}$
2.04	$7/2^-$	48% $\pi f_{7/2}^{-1} f_{5/2}^2$	14% $\pi f_{7/2}^{-1} p_{3/2}^2$	
2.65	$7/2^-$	35% $\pi f_{5/2}\nu d_{5/2}$	27% $\pi f_{7/2}^{-1} p_{3/2} f_{5/2}$	

Table 3.2: Wave-function composition for selected states in ^{79}Cu from the A3DA-m interaction. Private communication from [Tsu17]

does not portend deformation that would be worth noticing. The first $7/2^-$ state at 2.04 MeV contains a considerable $\pi f_{7/2}$ hole component, sharply raising its position from ^{77}Cu. For the second $7/2^-$ level at 2.65 MeV both proton and neutron excitations mix in. The verdict from experiment, which features in our article [Oli17b], shall be the topic of our final chapter.

Meanwhile with free g factors and effective charges of $e_\pi = 1.31e$ and $e_\nu = 0.46e$ the magnetic moment of the $1/2^+$ isomer in ^{79}Zn stays out of scope, a subject that summons concern in section 2.8 [Wra17]. Soon after the A3DA-m model space is enlarged to the whole *fpsdg* domain including the crucial $\nu s_{1/2}$ orbit, now correctly matching the moment [Xie19]. The calculated odd-even staggering of charge radii in zinc is stronger than what is measured but the mere ability to do so is a commendable feat. Adjusting the spin g_s factors to 0.75 times their free value and the orbital g_l factors to 1.1 for protons and -0.1 for neutrons, the interaction performs excellently for the electromagnetic moments of copper [DeG17].

In a paramount achievement the γ spectroscopy of ^{78}Ni is elucidated in section 2.9 [Tan19]. Realising the overriding importance of the extended model space to critically breach the spherical enclosure, shape coexistence is finally laid bare at the magic crossroads. The spherical 2_1^+ level arrives at 2.57 MeV, well below the deformed 2_2^+ one at 2.89 MeV. The prolate band with $\beta_2 \approx 0.3$ would harbour on average 2.5 particle-hole excitations for both protons and neutrons.

One may wonder whether type-II evolution would hide behind any deformation

in the copper isotopes. Rather than on the $\pi p_{1/2}$ orbital and the possibly related $1/2^-$ state that was seen Coulomb excitation and scrutinised in section 2.4, it would act on the πf components of the wave function, which are most susceptible to the tensor force. When $f_{7/2}$ protons stray across the $Z = 28$ gap into the $\pi p_{3/2}$ and $\pi f_{5/2}$ orbitals, however, many additional components might emerge in the wave function. The spectroscopic factors in transfer reactions would fade out, although γ bands at high spin would become visible in the deep-inelastic reactions that we mentioned in section 2.3 [Ish00].

The more profound appreciation of the tensor force also brings significant advances to our understanding of nuclei in the *p* and the *sd* shells. We abandoned their study after closing section 1.2 but briefly want to collect here some of the main insights and knit together the loose ends. The neutron drip-line in the oxygen isotopes is aptly tackled by the V_{MU} interaction, superseding SDPF and explicitly encompassing the $\pi + \rho$ tensor force [Yua12]. Applied to the silicon region, V_{MU} transmutes into SDPF-MU [Uts12]. Exhibiting a prime example of the Jahn-Teller effect, the tensor component is instrumental to lift the orbital degeneracy, pushing the ^{42}Si nucleus in a strongly oblate minimum whilst obtaining an accurate result for its 2^+ energy. The recent experimental progress at RIBF, which renders it possible to descend $N = 28$ even farther down, in turn incites SDPF-MU to correctly calculate the TNA and the 2^+ energy of the prolate rotor that emerges in ^{40}Mg [Cra14, Cra19]. The novel magicity of $N = 34$ in ^{54}Ca meanwhile would follow from a variation of the same model [Ste13]. We find an analogous declination of the V_{MU} interaction in the treatment of shape coexistence and quantum phase transitions in ^{100}Zr, which however we shall leave for another monographer in good season [Tog16].

3.5 Quasi and pseudosymmetry

Since the extensive essay by Poves and Zuker on nuclei in the *fp* shell [Pov81], several shell-model interactions have been developed in a fruitful collaboration between Madrid and Strasbourg. The paper is incidentally famous for its warning that “Data have the nice but treacherous habit to make us believe that a small diagonalisation, or

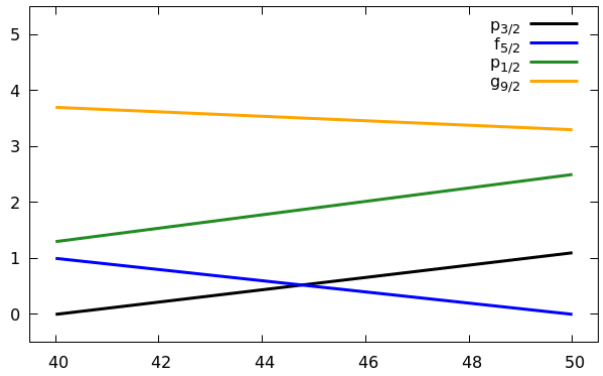

FIGURE 3.17: Evolution of proton single-particle energies in copper isotopes from the Duflo-Zuker interaction. Data taken from [Duf99]

even no diagonalisation at all, is sufficient to describe many of the interesting states. This habit is called Shell Model". An example of the statement is perhaps found in the purely phenomenological monopole Hamiltonian that is constructed by Jean Duflo at Orsay [Duf99]. With only six parameters to fit an anthology of experimental level energies from ^{39}Ca to ^{209}Bi, the single-particle energies for the copper isotopes are predicted up to $N = 50$. As the reader can deduce from figure 3.17, the outcome is altogether not so different than that from the much more sophisticated JUN45, V_{MU}, or A3DA interactions in figures 3.11, 3.14, and 3.15. Although the authors look with confidence upon the calculated spectra, prudence arguably prevents us from crossing the ford to an actual level scheme.

Heading for the steeper itinerary instead, we pick up the thread from our discussion in section 2.5 when experimental progress gains access to the $N = 40$ subshell closure and a force is proposed that for lack of a proper name we call the Madrid-Strasbourg Hamiltonian [Sor02]. The πfp and $\nu pf_{5/2}g_{9/2}$ valence orbitals bathing a core of ^{48}Ca are given life by a realistic interaction in which the fp two-body matrix elements stem from the KB3G force written in Madrid [Pov01], the link of $pf_{5/2}$ with $g_{9/2}$ is defined from the effort by Nowacki in Strasbourg [Now96], and that of $f_{7/2}$ with $g_{9/2}$ from an older strand of work at Brookhaven that we referred to in section 1.1 as KLS [Kah69]. To complete the recipe, the $\nu g_{9/2}$ single-particle energy and the $\pi f_{7/2}\nu g_{9/2}$ monopole strength are adjusted phenomenologically. The merit of the interaction lies contained in its ample model space, which should readily allow for proton excitations across the

$Z = 28$ gap.

As we reported upon in section 2.5, the calculated $B(E2)$ values for the even nickel isotopes confirm the experimentally observed closure of the neutron subshell in ^{68}Ni. The conjunction of proton core excitations bridging $Z = 28$ and neutron pair scattering surfing on $N = 40$, qualified as proton polarisability and neutron superfluidity in inspired prose, soon gnaws at the gap once ^{68}Ni is left behind. The upwards jump in the transition probability for ^{70}Ni, which is evidenced in figure 2.23 [Per06], nevertheless is questioned in the context of the further measurements shown in figure 2.25. Turning to copper, the level structure of ^{75}Cu ranked among our interests in section 2.4 [Dau10]. Weighing recent data from the Coulomb excitation of ^{80}Zn to adjust more finely the critical gap between the $\pi f_{7/2}$ and $\pi f_{5/2}$ orbitals, the $5/2^-$ ground-state spin of ^{75}Cu is correctly assessed. The $1/2^-$ and $3/2^-$ isomeric structures find their place close to each other in the lower part of the level scheme but the reader may recall that at this point the experimental situation is not yet settled.

An elaborate theoretical analysis of the nickel region is published separately [Sie10]. This time the interaction is outlined by Machleidt's charge-dependent Bonn potential [Mac01b], upon which the monopole terms are tuned to improve the agreement with selected data.[3] The proton single-particle energies are pictured in figure 3.18 and reveal a steady pattern in which the $\pi f_{7/2}$ and $\pi f_{5/2}$ spin-orbit partners reduce their reciprocal distance as one approaches $N = 50$, degrading the magicity at $Z = 28$ by 0.7 MeV. Interestingly a similar but weaker behaviour permeates for the $\pi p_{3/2}$ state with respect to its $\pi p_{1/2}$ kin. The authors refer to the work from the Tokyo team and recognise a tensor effect. The calculated levels in copper are brought together in figure 3.19. Looking out towards $N = 50$ the energy of the $5/2^-$ state obeys a straight descent that one may link to monopole migration, while for the $1/2^-$ level the trend is inverted as if it were as a suspension bridge between $N = 40$ and $N = 50$. The occupation numbers of the different orbitals in the wave function of the $1/2^-$ state as a matter of fact betray the presence of many components of equal value, corroborating its collective nature especially in the middle of the neutron subshell. The $3/2^-$ level claims a fair $\pi p_{3/2}$

[3] While [Dau10] derives its interaction from [Sor02], it relies in part on a future publication, by which apparently [Sie10] is meant. The charge-dependent Bonn potential, which is explicitly mentioned in [Sie10], is however entirely absent from [Sor02]

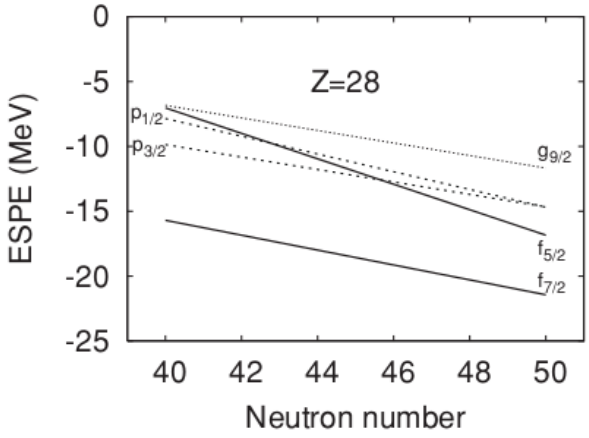

FIGURE 3.18: Evolution of proton single-particle energies in nickel isotopes from the Madrid-Strasbourg interaction. Taken from [Sie10]

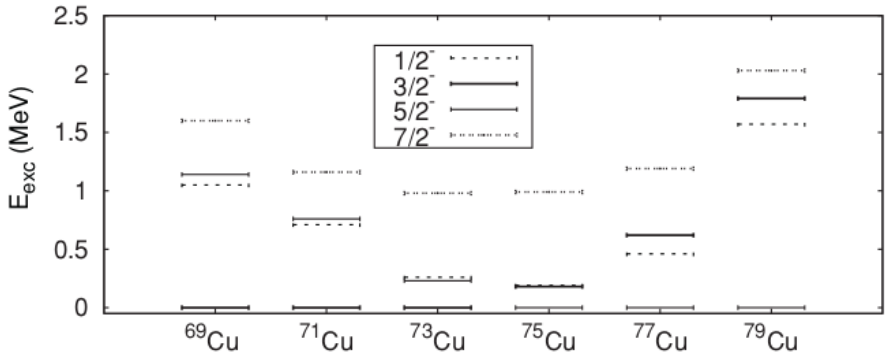

FIGURE 3.19: Theoretical level schemes of neutron-rich copper isotopes from the Madrid-Strasbourg interaction. Taken from [Sie10]

purity in ^{69,71,73}Cu, which it squanders in ^{75,77}Cu before recovering in ^{79}Cu. For the $5/2^-$ state the $\pi f_{5/2}$ contribution withers in ^{69}Cu but takes on an ever clearer stance as the neutron number increases.

Seeking to isolate the dowel that underpins the coexistence of collective and single-particle properties in the low-energy level schemes of copper, the role of the $f_{7/2}$ proton excitations is held under the microscope. For all odd isotopes from ^{69}Cu to ^{79}Cu the average number of holes in the orbital ticks off near 0.5, even exceeding so for the $5/2^-$ state in ^{69}Cu. Possibly this fact explains the puzzling spectroscopic factor that was observed for the level in the (d,τ) transfer reaction shown in figure 2.13 [Zei78]. The $7/2^-$ state itself stands out with a strong $\pi p_{3/2}$ component in ^{69,71,73}Cu but switches to a

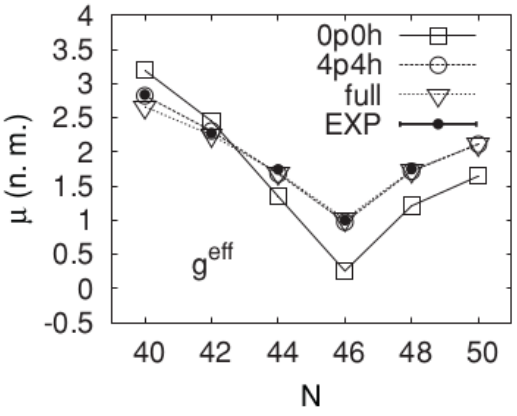

FIGURE 3.20: Magnetic moments of neutron-rich copper isotopes compared to calculations with the Madrid-Strasbourg interaction. Taken from [Sie10]

$\pi f_{5/2}$ one in ^{75,77,79}Cu. As if the ground-state proton remains stuck in its orbit, it forces a sizeable $\pi p_{3/2} \times 2^+$ or $\pi f_{5/2} \times 2^+$ configuration upon the $7/2^-$ level and attenuates a $\pi f_{7/2}$ hole character for it. Also neutron excitations across $N = 40$ add in a significant way to the wave functions, although their influence would diminish towards $N = 50$.

The electromagnetic properties are computed with effective charges of $e_\pi = 1.5e$ and $e_\nu = 0.5e$, scaling the spin g_s factors by a coefficient of 0.75 and setting the orbital g_l factors to 1.1 for protons and -0.1 for neutrons. Once again the particle-hole excitations are of vital importance to reach agreement between experiment and theory, the normalisation of the gyromagnetic ratios serving secondary consideration. Comparing figure 3.20 with figure 2.4, the improvement over jj44b and JUN45 thanks to the downwards extension of the model space is most admirable. Meanwhile the Madrid-Strasbourg force is integrated into a framework for β decay, nicely reproducing the half-lives of isotopes near ^{78}Ni displayed in figure 2.52 in section 2.7 [Xu14]. The additional data on ^{75}Cu that arrive a couple of years later and finally sort out the sequence of the γ rays in the level scheme confirm the adequacy of the theory, of which figure 2.22 in section 2.4 limpidly informs us [Pet16].

The deformation that is discovered in the chromium isotopes and that drew our attention in section 2.5 sets the scene for an upwards enlargement of the model space to the $\nu d_{5/2}$ orbital [Sor03]. By this choice quadrupole correlations between the $\nu g_{9/2}$ and $\nu d_{5/2}$ orbitals can be accommodated in the mechanism of quasi-SU(3) symmetry,

which expanding on Elliott's view traces the origin of collectivity to the interaction among the lowest $\Delta j = 2$ states within a given shell [Ell58, Zuk95]. Of equal importance, the corresponding reduction of the valence domain to the orbitals that are deemed relevant to the underlying physics brings down the dimension of the diagonalisation by typically two orders of magnitude. The supplementary matrix elements that are needed to implement the $\nu d_{5/2}$ particles are gracefully copied from Hjorth-Jensen's realistic G-matrix interaction. The neutron single-particle energies at $N = 40$ are plotted in figure 2.35 and are propelled downwards for a growing number of protons in $f_{7/2}$. The plausible effort that is undertaken to link their thrust to that of the tensor force might appear stymied, however, as we pointed out in our earlier discussion that a systematic differentiation of the $j_<$ and $j_>$ orbitals is at best unverified.

As the span of nuclei is increased also the collaboration is augmented. In the LNPS interaction the inner initials, which the reader can infer from above, are joined by those of Lenzi and Sieja [Len10]. The model space remains that of $\pi fp\ \nu pf_{5/2}g_{9/2}d_{5/2}$ but the two-body matrix elements are shaken up. The KB3gr force without providing details simply relieves its KB3G predecessor in the fp shell, the realistic G-matrix interaction from Hjorth-Jensen with empirically modified monopoles from Nowacki incorporates the $\nu g_{9/2}$ orbital, while the KLS potential tells the rule by which the $\nu d_{5/2}$ particles play. The single-particle energies are regulated by keeping the constraint that is imposed by the experimental $B(E2)$ value of ^{80}Zn on the $Z = 28$ gap mentioned above and cranking up the $N = 50$ divide to 5 MeV in order to match relevant particle-hole excitations in ^{82}Ge. The quadrupole interaction between the $\nu g_{9/2}$ and $\nu d_{5/2}$ quasi-SU(3) partners is reinforced by 20% to account for the absence of the $\nu s_{1/2}$ orbital, which is the nearest $\Delta j = 2$ state outside the model.

The primary motivation of the LNPS force is the description of the island of inversion around chromium and iron below ^{68}Ni, so the neutron single-particle energies that are reprinted in figure 2.37 focus on $N = 40$. The hopping intersection points of the quantum states when juxtaposing figure 2.35 do not perturb the eye much, but the more complete range of orbitals lends evidence to an identical treatment of the $j_<$ and $j_>$ orientations when $f_{7/2}$ protons are filled in. Paying particular heed to the nickel isotopes and the $N = 40$ isotones, from figure 3.21 we witness an excellent performance.

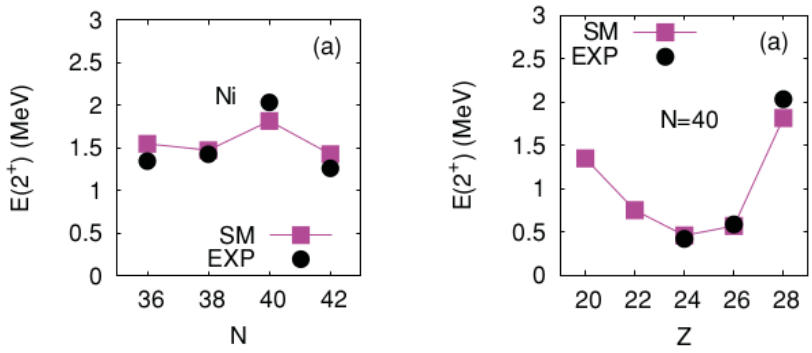

FIGURE 3.21: Experimental 2^+ energies compared to LNPS calculations for nickel isotopes (left) and $N = 40$ isotones (right). Taken from [Len10]

In ^{68}Ni excited 0^+ states are computed at energies of 1.2 and 2.4 MeV. While the 0^+_2 state is defined by a 2p-2h neutron configuration, the 0^+_3 one marks itself off through a pure 2p-2h proton configuration with a fair degree of collectivity. We remember from the previous section that the A3DA-m calculation agrees for 0^+_2 but adds four neutron particle-hole excitations to 0^+_3.

Venturing into the nickel realm, the LNPS monopoles are further redressed in line with the earlier work that has been specifically carried out for these nuclei [Sie12]. The wave function of ^{78}Ni reaches 79% of that of two closed shells, underscoring its enduring magicity. The 2^+ energy checks in at 4 MeV with a marked $\nu d_{5/2}$ occupancy of 1.35. Confronted with the controversial data on the $B(E2)$ values in ^{72,74}Ni from section 2.5, we may once more refer to figures 2.24 and 2.25 for the comparison between LNPS and experiment with effective charges fixed at $e_\pi = 1.5e$ and $e_\nu = 0.5e$ [Mar14, Kol16]. Resetting these to $e_\pi = 1.31e$ and $e_\nu = 0.46e$ the interaction determines the deformation lengths of ^{72,74}Ni with an equivalent outcome [Cor18]. As discussed above three 0^+ states are predicted in ^{68}Ni, clearing the premises for shape coexistence to gain due attention [Rec13]. Computing the half-life of the 0^+_3 state LNPS hits a point over A3DA, while we update in figure 2.32 the calculated 0^+_2 and 0^+_3 energies to 1.4 and 2.6 MeV [Cri16]. The role of LNPS in consolidating the quasi-SU(3) paradigm as a prescription for the island of inversion is put forward as we touched upon ^{64}Fe and ^{70}Fe [Lju10, Ben15]. A summary of 2^+ energies in nickel and chromium is gathered in figure 2.39.

Well equipped as we now are to describe both the excitations that break $Z = 28$

and $N = 50$, the need for the $\nu d_{5/2}$ state is instructively apparent from the $E2$ matrix elements in ^{70}Cu studied in section 2.6, for which we return to $e_\pi = 1.5e$ and $e_\nu = 0.5e$ [Rap11]. The explicit exclusion of the orbital deteriorates the concurrence for the $\Delta j = 2$ transitions, which figure 2.45 brings proof of. More information on collectivity comes from the lifetime measurements in ^{69,71,73}Cu that we evaluated in section 2.3 [Sah15]. From the LNPS calculations it dawns that three $7/2^-$ levels are present in these nuclei, the $\pi p_{3/2} \times 2^+$, $\pi f_{5/2} \times 2^+$, and $\pi f_{7/2}^{-1}$ configurations. Among these the hole state would suddenly come down to 1.1 MeV in ^{73}Cu, which is interpreted as a possible premonition of a reduced $Z = 28$ shell gap towards $N = 50$. While it may illustrate a different appreciation by different authors of the same numbers, it could also pull into the light a problem with the spin assignments in this nucleus. Jumping four neutrons to ^{77}Cu in section 2.7, the richness of the calculated level scheme is no match for the limited experimental data [Vaj18]. Nonetheless among the more important findings we mention the projected $\pi f_{7/2}$ hole state at 1.7 MeV, of which the strength function sketched in figure 2.57 is fragmented over several MeV of energy. In the proton knock-out from ^{77}Cu to ^{76}Ni, however, the $\pi f_{7/2}^{-1} f_{5/2}$ multiplet is situated near 4 MeV, pointing at a picture that might prove more complex [Ele19].

The constantly growing collection of experimental data lead to an improvement of the monopole and pairing parameters within the LNPS set of elements from which it comes out afresh as LNPS-m, while for the sake of minor detail we note that the $\nu p_{3/2}$ orbital drops out of the valence space [Sie14, San15]. In particular the proton single-particle energies pictured in figure 3.22 are of interest to us, the $\pi f_{7/2}$, $\pi p_{3/2}$, and $\pi p_{1/2}$ states in the nickel isotopes proceeding in a parallel fashion all the way from $N = 20$ to 50. The $\pi f_{5/2}$ state drifts across but only close to $N = 50$ would it affect the shell gap. Comparing the single-particle energies to those from the V_{MU} and A3DA forces in figures 3.14 and 3.15, the $f_{5/2}$ proton state now intersects the $\pi p_{3/2}$ orbital near $N = 48$ as it also does in A3DA but unlike the earlier crossing at $N = 45$ in V_{MU}.

The convergence between LNPS-m and A3DA is moreover confirmed by the mutual approach of the $\pi f_{7/2}$ and $\pi f_{5/2}$ single-particle energies towards $N = 50$. According to LNPS-m, the distance between the $\pi f_{5/2}$ and $\pi f_{7/2}$ partner orbitals is reduced from 8.7 to 5.0 MeV. In A3DA it narrows incisively from 9.4 to 5.0 MeV. For the

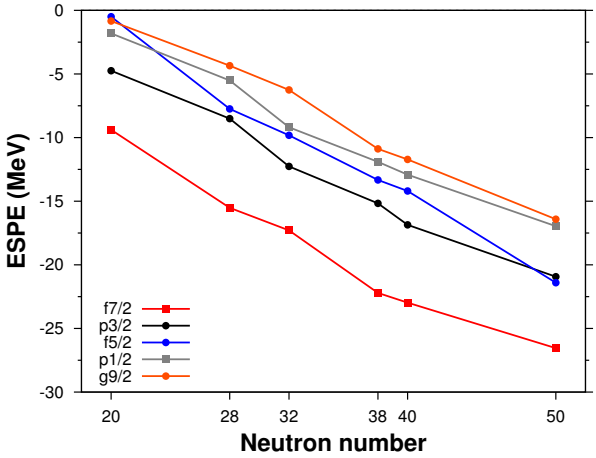

FIGURE 3.22: Evolution of proton single-particle energies in nickel isotopes from the LNPS-m interaction. Private communication from [Sie14]

$\pi p_{3/2}$-$\pi p_{1/2}$ pair on the other hand no erosion of the spin-orbit splitting is discernable. The $Z = 28$ shell gap would stay steady throughout and therefore the excitation energy of the uncorrelated $\pi f_{7/2}$ hole state would be kept unaltered. Neither model reveals a repulsion of the $\pi f_{7/2}$ orbital, as if truly in both forces similar underlying mechanisms would be at work.

Scrutinising the wave functions collected in table 3.3, we find that the ground state of ^{69}Cu reflects for 93% a closed nickel core with a $\pi p_{3/2}$ configuration sitting atop. The first excited $5/2^-$ state at 1.25 MeV contains a salient $\pi f_{5/2}$ contribution with a sizeable $\pi p_{3/2}$ component, as if the latter particle would remain stuck in its orbit. The first $7/2^-$ level at 1.86 MeV consists of a $p_{3/2}$ proton coupled to neutron perturbations. The wave function of the second $7/2^-$ state with an energy of 2.18 MeV is dominated by $\pi f_{5/2} \times 2^+_\nu$, expressing its nature as a member of the multiplet that is built on the first excited state. The diffusion of neutrons across $N = 50$ pulls protons along such that in both $7/2^-$ states a weak hole signature is present, promoting $\pi f_{7/2}$ particles across the $Z = 28$ gap into $\pi p_{3/2}$ or $\pi f_{5/2}$. Bit by bit the $Z = 28$ gap would be swept under the rug and the magicity of the ^{78}Ni core is put under pressure.

While the ground state of ^{71}Cu is still defined by a single $\pi p_{3/2}$ particle, its purity drops to 60% because of the appearance of a 2^+ neutron configuration. The first excited $5/2^-$ state arrives at 0.31 MeV instead of the experimental energy of 534 keV, whereas we note for the sake of reference that the original LNPS interaction put it at a position

E_x (MeV)	J^π	leading	second	third
0	$3/2^-$	93% $\pi p_{3/2} \times 0^+_\nu$		
1.25	$5/2^-$	37% $\pi f_{5/2} \times 0^+_\nu$	20% $\pi p_{3/2} \times 2^+_\nu$	16% $\pi f_{5/2} \times 2^+_\nu$
1.86	$7/2^-$	40% $\pi p_{3/2} \times 2^+_\nu$	22% $\pi p_{3/2} \times 4^+_\nu$	12% $\pi f^{-1}_{7/2} \times J^+_\nu$
2.18	$7/2^-$	52% $\pi f_{5/2} \times 2^+_\nu$	16% $\pi f^{-1}_{7/2} \times J^+_\nu$	14% $\pi f_{5/2} \times 4^+_\nu$
0	$3/2^-$	60% $\pi p_{3/2} \times 0^+_\nu$	14% $\pi p_{3/2} \times 2^+_\nu$	
0.31	$5/2^-$	36% $\pi f_{5/2} \times 0^+_\nu$	22% $\pi f_{5/2} \times 4^+_\nu$	
1.09	$7/2^-$	47% $\pi p_{3/2} \times 2^+_\nu$	11% $\pi p_{3/2} \times 4^+_\nu$	10% $\pi f^{-1}_{7/2} \times J^+_\nu$
1.41	$7/2^-$	42% $\pi f_{5/2} \times 2^+_\nu$	13% $\pi f^{-1}_{7/2} \times J^+_\nu$	12% $\pi f_{5/2} \times 4^+_\nu$

TABLE 3.3: Wave-function composition for selected states in ^{69}Cu (top) and ^{71}Cu (bottom) from the LNPS-m interaction. Private communication from [Sie14]

of 276 keV [Sah15]. Once again it converges on the $\pi f_{5/2}$ orbital. The calculated wave functions for the two $7/2^-$ levels at 1.09 and 1.41 MeV reveal a similar structure as in ^{69}Cu, that is centred on the $\pi p_{3/2}$ respectively $\pi f_{5/2}$ configurations enriched with significant neutron contributions and a smaller fragment of the $\pi f_{7/2}$ hole strength.

Postponing the comparison to the actual experiments we performed on ^{69,71}Cu to chapter 4 and our publications [Mor15b, Mor16b], elsewhere the LNPS-m facelift proves most successful, as back in section 2.5 we acknowledged how the 2^+ energies of ^{70,72}Fe and ^{66}Cr now closely adhere to the data [San15]. Leaving free g factors and chosing effective charges of $e_\pi = 1.31e$ and $e_\nu = 0.46e$ the magnetic moment of ^{79m}Zn examined in section 2.8 still suffers from a deficiency, which however the next iteration of the model will correct for [Wra17].

To better seize the incentive for the new force that is under preparation, we require a gallant step into symmetry concepts. Seeking a thorough theoretical understanding of the machinery that underlies the rise of collectivity, one must admit that the clout of the quadrupole force often appears hidden and perturbed by the monopole field [Zuk15]. To elucidate the levers at work both quasi-SU(3) and pseudo-SU(3) symmetry are investigated. Above we described how $f_{7/2}p_{3/2}$ protons and $g_{9/2}d_{5/2}$ neutrons team up in the quasi-SU(3) scheme, so essentially the deformation they develop occurs below

nickel where $\pi f_{7/2}^{-2n} p_{3/2}^{2n}$ quadrupole configurations are available and towards $N = 50$ where $\nu g_{9/2}^{-2n} d_{5/2}^{2n}$ excitations kick in. Pseudo-SU(3) is a mathematical trick borrowed from Akito Arima in which the angular momentum ℓ is substituted by $\tilde{\ell} = \ell - 1$, such that consecutive $j = \ell - 1/2$ and $j' = (\ell - 2) + 1/2$ orbitals can be grouped together in a single $j = \tilde{\ell} \pm 1/2$ structure [Ari69]. For the purpose of the isotones above $N = 50$ it renders it possible to replace the $g_{7/2}d_{5/2}d_{3/2}s_{1/2}$ neutron space by the $\tilde{f}_{7/2}\tilde{f}_{5/2}\tilde{p}_{3/2}\tilde{p}_{1/2}$ one. In the latter classical quadrupole coherence operates, at the same time rendering the shell-model calculations more manageable. At the proton side the cast is rooted in the $f_{5/2}p_{3/2}p_{1/2}$ particles beyond nickel, the act of which is played by the $\tilde{d}_{5/2}\tilde{d}_{3/2}\tilde{s}_{1/2}$ pseudo-orbitals. Working through the algebra solves our worry that not only the spin-orbit splitting but any haphazard monopole drift may instantly bring down the exact SU(3) system, since the quadrupole action can fortunately be recovered by the approximate quasi and pseudo-SU(3) structures.

Building on these fundamental bricks to make sure that no relevant orbital is left forgotten, the Strasbourg group proposed an interaction in the full harmonic $\pi fp\ \nu gds$ space, entering business under the tag of PFSDG-U [Now16]. The two-body matrix elements are moulded through the G-matrix formalism from the charge-dependent Bonn potential, once again chafing the monopole terms. The neutron single-particle energies are aligned to the measured binding energies of $^{68-72}$Ni, $^{90-98}$Zr, and neutron gaps in the $N = 50$ isotones. Their position in ^{79}Ni is gauged from experimental data in $N = 49$ and $N = 51$ nuclei, feeding back into the cross-shell proton-neutron monopoles. The proton energies are fixed from the single-particle spectrum of ^{79}Cu in the JUN45 Hamiltonian, further constrained by the $B(E2)$ values in zinc and germanium isotopes close to $N = 50$. In figure 2.39 the neutron single-particle energies at $N = 50$ are drafted, from which we can condense a likewise parallel behaviour of the spin-orbit partners as we could notice from figure 2.37 at $N = 40$.

The force predicts the emergence of a novel island of inversion below ^{78}Ni centred on ^{74}Cr. States that contain large quadrupole correlations in their wave function lower their excitation energy and are recognised as intruders. In ^{76}Fe this dashingly happens to the 0_2^+ state, as exemplified in figure 3.23. Arrestingly in ^{78}Ni the bolt freezes into shape coexistence. The calculated spectrum sports a first 2^+ state at 2.88 MeV, which

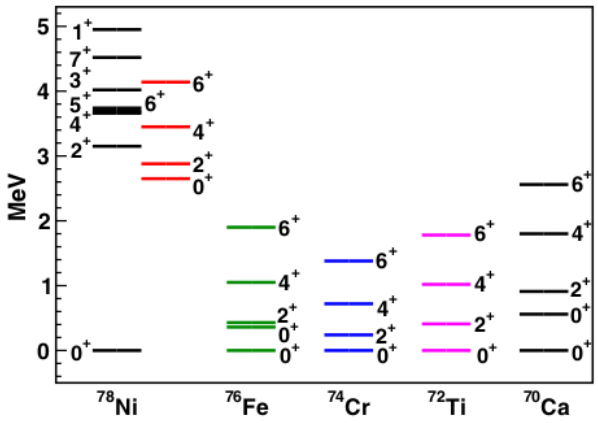

FIGURE 3.23: Theoretical level schemes of $N = 50$ isotones with the PFSDG-U interaction. The deformed intruder band in ^{78}Ni is coloured in red. Taken from [Now16]

hovers just above the prolate 0^+_2 band head sitting at 2.65 MeV. Both would share a neutron 2p-2h intruder signature. At 3.15 MeV we find the second 2^+ level, which with a 1p-1h configuration belongs to the spherical structure atop the ground state. The magicity in the ground-state wave function of ^{78}Ni falls back to 65%, sufficient to maintain its peculiar character at the edge of today's nuclear chart.

The 2^+ systematics in nickel and chromium in figure 2.39 at the end of section 2.5 are extended to $N = 50$, dramatically stressing the difference between both chains. The enigma of the $1/2^+$ isomer of ^{79}Zn meets its Oedipus, related in section 2.8 [Wra17]. The answer clearly lies in the addition of the $s_{1/2}$ orbital to the valence space, so with free g factors and effective charges of $e_\pi = 1.31e$ and $e_\nu = 0.46e$ the theoretical magnetic moment approaches the experimental one to 10%. Softening the spin gyromagnetic ratios g_s with a coefficient of 0.75 and implementing orbital g_l factors of 1.1 for protons and -0.1 for neutrons, the interaction keeps equal pace with A3DA-m along the electromagnetic moments of copper, however not drawing any particular advantage from its larger neutron space [DeG17]. The model moreover backs up the mass measurements of copper isotopes near $N = 50$, delineating mantically the magicity of ^{78}Ni [Wel17].

The bumpy potential-energy surface of ^{78}Ni revealed by figure 2.67 in section 2.9 may be compared with the simple smoothness obtained with the A3DA-m force in figure 3.16. Both schools, however, honed their theories once the first experimental

spectra of ^{78}Ni reached the community [Tan19]. Whereas A3DA-m extends its model space, LNPS and PFSDG-U are kneaded and rubbed together into the Large-Scale Shell Model, in short LSSM. To add precision to plasticity, the transition occurs at $N = 44$ and the proton and neutron gaps are somewhat narrowed down in order to make up for a slightly smaller valence space in which those orbitals with lesser relevance are removed. The outcome does not differ from PFSDG-U, however. At variance with A3DA-m the 2^+_1 state would be deformed and the 2^+_2 one spherical, a situation that is summed up in figure 3.23.

We briefly divert from the main track for a quick flashback to the *sd* shell, where the SDPF-U Hamiltonian from section 1.2 in the meantime has yielded to the SPDF-U-mix force, enriched with KLS cross-shell matrix elements, empirical monopoles, yet a reduced pairing in the isovector channel [Cau14]. The islands of inversion at $N = 20$ and $N = 28$ are united into one, among which the ^{42}Si nucleus is calculated anew to exemplary agreement. Intriguingly in the chain of silicon the $N = 28$ closure gives way to a minor magic number at $N = 32$ instead. Eventually SDPF-U and SDPF-U-mix also appear in the description of ^{40}Mg, next to SDPF-MU [Cra14, Cra19].

As we near the end of our brisk tour of theory, we may attempt to put into broader perspective the different paths that are taken with respect to the origin of collectivity. Unlike a drift of the monopole terms induced by the tensor force of Rarita and Schwinger, in which protons and neutrons directly interact with each other through type-I and type-II shell evolution as posited by the group in Tokyo, the quadrupole interaction derived from Elliott's SU(3) symmetry separates protons and neutrons in the quasi and pseudospaces conceived by the Strasbourg collaboration. It remains curious though that the $\pi p_{1/2}$ orbital, which is most prone to deformation at low energy in the copper isotopes, finds itself in the pseudo-SU(3) scheme coupled to the $\pi f_{5/2}$ partner, the resistance of which to correlations is most striking. If the fall of the latter to the ground state halfway the neutron subshell is engineered by the tensor force, it is however not matched by a reciprocal rise of the $\pi f_{7/2}$ orbital from underneath the Fermi surface. It is with this riddle in mind that we return to the area of experiment in the following chapter.

Chapter 4

Transfer at Ganil

4.1 The experiment

Historically transfer experiments made use of light incoming particles on targets of heavier nuclei. The advent of eams of exotic nuclei has inverted the kinematical conditions. Nowadays a heavy radioactive projectile can be accelerated and sent onto a stable target of an appropriate compound of hydrogen or deuterium, a tritium or helium-loaded metallic foil, or an isotopically pure gas or cryogenic target. Since it seems more sound to classify the reaction mechanism still in the same manner, we continue the practice of the notation $A(a,b)B$ where a and b stand for the lighter participants. In the present work we have investigated the ^{70,72}Zn(d,τ)^{69,71}Cu reactions with τ symbolising the nucleus of the ^{3}He particle.

The difference between direct and inverse experiments stretches farther than the simple laws of motion. In direct kinematics, the heavy reaction component often remains in the target and one measures the energy and outgoing angle of the light ejectile. For this a spectrometer is befitting, taking advantage of a large dispersive magnet to spread out the accepted energy range over the full focal plane that may cover a meter and where a position-sensitive detector is mounted with a resolution below a millimeter, thereby corresponding to a precision of ten keV in the excitation-energy spectrum. The angular distribution is then obtained by turning the spectrometer to the desired angle. The choice of field parameters is mostly such that the experimental conditions are favourable for one reaction channel only.

In inverse kinematics, the heavy nucleus comes out under small angles and is captured in a spectrometer or identified in a detector set-up at zero degree. The light particle now floods a wide range of angles and one resorts to a large silicon array for it to be registered efficiently, routinely reaching an intrinsic resolution of some tens of keV. The actual experimental performance, however, is considerably deteriorated by the energy straggling in the target, which remains unmeasured and cannot be corrected for accurately. Consequently the final peak widths in the spectra typically amount to several hundreds of keV. With the proper angular coverage several reaction channels can be studied simultaneously. Since the reactions rates often do not exceed 10^5 particles per second, the statistics are critical.

In this chapter we present the ^{70}Zn(d,τ)^{69}Cu reaction in direct kinematics and the ^{72}Zn(d,τ)^{70}Cu reaction in inverse kinematics in an endeavour to probe the $Z = 28$ proton shell on either side of the $N = 40$ subshell gap. The first experiment is quite straightforward and fits neatly into the canon of classical nuclear physics. Putting to use the single-gap split-pole spectrometer at Orsay [IPN73], angular distributions and spectroscopic factors were extracted from a conventional DWBA analysis. Although the energy matching of the reaction was insufficient, the purpose of the measurement was to gauge the LNPS-m shell-model calculations to the fraction of the strength that we could collect at low energy in order to extrapolate it to the part that was missing at high energy.

The second experiment homing in on the ^{70}Zn(d,τ)^{69}Cu reaction in inverse kinematics answers to the current state of the art in transfer experiments with radioactive ion beams. In this respect two recent separate developments can be spotted. The first major challenge is contained in the push to heavier beams, where the identification of the outgoing ejectile among an increasing number of contaminants is more arduous. Secondly, one seeks to improve on the expected spectral resolution through coincidence measurements with emitted γ radiation. The drawback is the geometrical arrangement of particle and γ detectors, for which compromises are unavoidable. In our work, we have been acutely confronted with the first issue, aware to venture above $Z = 28$. As to the second matter, we have thought it prudent to optimise the efficiency of particle detection whilst foregoing any attempt at γ measurements. We have, how-

ever, opted for a target that was as thin as possible with the aim to reduce at best the energy straggling. In doing so, we have consciously traded statistics for resolution.

Heading to Ganil with these considerations in mind, a ^{76}Ge beam was accelerated to 61.0 MeV per nucleon and made to hit a rotating disk of beryllium. Among the reaction products that entered the Ligne d'Ions Super Epluchés, better known as the Lise spectrometer [Ann92], we selected the ^{72}Zn nuclei at an energy of 37.6 MeV per nucleon. Four Must-2 detectors, specifically developed for the identification of light particles emitted in transfer reactions in inverse kinematics [Pol05], were supplemented with thin single-sided strip detectors. Surrounding the deuterated polypropylene target, they recorded the angular distributions of the fleeting τ particles, from which the spectroscopic factors were determined.

The dynamics of the single-particle energies that underlie the structure of the copper isotopes are most often masked by the superposition of correlations, such as the interaction with the open neutron shell. For instance the late crossing of the $\pi p_{3/2}$ and $\pi f_{5/2}$ orbitals in the A3DA and LNPS-m interactions can be compensated for by introducing a sufficient amount of higher-order corrections till the experimental swapping of these states in ^{75}Cu is reproduced. In the same vein the strength centroids systematically shift away from the single-particle energies. The calculated $\pi p_{3/2}$ centroid is thus located at 1.6 MeV above the actual ground state in ^{69}Cu and moves up to 2.0 MeV in ^{71}Cu.

In order to reproduce the experimental portfolio, the $\pi f_{5/2}$ state is forcibly set at a fairly low energy. The centroid of the calculated $5/2^-$ states comes down from 3.7 MeV in ^{69}Cu to 1.9 MeV in ^{71}Cu so it dips below the $\pi p_{3/2}$ one, even if in ^{71}Cu the single-particle states obey the opposite ordering. Since the $\pi f_{5/2}$ centroid settles close to the ground state, the available number of states is limited and the nucleus is left with little choice than to concentrate most of the spectroscopic strength in the first excited level only. The $\pi f_{7/2}$ orbital on the other hand spreads out into many other states with a centroid at 4.9 MeV in ^{69}Cu, which the addition of the two neutrons in ^{71}Cu pulls down to 3.5 MeV.

Comparing the theoretical predictions from the LNPS-m model to our experimental results for ^{69}Cu and ^{71}Cu, the measured portion of the $\pi f_{7/2}$ transfer strength returns

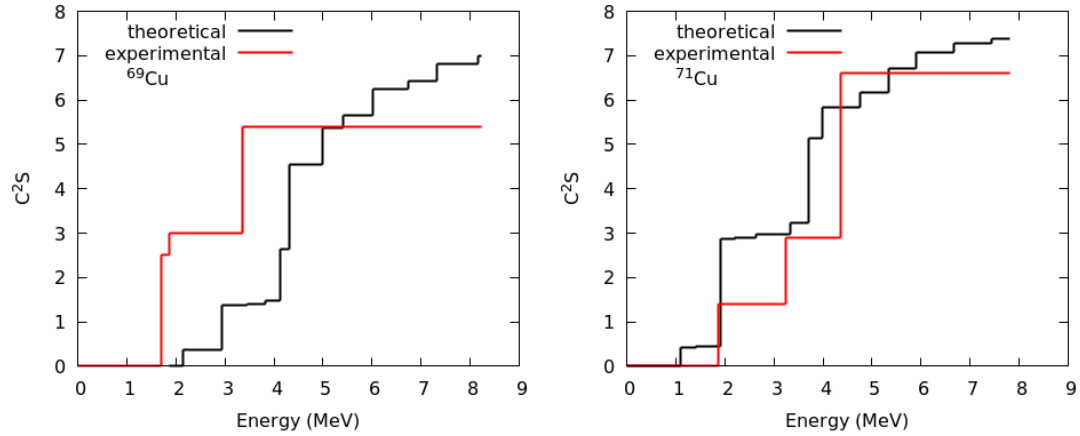

FIGURE 4.1: Cumulated experimental $\pi f_{7/2}$ spectroscopic strengths in proton pick-up towards ^{69}Cu (left) and ^{71}Cu (right) compared to calculations with the LNPS-m interaction. Data taken from [Mor15b, Mor16b]

us weighted averages that are situated at respectively 2.45 MeV and 3.76 MeV. While we are confident that we have measured most of the distribution in ^{71}Cu, this is not the case in ^{69}Cu. Striving to capture our performance in a single glance, we plot in figure 4.1 the cumulated strength as a function of excitation energy. In ^{69}Cu the theoretical $7/2^-$ states that carry the $\pi f_{7/2}$ force veer too high in energy, while the data remain insufficient to conclude on convergence. In ^{71}Cu we face the inverse behaviour, the calculated strength arriving earlier yet with a convergence that is quite satisfactory.

At the Fermi surface the $\pi f_{7/2}$ orbital is greeted by the $\pi p_{3/2}$ state, its reciprocal harbinger of quadrupole force. The theoretical high position of the transfer strength in ^{69}Cu could be explained if the calculations do not trigger the $\pi f_{7/2}$-$\pi p_{3/2}$ correlations sufficiently, neglecting to bring down the $\pi f_{7/2}^{-1}$ excitation. Also on the neutron side of things a problem might persist. If the $N = 40$ subshell gap is taken too rigid in ^{69}Cu, it would prove hard to excite neutrons across it and their interaction with the protons would be underestimated. The idea is reminiscent of the discussion of core polarisation in ^{70}Ni and indeed the calculations yield a somewhat better result for ^{71}Cu, where the neutron gap is weaker.

Wrapping up our discussion, the transfer experiments at Orsay and Ganil finally have brought us the evidence that the $\pi f_{7/2}$ hole strength lies at higher energies than the two $7/2^-$ levels that we had identified in the β decay at Lisol and the Coulomb

excitation at Isolde. From ^{69}Cu to ^{71}Cu its centroid moves by more than 1 MeV away from the Fermi surface deeper inside the nucleus, contrary to the simple tensor picture in which the $g_{9/2}$ neutrons tend to repel the orbital. The LNPS-m shell-model calculations reproduce our findings partially, although the strong fragmentation that accompanies its rise in energy warns us from drawing too stark a conclusion.

4.2 The articles

For the extensive discussion of the transfer experiments we refer to the doctoral thesis of Pierre Morfouace [Mor15a], while here we reproduce our two articles [Mor16b, Mor15b].

Single-particle strength in neutron-rich ^{69}Cu from the ^{70}Zn(d, ^{3}He)^{69}Cu proton pick-up reaction

P. Morfouace,[1] S. Franchoo,[1] K. Sieja,[2] I. Stefan,[1] N. de Séréville,[1] F. Hammache,[1] M. Assié,[1] F. Azaiez,[1] C. Borcea,[3] R. Borcea,[3] L. Grassi,[4] J. Guillot,[1] B. Le Crom,[1] L. Lefebvre,[1] I. Matea,[1] D. Mengoni,[5] D. Napoli,[6] C. Petrone,[3] M. Stanoiu,[3] D. Suzuki,[1] and D. Testov[1]

[1]*Institut de Physique Nucléaire et Université Paris-Sud, 91406 Orsay Cedex, France*
[2]*Université de Strasbourg, IPHC, CNRS, UMR7178, 67037 Strasbourg, France*
[3]*Institute of Atomic Physics, IFIN-HH, Bucharest-Mağurele, P.O. Box MG6, Romania*
[4]*Ruder Bošković Institute, Bijenička 54, 10000 Zagreb, Croatia*
[5]*Dipartimento di Fisica e Astronomia dell'Università and INFN, 35131 Padova, Italy*
[6]*INFN Laboratori Nazionali di Legnaro, 35020 Legnaro (Pd), Italy*

(Received 7 March 2016; published 7 June 2016)

We have performed the ^{70}Zn(d,^{3}He)^{69}Cu proton pick-up reaction in direct kinematics using a deuteron beam at 27 MeV. The outgoing ^{3}He particles were detected at the focal-plane detection system of an Enge split-pole spectrometer. The excitation-energy spectrum was reconstructed up to 7 MeV and spectroscopic factors were obtained after analysis of the angular distributions in the finite-range distorted-wave Born approximation. The results show three new angular distributions for which the $\pi f_{7/2}$ strength was measured and a lower limit of the centroid is established. State-of-the-art shell-model calculations are performed and predict a $\pi f_{7/2}$ strength that lies too high in energy in comparison to our experimental results.

DOI: 10.1103/PhysRevC.93.064308

I. INTRODUCTION

The development of the shell-model by Mayer, Haxel, Suess, and Jensen [1,2] in 1949 still accounts for much of our understanding in nuclear structure at low excitation energy. It gives a description of the observed shell gaps at nucleon number equal to one of the so-called magic numbers: 2, 8, 20, 28, 50, 82, and 126. It is of great interest nowadays to study the evolution of the single-particle states around shell closures when moving far from stability. The understanding of this evolution is crucial to constrain the nucleon-nucleon interaction and the nuclear models. It is well established that magic numbers evolve when one moves away from stability [3]. One can wonder about the evolution of the $Z = 28$ proton gap in neutron-rich isotope toward the key nucleus ^{78}Ni and especially between $N = 40$ and $N = 50$ with the filling of the $\nu g_{9/2}$ orbital. Very recently experimental results indicated a doubly magic ^{78}Ni by studying β-decay half-lives in its vicinity [4]. However it seems important to understand well the evolution of the $Z = 28$ proton gap that corresponds to the energy difference between the $\pi f_{7/2}$ orbital and the $\pi p_{3/2}$ or $\pi f_{5/2}$ orbitals. The behaviors of those orbitals will give a constraint on the πf-$\nu g_{9/2}$ proton-neutron interaction and it will allow us to test the strength of the tensor interaction and determine the spin-orbit splitting in this region. But to be able to constrain the gap evolution between $N = 40$ and $N = 50$, one needs to first determine the shell gap at $N = 40$, or the energy spacing between the $\pi f_{7/2}$ and the $\pi p_{3/2}$ orbital.

To probe the proton gap, the neutron-rich Cu isotopes are good candidates since they are composed of one proton outside a nickel core. In this article we propose to determine the proton gap in ^{69}Cu at $N = 40$. Indeed this isotope is a crucial starting point to see the evolution of the orbitals in more neutron-rich copper isotopes. Moreover the $N = 40$ region gives rise to a lot of experiments and theoretical work where the existence of a subshell was acknowledged [5]. More recently the unexpected small experimental $B(E2; 0^+_1 \rightarrow 2^+_1)$ value was interpreted as an erosion of $N = 40$ and shows the importance of the proton core excitations in the ^{68}Ni nucleus [6,7]. Many investigations have been performed since, revealing a third 0^+ state at 2511 keV [8] while the second 0^+ state was readjusted at 1604 keV [9], this value is consistent with more recent studies [10,11]. This leads to a richer interpretation in a shell model-model approach and in a Monte Carlo shell model (MCSM) of a shape coexistence in ^{68}Ni with a spherical ground state 0^+_1 and two deformed states: a 0^+_2 oblate and 0^+_3 prolate one [12,13].

It is known from the β decay of the neutron-rich Ni isotopes that the first $5/2^-$ excited state in ^{63,65,67,69}Cu remains between 1 and 1.2 MeV while it drops very rapidly at 534 keV in ^{71}Cu and 166 keV in ^{73}Cu [14]. The sudden energy shift arises above $N = 40$ with the filling of neutrons in the $\nu g_{9/2}$ orbital. A spin inversion between $3/2^-$ and $5/2^-$ was even observed in ^{75}Cu for the ground state [15]. From the Coulomb excitation of neutron-rich Cu isotopes we also see a strong reduction of the $B(E2)$ value for the transition to the $3/2^-$ ground state ($5/2^- \rightarrow 3/2^-_{\text{g.s.}}$) in ^{69,71,73}Cu around 3.0 to 4.4 W.u. while it has a value between 16 and 12.5 W.u. for ^{63,65,67}Cu. The low value of $B(E2)$ indicates a single-particle character of the $5/2^-$ states from $N = 40$ to at least $N = 44$ and one can link its energy shift to the position of the $\pi f_{5/2}$ orbital going down when adding a neutron in the $\nu g_{9/2}$ orbital. This suggests a strong attractive $\pi f_{5/2}$-$\nu g_{9/2}$ interaction. With all those experimental observations, one can naturally wonder about the behavior of the $\pi f_{7/2}$ spin-orbit partner.

In the present work we extract the spectroscopic factors of the $7/2^-$ levels in ^{69}Cu with the aim to obtain the $\pi f_{7/2}$ strength function at $N = 40$ and serve as a reference for the other more exotic Cu isotopes. We choose to do so using the ^{70}Zn(d,^{3}He)^{69}Cu proton pick-up reaction, which gives precisely access to the proton-hole states in ^{69}Cu. This reaction was already performed by Zeidman and Nolen

using a deuteron beam of 23.3 MeV [16]. In that experiment angular distributions were obtained for five peaks: the $3/2^-$ ground state, $1/2^-$ at 1.11 MeV, $5/2^-$ at 1.23 and two $7/2^-$ states at 1.74 and 1.87 MeV, respectively. The $5/2^-$ state shows a surprisingly high spectroscopic factor ($C^2S = 1.5$) and is larger than in ^{63,65,67}Cu, therefore the authors assume a probable $5/2^-$,$7/2^-$ doublet near 1.23 MeV. The sum of spectroscopic factors in the p-$f_{5/2}$ orbitals gives 3.36 while one expects naively only two protons in those orbitals in Zn isotopes. The sum of the $7/2^-$ gives a total of 3.15 protons that represents only 39.3% of the $\pi f_{7/2}$ strength. If one assumes a doublet at 1.23 MeV where a $5/2^-$ exhibits a spectroscopic factor of the order of 0.5 like in the other Cu isotopes, then the number of protons in the p-$f_{5/2}$ orbitals sums to 2.36, this is closer to the value we expect. Moreover the low-lying ^{69}Cu states were also populated from the $(\vec{t},\alpha)$ experiment using a polarized triton beam of 17 MeV [17]. Because of the polarized triton one should be able to differentiate between a $5/2^-$ and $7/2^-$ state since the analyzing power A_y has a completely different shape for two different spins. For the peak at 1.21 MeV, a $L = 3$ state is clearly assigned but the experimental A_y is not reproduced either by the $5/2^-$ or $7/2^-$ distribution. They conclude that it corresponds to two unresolved states and give a spectroscopic factor of 1.2 that corresponds to a $5/2^-$ state at this energy. Concerning the other states, they are in fair agreement with Zeidman and Nolen. The only strong difference is the value of the spectroscopic factor for the $7/2^-$ state at 1.71 MeV, which differs from 33% between these two experiments. Concerning states around 1.21 MeV from more recent works, a $5/2^-$ state was seen at 1.214 MeV and a $3/2^-$ state at 1.298 MeV from β decay [14] but no other state that could correspond to a $7/2^-$ level was observed.

In order to well establish the centroid of the $\pi f_{7/2}$ strength distribution it seems necessary to measure the complementary $7/2^-$ states at higher excitation energy by extracting the spectroscopic factor of every fragment. In several recent papers it has been pointed out that spectroscopic factors are not true observables [18,19]. Nevertheless it was shown that in a set of coherent parametrization, spectroscopic factors provide a valuable and consistent information on the nuclear structure [20,21]. In this article, we aim to use a set of a coherent parametrization to define the $\pi f_{7/2}$ centroid in ^{69}Cu at $N = 40$. It serves as reference for more exotic Cu isotopes [22] in order to establish the behavior of the $\pi f_{7/2}$ strength with the adding of neutrons in the $\nu g_{9/2}$ orbital. Moreover because of the $N = 40$ subshell gap, the correlations are minimized in ^{69}Cu, thus this nucleus is an essential test for shell-model calculation in order to constrain the position of single-particle orbitals (or proton-neutron monopole interaction).

II. EXPERIMENT

The ^{70}Zn$(d,^3$He$)^{69}$Cu reaction was studied at the Alto facility at Orsay, France. A deuteron beam of about 200 nA was produced by the duoplasmatron ion source and accelerated by the 15 MV tandem to an energy of 27 MeV. The beam was transported to the target located at the object focal point of an Enge split-pole magnetic spectrometer [24]. An enriched ^{70}Zn target with a thickness of 18.7(9) μg/cm^2 on a backing

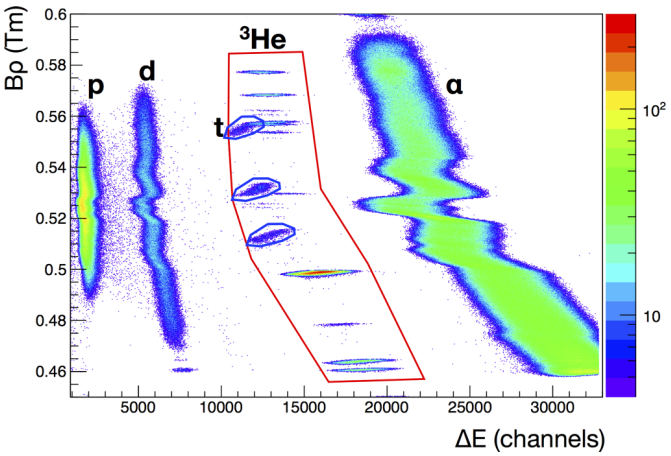

FIG. 1. Particle identification spectrum (magnetic rigidity versus energy loss) obtained with the focal-plane detector. The red contour indicates the $A = 3$ particles. All horizontal lines inside the red contour correspond to ^{3}He. The groups circled in blue correspond to tritons.

of carbon was used. The target thickness was determined through the Rutherford backscattering of α particles at the CSNSM, Orsay, France. With this method we could achieve an accuracy of 5% for the target thickness. The light charged particles from the reaction entered the split-pole spectrometer through a rectangular aperture covering a 1.16 msr solid angle, and were momentum analyzed and focused on the focal-plane detection system [25] as it is described in Ref. [26]. It consists of a 50 cm long position-sensitive proportional counter that gives the position of the particle, which is proportional to the magnetic rigidity $B\rho$. The position information is given by the time difference between the two sides of the delay line. A second detector is a proportional gas counter that provides a ΔE that corresponds to the energy loss in the gas. The gas used in the detector is isobutane at a pressure of 300 mbar. Finally, behind the position detector, there is a plastic scintillator measuring the residual energy of the particle. The active area of this plastic is smaller than the position detector reducing he achievable range of excitation energy for the residual nucleus. That is why, no condition on the plastic is applied in order not to reduce the excitation energy area. Particle identification was achieved through energy loss versus magnetic rigidity measurement as one can see in Fig. 1. The different masses are well identified, although with this method the triton and the ^{3}He are not well separated. Nevertheless the position of the focal-plane detection system was set up for our $(d,^3$He$)$ reaction of interest while the (d,t) reaction has a very different kinematics: the slope of the (d,t) reaction is much larger than the $(d,^3$He$)$ one. That is why the triton peaks are broad and their contribution will be easily identified in the final spectrum. Moreover the tritons we detect correspond only to the ^{12}C$(d,t)^{11}$C reaction that populates states in ^{11}C around 8 MeV of excitation energy.

After selection, the excitation-energy spectrum of ^{69}Cu was obtained. Angular distribution measurements were performed at spectrometer angles of $6°$,$9°$,$12°$,$15°$,$18°$,$21°$, and $24°$. The elastic scattering measurement was done at two other

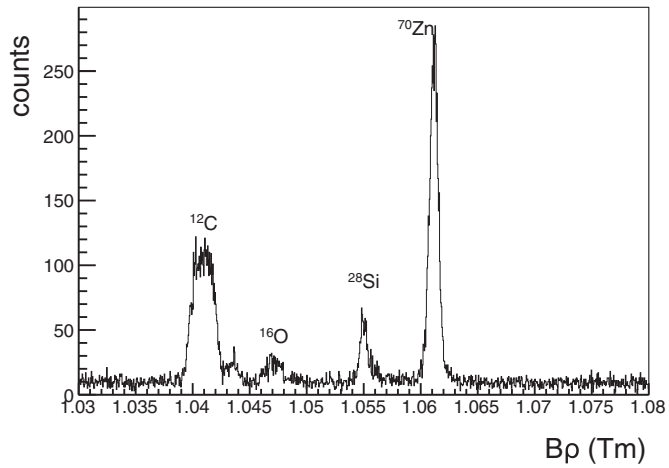

FIG. 2. Measured magnetic rigidity $B\rho$ for the elastic scattering of the deuteron on the target at $\theta_{\rm lab} = 40^\circ$.

angles of 30° and 40°. For each angle the position of the focal-plane detection system was adjusted to take into account the kinematic displacement and to have the final resolution as good as possible. With a unique setting of the magnetic field we measured the excitation-energy spectrum of ^{69}Cu up to 7 MeV with an average resolution for the excited states of $\sigma = 18(2)$ keV. Finally in order to measure the incident deuteron beam intensity we have used a Faraday cup at zero degree, which was performed with one current integrator.

III. DATA ANALYSIS AND RESULTS

A. Excitation-energy spectrum and peak identification

To quantify all the elements present in the target, elastic scattering at a large angle of 40° was measured in order to well spread the different elements. Besides ^{70}Zn and ^{12}C, the elastic scattering shows clearly the presence of ^{28}Si and ^{16}O as one can see in Fig. 2 where the magnetic rigidity of the scattered deuteron is displayed. The different peaks confirm the presence of different elements in the target. One can note that the resolution is degrading from zinc to carbon. This is due to the different slopes of the kinematic lines and in this run the kinematic displacement was adjusted for the ^{70}Zn(d,d) reaction. A $B\rho$ calibration of the focal-plane detector was performed using the elastic scattering with the different elements present in the target: ^{70}Zn, ^{28}Si, ^{16}O, and ^{12}C. The ground state of ^{11}B strongly populated from the well known ^{12}C$(d,^3$He$)^{11}$B reaction was also chosen for the calibration, in which the energy loss in the target was taken into account.

The $(d,^3$He) pick-up reaction with all the elements will populate discrete states in our excitation-energy window that one has to carefully identify in the final spectrum. As mentioned earlier, tritons and ^{3}He are not well separated, that is why the (d,t) reaction will also be a contamination in our spectrum. Nevertheless in our set of magnetic field, only the ^{12}C$(d,t)^{11}$C will populate discrete state in our spectrum and because of the very different kinematics they are easily identified as one can see in Fig. 3 where the excitation-energy spectrum of ^{69}Cu at $\theta_{\rm lab} = 21^\circ$ is shown. The other (d,t) reactions are situated in the continuum and can give a continuum flat background.

In Fig. 3, one can see that eight states have been populated and identified in ^{69}Cu at an energy of 0, 1.11, 1.23, 1.71, 1.87, 3.35, 3.70, and 3.94 MeV. For each of these peaks a Gaussian plus linear background fit was performed to determine the integral peak by peak at each angle to deduce the angular distributions. For all of these peaks, an average width of $\sigma = 18(2)$ keV is obtained and no peak are broader. From this work there is no evidence of a broader peak at 1.23 MeV so it seems that there is no doublet as it was suggested by previous works [16,17].

B. Angular distributions

In order to constrain the input parameters for the DWBA calculation but also to check the normalization procedure, the elastic scattering at eight different angles was measured. At each measured angle, the elastic peak was integrated and a careful normalization was performed by taking into account

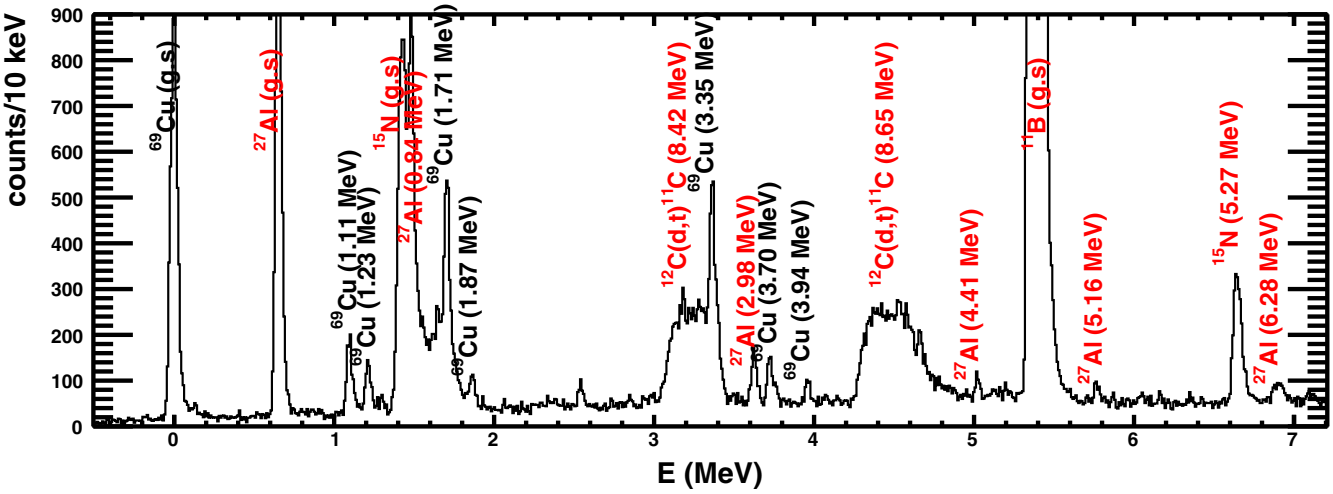

FIG. 3. Reconstructed excitation-energy spectrum of ^{69}Cu at $\theta_{\rm lab} = 21^\circ$ from the ^{70}Zn$(d,^3$He$)^{69}$Cu kinematics after gating on the $A = 3$ light charged particles.

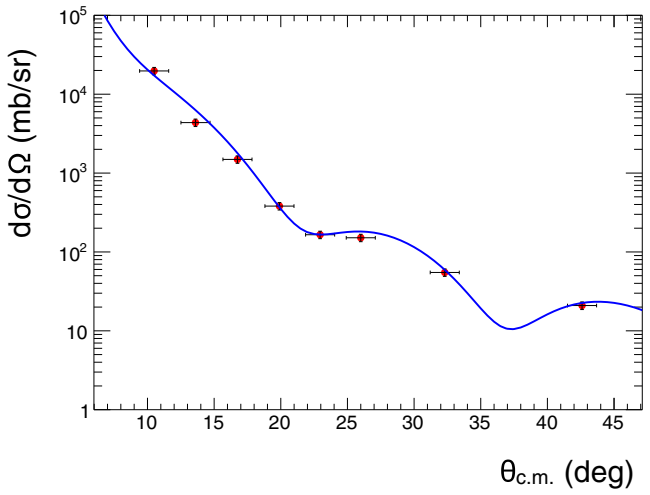

FIG. 4. Angular distribution of the elastic scattering for ^{70}Zn (red points) with the calculation where the Daehnick-F optical potential was used [28] (blue line).

the accumulated charges (beam intensity multiplied by the duration of the run), the target thickness, the aperture of the spectrometer and the Jacobian of the reaction for each excited states. In Fig. 4, the angular distribution of the elastic scattering is displayed together with the calculation. We have a good agreement between the experimental points and the calculation where the Daehnick-F optical potential was used [28], no scaling of the data has been done on top of the normalization, giving confidence in the normalization and in the input parameters used for the DWBA calculation as well. The Daehnick-L potential has been used for comparison in our previous study about ^{71}Cu [22], however this potential was not able to reproduce the data while the Daehnick-F reproduces well the elastic scattering (see Fig. 5 in Ref. [23]). To be consistent with our previous study, we decided to use the same optical potential for the ^{69}Cu case where we also observe a very good agreement between the experimental data and the calculation.

The same procedure was followed to extract the angular distributions for the populated states in ^{69}Cu. In a first step the distorted-wave Born approximation (DWBA) calculations were made in a similar way to those in Ref. [16] using the zero-range framework with the DWUCK-4 code [27] and the same bound-state parameters as in that paper ($r_0 = 1.20$ fm and $a_0 = 0.70$ fm), in such a way that direct comparisons could be made. For the incoming channel, the Daehnick-F optical potential was used [28], which reproduces well the angular distribution of the elastic scattering. For the outgoing channel, we used the Perey and Perey parametrization [29]. The second set of calculations were identical to the first, except that we adopted the commonly used bound-state parameters ($r_0 = 1.25$ fm and $a_0 = 0.65$). Finally a third set of calculations was performed in a finite-range framework using the DWUCK-5 finite-range code [30] and we used the Brida potential for the overlap between the deuteron and the ^{3}He particle [31]. In Fig. 5 we display the experimental angular distributions together with the DWBA calculations. The results of these calculations are listed in Table I. The errors given for our work correspond to the statistical ones.

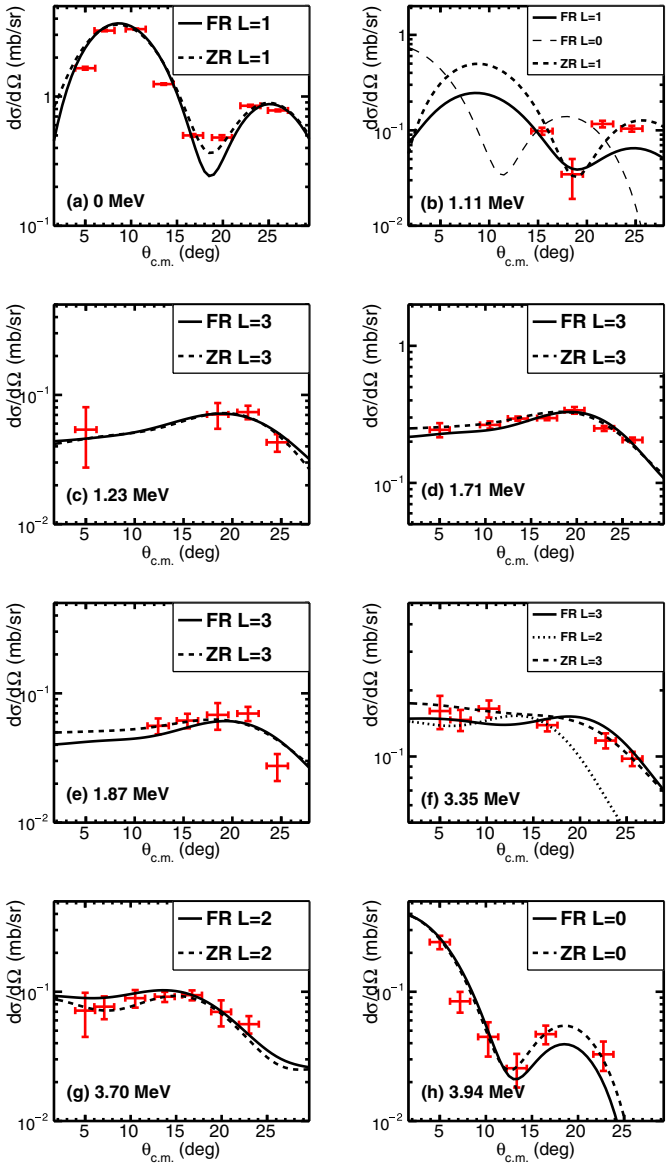

FIG. 5. Angular distributions of the states at 0 MeV (a), 1.11 MeV (b), 1.23 MeV (c), 1.71 MeV (d), 1.87 MeV (e), 3.35 MeV (f), 3.70 MeV (g), and 3.94 MeV (h). Both zero-range and finite-range calculations are shown.

As one can see in the first part of Table I where we use $r_0 = 1.20$ and $a_0 = 0.70$ fm and the zero-range DWBA calculation, our results are in fair agreement (within 25%) with the ones of Ref. [16] for the $3/2^-$ ground state and for the two $7/2^-$ excited states at 1.71 and 1.87 MeV. Our reported values are closer to the one from Ref. [16], except for the state at 1.87 MeV where the value is closer to Ref. [17]. For the $5/2^-$ state at 1.23 MeV we have a discrepancy of 40% between our values and the one from Ref. [16]. In this work we obtain a smaller value for the spectroscopic factor and the peak is as broad as the other one. This suggests that there is no doublet and that there is only one state located at 1.23 MeV, which is consistent from the β-decay experiment [14] where no other γ transition was observed around this energy. For the state at 1.11 MeV the contamination was very important for most of

TABLE I. Position in energy of the different populated states in ^{69}Cu, the transferred angular momentum L, the spin-parity J^π (parenthesis means tentative assignment from this work), and the associated spectroscopic factor C^2S for different values of r_0 and a_0. ZR stands for zero-range DWBA calculation while FR stands for finite-range calculation. In Refs. [16,17] the calculations are done using the zero-range approximation.

E (MeV)	$r_0 = 1.20$ fm, $a_0 = 0.70$ fm				$C^2S(ZR)$ (This work)	$r_0 = 1.25$ fm, $a_0 = 0.65$ fm	
	L	J^π	C^2S [16]	C^2S [17]		$C^2S(ZR)$ (This work)	$C^2S(FR)$ (This work)
0	1	$3/2^-$	1.3	1.03	1.60(11)	1.40(15)	1.50(17)
1.11	1	$1/2^-$	0.46	0.41	–	–	0.35(11)[a]
1.23	3	$5/2^-$	1.5	1.2	0.90(13)	0.80(11)	0.70(10)
1.71	3	$7/2^-$	2.7	1.8	2.70(10)	2.00(11)	2.50(14)
1.87	3	$7/2^-$	0.45	0.5	0.55(12)	0.40(10)	0.50(10)
3.35	3	$(7/2^-)$	–	–	2.00(8)	1.60(10)	2.40(15)
3.70	2	$(3/2^+)$	–	–	2.60(21)	1.90(25)	1.50(20)
3.94	0	$(1/2^+)$	–	–	0.80(6)	0.70(06)	0.70(10)

[a]Only four angles were used for the angular distribution, see text for more details.

the angles and the integration of this peak was possible only for $\theta_{\text{lab}} = 15$, 18, 21, and 24°. The L assignment for this state is therefore difficult to make. If we refer to previous work [16,17] a spin assignment of $1/2^-$, hence $L = 1$, was given with a spectroscopic factor of 0.46 and 0.41, respectively. As one can see in Fig. 5(b) the angular distribution of this state in our present work can be fitted with a $L = 1$ distribution. Assuming a $L = 1$ distribution, the finite-range DWBA calculation gives a spectroscopic factor of $C^2S = 0.35(11)$, which is compatible with previous work.

Even though the authors in Ref. [16] mention other states at higher excitation energy, the highest excitation energy for which angular distribution is given is 1.87 MeV. We report here three new angular distributions for the states at 3.35, 3.70, and 3.94 MeV as one can see in Fig. 5. The states at 3.70 MeV and 3.94 MeV exhibit a $L = 2$ and a $L = 0$ distribution, respectively, that probably comes from the inner sd shell of the nucleus. Concerning the state at 3.35 MeV, it corresponds to a $L = 3$ distribution for which we extract a spectroscopic factor of 2.40(15) in the finite-range calculation.

It is interesting to note that when looking at the result of the finite-range calculation, the $pf_{5/2}$ orbitals have a sum of 2.20(20) protons if we do not take into account our result for the $1/2^-$ state at 1.23 MeV. We get 2.55(23) if we take into account a spectroscopic factor of 0.35(11) for the $1/2^-$ state. The last result is quite large since one expects only two protons above the $\pi f_{7/2}$ orbital. In the case that 0.55 particles from the $\pi f_{7/2}$ orbital are situated in the $pf_{5/2}$ orbitals, we do not expect eight protons anymore in this $\pi f_{7/2}$ orbital but 7.45. Concerning the $7/2^-$ states, the sum of the spectroscopic factors gives 5.40 and the centroid of the $\pi f_{7/2}$ strength is

$$E(f_{7/2}) = \sum \frac{C^2S(7/2^-)E(7/2^-)}{C^2S(7/2^-)} = 2.45 \text{ MeV}. \quad (1)$$

This centroid corresponds to a lower limit since a part of the strength remains undetected. We have extracted only 5.40 over 8, which corresponds to 67% of the strength. As aforementioned, if one expects only 7.45, then it corresponds to 72% of the strength. We miss a part of the strength that must lie at higher excitation energy. Indeed the matching of the reaction was not sufficient in this experiment to populate $L = 3$ states at high energy. Figure 6 shows the evolution of the matching for the $(d,{}^3\text{He})$ reaction as a function of the total kinetic energy of the deuteron beam. The matching for the ground state with a 27 MeV deuteron beam is $0.76\hbar$. A deuteron beam around 75 to 90 MeV is indeed well matched for $L = 3$. The cross section for a $L = 3$ state calculated with Dwuck-5 drops very rapidly with the excitation energy in our case. It explains why we do not see other states above 4 MeV. In our experiment, considering the flat background in the spectrum (cf Fig. 3), we have determined that at least 130 counts are needed in a peak to be detected with a confidence level of 95%. We have translated this number of counts to a spectroscopic factor for a given excitation energy (cf Fig. 7). We can then define two different zones: the first one above the line corresponds to the detectable zone in our experiment while

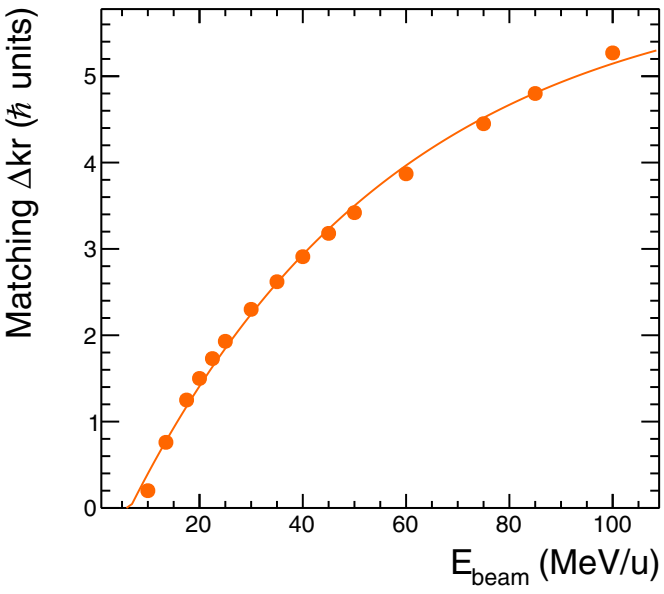

FIG. 6. Matching Δkr of the reaction to the ground state as a function of the total kinetic energy of the deuteron beam. The line corresponds to an exponential fit of the points.

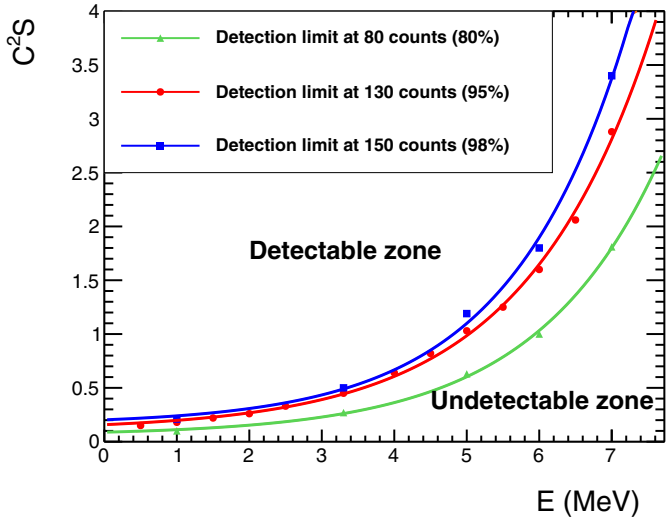

FIG. 7. Limit of spectroscopic factor as a function of the excitation energy. Two zones are defined: the detectable zone above the line and the undetectable one below the line.

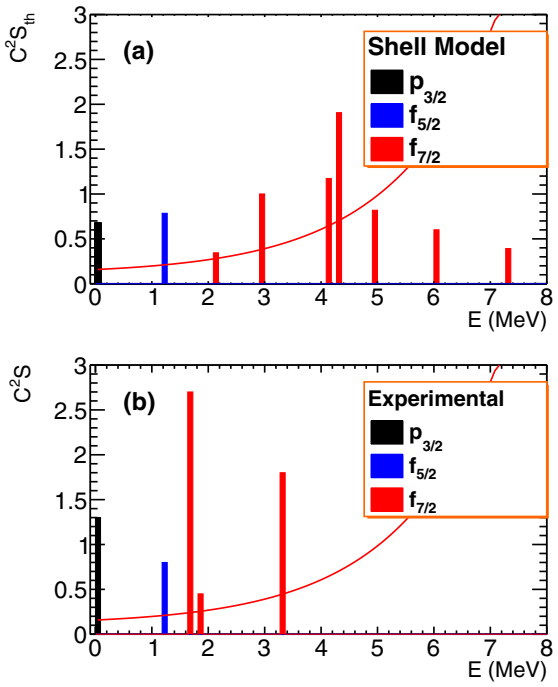

FIG. 8. States calculated from shell-model calculation with $C^2S_{th} > 0.3$ (a) compared to experimental data (b). The x axis represents the energy position of the states while the y axis shows the associated spectroscopic factor. The red line corresponds to the frontier between the detectable zone and the undetectable zone from Fig. 7. Peaks below this line cannot be measured in this experiment.

the second one, below the line, corresponds to the undetectable zone. For instance, it means that if there was a $L = 3$ state at 5 MeV, the associated spectroscopic factor is necessarily lower than 1 because we did not see any peak at this energy in our experiment. The undetectable zone grows exponentially with the excitation energy. This is so because the cross section to populate a $L = 3$ state decreases exponentially as a function of the excitation energy. In this experiment, since we did not detect all of the strength we can only give a lower limit for the energy centroid.

It appears clearly that the population of $L = 3$ state in a neutron-rich region around nickel isotopes using a $(d,{}^3\mathrm{He})$ pick-up reaction where the Q values are very negative (-5.62 MeV in this case), needs to be performed around 40 MeV/u to be well matched and extract the maximum of the strength.

C. Shell-model calculation

Shell-model calculations within the $fpgd$ valence space and enacting the LNPS Hamiltonian [32] with further modifications to assure a proper evolution of the proton gap ($Z = 28$) between ^{68}Ni and ^{78}Ni [33] were carried out. The same Hamiltonian was used in our earlier study on ^{71}Cu [22] and in recent work on $^{69-73}$Cu [34]. Due to the large size of the configuration space, the calculations were truncated to $9p$-$9h$ across $Z = 28$ and $N = 40$. As one can see in Fig. 8, the calculation reproduces the $3/2^-$ as a ground state, however there is a factor of two difference in C^2S between the shell-model calculation and the extracted one using the finite-range DWBA calculation. The spectroscopic factor of the first $5/2^-$ excited state calculated at 1.25 MeV is satisfactorily reproduced while the main $7/2^-$ fragments are shifted up more than 1 MeV between the calculation and the experimental data.

In addition to the strength functions, calculations to determine the composition of the first low-lying states were performed using the NATHAN code (see Table II). According to the shell-model calculation, the $3/2^-$ ground state corresponds largely to a single proton in the $p_{3/2}$ orbital. The dominant part of the $5/2^-$ state corresponds to a single proton in the $\pi f_{5/2}$ and is adequately located. The first $7/2^-$ state calculated at 1.86 MeV has a large part coming from the coupling $|2^+_\nu \otimes \pi p_{3/2}\rangle$ and has a large transition strength to the ground state of $B(E2) = 46\ e^2\mathrm{fm}^4$. However this state has a very low calculated spectroscopic factor and is not visible in Fig. 8. This state is remarkably close to the experimental level at 1.87 MeV where a strong $E2$ transition to the ground state has been observed with a measured $B(E2) = 77(12)\ e^2\mathrm{fm}^4$ [35]. The

TABLE II. Dominating components of the wave functions for the lowest calculated states in ^{69}Cu.

Energy (MeV)	J^π	Percentage	Composition
0	$3/2^-$	93%	$\|0^+_\nu \otimes \pi p_{3/2}\rangle$
1.25	$5/2^-$	37%	$\|0^+_\nu \otimes \pi f_{5/2}\rangle$
		20%	$\|2^+_\nu \otimes \pi p_{3/2}\rangle$
		16%	$\|2^+_\nu \otimes \pi f_{5/2}\rangle$
1.86	$7/2^-$	40%	$\|2^+_\nu \otimes \pi p_{3/2}\rangle$
		22%	$\|4^+_\nu \otimes \pi p_{3/2}\rangle$
		12%	$\|J^+_\nu \otimes \pi f^{-1}_{7/2}\rangle$
2.18	$7/2^-$	52%	$\|2^+_\nu \otimes \pi f_{5/2}\rangle$
		14%	$\|4^+_\nu \otimes \pi f_{5/2}\rangle$
		16%	$\|J^+_\nu \otimes \pi f^{-1}_{7/2}\rangle$

second calculated $7/2^-$ state at 2.18 MeV corresponds also to a coupling in particular with $\pi f_{5/2}$ but has a very low $B(E2)$ value (0.05 $e^2\text{fm}^4$) because the overlap with the $\pi p_{3/2}$ wave function of the ground state is small. Moreover, this state has a small calculated spectroscopic factor (0.34) and therefore does not match with the experimental level at 1.71 MeV. The first calculated $7/2^-$ state with large C^2S arises at 2.93 MeV and is situated 1.2 MeV above the 1.71 MeV experimental level. One should however note that the proton gap calculated in the shell model is 6.1 MeV on the monopole level and is reduced to 5.8 MeV when correlations are added. These values are in a good agreement with the experimental value extracted from masses (5.9 MeV) [36]. In addition, in the neighboring ^{71}Cu nucleus the position of the $f_{7/2}$ centroid seems to be well reproduced in the present shell model [22]. The correlation mechanism that could bring down the $f_{7/2}$ strength at $N = 40$ in the calculations is thus not understood. Interestingly, a similar problem has been encountered in the calculations for the $d_{5/2}$ strength in ^{67}Ni [37]. Thus, the fact that the $\pi f_{7/2}$ orbital is lower that the prediction implies that it should favor quadrupole collectivity between the $f_{7/2}$-$p_{3/2}$ proton orbitals. More investigations have to be performed in the future to pin down the single-particle strength in this neutron-rich region.

IV. CONCLUSION

The ^{70}Zn$(d,^3$He$)^{69}$Cu transfer reaction was performed in direct kinematics and states up to excitation energies of 4 MeV were populated. From this work, there is no evidence of a doublet in the peak at 1.23 MeV, three new angular distributions have been measured, and spectroscopic factors were determined from comparison with finite-range DWBA calculations. Due to the poor matching of the reaction the higher-lying part of the $\pi f_{7/2}$ strength was not measured and a lower limit on the centroid of the strength is established at 2.45 MeV. A state-of-the-art shell-model calculation was performed and reproduces the $3/2^-$ and $5/2^-$ states but localizes the main fragments of the $7/2^-$ strength too high in energy.

ACKNOWLEDGMENTS

The continuous support of the staff of the Alto facility as well as the target laboratory staff as well as the CSNSM is gratefully acknowledged as well as the Romanian National Authority for Scientific Research, CNCS-UEFISCDI, Project No. PN-II-ID-PCE-2011-3-0487.

[1] M. Goeppert-Mayer, Phys. Rev. **75**, 1969 (1949).
[2] O. Haxel, J. H. D. Jensen, and H. E. Suess, Phys. Rev. **75**, 1766 (1949).
[3] O. Sorlin and M.-G. Porquet, Prog. Part. Nucl. Phys. **61**, 602 (2008).
[4] Z. Y. Xu *et al.*, Phys. Rev. Lett. **113**, 032505 (2014).
[5] M. Bernas, P. Dessagne, M. Langevin, J. Payet, F. Pougheon, and P. Roussel, Phys. Lett. B **113**, 279 (1982).
[6] O. Sorlin *et al.*, Phys. Rev. Lett. **88**, 092501 (2002).
[7] K. Langanke, J. Terasaki, F. Nowacki, D. J. Dean, and W. Nazarewicz, Phys. Rev. C **67**, 044314 (2003).
[8] W. F. Mueller *et al.*, Phys. Rev. C **61**, 054308 (2000).
[9] F. Recchia *et al.*, Phys. Rev. C **88**, 041302(R) (2013).
[10] F. Flavigny *et al.*, Phys. Rev. C **91**, 034310 (2015).
[11] S. Suchyta, S. N. Liddick, Y. Tsunoda, T. Otsuka, M. B. Bennett, A. Chemey, M. Honma, N. Larson, C. J. Prokop, S. J. Quinn, N. Shimizu, A. Simon, A. Spyrou, V. Tripathi, Y. Utsuno, and J. M. VonMoss, Phys. Rev. C **89**, 021301(R) (2014).
[12] A. Dijon *et al.*, Phys. Rev. C **85**, 031301(R) (2012).
[13] Y. Tsunoda, T. Otsuka, N. Shimizu, M. Honma, and Y. Utsuno, Phys. Rev. C **89**, 031301(R) (2014).
[14] S. Franchoo, M. Huyse, K. Kruglov, Y. Kudryavtsev, W. F. Mueller, R. Raabe, I. Reusen, P. VanDuppen, J. VanRoosbroeck, L. Vermeeren, A. Wohr, K. L. Kratz, B. Pfeiffer, and W. B. Walters, Phys. Rev. Lett. **81**, 3100 (1998).
[15] K. T. Flanagan *et al.*, Phys. Rev. Lett. **103**, 142501 (2009).
[16] B. Zeidman and J. A. Nolen, Phys. Rev. C **18**, 2122 (1978).
[17] F. Ajzenberg-Selove *et al.*, Phys. Rev. C **24**, 1762 (1981).
[18] R. J. Furnstahl and H.-W. Hammer, Phys. Lett. B **531**, 203 (2002).
[19] T. Duguet and G. Hagen, Phys. Rev. C **85**, 034330 (2012).
[20] J. P. Schiffer, C. R. Hoffman, B. P. Kay, J. A. Clark, C. M. Deibel, S. J. Freeman, A. M. Howard, A. J. Mitchell, P. D. Parker, D. K. Sharp, and J. S. Thomas, Phys. Rev. Lett. **108**, 022501 (2012).
[21] M. B. Tsang, J. Lee, and W. G. Lynch, Phys. Rev. Lett. **95**, 222501 (2005).
[22] P. Morfouace *et al.*, Phys. Lett. B **751**, 306 (2015).
[23] A. Matta *et al.*, J. Phys. G: Nucl. Part. Phys. **43**, 045113 (2016).
[24] J. E. Spencer and J. Sherman, Nucl. Instrum. Methods **49**, 181 (1967).
[25] R. G. Markham and R. G. Robertson, Nucl. Instrum. Methods **129**, 131 (1975).
[26] S. Benamara, N. deSereville, A. M. Laird, F. Hammache, I. Stefan, P. Roussel, S. Ancelin, M. Assie, A. Coc, I. Deloncle, S. P. Fox, J. Kiener, L. Lefebvre, A. Lefebvre-Schuhl, G. Mavilla, P. Morfouace, A. M. Sanchez-Benitez, L. Perrot, M. Sinha, V. Tatischeff, and M. Vandebrouck, Phys. Rev. C **89**, 065805 (2014).
[27] P. D. Kunz, computer code DWUCK4, University of Colorado (unpublished).
[28] W. W. Daehnick, J. D. Childs, and Z. Vrcelj, Phys. Rev. C **21**, 2253 (1980).
[29] C. Perey and F. Perey, At. Data Nucl. Data Tables **17**, 1 (1976).
[30] P. D. Kunz, computer code DWUCK5, University of Colorado (unpublished).
[31] I. Brida, S. C. Pieper, and R. B. Wiringa, Phys. Rev. C **84**, 024319 (2011).
[32] S. M. Lenzi, F. Nowacki, A. Poves, and K. Sieja, Phys. Rev. C **82**, 054301 (2010).
[33] K. Sieja and F. Nowacki, Phys. Rev. C **85**, 051301(R) (2012).
[34] E. Sahin *et al.*, Phys. Rev. C **91**, 034302 (2015).
[35] I. Stefanescu *et al.*, Phys. Rev. Lett. **100**, 112502 (2008).
[36] M. Wang, G. Audi, A. H. Wapstra, F. G. Kondev, M. MacCormick, X. Xu, and B. Pfeiffer, Chin. Phys. C **36**, 1603 (2012).
[37] J. Diriken *et al.*, Phys. Lett. B **736**, 533 (2014).

Physics Letters B 751 (2015) 306–310

Contents lists available at ScienceDirect

Physics Letters B

www.elsevier.com/locate/physletb

Evolution of single-particle strength in neutron-rich ^{71}Cu

P. Morfouace [a,*], S. Franchoo [a], K. Sieja [b], I. Matea [a], L. Nalpas [c], M. Niikura [a], A.M. Sánchez-Benítez [d], I. Stefan [a], M. Assié [a], F. Azaiez [a], D. Beaumel [a], S. Boissinot [c], C. Borcea [e], R. Borcea [e], G. Burgunder [f], L. Cáceres [f], N. De Séréville [a], Zs. Dombrádi [g], J. Elseviers [h], B. Fernández-Domínguez [i], A. Gillibert [c], S. Giron [a], S. Grévy [j], F. Hammache [a], O. Kamalou [f], V. Lapoux [c], L. Lefebvre [a], A. Lepailleur [f], C. Louchart [c], G. Marquinez-Duran [d], I. Martel [d], A. Matta [a], D. Mengoni [k], D.R. Napoli [l], F. Recchia [k], J.-A. Scarpaci [a], D. Sohler [g], O. Sorlin [f], M. Stanoiu [e], C. Stodel [f], J.-C. Thomas [f], Zs. Vajta [g]

[a] Institut de Physique Nucléaire et Université Paris-Sud, 91406 Orsay Cedex, France
[b] Université de Strasbourg, IPHC, 67037 Strasbourg, France
[c] CEA Saclay, IRFU/SPhN, 91191 Gif-sur-Yvette Cedex, France
[d] Universidad de Huelva, 21071 Huelva, Spain
[e] Institute of Atomic Physics, IFIN-HH, Bucharest-Măgurele, P.O. Box MG6, Romania
[f] Grand Accélérateur National d'Ions Lourds, 14076 Caen Cedex 5, France
[g] Institute for Nuclear Research, Hungarian Academy of Sciences, 4026 Debrecen, Hungary
[h] Instituut voor Kern- en Stralingsfysica, University of Leuven, 3001 Leuven, Belgium
[i] Universidade de Santiago de Compostela, 15754 Santiago de Compostela, Spain
[j] Centre d'Études Nucléaires de Bordeaux Gradignan, 33175 Gradignan, France
[k] Dipartimento di Fisica e Astronomia dell'Università and INFN, 35131 Padova, Italy
[l] INFN, Laboratori Nazionali di Legnaro, 35020 Legnaro, Italy

ARTICLE INFO

Article history:
Received 7 April 2015
Received in revised form 12 October 2015
Accepted 23 October 2015
Available online 27 October 2015
Editor: V. Metag

ABSTRACT

The strength functions of the $\pi f_{5/2}$, $\pi p_{3/2}$ and $\pi f_{7/2}$ orbitals in neutron-rich ^{71}Cu were obtained in a ^{72}Zn(d,^{3}He)^{71}Cu proton pick-up reaction in inverse kinematics using a radioactive beam of ^{72}Zn at 38 MeV/u. A dedicated set-up was developed to overcome the experimental challenges posed by the low cross section of the reaction and the low energy of the outgoing ^{3}He particles. The excitation-energy spectrum was reconstructed and spectroscopic factors were obtained after analysis of the angular distributions with the finite-range Distorted-Wave Born Approximation (DWBA). The results show that unlike for the $\pi f_{5/2}$ orbital and contrary to earlier interpretation, the $\pi f_{7/2}$ single-particle strength distribution is not appreciably affected by the addition of neutrons beyond $N = 40$.

1. Introduction

With a long and fruitful history to its credit, the shell model still accounts for much of our understanding of nuclear structure at low excitation energy [1]. The bulk of the interaction within the nuclear many-body system is well represented by a mean field that gives rise to a shell structure characterized by the well-known magic numbers 8, 20, 28, 50, … which originally defined either proton or neutron closed shells. These magic numbers, however, are not absolute and universal but are subject to evolution as one moves away from the valley of stability into the realm of exotic isotopes, where the numbers of protons and neutrons are out of their ordinary balance.

The fate of a presumed doubly magic nucleus like ^{78}Ni therefore carries much interest, as its closed-shell character comes under scrutiny. While the ^{78}Ni isotope was observed for the first time two decades ago [2], only its half-life is known so far [3], which was measured more precisely recently [4] and direct spectroscopic information is not yet available. In this article, we investigate the $Z = 28$ gap that corresponds to the energy splitting between the

* Corresponding author.
E-mail address: morfouac@nscl.msu.edu (P. Morfouace).

http://dx.doi.org/10.1016/j.physletb.2015.10.064

$\pi f_{7/2}$ orbital and the $\pi p_{3/2}$ or $\pi f_{5/2}$ orbital. This is the first shell gap that originates from the spin-orbit interaction and its evolution away from stability gives insight into the isospin dependence of the spin-orbit force. The neutron-rich copper isotopes with one proton outside a nickel core present an ideal opportunity to probe the movement of a single-proton orbit in the field of a closed-shell nucleus. Proceeding along the copper isotopic chain, while filling of the $\nu g_{9/2}$ orbital ($40 < N \leq 50$), one is able to explore the influence of the occupation of the neutron orbitals on the nuclear structure.

Of particular interest is the transition at $N = 40$. Because the first excited state in ^{68}Ni is located at a rather high energy and shows a spin and parity of 0^+, the existence of a subshell gap at $N = 40$ was rapidly acknowledged [5]. Nevertheless the small experimental $B(E2; 0_1^+ \rightarrow 2_1^+)$ value [6] was argued not to be a strong evidence for a magic ^{68}Ni nucleus [7]. Much experimental work has been done since, revealing a third 0^+ state at 2511 keV [8] and readjusting the second 0^+ energy to 1604 keV [9], which is consistent with a more recent study [10]. This has in turn spurred new theoretical activity, leading to a richer interpretation that advances the coexistence of spherical and deformed shapes in ^{68}Ni [11,12].

The first excited state of spin and parity $5/2^-$ is situated in a stable manner at an energy between 1 and 1.2 MeV in the ^{63,65,67,69}Cu isotopes. In the β-decay of ^{71}Ni, it was observed that it suddenly comes down to 534 keV in ^{71}Cu [13]. This distinctive feature coincides with the addition of neutrons beyond $N = 40$. Because of the large spectroscopic factor of $C^2S = 1.5$ deduced in the ^{70}Zn(d,^{3}He)^{69}Cu proton pick-up reaction [14], the level can be interpreted as mainly corresponding to the $\pi f_{5/2}$ single-particle state in ^{69}Cu. For the level at 1190 keV in ^{71}Cu, seen in the $E2$ cascade that deexcites a $19/2^-$ microsecond isomer, a $7/2^-$ assignment was made [15,16]. Based on a lower limit for the log ft value of 5.9 in the β-decay of ^{71}Ni, the ground state of which is conjectured to consist of a $9/2^+$ configuration, and the similarity of the γ branching pattern between ^{69}Cu and ^{71}Cu, a spin and parity of $7/2^-$ was suggested for the level at 981 keV. This was corroborated by calculations within the particle-core coupling model (PCM) that linked the state to the $f_{7/2}^{-1}$ proton hole, onto which a 2p–1h quasiband would dwell in the same manner as for ^{69}Cu [17]. The Coulomb excitation of ^{71}Cu accordingly revealed a value of 10.7(12) Weisskopf units for the 1190-keV level, while the 981-keV state was not observed and suggested to be of single-particle nature [18]. Finally the lifetime of the 981-keV state was measured in a recent study, which corresponds to $B(E2) = 44(20)$ e^2 fm^4 [19]. In this article, since the theoretical value of the $B(E2)$ is much higher compared to the experimental one the authors exclude a particle-hole character for this state. Nevertheless one has to obtain spectroscopic factor for this state to confirm it.

The ^{71}Cu nucleus is an essential test for shell-model calculations because of the sudden change in the energy of the $\pi f_{5/2}$ orbital. The position of its spin-orbit partner, the $\pi f_{7/2}$ orbital, is important to measure the energy gap of the $Z = 28$ shell closure. In the present work, we set off to extract the spectroscopic factors of the $7/2^-$, $3/2^-$ and $5/2^-$ levels with the aim of obtaining the strength function of the single-particle states. We chose to do so in the ^{72}Zn(d,^{3}He)^{71}Cu proton pick-up reaction, as it should selectively populate the hole states in ^{71}Cu. Several papers have questioned the interpretation of spectroscopic factors as observables of single-particle components in nuclear wave-functions [20,21]. Nevertheless, it was shown that within a coherent parametrization of potential parameters, spectroscopic factors provide self-consistent information and are good indicators of orbital structures [22,23].

2. Experimental setup

The experiment took place at the Ganil laboratory in Caen, France. A radioactive beam of ^{72}Zn at 38 MeV/u and a rate of 1.5 10^5 particles per second was obtained from the fragmentation of a primary ^{76}Ge beam on a Be target of 733 µm thickness. The reaction products were selected with the Lise spectrometer, resulting in a beam purity of 55% with ^{74}Ga as main contaminant (30%). Thanks to their time-of-flight difference, one is able to separate ^{72}Zn from ^{74}Ga and get a relative purity of 90.6%. After passing through two Cats beam-tracking detectors [24], the beam impinged on a deuterated polypropylene target of 0.26 mg/cm^2.

The target was surrounded by four Must2 telescopes [25], covering forward angles from 8 to 50° in the laboratory. The energy range of ^{3}He reaction product was below 21 MeV for laboratory angles lower than 46°. Since they would have been stopped already in the first stage of Must2, a double-sided silicon strip detector (DSSSD) of 300 µm, four silicon strip detectors with nominal thickness of 20 µm were added in front of the Must2 array. From transmission measurements with an α-source it appeared that the actual non-uniformity of the thickness varies up to 25%. Only after a pixel-by-pixel mapping on a 1-mm^2 grid was carried out to correct for the variation in energy loss (ΔE), the necessary resolution for particle identification could be achieved. Two Must2 telescopes covering the angles from $\theta_{lab} = 69°$ to $\theta_{lab} = 90°$ were installed in order to measure the elastic scattering, check the normalization and validate the optical potential in the incoming channel. Downstream from the experiment an ionization chamber was installed for detecting the outgoing heavy particles. The electronic dead time was kept at 15% throughout the experiment.

3. Data analysis and results

3.1. Excitation-energy spectrum and angular distributions

The ^{3}He particles of interest were identified by combination of their time-of-flight, ΔE signal in the 20-µm strip detectors and E deposit in the Must2 DSSSD. For each selected event, the excitation energy was reconstructed by the missing-mass method. The spectrum was further purified by requiring the presence of a heavy recoil in the ionization chamber. After the subtraction of background stemming from reactions on the carbon nuclei in the target (obtained in a separate run with a carbon target and shown in blue in Fig. 1), five peaks with an average resolution of $\sigma = 290$ keV (680 keV in FWHM) could be distinguished in the spectrum, as can be seen in Fig. 1 (a). The remaining events at negative energy, observed with low statistics, can be understood as stemming from the 9.4% beam contamination of ^{74}Ga. When comparing Figs. 1 (a) and 1 (b) one sees that the condition on the ionization chamber indeed reduces the ^{74}Ga counts.

Because of the limited angular coverage of the ionization chamber, its efficiency for our case amounted to 43% and its inclusion in the analysis reduces the statistics. Once the peaks in the excitation-energy spectrum are identified, we therefore remove the condition on the ionization chamber. The resulting spectrum is shown in Fig. 1 (b). The width of the first peak is larger than the expected experimental resolution of $\sigma = 306$ keV (720 keV in FWHM) indicating the presence of a doublet. From the known level scheme [13,18], the doublet can include two or more states among the $3/2^-$ ground state, the $1/2^-$ state at 454 keV and the $5/2^-$ state at 534 keV. For the latter a single-particle interpretation of $\pi f_{5/2}$ has been put forward and we should populate it in a similar manner as in ^{69}Cu [14]. The spectroscopic factor of the $1/2^-$ excited state in ^{69}Cu is three times weaker than for the $3/2^-$ ground state and its $B(E2)$ value is two times smaller than in ^{71}Cu, where

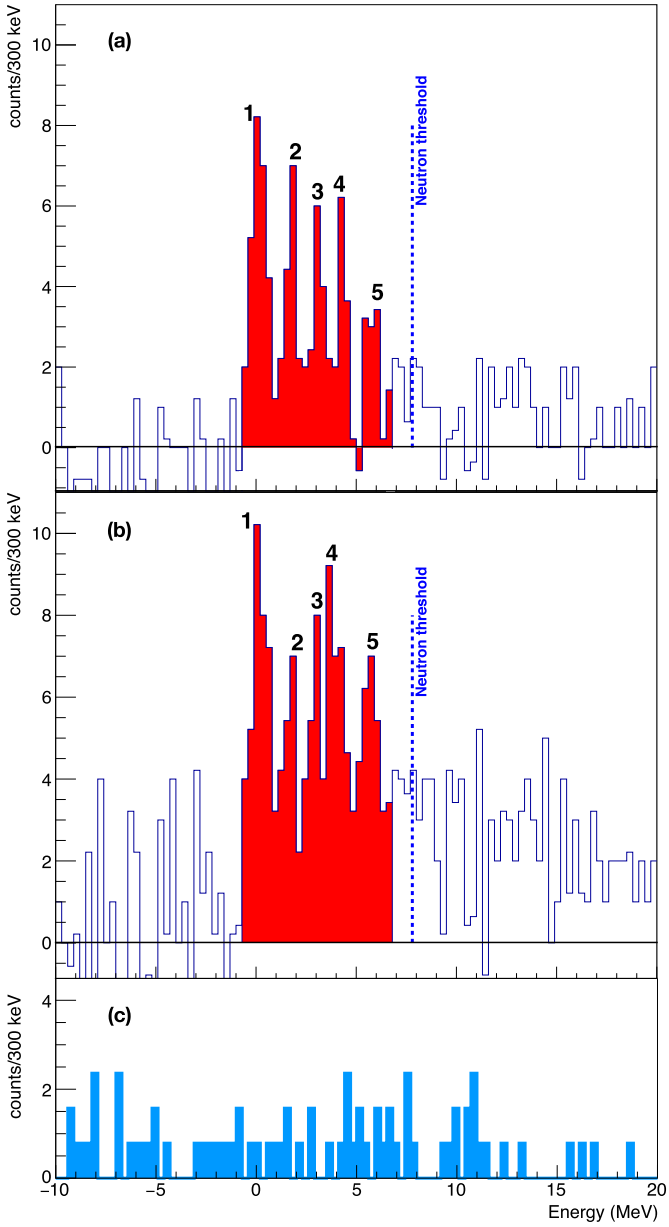

Fig. 1. Excitation-energy spectrum of ^{71}Cu (a) with and (b) without condition on the ionization chamber. The red part corresponds to the identified states in ^{71}Cu. The blue dotted line shows the neutron threshold. The normalized carbon background (c) has been subtracted in the excitation-energy spectrum. (For interpretation of the references to color in this figure legend, the reader is referred to the web version of this article.)

it is known to be of a strongly collective nature [18]. We do not expect to see it in our pick-up reaction, therefore its possible contribution was not taken into account. The peak was fitted with a sum of two Gaussians, fixed at E_0 and $E_0 + 0.534$ MeV. The result is $E_0 = 0.18(19)$ MeV and is consistent with zero within the statistical uncertainty. If the mean energy of the first peak is corrected for this offset, we find 0.11(19) MeV. In Table 1 we list the energies of the five identified peaks, corrected for the offset.

The angular distributions of the emitted ^{3}He particles were fitted with functions calculated within the finite-range Distorted-Wave Born Approximation (DWBA) using the DWUCK5 code. For the incoming channel, the relativistic Daehnick-F optical potential was taken [26] since it reproduces very well the angular distribution of the elastic scattering measured with the two Must2 detectors at 90°. For the outgoing channel, where the elastic scattering was not measured, we used the Perey and Perey parametrization [27]. The Pang potential [28] was also tested and a lower variation of 20% was observed for the spectroscopic factors. Nonetheless, after minimization, the χ^2 is worse since the shape of the calculated distribution using the Pang potential does not reproduce the experimental one as well as the Perey and Perey distribution does. For the overlap between the deuteron and the ^{3}He we chose the Brida potential [29]. Finally for the form factor the standard values of $r_0 = 1.25$ fm and $a_0 = 0.65$ fm were chosen. In our case, the use of different potentials affects the absolute normalization as expected but it does not affect the position of the centroid of the energy distribution.

Table 1
Position in energy of the different populated states in ^{71}Cu with their width *FWHM*, the transferred angular momentum L, the proposed spin-parity J^π and the spectroscopic factor C^2S.

State	E (MeV)	*FWHM* (MeV)	$L(J^\pi)$	C^2S
1	0.11(19)	0.95	1 ($3/2^-$)	0.8(2)
			3 ($5/2^-$)	1.4(6)
2	1.86(15)	0.61	3 ($7/2^-$)	1.4(2)
3	3.24(20)	0.61	3 ($7/2^-$)	1.5(3)
4	4.36(17)	0.94	3 ($7/2^-$)	3.7(6)
5	5.92(18)	0.94	0 ($1/2^+$)	0.4(1)
			2 ($3/2^+$)	3.0(5)

After a χ^2 minimization, we found that the differential cross section of the first peak could be fitted with a combination of $L = 1$ and $L = 3$ distributions (Fig. 2 (a)) assuming that it is a doublet, which is also consistent with the width of the peak. The $L = 1$ component shows a spectroscopic factor of $C^2S = 0.8(2)$ (see Table 1), which we attribute to the $3/2^-$ ground state. The $L = 3$ contribution yields $C^2S = 1.4(6)$ and we attribute it to the $5/2^-$ state at 534 keV, for which we infer a dominant $\pi f_{5/2}$ configuration. We note that the large spectroscopic factor exhausts the available $f_{5/2}$ proton strength as it was seen for the other lighter copper isotopes [14]. From the integrated cross sections of the $L = 1$ and $L = 3$ components taking into consideration their spectroscopic factors C^2S, we can determine the mean energy of the ground-state doublet. This gives 0.13 MeV, which agrees with the mean energy of the first peak of 0.11(19) MeV. The sum in the $\pi p_{3/2}$ and the $\pi f_{5/2}$ orbitals gives 2.2(6), which is compatible with the expected value of 2 protons in the zinc isotopes above $Z = 28$ and with former literature [14,30].

The next three peaks were best fitted with $L = 3$ functions. The fourth peak is also wider and might contain at least two states but its angular distribution is well fitted with only $L = 3$. The weighted centroid for all the peaks gives 3.8 MeV. Since the shape of the $L = 3$ angular distribution does not change between 1.5 and 5 MeV excitation energy in the present reaction, the angular distribution of the three peaks together was fitted with a state at 3.8 MeV in the DWBA calculations. The result of the fit gives a spectroscopic strength of $C^2S = 6.9(8)$ (Fig. 2 (b)), which is compatible with the sum of the respective spectroscopic factors ($\sum C^2S_{7/2^-} = 6.6(7)$). This corresponds to $86 \pm 12\%$ of the $\pi f_{7/2}$ strength with an experimental centroid at 3.8 MeV, which represents a lower limit as far as part of the strength stays undetected. One can see that the sum of the spectroscopic factors in the pf orbitals gives 9.1 ± 1.0, which is close to the expected value of 10 protons [31]. The fifth peak in the excitation-energy spectrum was fitted with a superposition of $L = 0$ and $L = 2$ distributions even though in this case the χ^2 value is quite high ($\chi^2/NDF = 6.2/2$). One can infer that these states likely originate from hole excitations in the deeper *sd* shell.

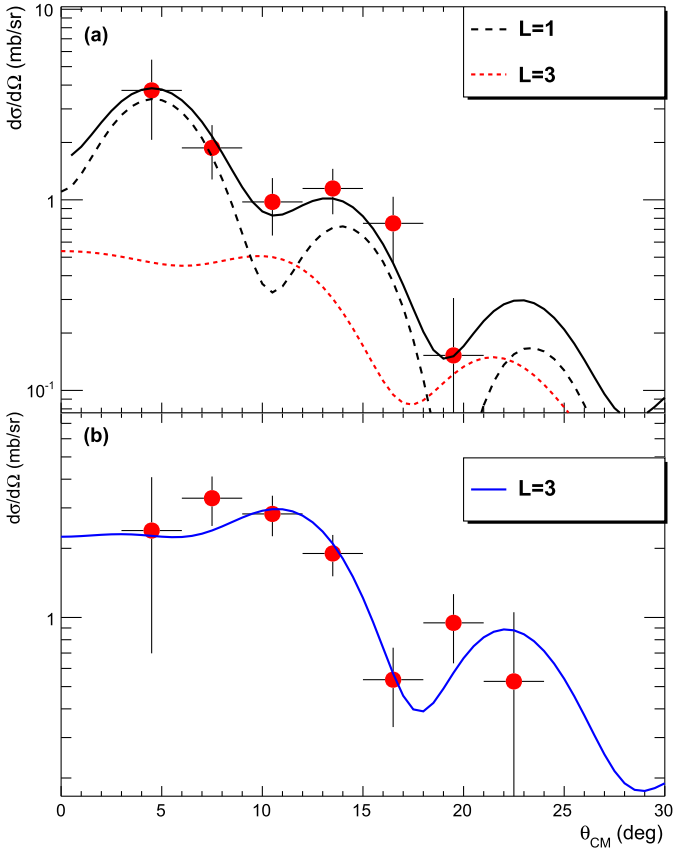

Fig. 2. (a) Angular distribution of the first peak where a $L=1$ and $L=3$ angular distribution are needed. The black line corresponds to the minimization where both contributions are taken into account. (b) Summed angular distribution for the second, third and fourth peak in the excitation-energy spectrum of ^{71}Cu showing a $L=3$ angular distribution.

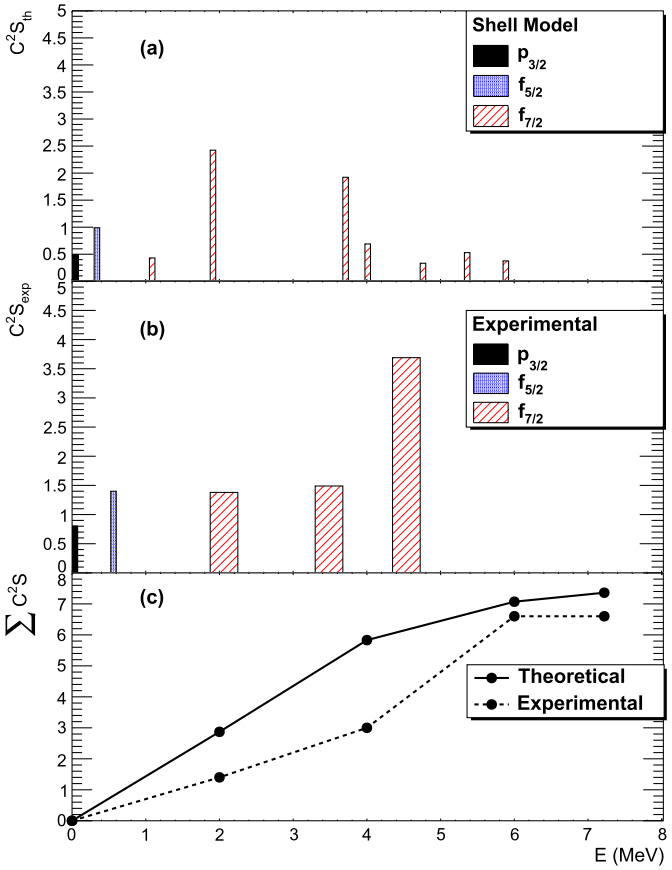

Fig. 3. States from shell-model calculations with $C^2S_{th} > 0.3$ (a) compared to experimental data (b). The larger area for the experimental data stands for the experimental uncertainties for the $7/2^-$ states. Figure (c) corresponds to the accumulated strength both experimentally and theoretically.

3.2. Shell-model calculations

Shell-model calculations within a *fpgd* valence space and originating from a Hamiltonian from earlier published work [32,33] with minor modifications [19] were carried out. This valence space includes $\Delta l = 2$ valence orbitals for neutrons ($0g_{9/2}1d_{5/2}$) and protons ($0f_{7/2}1p_{3/2}$), which naturally favor quadrupole correlations and generate collectivity through the Elliott's $SU(3)$ symmetry [34]. One can see in Fig. 3 the comparison between the theoretical levels (C^2S_{th}) and the experimental ones (C^2S_{exp}). We can see in blue the strength function of the $\pi f_{5/2}$ levels. The experimental state situated at 534 keV is reproduced by the calculations at 310 keV. Concerning the strength function of the $f_{7/2}$ proton orbital, it appears more fragmented than the measurement could establish. Nevertheless, most of the distribution spreads around 2 and 4 MeV. The other smaller splinters remain below the experimental sensitivity. One can evaluate the evolution of the cumulative $\pi f_{7/2}$ strength by step of 2 MeV both experimentally and theoretically and note that the shapes of both curves are in fair agreement (cf. Fig. 3 (c)), giving confidence in the calculated trend even though the cumulative theoretical strength is larger than its experimental counterpart. This can be understood from the role of short and long-range correlations in the quenching of spectroscopic factors [35,36].

In addition to the strength functions, calculations to determine the composition of the first low-lying states were performed (see Table 2). We clearly see that the $3/2^-$ ground state mainly corresponds to a single proton in the $\pi p_{3/2}$ orbital. The $5/2^-$ is reasonably located and its dominant part corresponds to a single proton in the $\pi f_{5/2}$ orbital. It has to be noted that the energy gap between the effective single-particle energy (ESPE) from the shell-model calculations is decreasing between $\pi f_{5/2}$ and $\pi p_{3/2}$ due to the more attractive $\nu g_{9/2} - \pi f_{5/2}$ neutron–proton interaction. The high extracted spectroscopic factor combined with the calculations confirm the single-particle character of the $5/2^-$ state and the gradual weakening of the gap between the $\pi p_{3/2}$ and $\pi f_{5/2}$ orbitals.

Table 2
Dominating components of the wave functions for the lowest calculated states in ^{71}Cu.

E (MeV)	J^π	Percentage	Composition
0	$3/2^-$	60%	$\|0^+_\nu \otimes \pi p_{3/2}\rangle$
		14%	$\|2^+_\nu \otimes \pi p_{3/2}\rangle$
0.31	$5/2^-$	36%	$\|0^+_\nu \otimes \pi f_{5/2}\rangle$
		22%	$\|4^+_\nu \otimes \pi f_{5/2}\rangle$
1.09	$7/2^-$	47%	$\|2^+_\nu \otimes \pi p_{3/2}\rangle$
		11%	$\|4^+_\nu \otimes \pi p_{3/2}\rangle$
		10%	$\|J^+_\nu \otimes \pi f^{-1}_{7/2}\rangle$
1.41	$7/2^-$	42%	$\|2^+_\nu \otimes \pi f_{5/2}\rangle$
		12%	$\|4^+_\nu \otimes \pi f_{5/2}\rangle$
		13%	$\|J^+_\nu \otimes \pi f^{-1}_{7/2}\rangle$

We now come back to the nature of the two first $7/2^-$ states at 981 and 1190 keV respectively that are part of two γ cascades in ^{71}Cu. The one including the 1190-keV state shows an $E2$ sequence built on the $3/2^-$ ground state [15,16]. The one includ-

ing the 981-keV state forms a $\Delta L = 1$ pattern on top of the first $5/2^-$ level at 534 keV [37]. In our experiment, no pick-up strength was detected below 1.3 MeV except for the $L = 3$, $5/2^-$ state at 534 keV. Therefore, our data do not support the presence of a strong $L = 3$ component in the wave function of the $7/2^-$ state at 981 nor 1190 keV. As a matter of fact, the first calculated $7/2^-$ state at 1.09 MeV is dominated by the coupling $|2^+_\nu \otimes \pi p_{3/2}\rangle$ and is associated with a strong calculated $B(E2)$ value to the ground state (179 e^2 fm^4 or 10.25 W.u). It can be associated to the collective state at 1189 keV, which was observed in Coulomb excitation [18] with a measured value of $B(E2) = 10.7$ W.u. The wave function of the second calculated $7/2^-$ state has a large contribution coming from the coupling $|2^+_\nu \otimes \pi f_{5/2}\rangle$. It decays to the $5/2^-$ state and has a small calculated $B(E2)$ value (14.4 e^2 fm^4 or 0.82 W.u) to the ground state. On the contrary, it has a strong calculated $B(M1)$ value to the $5/2^-$ state ($0.168\mu_N^2$). This state would correspond to the experimental level at 981 keV. We interpret the experimental results combined with the shell-model calculations as a dominant $M1$ character and it explains why this $7/2^-$ level at 981 keV was not seen in Coulomb excitation. Indeed it would involve a structurally different configuration, which would not be as favorable as the excitation to the $7/2^-$ level at 1190 keV. Taking together the preceding arguments, the non-observation of the level at 981 keV in our work excludes a $\pi f^{-1}_{7/2}$ interpretation of the level at 981 keV. The calculated spectroscopic factors of these two $7/2^-$ states are 0.43 and 0.007 respectively, which is below our experimental sensitivity and which can now be understood from the fact that these two states arise mainly from proton-core couplings. The $7/2^-$ states with a high spectroscopic factor are situated above 1.9 MeV both experimentally and theoretically. It indicates that the gap between $\pi f_{7/2}$ and $\pi p_{3/2}$ is not significantly reduced. The neutron–proton interaction is almost the same between $\nu g_{9/2} - \pi f_{7/2}$ and $\nu g_{9/2} - \pi p_{3/2}$ leading to the fact that the $Z = 28$ gap defined as the energy difference between the $\pi f_{7/2}$ and $\pi p_{3/2}$ ESPEs remains unchanged while the $\pi f_{5/2}$ orbital is getting closer to the $\pi p_{3/2}$ orbital.

From different experimental works [15,16,19,37] and from this work, we see that three $7/2^-$ structures exist. In transfer we see that the $\pi f_{7/2}$ centroid does not come down therefore the $7/2^-$ levels at 981 and 1190 keV are not proton-hole states but from shell model calculations we identify them as $|2^+_\nu \otimes \pi f_{5/2}\rangle$ and $|2^+_\nu \otimes \pi p_{3/2}\rangle$ respectively. The last one was indeed seen in Coulomb excitation [18] while the first one was not observed because of its very low $B(E2)$ value. In this way, the results from β-decay, Coulomb excitation, deep-inelastic and transfer reaction are consistent with the present shell-model calculations.

The experimental data as well as the shell-model calculations show that the $f_{7/2}$ proton single-particle strength remains at several MeV of excitation energy in ^{71}Cu. It does not come down appreciably and does not follow the sharp decline of the $\pi f_{5/2}$ state, preventing a rapid reduction of the $Z = 28$ gap. It should be kept in mind, however, that the $\pi f_{7/2}$ orbital resides farther away from the Fermi surface and its influence on the nuclear structure at low energy is less immediate. Instead it appears more susceptible to fragmentation and therefore any change in its centroid is less visible than it is for its $\pi f_{5/2}$ spin-orbit partner. This is similar to observations of orbital energies in the $Z = 20$ region, where the experimental data [1,38,39] and the theoretical calculations [40] indicate a reduction of the $\pi d_{3/2} - \pi s_{1/2}$ gap in the potassium isotopes correlated with filling the $\nu f_{7/2}$ orbital, but the weakening of the gap between the $\pi d_{5/2} - \pi s_{1/2}$ orbitals is much less pronounced. From our findings, one can point to a parallel behavior in the copper isotopes where the $\pi f_{5/2} - \pi p_{3/2}$ gap is quenched with the filling of the $\nu g_{9/2}$ orbital, while we do not see any reduction of the $\pi f_{7/2} - \pi p_{3/2}$ gap.

4. Conclusion

Notwithstanding the low cross section of the order of 10 mb and the low energy of the outgoing light particles that did not exceed 7 MeV/u for the angles of interest leading to a challenging experimental setup, it has been possible for the first time to extract the spectroscopic factors for the (d,^{3}He) proton pick-up reaction with a ^{72}Zn radioactive beam in the neutron-rich copper region beyond $N = 40$. We confirm the weakening of the gap between the $\pi p_{3/2}$ and $\pi f_{5/2}$ orbitals and three levels carrying $\pi f_{7/2}$ strength were found in ^{71}Cu. Their spectroscopic factors were determined from the comparison of the experimental angular distributions with finite-range DWBA calculations. We found $86 \pm 12\%$ of the $f_{7/2}$ proton strength and the centroid of the $\pi f_{7/2}$ force remains situated at several MeV of excitation energy contrary to earlier interpretation [17,18], showing that there is no collapse of the $Z = 28$ shell gap in the neutron-rich copper isotopes.

Acknowledgements

The authors are thankful to the Ganil accelerator staff, informatics service and to the IPN design office. We are grateful for the grant of the Romanian National Authority for Scientific Research, CNCS – UEFISCDI, project number PN-II-ID-PCE-2011-3-048, to the grant FPA2010-22131-C02-01 from the Spanish government and to the OTKA contract No. K100835.

References

[1] O. Sorlin, M.-G. Porquet, Prog. Part. Nucl. Phys. 61 (2008) 602.
[2] C. Engelmann, et al., Z. Phys. A 352 (1995) 351.
[3] P. Hosmer, et al., Phys. Rev. Lett. 94 (2005) 112501.
[4] Z.Y. Xu, et al., Phys. Rev. Lett. 113 (2014) 032505.
[5] M. Bernas, P. Dessagne, M. Langevin, J. Payet, F. Pougheon, P. Roussel, Phys. Lett. B 113 (1982) 279.
[6] O. Sorlin, et al., Phys. Rev. Lett. 88 (2002) 092501.
[7] K. Langanke, et al., Phys. Rev. C 67 (2003) 044314.
[8] W. Mueller, et al., Phys. Rev. C 61 (2000) 054308.
[9] F. Recchia, et al., Phys. Rev. C 88 (2013) 041302.
[10] S. Suchyta, et al., Phys. Rev. C 89 (2014) 021301(R).
[11] A. Dijon, et al., Phys. Rev. C 85 (2012) 031301(R).
[12] Y. Tsunoda, T. Otsuka, N. Shimizu, M. Honma, Y. Utsuno, Phys. Rev. C 89 (2014) 031301.
[13] S. Franchoo, et al., Phys. Rev. Lett. 81 (1998) 3100.
[14] B. Zeidman, J.A. Nolen, Phys. Rev. C 18 (1978) 2122.
[15] R. Grzywacz, et al., Phys. Rev. Lett. 81 (1998) 766.
[16] T. Ishii, et al., Phys. Rev. Lett. 81 (1998) 4100.
[17] A. Oros-Peusquens, P. Mantica, Nucl. Phys. A 669 (2000) 81.
[18] I. Stefanescu, et al., Phys. Rev. Lett. 100 (2008) 112502.
[19] E. Sahin, et al., Phys. Rev. C 91 (2015) 034302.
[20] R.J. Furnstahl, H.-W. Hammer, Phys. Lett. B 531 (2002) 203.
[21] T. Duguet, G. Hagen, Phys. Rev. C 85 (2012) 034330.
[22] J.P. Schiffer, et al., Phys. Rev. Lett. 108 (2012) 022501.
[23] J.P. Schiffer, et al., Phys. Rev. C 87 (2013) 034306.
[24] S. Ottini, et al., Nucl. Instrum. Methods Phys. Res., Sect. A 431 (1999) 476.
[25] E. Pollacco, et al., Eur. Phys. J. A 25 (2005) 287.
[26] W.W. Daehnick, J.D. Childs, Z. Vrcelj, Phys. Rev. C 21 (1980) 2253.
[27] C. Perey, F. Perey, At. Data Nucl. Data Tables 17 (1) (1976).
[28] D.Y. Pang, et al., Phys. Rev. C 79 (2009) 024615.
[29] I. Brida, S.C. Pieper, R.B. Wiringa, Phys. Rev. C 84 (2011) 024319.
[30] G. Rotbard, et al., Phys. Rev. C 18 (1978) 86.
[31] P.G. Hansen, J.A. Tostevin, Annu. Rev. Nucl. Part. Sci. 53 (2003) 219.
[32] S.M. Lenzi, F. Nowacki, A. Poves, K. Sieja, Phys. Rev. C 82 (2010) 054301.
[33] K. Sieja, F. Nowacki, Phys. Rev. C 85 (2012) 051301(R).
[34] J.P. Elliott, et al., Proc. R. Soc. A 245 (1958) 128.
[35] W.H. Dickhoff, C. Barbieri, Prog. Part. Nucl. Phys. 52 (2004) 377.
[36] C. Barbieri, Phys. Rev. Lett. 103 (2009) 202502.
[37] G. De Angelis, Phys. Scr. T 150 (2012) 014010.
[38] P. Doll, et al., Nucl. Phys. A 263 (1976) 210.
[39] S.M. Banks, et al., Nucl. Phys. A 437 (1984) 381.
[40] N.A. Smirnova, et al., Phys. Lett. B 686 (2010) 109.

Chapter 5

Gamma spectroscopy at RIBF

5.1 The experiment

Unlike particle spectroscopy, the measurement of γ rays appears more straightforward yet considerable effort is involved in sorting out the sundry transitions that one observes and obtaining a level scheme from these. The utterly low intensity of the most exotic beams turns the high efficiency of the detection set-up nearly always into the primary objective, relegating the resolution to the role of a luxury one cannot afford. Opting for large scintillator multidetectors in experiments with fast beams, the granularity of the array becomes of paramount importance to achieve a reasonable Doppler correction. To increase the luminosity a thick target can be chosen, the straggling in which must be quantified as accurately as possible by additional tracking devices.

The Seastar campaign at RIBF was dictated by this logic. The in-flight fission of a ^{238}U beam speeding at 345 MeV per nucleon into a beryllium target gave access to an extraordinary range of nuclei [Kub12, Fuk13]. The Bigrips separator was tuned to transmit a composite beam centred on ^{80}Zn, the impact of which on a cryogenic hydrogen target created the ^{79}Cu particles carrying our interest at an average energy of 270 MeV per nucleon. While the emerging residue was identified in the Zerodegree spectrometer, the emitted protons were recorded in the Minos time-projection chamber cylindrically enclosing the target, enabling to select the (p,2p) knock-out channel and resolve the interaction position [Obe14]. A smaller contribution to the ^{79}Cu yield of 7.7% originated from the ^{81}Ga(p,3p) reaction. The Dali-2 assembly of 186 NaI(Tl)

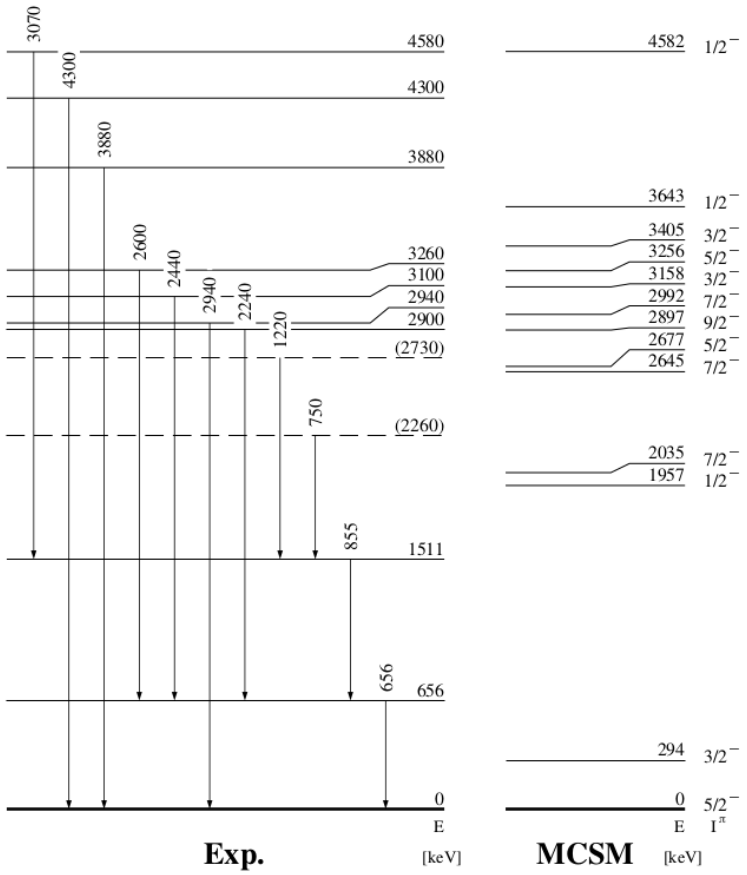

FIGURE 5.1: Experimental level scheme of ^{79}Cu compared to the prediction from the A3DA-m interaction. Taken from [Oli17b]

crystals surrounding Minos in close geometry collected the associated γ rays [Tak14].

Calculations with the A3DA-m force provide a promising handle on the structure we may expect. The proton can be removed from the $\pi p_{3/2} f_{5/2}$ orbitals in the ^{80}Zn ground state, which is described as a superposition of 47% of $\pi f^2_{5/2}$ and 22% of $\pi p^2_{3/2}$. Digging deeper we mine the rich artery of $f_{7/2}$ protons, populating a predicted $7/2^-$ level at 2.04 MeV of energy with a spectroscopic factor of 5.58. A number of weaker states arguably exist higher up, each claiming a remnant of the fragmented strength. The determination of their centroid above the $\pi f_{5/2}$ ground state would then strikingly reveal the magnitude of the spin-orbit splitting at $N = 50$. However, instead of the simple spectrum of the three $\pi f_{5/2}$, $\pi p_{3/2}$, and $\pi f^{-1}_{7/2}$ structures, the experiment and the extracted level scheme we present in figure 5.1 burst into a treasure grove of nuclear transitions.

So what happened? Not only is the knock-out strength shattered, it comes in at a much more elevated energy. We recall from section 2.7 that perhaps not by chance also in the proton removal from ^{77}Cu to ^{76}Ni several states are accessed with similar energies near 4 MeV. Gauging ^{77}Cu attentively, the relatively low energy of 990 keV at which the 2^+ state is found in ^{76}Ni forces the core-coupling multiplet to cluster near 1 MeV. From figure 2.54 and 2.56 we learn that the $\pi f_{7/2}^{-1}$ state sticks out above the multiplet at 2068 keV or higher and receives clear and direct feeding. In ^{79}Cu, one expects the particle-core combinations to step in close to the 2_1^+ excitation energy of ^{78}Ni at 2600 keV with a second series sourced by the 2_2^+ state at 2910 keV. The $\pi f_{7/2}$ hole strength dives below these, mixing with the $7/2^-$ members that are at hand. Sending its sparkles throughout the upper reaches of the spectrum, the strong spectroscopic factor that is foreseen for the theoretical $7/2^-$ level at 2.04 MeV vanishes. Inversely, the appearance of a set of states between 2.7 and 3.3 MeV corresponding to the coupling of the ground and first excited state to the underlying 2^+ excitations of the nickel core implies the sizeable energies of the latter and the persistence of ^{78}Ni as a crux of magic matter.

In the lower part of the level scheme the rigidity of the nickel core would ensure that the simple picture is held up. The absence of direct knock-out feeding to the 1511-keV level renders a spin and parity of $7/2^-$ unlikely and instead it may embody a low-spin single-particle state. In particular it could correspond to the $1/2^-$ level that is calculated at 1.96 MeV and according to table 3.2 contains a 49% contribution from the $\pi p_{1/2}$ configuration. The rather pure nature it reflects stands stark against the solid collectivity of the $1/2^-$ level in ^{71,73}Cu that was observed in Coulomb excitation and discussed in section 2.5. It betrays the magicity of ^{78}Ni, where indeed deformation is replaced by shape coexistence. The experimental energy of the first excited level rises steeply from 293 keV in ^{77}Cu to 656 keV in ^{79}Cu, whereas in theory it remains flat. We connect it to the $\pi p_{3/2}$ single-particle state above the $\pi f_{5/2}$ ground state, their respective monopole migration steadily progressing.

The transfer reactions on the lighter copper isotopes in the previous chapter confronted us with the same elusiveness of the $\pi f_{7/2}$ orbital, contrary to the tractable disposition of its $\pi f_{5/2}$ spin-orbit partner. From the single-particle diagram in 3.15 it is

undeniable that something specific is affecting the $\pi f_{5/2}$ orbital and the relation with the $g_{9/2}$ neutrons juts out. Perhaps, however, it only translates its closeness to the Fermi surface and thereby its sensitivity to experimental scrutiny. The behaviour of the $\pi f_{7/2}$ orbital meanwhile can at best be qualified as decorrelated and whether a tensor effect is at work to weaken the spin-orbit splitting in exotic nuclei or instead quadrupole correlations lead the dance, is hard to answer.

Seeking to plait the strands together, in the end the descent of the $\pi f_{5/2}$ state left on its own does not affect the $Z = 28$ gap much, merely fixing its definition by means of a different orbital. From the spectroscopy of the neutron-rich copper isotopes we establish a collectivity that fizzles out as one progresses towards ^{78}Ni and a $Z = 28$ gap at $N = 50$ that supports the restoration of single-particle properties in ^{79}Cu. A natural pathway is pointed out from shape coexistence in magic nuclei to weak coupling in their odd neighbours and actual deformation farther afield. With the rolling landscape that thus unfolds we can only reaffirm the closing words of Maria Goeppert-Mayer in her Nobel lecture that "There are enough nuclei to investigate so that the shell model-lists will not soon be unemployed" [Goe63]. While the journey is long, the itinerary is nonetheless written bit by bit.

5.2 The articles

The γ-spectroscopy experiment is treated in great detail in the doctoral thesis of Louis Olivier [Oli17a]. On the following pages we reprint the article [Oli17b, Oli18] and the perhaps more accessible release that was issued by IN2P3 [Act18].

Persistence of the $Z = 28$ Shell Gap Around ^{78}Ni: First Spectroscopy of ^{79}Cu

L. Olivier,[1] S. Franchoo,[1] M. Niikura,[2] Z. Vajta,[3] D. Sohler,[3] P. Doornenbal,[4] A. Obertelli,[5,4] Y. Tsunoda,[6] T. Otsuka,[2,4,6] G. Authelet,[5] H. Baba,[4] D. Calvet,[5] F. Château,[5] A. Corsi,[5] A. Delbart,[5] J.-M. Gheller,[5] A. Gillibert,[5] T. Isobe,[4] V. Lapoux,[5] M. Matsushita,[7] S. Momiyama,[2] T. Motobayashi,[4] H. Otsu,[4] C. Péron,[5] A. Peyaud,[5] E. C. Pollacco,[5] J.-Y. Roussé,[5] H. Sakurai,[2,4] C. Santamaria,[5,4] M. Sasano,[4] Y. Shiga,[4,8] S. Takeuchi,[4] R. Taniuchi,[2,4] T. Uesaka,[4] H. Wang,[4] K. Yoneda,[4] F. Browne,[9] L. X. Chung,[10] Z. Dombradi,[3] F. Flavigny,[1] F. Giacoppo,[11,*] A. Gottardo,[1] K. Hadyńska-Klęk,[11] Z. Korkulu,[3] S. Koyama,[2] Y. Kubota,[4,7] J. Lee,[12] M. Lettmann,[13] C. Louchart,[13] R. Lozeva,[14,†] K. Matsui,[2,4] T. Miyazaki,[2] S. Nishimura,[4] K. Ogata,[15] S. Ota,[7] Z. Patel,[16] E. Sahin,[11] C. Shand,[16] P.-A. Söderström,[4] I. Stefan,[1] D. Steppenbeck,[7] T. Sumikama,[17] D. Suzuki,[1] V. Werner,[13] J. Wu,[4,18] and Z. Xu[12]

[1]*Institut de Physique Nucléaire, IN2P3-CNRS, Université Paris-Sud, Université Paris-Saclay, 91406 Orsay Cedex, France*
[2]*Department of Physics, University of Tokyo, 7-3-1 Hongo, Bunkyo, Tokyo 113-0033, Japan*
[3]*MTA Atomki, P.O. Box 51, Debrecen H-4001, Hungary*
[4]*RIKEN Nishina Center, 2-1 Hirosawa, Wako, Saitama 351-0198, Japan*
[5]*IRFU, CEA, Université Paris-Saclay, F-91191 Gif-sur-Yvette, France*
[6]*Center for Nuclear Study, University of Tokyo, 7-3-1 Hongo, Bunkyo, Tokyo 113-0033, Japan*
[7]*Center for Nuclear Study, University of Tokyo, RIKEN campus, Wako, Saitama 351-0198, Japan*
[8]*Department of Physics, Rikkyo University, 3-34-1 Nishi-Ikebukuro, Toshima, Tokyo 172-8501, Japan*
[9]*School of Computing Engineering and Mathematics, University of Brighton, Brighton BN2 4GJ, United Kingdom*
[10]*Institute for Nuclear Science & Technology, VINATOM, P.O. Box 5T-160, Nghia Do, Hanoi, Vietnam*
[11]*Department of Physics, University of Oslo, N-0316 Oslo, Norway*
[12]*Department of Physics, The University of Hong Kong, Pokfulam, Hong Kong*
[13]*Institut für Kernphysik, Technische Universität Darmstadt, 64289 Darmstadt, Germany*
[15]*IPHC, CNRS/IN2P3, Université de Strasbourg, F-67037 Strasbourg, France*
[15]*Research Center for Nuclear Physics (RCNP), Osaka University, Ibaraki 567-0047, Japan*
[16]*Department of Physics, University of Surrey, Guildford GU2 7XH, United Kingdom*
[17]*Department of Physics, Tohoku University, Sendai 980-8578, Japan*
[18]*State Key Laboratory of Nuclear Physics and Technology, Peking University, Beijing 100871, People's Republic of China*

(Received 1 February 2017; revised manuscript received 20 September 2017; published 6 November 2017)

In-beam γ-ray spectroscopy of ^{79}Cu is performed at the Radioactive Isotope Beam Factory of RIKEN. The nucleus of interest is produced through proton knockout from a ^{80}Zn beam at 270 MeV/nucleon. The level scheme up to 4.6 MeV is established for the first time and the results are compared to Monte Carlo shell-model calculations. We do not observe significant knockout feeding to the excited states below 2.2 MeV, which indicates that the $Z = 28$ gap at $N = 50$ remains large. The results show that the ^{79}Cu nucleus can be described in terms of a valence proton outside a ^{78}Ni core, implying the magic character of the latter.

DOI: 10.1103/PhysRevLett.119.192501

The shell model constitutes one of the main building blocks of our understanding of nuclear structure. Its robustness is well proven for nuclei close to the valley of stability, where it successfully predicts and explains the occurrence of magic numbers [1,2]. However, these magic numbers are not universal throughout the nuclear chart and their evolution far from stability, observed experimentally over the last decades, has generated much interest [3]. For example, the magic numbers $N = 20$ and 28 may disappear [4–7] while new magic numbers arise at $N = 14$, 16 and 32, 34, respectively [8–13]. Although shell gaps, defined within a given theoretical framework as differences of effective single-particle energies (ESPE), are not observables [14], they are useful quantities to assess the underlying structure of nuclei [15–17]. The nuclear potential acting on nuclei far from stability can induce drifts of the single-particle orbitals and their behavior as a function of isospin can be understood within the shell model [18–22]. Difficulties arise, however, when the single-particle properties are masked by correlations that stem from residual interactions and discriminating between the two effects is nontrivial.

In the shell model as it was initially formulated, the proton $\pi f_{7/2}$ orbital separates from the $3\hbar\omega$ harmonic oscillator shell because of the spin-orbit splitting and forms the $Z = 28$ gap. The neutron $\nu g_{9/2}$ orbital splits off from the $4\hbar\omega$ shell to join the $3\hbar\omega$ orbits and creates a magic number at $N = 50$. With 28 protons and 50 neutrons, the ^{78}Ni nucleus is thus expected to be one of the most neutron-rich doubly magic nuclei, making it of great interest for nuclear structure. Up to now, no evidence has been found for the disappearance of the shell closures at $Z = 28$

and $N = 50$, even if recent studies hint at a possible weakening of the $N=50$ magic number below ^{78}Ni [23,24]. On the contrary, the half-life of ^{78}Ni was determined at 122.2(5.1) ms, suggesting a survival of magicity [25], and calculations predict a first excited state in ^{78}Ni above 2 MeV [24,26–28]. But so far no other information about ^{78}Ni is available, with the exception of indirect ones such as the mass of ^{79}Cu, measured recently [29].

The size of the $Z = 28$ gap might be affected by a drift of the single-particle energies. When adding neutrons in the $\nu g_{9/2}$ orbital above the $N = 40$ subshell gap, there is a sudden decrease of the energy of the first $5/2^-$ excited state relative to the $3/2^-$ ground state in ^{71,73}Cu, which was established from β decay [30]. The subsequent inversion of these two states in ^{75}Cu was evidenced from collinear laser spectroscopy [31]. Theoretically, these $3/2^-$ and $5/2^-$ levels are linked through the main components in their respective wave functions with the $p_{3/2}$ and $f_{5/2}$ proton single-particle states [18,32,33].

The behavior of the $\pi f_{7/2}$ spin-orbit partner is more difficult to determine. This orbital is of primary importance as it is one of the two orbitals defining the $Z = 28$ gap. Access to this hole state is possible through proton transfer or knockout reactions [34]. While spectroscopic factors extracted in proton pickup reactions allow in principle for the measurement of strength functions, it is a challenge to identify the smallest components or those that are situated at high excitation energy. Moreover, away from the valley of stability, the resort to inverse kinematics with radioactive ion beams limits the count rate as well as the resolution that can be achieved. Today, data are available for the ^{70}Zn$(d,{}^3$He$)^{69}$Cu [35,36] and ^{72}Zn$(d,{}^3$He$)^{71}$Cu [37] reactions, on both sides of the $N = 40$ subshell gap. The measured part of the $\pi f_{7/2}^{-1}$ centroid was seen to remain at 3.8 MeV in ^{71}Cu, compared to a lower limit of 2.45 MeV in ^{69}Cu. While it is not possible to clarify in what direction or to what extent the energy of the centroid shifts, it remains sufficiently high and the $Z = 28$ gap does not appear to be appreciably affected.

In this Letter we report on our measurement of the proton knockout of ^{80}Zn into ^{79}Cu, at $N = 50$. The reaction mechanism favors proton hole states, including the $\pi f_{7/2}^{-1}$ one. It sheds the first light on the evolution of nuclear structure in the most neutron-rich copper isotopes available today, in the close vicinity of ^{78}Ni.

The experiment was performed at the Radioactive Isotope Beam Factory (RIBF), operated jointly by the RIKEN Nishina Center and the Center for Nuclear Study of the University of Tokyo. A ^{238}U beam with an energy of 345 MeV per nucleon and an average intensity of 12 pnA was sent on a 3-mm thick ^{9}Be target for in-flight fission. The secondary ^{80}Zn beam was selected in the BigRIPS separator [38]. A secondary target was placed at the end of BigRIPS. The isotopes before and after the secondary target were identified on an event-by-event basis in the BigRIPS and ZeroDegree spectrometers, respectively, with the TOF-$B\rho$-ΔE method [39]. The average ^{80}Zn intensity was 260 particles per second. The detector setup installed between the two spectrometers was composed of the MINOS device [40] mounted inside the DALI2 γ-ray multidetector [41]. MINOS consists of a liquid-hydrogen target surrounded by a cylindrical time-projection chamber (TPC). The target was 102(1) mm long with a density of 70.97 kg/m^3. The energy of the isotopes was 270 and 180 MeV per nucleon at the entrance and exit of MINOS, respectively. The ^{79}Cu nucleus was produced mainly through proton knockout from the incoming ^{80}Zn isotopes, the $(p,3p)$ channel from ^{81}Ga contributing to only 8%. The emitted protons were tracked in the TPC, while the beam trajectory was given by two parallel-plate avalanche counters [42] before the target. For the events with at least one proton detected in the TPC, this ensured the reconstruction of the interaction-vertex position with 95% efficiency and a 5-mm uncertainty (full width at half maximum) along the beam axis. The DALI2 array consists of 186 NaI scintillator crystals that were calibrated with ^{60}Co, ^{137}Cs, and ^{88}Y sources. When several crystals separated by no more than 15 cm were hit by γ rays, the energies were summed before Doppler correction and the event was considered as one single γ ray, a method known as add back. The photopeak

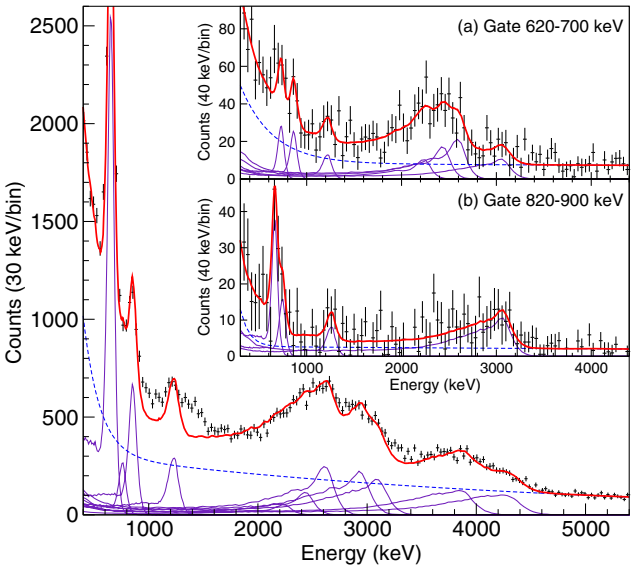

FIG. 1. γ-ray spectrum of ^{80}Zn$(p,2p)^{79}$Cu after Doppler correction, with multiplicities below 4. The experimental data points are in black, with the double-exponential background as the blue dashed line, the simulated response function of each transition in purple, and the sum of the simulated response functions with the background in red. Discrepancies between the data and the fit are due to nonidentified transitions (see text). The inset shows γ-γ coincidences after background subtraction for a gate set on the 656-keV [subpanel (a)] and 855-keV [subpanel (b)] transitions.

detection efficiency with add back was 27% and the energy resolution was $\sigma = 45$ keV for a 1 MeV transition emitted in flight at 250 MeV per nucleon.

The γ-ray spectrum obtained for ^{80}Zn$(p,2p)^{79}$Cu after Doppler correction is shown in Fig. 1. Two clear transitions were found at 656(5) and 855(6) keV, while three structures were seen in the ranges 1.0–1.5 MeV, 2.0–3.4 MeV, and 3.4–4.5 MeV. γ-γ coincidences with background subtraction were performed, gating on the 656- and 855-keV transitions. The corresponding coincidence spectra are shown in the insets of Fig. 1. Seven transitions are observed when a gate is set around 656 keV: 750(20), 860(10), 1220(30), 2240(40), 2440(40), 2600(40), and 3070(30) keV. When a gate is set around 855 keV, peaks at 660(20), 760(30), 1250(30), and 3050(30) keV are seen. Three other γ rays were found at 2940(60), 3880(40), and 4300(40) keV with no coincidence with any other transition. All transitions observed are listed in Table I. The uncertainties on the energies were obtained by adding quadratically calibration (5 keV) and statistical uncertainties.

The response functions of DALI2 for all transitions were obtained from Geant4 simulations [43], taking into account the measured intrinsic resolution of each crystal. While the simulated efficiency agreed within 5% with measurements made with sources and solid targets in previous experiments, we allowed for a larger margin of 10% to account for the thick liquid target that was used here. The ^{79}Cu spectrum was fitted with these response functions as well as with a background composed of two exponential functions, as shown in Fig. 1, in order to obtain the intensity of each transition. The structure between 3.4 and 4.5 MeV is well fitted, while discrepancies are observed for the two other structures, mainly between 1.0 and 1.5 MeV. This indicates that other transitions are present in the spectrum. The uncertainties on the intensities in Table I have been estimated by taking into account these discrepancies.

TABLE I. Transitions seen in the ^{80}Zn$(p,2p)^{79}$Cu spectrum. Intensities are normalized with respect to the intensity of the 656-keV transition, and take into account all multiplicities.

Energy (keV)	Intensity (relative)
656(5)[b]	100(11)
750(20)[a,b]	9(2)
855(6)[a]	33(4)
1220(30)[a,b]	16(4)
2240(40)[a]	4(2)
2440(40)[a]	21(3)
2600(40)[a]	40(7)
2940(60)	33(6)
3070(30)[a,b]	28(6)
3880(40)	34(4)
4300(40)	31(4)

[a]Transitions observed in the γ-γ spectrum when gating on the 656-keV transition.
[b]Transitions observed in the γ-γ spectrum when gating on the 855-keV transition.

The level scheme for ^{79}Cu, based on the intensities of the transitions and the γ-γ coincidences, is shown in Fig. 2. Considering the intensities of the 656- and 855-keV transitions, the latter is placed on top of the former. No γ transition was seen below 656 keV, while it was possible elsewhere in the data set to detect peaks down to 200 keV. We place the first excited state of ^{79}Cu at 656(5) keV and the second one at 1511(8) keV. A direct decay of the 1511-keV level to the ground state cannot be excluded but has not been observed: by fitting the spectrum, a limit can be put that is equal to one third of the intensity of the 855-keV transition. The 750-, 1220-, and 3070-keV transitions, found in coincidence with both the 656- and 855-keV ones, are placed on top of the 1511-keV level. This gives three levels at 2260(20), 2730(30), and 4580(30) keV, respectively. The 2260- and 2730-keV levels are shown as dashed lines because we cannot exclude the coincidence of the 750- and 1220-keV transitions with other γ rays due to low statistics.

No information about the half-lives of levels was available and therefore we considered all decays to be prompt. A half-life of several tens of picoseconds could change the energy by a few percent, but it would not affect the placement of the transitions in the scheme. For example, a 100 ps half-life corresponds to an offset of 24 keV for a 656-keV transition.

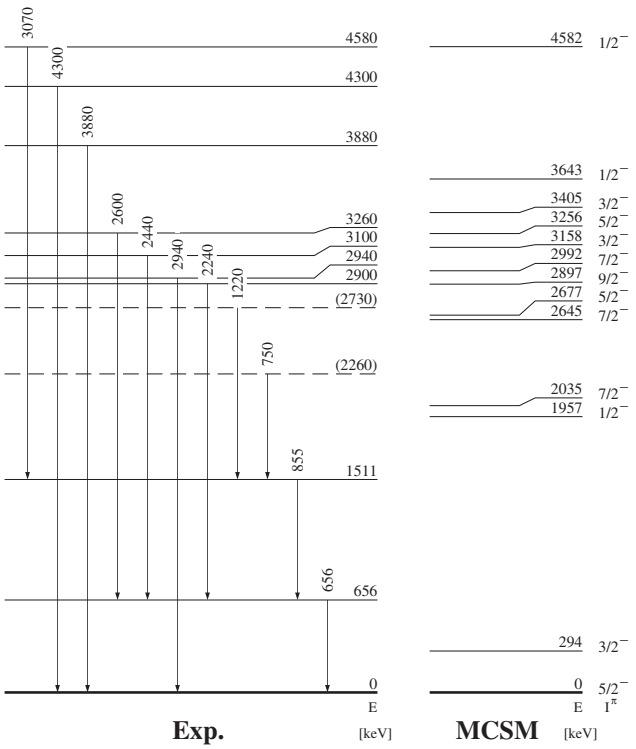

FIG. 2. Proposed level scheme for ^{79}Cu. The experimental results (left) are compared to Monte Carlo shell-model (MCSM) calculations (right).

TABLE II. Occupation numbers of proton orbits and spectroscopic factors (SF) for the lowest and the three first $7/2^-$ calculated states in ^{79}Cu, as well as for the ground state of ^{80}Zn.

	E (MeV)	J^π	$f_{7/2}$	$f_{5/2}$	$p_{3/2}$	$p_{1/2}$	$g_{9/2}$	$d_{5/2}$	SF
^{79}Cu	0	$5/2^-$	7.73	1.05	0.15	0.02	0.03	0.01	1.33
	0.294	$3/2^-$	7.73	0.17	1.02	0.03	0.04	0.01	0.57
	1.957	$1/2^-$	7.57	0.48	0.29	0.62	0.03	0.01	0.04
	2.035	$7/2^-$	6.82	1.49	0.57	0.04	0.07	0.01	5.58
	2.645	$7/2^-$	7.22	1.09	0.61	0.03	0.04	0.01	0.15
	2.992	$7/2^-$	7.54	1.00	0.37	0.05	0.03	0.00	0.43
^{80}Zn	0	0^+	7.66	1.43	0.73	0.06	0.10	0.01	—

Monte Carlo shell-model (MCSM) calculations were carried out in the $pfg_{9/2}d_{5/2}$ model space of protons and neutrons with an A3DA Hamiltonian [27]. Previous results are reproduced within this theoretical framework, like the structure of ^{80,82}Zn [44] and ^{77}Cu [45]. Calculated occupation numbers of proton orbits for the wave functions of the ground state of ^{80}Zn as well as for the lowest calculated states in ^{79}Cu are given in Table II. Spectroscopic factors, corresponding to the overlap between the initial (^{80}Zn) and final (^{79}Cu) wave functions, are also given. The ground state of ^{80}Zn is characterized by a proton component that is distributed over the $\pi f_{5/2}$ and $\pi p_{3/2}$ orbitals. The unpaired proton in ^{79}Cu, after one-proton removal from ^{80}Zn, is expected to reside mainly in the pf orbitals and therefore generates negative-parity final states.

We propose a $5/2^-$ spin for the ground state of ^{79}Cu and a $3/2^-$ spin for the first excited state at 656 keV from the systematics of the copper isotopic chain, as shown in Fig. 3, as well as the systematics of the $N = 50$ isotonic chain above ^{79}Cu [48,49]. The present MCSM calculations support this conclusion. The calculated wave functions for the lowest $5/2^-$ and $3/2^-$ states correspond closely to those of the $\pi f_{5/2}$ (75.3%) and $\pi p_{3/2}$ (74.2%) single-particle states, respectively. From the comparison with ^{77}Cu

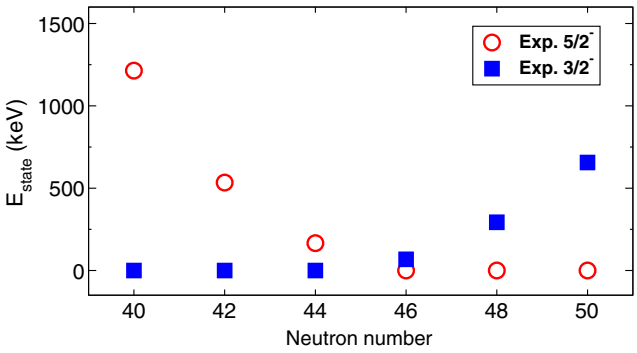

FIG. 3. Systematics of the first $3/2^-$ and $5/2^-$ states in copper isotopes. Data taken from Refs. [30,31,35,45–47] and this work. The error bars are smaller than the data points.

[45,46], the $3/2^-$ level is seen to rise and illustrates the continuation of the inversion of the $\pi p_{3/2}$ and $\pi f_{5/2}$ orbitals that is known from the preceding copper isotopes.

For the second excited state at 1511 keV, the calculation offers two possibilities: a $1/2^-$ state at 1957 keV, with 48.3% $\pi p_{1/2}$ single-particle character, or a $7/2^-$ state at 2035 keV, whose 64.1% of the wave function is built from a $\pi f_{7/2}^{-1}$ hole and two protons in $\pi f_{5/2}p_{3/2}$. The absence of direct feeding in the knockout reaction disfavors the $7/2^-$ assignment, for which the calculated spectroscopic factor is high. Comparing the transition strengths for $1/2^-$ and $7/2^-$ spins obtained from calculated $B(M1)$ and $B(E2)$ values and experimental energies, we find that the ratio $\lambda(1/2_1^- \to 5/2_{gs}^-)/\lambda(1/2_1^- \to 3/2_1^-)$ equals 3.2 while $\lambda(7/2_1^- \to 5/2_{gs}^-)/\lambda(7/2_1^- \to 3/2_1^-)$ is 427, so we would expect the 1511-keV transition to be stronger than the 855-keV one. We do not see a 1511-keV transition to the ground state because of the limited resolution, but we can put an upper limit of 10(2) for its intensity compared to 33(4) for the 855-keV one, namely, a ratio of 0.30(7). This is closer to the expected value for $1/2^-$ than for $7/2^-$. If this level is a $1/2^-$ state, the low ratio of 0.30(7) would rather support a $\pi p_{1/2}$ single-particle nature for this state, unlike the strongly collective $1/2^-$ state seen at low energy in ^{69,71,73,75}Cu [47,50].

The multiplet of states between 2.7 and 3.3 MeV is interpreted as the coupling of a proton in the $\pi f_{5/2}$ or $\pi p_{3/2}$ orbital with the first 2^+ state of ^{78}Ni, in agreement with the present MCSM calculations for which all calculated states shown above 2.6 MeV are core-coupling states. We can therefore estimate the first 2^+ state of ^{78}Ni at about 3 MeV excitation energy, in accordance with the MCSM calculations and other theoretical studies [24,26–28]. Such a 3-MeV 2_1^+ state in ^{78}Ni, compared to 992 keV in ^{76}Ni [51], indicates a good shell closure at $N = 50$.

In the experimental level scheme, we find that the knockout of a proton results in a final nucleus at high excitation energy, populating several configurations. Because of the structure of the wave function of the ^{80}Zn ground state, we may expect the reaction to populate the $\pi f_{7/2}^{-1}f_{5/2}^2$ hole but also the $\pi f_{7/2}^{-1}f_{5/2}p_{3/2}$ and $\pi f_{7/2}^{-1}p_{3/2}^2$ configurations. The $\pi f_{7/2}^{-1}$ single-particle wave function will mix with the $7/2^-$ members of the $\pi(f_{5/2}, p_{3/2}) \otimes 2^+$ multiplets, resulting in a fragmentation of the strength over several levels. We have no evidence for a strongly fed $7/2^-$ state below 2.2 MeV and we conclude on the absence of a significant part of the $\pi f_{7/2}^{-1}$ strength below this energy.

Concerning cross sections, we determined an inclusive cross section of 7.9(4) mb for the ^{80}Zn$(p, 2p)^{79}$Cu reaction, but reliable exclusive cross sections could not be extracted as the feeding ratio of each level could be affected by nonobserved transitions between high-energy levels. Only an upper limit of 3.8(8) mb for the ground state and a small

value of 0.04(29) mb for the first excited state were found, leaving at least 4.1(9) mb that will mainly belong to states that in their wave function contain a hole in the $\pi f_{7/2}$ orbital. Theoretical single-particle cross sections were calculated using the distorted-wave impulse approximation (DWIA) framework [52] and averaged along the thick target, the beam energy decreasing from 270 to 180 MeV per nucleon. The optical potentials for the incoming proton and the outgoing two protons are obtained by a microscopic framework; the Melbourne nucleon-nucleon G-matrix interaction [53] is folded by a nuclear density calculated with the Bohr-Mottelson single-particle potential [54]. For the ground state, the low-lying $\pi p_{3/2}$ state and the knockout of a $f_{7/2}$ proton, we obtained 2.1, 2.6, and 2.3 mb, respectively, and these numbers should be multiplied by the corresponding spectroscopic factors from the MCSM given in Table II. We did not identify a strongly populated $7/2^-$ state; our observation shows more fragmentation of the single-particle strength than predicted. Although this could be partly explained by the existence of unobserved γ rays, it is also possible that a part of the $\pi f_{7/2}^{-1}$ strength lies above the neutron-separation threshold. Somewhat discrepant with the presented shell-model calculations, this main result calls for further experimental and theoretical investigations.

The $Z = 28$ gap corresponds to the $\pi f_{5/2} f_{7/2}$ ESPE splitting, as the $\pi p_{3/2}$ and $\pi f_{5/2}$ orbitals are inverted and the MCSM calculations put it at 4.9 MeV. Experimentally, we found a lower limit of 2.2 MeV for the $\pi f_{7/2}^{-1}$ hole strength. Even if the latter cannot be directly related to the ESPE because of model-dependent correlations, both experiment and theory show that although the orbital content of the $Z = 28$ gap is changing along the copper isotopic chain, its magicity persists. Therefore, ^{79}Cu can be described as a ^{78}Ni core plus a valence proton. This is in line with the depiction of ^{80}Zn as two-proton configurations with a ^{78}Ni core [44].

In conclusion, we performed the first spectroscopy of ^{79}Cu and compared the results with MCSM calculations. These calculations show the restoration of the single-particle nature of the low-lying states, which is supported by the experiment. There is no significant knockout feeding to the excited states below 2.2 MeV, indicating that the $Z = 28$ gap remains large. The ability to describe the ^{79}Cu nucleus as a valence proton outside a ^{78}Ni core presents us with indirect evidence of the magic character of the latter. Spectroscopy and mass measurement of ^{78}Ni are the next steps for a direct proof of its double magicity.

The authors are thankful to the RIBF and BigRIPS teams for the stable operation and high intensity of the uranium primary beam, and production of secondary beams during the experiment. The development of MINOS and the core MINOS team have been supported by the European Research Council through the ERC Grant No. MINOS-258567. A. O. was supported by JSPS long-term fellowship L-13520 from September 2013 to June 2014 at the RIKEN Nishina Center. A. O. deeply thanks the ERC and JSPS for their support. C. S. was supported by the IPA program at the RIKEN Nishina Center. A. O. and C. S. are grateful to the RIKEN Nishina Center for its hospitality. This work was supported by JSPS Grant-in-Aid for a JSPS Research Fellow (No. 268718). The MCSM calculations were performed on the K computer at RIKEN AICS (hp150224, hp160211). This work was supported in part by the HPCI Strategic Program ("The Origin of Matter and the Universe") and the "Priority Issue on Post-K computer" ("Elucidation of the Fundamental Laws and Evolution of the Universe") from MEXT and JICFuS. Z. D. and Z. V. were supported by the GINOP-2.3.3-15-2016-00034 contract. L. X. C. would like to thank MOST for its support. M. L. and V. W. acknowledge the German BMBF with the supporting No. 05P15RDFN1 and No. 05P12RDFN8. We thank N. Paul for her careful reading of the Letter.

*Present address: Helmholtz Institute Mainz, 55099 Mainz, Germany and GSI Helmholtzzentrum für Schwerionenforschung, 64291 Darmstadt, Germany.
†Present address: CSNSM, IN2P3-CNRS, Université Paris-Sud, Université Paris-Saclay, 91406 Orsay Cedex, France.

[1] M. Goeppert-Meyer, Phys. Rev. **75**, 1969 (1949).
[2] O. Haxel, J. H. D. Jensen, and H. E. Suess, Phys. Rev. **75**, 1766 (1949).
[3] O. Sorlin and M.-G. Porquet, Prog. Part. Nucl. Phys. **61**, 602 (2008).
[4] D. Guillemaud-Mueller, C. Detraz, M. Langevin, F. Naulin, M. de Saint-Simon, C. Thibault, F. Touchard, and M. Epherre, Nucl. Phys. **A426**, 37 (1984).
[5] T. Motobayashi *et al.*, Phys. Lett. B **346**, 9 (1995).
[6] C. M. Campbell *et al.*, Phys. Rev. Lett. **97**, 112501 (2006).
[7] B. Bastin *et al.*, Phys. Rev. Lett. **99**, 022503 (2007).
[8] A. Huck, G. Klotz, A. Knipper, C. Miehe, C. Richard-Serre, G. Walter, A. Poves, H. L. Ravn, and G. Marguier, Phys. Rev. C **31**, 2226 (1985).
[9] P. G. Thirolf *et al.*, Phys. Lett. B **485**, 16 (2000).
[10] E. Becheva *et al.*, Phys. Rev. Lett. **96**, 012501 (2006).
[11] A. Gade *et al.*, Phys. Rev. C **74**, 021302(R) (2006).
[12] C. R. Hoffman *et al.*, Phys. Lett. B **672**, 17 (2009).
[13] D. Steppenbeck *et al.*, Nature (London) **502**, 207 (2013).
[14] T. Duguet, H. Hergert, J. D. Holt, and V. Somà, Phys. Rev. C **92**, 034313 (2015).
[15] A. Poves and A. Zuker, Phys. Rep. **70**, 235 (1981).
[16] T. Otsuka, R. Fujimoto, Y. Utsuno, B. A. Brown, M. Honma, and T. Mizusaki, Phys. Rev. Lett. **87**, 082502 (2001).
[17] E. Caurier, G. Martínez-Pinedo, F. Nowacki, A. Poves, and A. P. Zuker, Rev. Mod. Phys. **77**, 427 (2005).

[18] T. Otsuka, T. Suzuki, R. Fujimoto, H. Grawe, and Y. Akaishi, Phys. Rev. Lett. **95**, 232502 (2005).
[19] T. Otsuka, T. Suzuki, M. Honma, Y. Utsuno, N. Tsunoda, K. Tsukiyama, and M. Hjorth-Jensen, Phys. Rev. Lett. **104**, 012501 (2010).
[20] N. A. Smirnova, B. Bally, K. Heyde, F. Nowacki, and K. Sieja, Phys. Lett. B **686**, 109 (2010).
[21] T. Otsuka, Phys. Scr. **T152**, 014007 (2013).
[22] T. Otsuka and Y. Tsunoda, J. Phys. G **43**, 024009 (2016).
[23] C. Santamaria *et al.*, Phys. Rev. Lett. **115**, 192501 (2015).
[24] F. Nowacki, A. Poves, E. Caurier, and B. Bounthong, Phys. Rev. Lett. **117**, 272501 (2016).
[25] Z. Y. Xu *et al.*, Phys. Rev. Lett. **113**, 032505 (2014).
[26] K. Sieja and F. Nowacki, Phys. Rev. C **85**, 051301(R) (2012).
[27] Y. Tsunoda, T. Otsuka, N. Shimizu, M. Honma, and Y. Utsuno, Phys. Rev. C **89**, 031301(R) (2014).
[28] G. Hagen, G. R. Jansen, and T. Papenbrock, Phys. Rev. Lett. **117**, 172501 (2016).
[29] A. Welker *et al.*, following Letter, Phys. Rev. Lett. **119**, 192502 (2017).
[30] S. Franchoo, M. Huyse, K. Kruglov, Y. Kudryavtsev, W. F. Mueller, R. Raabe, I. Reusen, P. Van Duppen, J. Van Roosbroeck, L. Vermeeren, A. Wohr, and K. L. Kratz, B. Pfeiffer, and W. B. Walters, Phys. Rev. Lett. **81**, 3100 (1998).
[31] K. T. Flanagan *et al.*, Phys. Rev. Lett. **103**, 142501 (2009).
[32] N. A. Smirnova, A. De Maesschalck, A. Van Dyck, and K. Heyde, Phys. Rev. C **69**, 044306 (2004).
[33] K. Sieja and F. Nowacki, Phys. Rev. C **81**, 061303(R) (2010).
[34] P. G. Hansen and J. A. Tostevin, Annu. Rev. Nucl. Part. Sci. **53**, 219 (2003).
[35] B. Zeidman and J. A. Nolen, Phys. Rev. C **18**, 2122 (1978).
[36] P. Morfouace *et al.*, Phys. Rev. C **93**, 064308 (2016).
[37] P. Morfouace *et al.*, Phys. Lett. B **751**, 306 (2015).
[38] T. Kubo *et al.*, Prog. Theor. Exp. Phys. **2012**, 03C003 (2012).
[39] N. Fukuda, T. Kubo, T. Ohnishi, N. Inabe, H. Takeda, D. Kameda, and H. Suzuki, Nucl. Instrum. Methods Phys. Res., Sect. B **317**, 323 (2013).
[40] A. Obertelli *et al.*, Eur. Phys. J. A **50**, 8 (2014).
[41] S. Takeuchi, T. Motobayashi, Y. Togano, M. Matsushita, N. Aoi, K. Demichi, H. Hasegawa, and H. Murakami, Nucl. Instrum. Methods Phys. Res., Sect. A **763**, 596 (2014).
[42] H. Kumagai, A. Ozawa, N. Fukuda, K. Sümmerer, and I. Tanihata, Nucl. Instrum. Methods Phys. Res., Sect. A **470**, 562 (2001).
[43] S. Agostinelli *et al.*, Nucl. Instrum. Methods Phys. Res., Sect. A **506**, 250 (2003).
[44] Y. Shiga *et al.*, Phys. Rev. C **93**, 024320 (2016).
[45] E. Sahin *et al.*, Phys. Rev. Lett. **118**, 242502 (2017).
[46] U. Köster, N. J. Stone, K. T. Flanagan, J. R. Stone, V. N. Fedosseev, K. L. Kratz, B. A. Marsh, T. Materna, L. Mathieu, P. L. Molkanov, M. D. Seliverstov, O. Serot, A. M. Sjödin, and Y. M. Volkov, Phys. Rev. C **84**, 034320 (2011).
[47] C. Petrone, J. M. Daugas, G. S. Simpson, M. Stanoiu, C. Plaisir, T. Faul, C. Borcea, R. Borcea, L. Caceres, S. Calinescu, R. Chevrier, L. Gaudefroy, G. Georgiev, G. Gey, O. Kamalou, F. Negoita, F. Rotaru, O. Sorlin, and J. C. Thomas, Phys. Rev. C **94**, 024319 (2016).
[48] D. Verney, F. Ibrahim, C. Bourgeois, S. Essabaa, S. Gales, L. Gaudefroy, D. Guillemaud-Mueller, F. Hammache, C. Lau, F. LeBlanc, A. C. Mueller, O. Perru, F. Pougheon, B. Roussiere, J. Sauvage, and O. Sorlin, Phys. Rev. C **76**, 054312 (2007).
[49] B. Cheal *et al.*, Phys. Rev. Lett. **104**, 252502 (2010).
[50] I. Stefanescu *et al.*, Phys. Rev. Lett. **100**, 112502 (2008).
[51] C. Mazzocchi *et al.*, Phys. Lett. B **622**, 45 (2005).
[52] T. Wakasa, K. Ogata, and T. Noro, Prog. Part. Nucl. Phys. **96**, 32 (2017).
[53] K. Amos, P. J. Dortmans, H. V. von Geramb, S. Karataglidis, and J. Raynal, Adv. Nucl. Phys. **25**, 276 (2000).
[54] A. Bohr and B. R. Mottelson, *Nuclear Structure* (Benjamin, New York, 1969), Vol. I.

Erratum: Persistence of the $Z = 28$ Shell Gap Around ^{78}Ni: First Spectroscopy of ^{79}Cu [Phys. Rev. Lett. 119, 192501 (2017)]

L. Olivier, S. Franchoo, M. Niikura, Z. Vajta, D. Sohler, P. Doornenbal, A. Obertelli, Y. Tsunoda, T. Otsuka, G. Authelet, H. Baba, D. Calvet, F. Château, A. Corsi, A. Delbart, J.-M. Gheller, A. Gillibert, T. Isobe, V. Lapoux, M. Matsushita, S. Momiyama, T. Motobayashi, H. Otsu, C. Péron, A. Peyaud, E. C. Pollacco, J.-Y. Roussé, H. Sakurai, C. Santamaria, M. Sasano, Y. Shiga, S. Takeuchi, R. Taniuchi, T. Uesaka, H. Wang, K. Yoneda, F. Browne, L. X. Chung, Z. Dombradi, F. Flavigny, F. Giacoppo, A. Gottardo, K. Hadyńska-Klęk, Z. Korkulu, S. Koyama, Y. Kubota, J. Lee, M. Lettmann, C. Louchart, R. Lozeva, K. Matsui, T. Miyazaki, S. Nishimura, K. Ogata, S. Ota, Z. Patel, E. Sahin, C. Shand, P.-A. Söderström, I. Stefan, D. Steppenbeck, T. Sumikama, D. Suzuki, V. Werner, J. Wu, and Z. Xu

(Received 6 August 2018; published 31 August 2018)

DOI: 10.1103/PhysRevLett.121.099902

In this Letter, we presented experimental inclusive and exclusive cross sections for the $^{80}\mathrm{Zn}(p, 2p)^{79}\mathrm{Cu}$ reaction and compared them to theoretical single-particle cross sections that were calculated within the distorted-wave impulse approximation (DWIA) [1]. For the ground state, the low-lying $\pi p_{3/2}$ state and the knockout of a $f_{7/2}$ proton, these numbers were to be multiplied by the corresponding spectroscopic factors from the Monte Carlo shell model [2] to yield the total theoretical cross section.

By considering the treatment of two identical protons, the total (p, p) cross section σ_{pp} is defined by a differential cross section $d\sigma_{pp}/d\Omega$ integrated over the solid angle Ω and divided by two. The triple differential cross section (TDX) $d^3\sigma_{p2p}/dE_1 d\Omega_1 d\Omega_2$, where E_1 (Ω_1) is the energy (solid angle) of one outgoing proton and Ω_2 is the solid angle of the other proton, corresponds to $d\sigma_{pp}/d\Omega$ specified by the kinematics of the incoming proton and the outgoing protons, taking into account distortion effects, momentum distribution of the nucleon inside a target, and a phase space factor. The $(p, 2p)$ cross section σ_{p2p} is then defined by the TDX integrated over E_1, Ω_1, and Ω_2, divided by two. Since we counted the number of events in which two protons are detected to evaluate σ_{p2p}, the theoretical values that we reported in this Letter should accordingly be divided by two for all single-particle configurations.

The DWIA transition matrix was furthermore evaluated with a better numerical accuracy. For the ground state, the low-lying $\pi p_{3/2}$ state, and the knockout of a $f_{7/2}$ proton, the single-particle cross sections become 1.0, 1.3, and 1.1 mb, respectively. They depend only weakly on the excitation energy. Multiplied by the theoretical spectroscopic factors, a total cross section of 9.3 mb can be obtained compared to the measurement of 7.9(4) mb. The result does not affect the conclusions of this Letter, but it shows that there is good agreement between experiment and theory since the amount of correlations that are incorporated in the shell-model calculation and that reduce the theoretical cross section are better taken care of than we found initially.

[1] T. Wakasa, K. Ogata, and T. Noro, Prog. Part. Nucl. Phys. **96**, 32 (2017).
[2] Y. Tsunoda, T. Otsuka, N. Shimizu, M. Honma, and Y. Utsuno, Phys. Rev. C **89**, 031301(R) (2014).

Etudier le noyau atomique du cuivre, pour mieux comprendre le nickel

09 janvier 2018

RÉSULTATS SCIENTIFIQUES PHYSIQUE NUCLÉAIRE

Deux nouvelles études menées par des équipes internationales où sont impliqués l'Institut de physique nucléaire d'Orsay (IPNO, CNRS/Université Paris-Sud), le Centre de sciences nucléaires et de sciences de la matière (CSNSM, CNRS/Université Paris-Sud) et l'Institut pluridisciplinaire Hubert Curien (IPHC, CNRS/Université de Strasbourg), indiquent que le nickel-78 est probablement un noyau doublement magique. Cette découverte éclaire notre connaissance de la structure de ce noyau très riche en neutrons intervenant notamment dans la nucléosynthèse stellaire.

Les noyaux doublement magiques [1] ont une stabilité accrue grâce aux couches énergétiques remplies. Ces noyaux particuliers sont des points de repère dans le modèle en couches de la structure nucléaire. Parmi eux, le nickel-78 est l'un des plus riches en neutrons connu à ce jour. Mais compte tenu de sa richesse en neutrons (50 par rapport aux 28 protons), les physiciens s'attendaient à ce que sa structure diffère de celle de ses cousins eux aussi magiques mais proche de la stabilité (le nickel stable le plus proche contient entre 14 et 20 neutrons de moins).

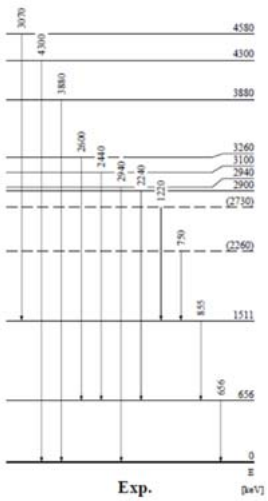

Etats excités du 79Cu © DR

Cette différence soulève une des plus grandes questions de la physique nucléaire aujourd'hui : les propriétés des noyaux magiques s'appliquent-elles à des noyaux aussi exotiques ? Une interrogation d'autant plus légitime, puisqu'il a été montré que pour certains noyaux plus légers,

comme le magnesium-32 (12 protons et 20 neutrons) ou encore le silicium-42 (14 protons et 28 neutrons), les nombres magiques de neutrons ne permettent pas de préserver leurs formes sphériques.

Une étude indirecte du nickel-78 via le cuivre-79, avec un proton de plus

Pour répondre à cette question, deux approches, remarquables pour leur complémentarité, ont été utilisées : une avec les ions ralentis et l'autre avec un faisceau relativiste.

Une équipe internationale à laquelle participe le CSNSM a mesuré avec une très grande précision la masse du noyau du cuivre-79, avec le spectromètre Isoltrap installé au Cern. Tandis qu'une autre équipe internationale dont l'IPNO fait partie a réalisé le premier spectre d'excitation du cuivre-79 à l'aide d'une réaction *knock-out* avec protons au RIKEN, au Japon.

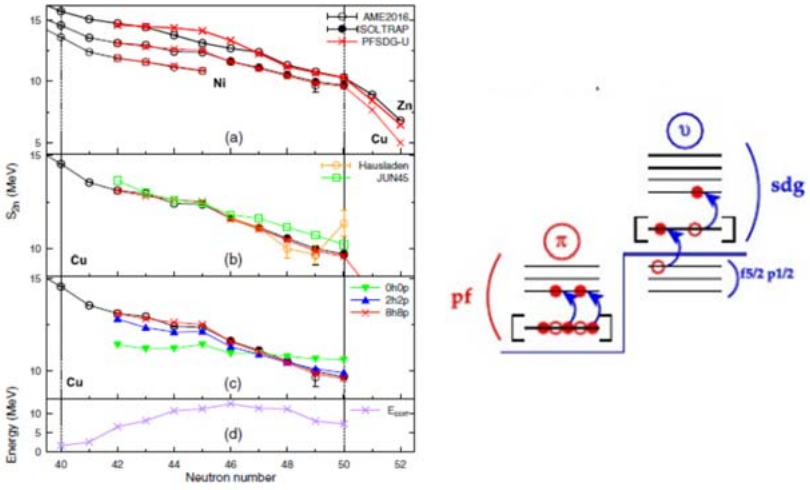

À gauche : masses comparées des différents isotopes du nickel et du cuivre. À droite : schéma de remplissage des couches énergétiques selon le modèle PFSDG-U © DR

Afin d'interpréter les résultats de ces deux mesures, des calculs théoriques ont été développés à la fois en France à Strasbourg et à l'Université de Tokyo. Une collaboration entre l'IPHC et l'université de Madrid a permis de révéler la structure "duale" du nickel-78 comme à la fois doublement magique mais avec des modes d'excitations faciles (proches en énergie). L'étude théorique menée par l'université de Tokyo s'est appuyée sur le modèle en couches "Monte-Carlo" effectué sur le super-ordinateur K [2] au RIKEN. Il ressort de cette étude que le noyau du 79-Cu peut être interprété d'une façon simple comme un seul proton de valence autour d'un cœur bien doublement magique de nickel-78 – en accord avec les résultats obtenus à Strasbourg.

Même si le nickel-78 n'est pas tout à fait sphérique, comme les autres noyaux doublement magiques, sa déformation reste très faible. Il semblerait que l'interaction tensorielle, qui dicte le comportement des noyaux plus légers, cède à l'interaction spin-orbite [3] pour les noyaux de masse intermédiaire.

Ces deux méthodes d'études indirectes fournissent des indices que le nickel-78 garderait ses propriétés de noyau doublement magique. Ce résultat renforce notre connaissance des noyaux riches en neutrons situés sur les chemins des processus de nucléosynthèse stellaire.

Pour en savoir plus

- L'article de la spectroscopie à RIKEN avec l'IPNO (en anglais)

- L'article de la collaboration ISOLTRAP avec le CSNSM et l'IPHC (en anglais)

Notes

1. Dans les années 1940, les physiciens et les physiciennes nucléaires constatent que les noyaux ayant un nombre de protons ou de neutrons égal à 2, 8, 20, 28, 50, 82 et 126 ont une énergie de liaison plus grande que celle de leurs voisins les plus proches. Autrement dit, ils sont beaucoup plus stables que tous les autres. De tels noyaux ont alors été appelés "noyau magique". Mais lorsque les nombres de neutrons et de protons correspondent aux chiffres cités plus haut, le noyau est dit "doublement magique" et sa stabilité est accrue.
2. Le K computer produit par Fujitsu au RIKEN, est un puissant superordinateur pouvant atteindre 10,51 pétaFLOPS.
3. L'interaction spin-orbite, qualifie toute interaction entre le spin d'une particule et son mouvement. En physique nucléaire elle est responsable des grandes caractéristiques du modèle en couches, en particulier les nombres magiques.

Contact

Serge Francho

Serge.Franchoo@cern.ch

David Lunney

david.lunney@csnsm.in2p3.fr

Frédéric Nowacki

frederic.nowacki@iphc.cnrs.fr

Bibliography

[Act18] Actualités de l'IN2P3 (Paris, 2018), available from https://in2p3.cnrs.fr/fr/cnrsinfo/etudier-le-noyau-atomique-du-cuivre-pour-mieux-comprendre-le-nickel

[Adr08] P. Adrich *et al.*, Physical Review C 77, 054306 (2008)

[Ajz81] F. Ajzenberg-Selove, R. Brown, E. Flynn, and J. Sunier, Physical Review C 24, 1762 (1981)

[Alk92] G. Alkhazov *et al.*, Nuclear Instruments and Methods in Physics Research B 69, 517 (1992)

[Ann92] R. Anne and A. Mueller, Nuclear Instruments and Methods in Physics Research B 70, 276 (1992)

[Aoi10] N. Aoi *et al.*, Physics Letters B 692, 302 (2010)

[Ari69] A. Arima, M. Harvey, and K. Shimizu, Physics Letters B 30, 517 (1969)

[Arm67] D. Armstrong, A. Blair, and H. Thomas, Physical Review 155, 1254 (1967)

[Aud06] G. Audi, International Journal of Mass Spectrometry 251, 85 (2006)

[Bac67] D. Bachner *et al.*, Nuclear Physics A 99, 487 (1967)

[Ban64] R. Bansal and J. French, Physics Letters 11, 145 (1964)

[Bar32a] J. Bartlett, Nature 130, 165 (1932)

[Bar32b] J. Bartlett, Physical Review 42, 145 (1932)

[Bas07] B. Bastin *et al.*, Physical Review Letters 99, 022503 (2007)

[Bau87] P. Baumann *et al.*, Physical Review C 36, 765 (1987)

[Bau89] P. Baumann *et al.*, Physics Letters B 228, 458 (1989)

[Bau07] T. Baumann *et al.*, Nature 449, 1022 (2007)

[Bel20] F. Bello Garrote *et al.*, Physical Review C 102, 034314 (2020)

[Ben15] G. Benzoni *et al.*, Physics Letters B 751, 107 (2015)

[Ber81] A. Bernstein, V. Brown and V. Madsen, Physics Letters B 103, 255 (1981)

[Ber82] M. Bernas *et al.*, Physics Letters B 113, 279 (1982)

[Bia10] L. Bianco *et al.*, Physics Letters B 690, 15 (2010)

[Bis16] M. Bissell *et al.*, Physical Review C 93, 064318 (2016)

[Bla65] A. Blair, Physical Review 140, B648 (1965)

[Bog02] S. Bogner, T. Kuo, L. Coraggio, A. Covello, and N. Itaco, Physical Review C 65, 051301 (2002)

[Boh53] A. Bohr and B. Mottelson, Matematisk-fysiske meddelelser Kongelige Danske Videnskabernes Selskab 27, 16 (1953)

[Bor03] I. Borzov, Physical Review C 67, 025802 (2003)

[Bor05] I. Borzov, Physical Review C 71, 065801 (2005)
[Bos88] U. Bosch *et al.*, Nuclear Physics A 477, 89 (1988)
[Bou87] J. Bounds *et al.*, Physical Review C 36, 2560 (1987)
[Bre60] M. Brennan and A. Bernstein, Physical Review 120, 927 (1960)
[Bri76] R. Britton and D. Watson, Nuclear Physics A 272, 91 (1976)
[Bro66] G. Brown and A. Green, Nuclear Physics 85, 87 (1966)
[Bro95] R. Broda *et al.*, Physical Review Letters 74, 868 (1995)
[Bro98] R. Broda *et al.*, in Proceedings of the International Conference on Fission and Properties of Neutron-Rich Nuclei, Sanibel Island, 1997, edited by J. Hamilton and A. Ramayya (World Scientific, Singapore, 1998), p. 202
[Bru77] P. Brussaard and P. Glaudemans, Shell-Model Applications in Nuclear Spectroscopy (North-Holland Publishing Company, Amsterdam, 1977)
[Bur14] G. Burgunder *et al.*, Physical Review Letters 112, 042502 (2014)
[Cam75] X. Campi, H. Flocard, A. Kerman, and S. Koonin, Nuclear Physics A 251, 193 (1975)
[Cas50] K. Case and A. Pais, Physical Review 80, 203 (1950)
[Cas63] H. Casimir, On the Interaction between Atomic Nuclei and Electrons (Freeman, San Francisco, 1963)
[Cau04] E. Caurier, F. Nowacki, and A. Poves, Nuclear Physics A 742, 14 (2004)
[Cau14] E. Caurier, F. Nowacki, and A. Poves, Physical Review C 90, 014302 (2014)
[Che10] B. Cheal *et al.*, Physical Review Letters 104, 252502 (2010)
[Chi11] C. Chiara *et al.*, Physical Review C 84, 037304 (2011)
[Chi12] C. Chiara *et al.*, Physical Review C 86, 041304 (2012)
[Coh61] B. Cohen and R. Price, Physical Review 121, 1441 (1961)
[Coh62a] B. Cohen, Physical Review 125, 1358 (1962)
[Coh62b] B. Cohen, Physical Review 127, 597 (1962)
[Cor14] L. Coraggio, A. Covello, A. Gargano, and N. Itaco, Physical Review C 89, 024319 (2014)
[Cor18] M. Cortés *et al.*, Physical Review C 97, 044315 (2018)
[Cot98] P. Cottle and K. Kemper, Physical Review C 58, 3761 (1998)
[Cra14] H. Crawford *et al.*, Physical Review C 89, 041303 (2014)
[Cra19] H. Crawford *et al.*, Physical Review Letters 122, 052501 (2019)
[Cri16] B. Crider *et al.*, Physics Letters B 763, 108 (2016)
[Dan99] I. Danko *et al.*, Physical Review C 59, 1956 (1999)
[Dau00] J.M. Daugas *et al.*, Physics Letters B 476, 213 (2000)
[Dau10] J.M. Daugas *et al.*, Physical Review C 81, 034304 (2010)
[Dau11] J.M. Daugas *et al.*, Physical Review C 83, 054312 (2011)
[DeA12] G. De Angelis, Physica Scripta T150, 014010 (2012)
[DeG17] R. de Groote *et al.*, Physical Review C 96, 041302 (2017)
[DeG20] R. de Groote *et al.*, Nature Physics 16, 620 (2020)
[Del16] M.-C. Delattre, Thèse de doctorat (Orsay, 2016)
[DeS53] A. de-Shalit and M. Goldhaber, Physical Review 92, 1211 (1953)

[DeS63] A. de-Shalit and I. Talmi, Nuclear Shell Theory (Academic Press, New York, 1963)
[DeS74] A. de-Shalit and H. Feshbach, Theoretical Nuclear Physics Volume I: Nuclear Structure (John Wiley & Sons, New York, 1974)
[Dew12] A. Dewald, O. Möller, and P. Petkov, Progress in Particle and Nuclear Physics 67, 786 (2012)
[Dij12] A. Dijon *et al.*, Physical Review C 85, 031301 (2012)
[Dob94] J. Dobaczewski, I. Hamamoto, W. Nazarewicz, and J. Sheikh, Physical Review Letters 72, 981 (1994)
[Dol76] P. Doll, G. Wagner, K. Knöpfle, and G. Mairle, Nuclear Physics A 263, 210 (1976)
[Dom03] Z. Dombradi *et al.*, Nuclear Physics A 727, 195 (2003)
[Doo07] P. Doornenbal *et al.*, Physics Letters B 647, 237 (2007)
[Duf99] J. Duflo and A. Zuker, Physical Review C 59, 2347 (1999)
[Ele19] Z. Elekes *et al.*, Physical Review C 99, 014312 (2019)
[Ell58] J. Elliott, Proceeding of the Royal Society A 245, 128 (1958)
[Els34a] W. Elsasser, Journal de Physique et le Radium 5, 389 (1934)
[Els34b] W. Elsasser, Journal de Physique et le Radium 5, 635 (1934)
[Eng95] C. Engelmann *et al.*, Zeitschrift für Physik A 352, 351 (1995)
[Eng99] J. Engel, M. Bender, J. Dobaczewski, W. Nazarewicz, and R. Surman, Physical Review C 60, 014302 (1999)
[Fed79] P. Federman and S. Pittel, Physical Review C 20, 820 (1979)
[Fed84] P. Federman, S. Pittel, and A. Etchegoyen, Physics Letters B 140, 269 (1984)
[Fed00] V. Fedoseyev *et al.*, Hyperfine Interactions 127, 409 (2000)
[Fee49a] E. Feenberg and K. Hammack, Physical Review 75, 1877 (1949)
[Fee49b] E. Feenberg, K. Hammack and L. Nordheim, Physical Review 75, 1968 (1949)
[Fei56] A. Feingold, Physical Review 101, 258 (1956)
[Fie37] M. Fierz, Zeitschrift für Physik 104, 553 (1937)
[Fir96] R. Firestone, Table of Isotopes: CD-Rom Edition 1.0 (John Wiley & Sons, New York, 1996)
[Fla09] K. Flanagan *et al.*, Physical Review Letters 103, 142501 (2009)
[Fla10] K. Flanagan *et al.*, Physical Review C 82, 041302 (2010)
[Fla15] F. Flavigny *et al.*, Physical Review C 91, 034310 (2015)
[Fla19] F. Flavigny *et al.*, Physical Review C 99, 054332 (2019)
[For10] C. Force *et al.*, Physical Review Letters 105, 102501 (2010)
[Fra98] S. Franchoo *et al.*, Physical Review Letters 81, 3100 (1998)
[Fra99] S. Franchoo, Doctoral Thesis (Louvain, 1999)
[Fra01] S. Franchoo *et al.*, Physical Review C 64, 054308 (2001)
[Fri05] J. Fridmann *et al.*, Nature 435, 922 (2005)
[Fuk13] N. Fukuda *et al.*, Nuclear Instruments and Methods in Physics Research B 317, 323 (2013)
[Gad10] A. Gade *et al.*, Physical Review C 81, 051304 (2010)
[Gau07] L. Gaudefroy *et al.*, Physical Review Letters 97, 092501 (2006) and 99, 099202

(2007)
[Gir88] M. Girod *et al.*, Physical Review 37, 2600 (1988)
[Gla97] T. Glasmacher *et al.*, Physics Letters B 395, 163 (1997)
[Goe49] M. Goeppert-Mayer, Physical Review 75, 1969 (1949)
[Goe63] M. Goeppert-Mayer, Nobel Lecture (Stockholm, 1963)
[Goo77] A. Goodman, Nuclear Physics A 287, 1 (1977)
[Goo78] A. Goodman and J. Borysowicz, Nuclear Physics A 295, 333 (1978)
[Got20] A. Gottardo *et al.*, Physical Review 102, 014323 (2020)
[Gra99] H. Grawe *et al.*, in Proceedings of the Workshop on Beta Decay, from Weak Interaction to Nuclear Structure, Strasbourg, 1999, edited by P. Dessagne, A. Michalon, and C. Miehe (Ires, Strasbourg, 1999), p. 211
[Gra02] H. Grawe *et al.*, Nuclear Physics A 704, 211 (2002)
[Gre05] S. Grévy *et al.*, European Physical Journal A 25, 111 (2005)
[Gro09] C. Gross *et al.*, Acta Physica Polonica B 40, 447 (2009)
[Grz98] R. Grzywacz *et al.*, Physical Review Letters 81, 766 (1998)
[Gue07] C. Guénaut *et al.*, Physical Review C 75, 044303 (2007)
[Gug34] K. Guggenheimer, Journal de Physique et le Radium 5, 253 (1934)
[Hag16] G. Hagen, G. Jansen, and T. Papenbrock, Physical Review Letters 117, 172501 (2016)
[Han79] O. Hansen, M. Harakeh, J. Maher, L. Put, and J. Vermeulen, Nuclear Physics A 313, 95 (1979)
[Han99] M. Hannawald *et al.*, Physical Review Letters 82, 1391 (1999)
[Han03] P. Hansen and J. Tostevin, Annual Review of Nuclear and Particle Science 53, 219 (2003)
[Har95] K. Hara and Y. Sun, International Journal of Modern Physics E 4, 637 (1995)
[Hau06] P. Hausladen *et al.*, International Journal of Mass Spectrometry 251, 119 (2006)
[Hax49] O. Haxel, H. Jensen and H. Suess, Physical Review 75, 1766 (1949)
[Her14] H. Hergert *et al.*, Physical Review C 90, 041302 (2014)
[Hey67] K. Heyde and P. Brussaard, Nuclear Physics A 104, 81 (1967)
[Hey83] K. Heyde, P. Van Isacker, M. Waroquier, J. Wood, and R. Meyer, Physics Reports 102, 291 (1983)
[Hey87] K. Heyde *et al.*, Nuclear Physics A 466, 189 (1987)
[Hey94] K. Heyde, The Nuclear Shell Model (Springer Verlag, Berlin, Heidelberg, and New York, 1994)
[Hjo95] M. Hjorth-Jensen, T. Kuo, and E. Osnes, Physics Reports 261, 125 (1995)
[Hof81] P. Hoff and B. Fogelberg, Nuclear Physics A 368, 210 (1981)
[Hon02] M. Honma, T. Otsuka, B. Brown, and T. Mizusaki, Physical Review C 65, 061301 (2002)
[Hon05] M. Honma, T. Otsuka, B. Brown, and T. Mizusaki, European Physical Journal A 25, 499 (2005)
[Hon06] M. Honma, T. Otsuka, T. Mizusaki, and M. Hjorth-Jensen, Journal of Physics Conference Series 49, 45 (2006)

[Hon09] M. Honma, T. Otsuka, T. Mizusaki, and M. Hjorth-Jensen, Physical Review C 80, 064323 (2009)
[Hos05] P. Hosmer *et al.*, Physical Review Letters 94, 112501 (2005)
[Hos10] P. Hosmer *et al.*, Physical Review C 82, 025806 (2010)
[Ich19] Y. Ichikawa *et al.*, Nature Physics 15, 321 (2019)
[Ily09] S. Ilyushkin *et al.*, Physical Review C 80, 054304 (2009)
[Ing36] D. Inglis, Physical Review 50, 783 (1936)
[IPN73] Groupe tandem, Annuaire de l'Institut de Physique Nucléaire, N21 (1973)
[Ish97] T. Ishii *et al.*, Nucl. Instr. Meth. A 395, 210 (1997)
[Ish98] T. Ishii *et al.*, Physical Review Letters 81, 4100 (1998)
[Ish00] T. Ishii *et al.*, Physical Review Letters 84, 39 (2000)
[Ish02] T. Ishii *et al.*, European Physical Journal A 13, 15 (2002)
[Ji88] X. Ji and B. Wildenthal, Physical Review C 37, 1256 (1988)
[Ji89] X. Ji and B. Wildenthal, Physical Review C 40, 389 (1989)
[Joh92] C. Johnson, S. Koonin, G. Lang, and W. Ormand, Physical Review Letters 69, 3157 (1992)
[Kah69] S. Kahana, H. Lee, and C. Scott, Physical Review 180, 956 (1969)
[Kan08] K. Kaneko, Y. Sun, M. Hasegawa, and T. Mizusaki, Physical Review C 78, 064312 (2008)
[Kan14] K. Kaneko, T. Mizusaki, Y. Sun, and S. Tazaki, Physical Review 89, 011302 (2014)
[Kei51] J. Keilson, Physical Review 82, 759 (1951)
[Kel39] J. Kellogg, I. Rabi, N. Ramsey Jr., and J. Zacharias, Physical Review 55, 318 (1939)
[Koe00a] U. Koester *et al.*, Hyperfine Interactions 127, 417 (2000)
[Koe00b] U. Koester *et al.*, Nuclear Instruments and Methods in Physics Research B 160, 528 (2000)
[Koe11] U. Koester *et al.*, Physical Review C 84, 034320 (2011)
[Kol16] K. Kolos *et al.*, Physical Review Letters 116, 122502 (2016)
[Kor12] A. Korgul *et al.*, Physical Review C 86, 024307 (2012)
[Kou05] H. Koura, T. Tachibana, M. Uno, and M. Yamada, Progress of Theoretical Physics 113, 305 (2005)
[Kub12] T. Kubo *et al.*, Progress in Theoretical and Experimental Physics 2012, 03C003 (2012)
[Lan03a] K. Langanke, J. Terasaki, F. Nowacki, D. Dean, and W. Nazarewicz, Physical Review C 67, 044314 (2003)
[Lan03b] K. Langanke and G. Martínez-Pinedo, Reviews of Modern Physics 75, 819 (2003)
[Len10] S. Lenzi, F. Nowacki, A. Poves, and K. Sieja, Physical Review C 82, 054301 (2010)
[Lis04] A. Lisetskiy, B. Brown, M. Horoi, and H. Grawe, Physical Review C 70, 044314 (2004)
[Lis05] A. Lisetskiy, B. Brown, and M. Horoi, European Physical Journal A 25, 95 (2005)

[Lju10] J. Ljungvall *et al.*, Physical Review C 81, 061301 (2010)
[Mac01a] H. Mach *et al.*, in Proceedings of the International Symposium on Nuclear Structure Physics, Göttingen, 2001 (World Scientific, Singapore, 2001), p. 379
[Mac01b] R. Machleidt, Physical Review C 63, 024001 (2001)
[Mai93] G. Mairle *et al.*, Physical Review C 47, 2113 (1993)
[Mar14] T. Marchi *et al.*, Physical Review Letters 113, 182501 (2014)
[May72] E. May and S. Lewis, Physical Review C 5, 117 (1972)
[Maz05] C. Mazzocchi *et al.*, Physics Letters B 622, 45 (2005)
[Mil75] D. Millener and D. Kurath, Nuclear Physics A 255, 315 (1975)
[Mis87] V. Mishin *et al.*, Optics Communications 61, 383 (1987)
[Moe03] P. Moeller, B. Pfeiffer, and K.-L. Kratz, Physical Review C 67, 055802 (2003)
[Mor56] H. Morinaga, Physical Review 101, 254 (1956)
[Mor15a] P. Morfouace, Thèse de doctorat (Orsay, 2015)
[Mor15b] P. Morfouace *et al.*, Physics Letters B 751, 306 (2015)
[Mor16a] A. Morales *et al.*, Physical Review C 93, 034328 (2016)
[Mor16b] P. Morfouace *et al.*, Physical Review C 93, 064308 (2016)
[Mor17] A. Morales *et al.*, Physics Letters B 765, 328 (2017)
[Mor18] A. Morales *et al.*, Physics Letters B 781, 706 (2018)
[Mou10] B. Mouginot, Thèse de doctorat (Orsay, 2010)
[Mue99] W. Mueller *et al.*, Physical Review Letters 83, 3613 (1999)
[Mue00] W. Mueller *et al.*, Physical Review C 61, 054308 (2000)
[Nii12] M. Niikura *et al.*, Physical Review C 85, 054321 (2012)
[Nik05] T. Nikšić, T. Marketin, D. Vretenar, N. Paar, and P. Ring, Physical Review C 71, 014308 (2005)
[Nor49] L. Nordheim, Physical Review 75, 1894 (1949)
[Now96] F. Nowacki, Thèse de doctorat (Strasbourg, 1996)
[Now09] F. Nowacki and A. Poves, Physical Review C 79, 014310 (2009)
[Now16] F. Nowacki, A. Poves, E. Caurier, and B. Bounthong, Physical Review Letters 117, 272501 (2016)
[Num01] S. Nummela *et al.*, Physical Review C 63, 044316 (2001)
[Obe14] A. Obertelli *et al.*, European Physical Journal A 50, 8 (2014)
[Oli17a] L. Olivier, Thèse de doctorat (Orsay, 2017)
[Oli17b] L. Olivier *et al.*, Physical Review Letters 119, 192501 (2017)
[Oli18] L. Olivier *et al.*, Physical Review Letters 121, 099902 (2018)
[Oln71] J. Olness *et al.*, Physical Review C 3, 2323 (1971)
[Orl15] R. Orlandi *et al.*, Physics Letters B 740, 298 (2015)
[Oro00] A. Oros-Peusquens and P. Mantica, Nuclear Physics A 669, 81 (2000)
[Ots99] T. Otsuka, T. Mizusaki, and M. Honma, Journal of Physics G 25, 699 (1999]
[Ots01a] T. Otsuka *et al.*, Physical Review Letters 87, 082502 (2001)
[Ots01b] T. Otsuka, M. Honma, T. Mizusaki, N. Shimizu, and Y. Utsuno, Progress in Particle and Nuclear Physics 47, 319 (2001)
[Ots02] T. Otsuka, Progress of Theoretical Physics Supplement 146, 6 (2002)

[Ots05] T. Otsuka, T. Suzuki, R. Fujimoto, H. Grawe, and Y. Akaishi, Physical Review Letters 95, 232502 (2005)
[Ots06] T. Otsuka, T. Matsuo, and D. Abe, Physical Review Letters 97, 162501 (2006)
[Ots10] T. Otsuka *et al.*, Physical Review Letters 104, 012501 (2010)
[Oza00] A. Ozawa, T. Kobayashi, T. Suzuki, K. Yoshida, and I. Tanihata, Physical Review Letters 84, 5493 (2000)
[Paa79] V. Paar, Nuclear Physics A 331, 16 (1979)
[Paa81] V. Paar, Nuclear Physics A 351, 1 (1981)
[Pat09] N. Patronis *et al.*, Physical Review C 80, 034307 (2009)
[Pau08] D. Pauwels *et al.*, Physical Review C 78, 041307 (2008)
[Pau10] D. Pauwels *et al.*, Physical Review C 82, 027304 (2010)
[Paw94] T. Pawłat *et al.*, Nuclear Physics A 574, 623 (1994)
[Pea96] J. Pearson, R. Nayak, and S. Goriely, Physics Letters B 387, 455 (1996)
[Per06] O. Perru *et al.*, Physical Review Letters 96, 232501 (2006)
[Per14] S. Péru and M. Martini, European Physical Journal A50, 88 (2014)
[Pet16] C. Petrone *et al.*, Physical Review C 94, 024319 (2016)
[Pfü97] M. Pfützner, R. Grzywacz, M. Lewitowicz, and K. Rykaczewki, Nuclear Physics A 626, 259 (1997)
[Pol05] E. Pollacco *et al.*, European Physical Journal 25, 287 (2005)
[Por11] M.-G. Porquet *et al.*, Physical Review C 84, 054305 (2011)
[Pou86] F. Pougheon *et al.*, Europhysics Letters 2, 505 (1986)
[Pov81] A. Poves and A. Zuker, Physics Reports 70, 235 (1981)
[Pov87] A. Poves and J. Retamosa, Physics Letters B 184, 311 (1987)
[Pov01] A. Poves, J. Sánchez-Solano, E. Caurier, and F. Nowacki, Nuclear Physics A 694, 157 (2001)
[Pri99] J. Prisciandaro *et al.*, Physical Review C 60, 054307 (1999)
[Pro15] C. Prokop *et al.*, Physical Review C 92, 061302 (2015)
[Rah07] S. Rahaman *et al.*, European Physical Journal 34, 5 (2007)
[Rai50] J. Rainwater, Physical Review 79, 432 (1950)
[Raj12] M. Rajabali *et al.*, Physical Review C 85, 034326 (2012)
[Rap11] E. Rapisarda *et al.*, Physical Review C 84, 064323 (2011)
[Rar41] W. Rarita and J. Schwinger, Physical Review 59, 436 (1941)
[Rec13] F. Recchia *et al.*, Physical Review C 88, 041302 (2013)
[Rei75] W. Reiter, W. Breunlich, and P. Hille, Nuclear Physics A 249, 166 (1975)
[Rei86] P.-G. Reinhard, M. Rufa, J. Maruhn, W. Greiner, and J. Friedrich, Zeitschrift für Physik A 323, 13 (1986)
[Ret97] J. Retamosa, E. Caurier, F. Nowacki, and A. Poves, Physical Review C 55, 1266 (1997)
[Rob16] C. Robin and E. Litvinova, European Physical Journal A 52, 205 (2016)
[Rot78] G. Rotbard *et al.*, Physical Review C 18, 86 (1978)
[Rou70] P. Roussel, G. Bruge, A. Bussière, H. Faraggi, and J. Testoni, Nuclear Physics A 155, 306 (1970)

[Run85] E. Runte *et al.*, Nuclear Physics A 441, 237 (1985)
[Sah15] E. Sahin *et al.*, Physical Review C 91, 034302 (2015)
[Sah17a] E. Sahin *et al.*, Physical Review Letters 118, 242502 (2017)
[Sah17b] E. Sahin, private communication (2017)
[Sak99] H. Sakurai *et al.*, Physics Letters B 448, 180 (1999)
[San15] C. Santamaria *et al.*, Physical Review Letters 115, 192501 (2015)
[Sat83] G. Satchler, Direct Nuclear Reactions (Clarendon Press, Oxford, 1983)
[Saw03] M. Sawicka *et al.*, Physical Review C 68, 044304 (2003)
[Sch76] R. Scheerbaum, Physics Letters B 63, 381 (1976)
[Sch96] H. Scheit *et al.*, Physical Review Letters 77, 3967 (1996)
[Sch13] J. Schiffer *et al.*, Physical Review C 87, 034306 (2013)
[See91] M. Seeger *et al.*, Nuclear Physics A 533, 1 (1991)
[Sha93] M. Sharma, M. Nagarajan, and P. Ring, Physics Lettters B 312, 377 (1993)
[She77] J. Sherman, E. Flynn, O. Hansen, N. Stein, and J. Sunier, Physics Letters B 67, 275 (1977)
[She02] J. Shergur *et al.*, Physical Review C 65, 034313 (2002)
[Shi12] N. Shimizu *et al.*, Progress in Theoretical and Experimental Physics 2012, 01A205 (2012)
[Shi16] Y. Shiga *et al.*, Physical Review C 93, 024320 (2016)
[Sie10] K. Sieja and F. Nowacki, Physical Review C 81, 061303 (2010)
[Sie12] K. Sieja and F. Nowacki, Physical Review C 85, 051301 (2012)
[Sie14] K. Sieja, private communication (2014)
[Sin92] J. Sinatkas, L. Skouras, D. Strottman, and J. Vergados, Journal of Physics G 18, 1377 (1992) and 18, 1401 (1992)
[Smi68] D. Smith, H. Chen, and H. Enge, Nuclear Physics A 107, 639 (1968)
[Smi04] N. Smirnova, A. De Maesschalck, A. Van Dyck, and K. Heyde, Physical Review C 69, 044306 (2004)
[Smi10] N. Smirnova, B. Bally, K. Heyde, F. Nowacki, and K. Sieja, Physics Letters B 686, 109 (2010)
[Söd15] P.-A. Söderström *et al.*, Physical Review C 92, 051305 (2015)
[Sor84] R. Sorensen, Nuclear Physics A 420, 221 (1984)
[Sor02] O. Sorlin *et al.*, Physical Review Letters 88, 092501 (2002)
[Sor03] O. Sorlin *et al.*, European Physical Journal A 16, 55 (2003)
[Sta04] M. Stanoiu *et al.*, Physical Review C 69, 034312 (2004)
[Ste07] I. Stefanescu *et al.*, Physical Review Letters 98, 122701 (2007)
[Ste08] I. Stefanescu *et al.*, Physical Review Letters 100, 112502 (2008)
[Ste09a] I. Stefanescu *et al.*, Physical Review C 79, 034319 (2009)
[Ste09b] I. Stefanescu *et al.*, Physical Review C 79, 044325 (2009)
[Ste09c] I. Stefanescu *et al.*, Physical Review C 79, 064302 (2009)
[Ste13] D. Steppenbeck *et al.*, Nature 502, 207 (2013)
[Sto83] M. Storm, A. Watt, and R. Whitehead, Journal of Physics G 9, L165 (1983)
[Sto08] N. Stone *et al.*, Physical Review C 77, 014315 (2008)

[Suc14a] S. Suchyta *et al.*, Physical Review C 89, 021301 (2014)
[Suc14b] S. Suchyta *et al.*, Physical Review C 89, 067303 (2014)
[Sum17] T. Sumikama *et al.*, Physical Review C 95, 051601 (2017)
[Sun09] Y. Sun *et al.*, Physical Review C 80, 054306 (2009)
[Tac95] T. Tachibana *et al.*, in Proceedings of the International Conference on Exotic Nuclei and Atomic Masses, Arles, 1995, edited by M. de Saint Simon and O. Sorlin (Editions Frontières, Gif-sur-Yvette, 1995), p. 763
[Taf71] L. Taff, B. Koene, and J. van Klinken, Nuclear Physics A 164, 565 (1971)
[Tak12] S. Takeuchi *et al.*, Physical Review Letters 109, 182501 (2012)
[Tak14] S. Takeuchi *et al.*, Nuclear Instruments and Methods A 763, 596 (2014)
[Tal62] I. Talmi, Reviews of Modern Physics 34, 704 (1962)
[Tan19] R. Taniuchi *et al.*, Nature 569, 53 (2019)
[Ter60] T. Terasawa, Progress of Theoretical Physics 23, 87 (1960)
[Thi75] C. Thibault *et al.*, Physical Review C 12, 644 (1975)
[Thi00] P. Thirolf *et al.*, Physics Letters B 485, 16 (2000)
[Tho06] J.-C. Thomas *et al.*, Physical Review C 74, 054309 (2006)
[Tod04] B. Todd-Rutel, J. Piekarewicz, and P. Cottle, Physical Review C 69, 021301 (2004)
[Tog16] T. Togashi, Y. Tsunoda, T. Otsuka, and N. Shimizu, Physical Review Letters 117, 172502 (2016)
[Tsu11] N. Tsunoda, T. Otsuka, K. Tsukiyama, and M. Hjorth-Jensen, Physical Review C 84, 044322 (2011)
[Tsu14] Y. Tsunoda, T. Otsuka, N. Shimizu, M. Honma, and Y. Utsuno, Physical Review C 89, 031301 (2014)
[Tsu17] Y. Tsunoda, private communication (2016 and 2017)
[Unn63] I. Unna, Physical Review 132, 2225 (1963)
[Uts99] Y. Utsuno, T. Otsuka, T. Mizusaki, and M. Honma, Physical Review C 60, 054315 (1999)
[Uts12] Y. Utsuno *et al.*, Physical Review 86, 051301 (2012)
[Vaj18] Z. Vajta *et al.*, Physics Letters B 782, 99 (2018)
[Van04a] J. Van Roosbroeck *et al.*, Physical Review C 69, 034313 (2004)
[Van04b] J. Van Roosbroeck *et al.*, Physical Review Letters 92, 112501 (2004)
[Van05] J. Van Roosbroeck *et al.*, Physical Review C 71, 054307 (2005)
[Van14] P. Van Isacker and S. Heinze, Annals of Physics 349, 73 (2014)
[Ver79] M. Vergnes *et al.*, Physical Review C 19, 1276 (1979)
[Ver07] D. Verney *et al.*, Physical Review C 76, 054312 (2007)
[Vin10] P. Vingerhoets *et al.*, Physical Review C 82, 064311 (2010)
[Wak17] T. Wakasa, K. Ogata, and T. Noro, Progress in Particle and Nuclear Physics 96, 32 (2017)
[Wan65] W. Wang and E. Winhold, Physical Review 140, B882 (1965)
[War90] E. Warburton, J. Becker, and B. Brown, Physical Review C 41, 1147 (1990)
[Wat81] A. Watt, R. Singhal, M. Storm, and R. Whitehead, Journal of Physics G 7, L145

(1981)
[Wei02] L. Weissman *et al.*, Physical Review C 65, 024315 (2002)
[Wel17] A. Welker *et al.*, Physical Review Letters 119, 192502 (2017)
[Wer96] T. Werner *et al.*, Nuclear Physics A 597, 327 (1996)
[Wie10] A. Wiens *et al.*, Nuclear Instruments and Methods in Physics Research A 618, 223 (2010)
[Wie13] F. Wienholtz *et al.*, Nature 498, 346 (2013)
[Wie18] O. Wieland *et al.*, Physical Review C 98, 064313 (2018)
[Wig37] E. Wigner, Physical Review 51, 947 (1937)
[Win88] J. Winger *et al.*, Physical Review C 38, 285 (1988)
[Win08] J. Winger *et al.*, Acta Physica Polonica B 39, 525 (2008)
[Win09] J. Winger *et al.*, Physical Review Letters 102, 142502 (2009)
[Wra17] C. Wraith *et al.*, Physics Letters B 771, 385 (2017)
[Xie19] L. Xie *et al.*, Physics Letters B 797, 134805 (2019)
[Xu14] Z. Xu *et al.*, Physical Review Letters 113, 032505 (2014)
[Yan16] X. Yang *et al.*, Physical Review Letters 116, 182502 (2016)
[Yua12] C. Yuan, T. Suzuki, T. Otsuka, F. Xu, and N. Tsunoda, Physical Review C 85, 064324 (2012)
[Yuk38] H. Yukawa, S. Sakata, and M. Taketani, Proceedings of the Physico-Mathematical Society of Japan 20, 319 (1938)
[Zei78] B. Zeidman and J. Nolen Jr., Physical Review C 18, 2122 (1978)
[Zel83] N.Zeldes, T. Dumitrescu, and H. Koehler, Nuclear Physics A 399, 11 (1983)
[Zhi13] Q. Zhi *et al.*, Physical Review C 87, 025803 (2013)
[Zuk95] A. Zuker, J. Retamosa, A. Poves, and E. Caurier, Physical Review C 52, 1741 (1995)
[Zuk15] A. Zuker, A. Poves, F. Nowacki, and S. Lenzi, Physical Review C 92, 024320 (2015)

Video vos epilogum expectare, sed nimium desipitis, siquidem arbitramini, me quid dixerim etiam dum meminisse, cum tantam verborum farraginem effuderim. Vetus illud, μισω μναμονα συμποταν. Novum hoc, μισω μναμονα ακροατην. Quare valete, plaudite, vivite, bibite, Moriæ celeberrimi mystæ.

Je vois bien que vous attendez une péroraison ; mais en vérité vous vous trompez bien fort, si vous croyez que j'ai gardé dans ma mémoire tout le verbiage que je viens de vous débiter. Les Grecs disaient autrefois : Je hais un convive qui a trop bonne mémoire ; et moi je vous dis à présent : Je hais un auditeur qui se souvient de tout. Adieu donc, illustres et chers amis de la Folie, applaudissez-moi, portez-vous bien et divertissez-vous.

Erasmus Roterodamus, Stultitiæ Laus